Eshelman, Mark Alan

SOLIDIFICATION DYNAMICS IN BINARY ALLOY SYSTEMS

Iowa State University PH.D. 1987

PLEASE NOTE:

In all cases this material has been filmed in the best possible way from the available copy. Problems encountered with this document have been identified here with a check mark ✓.

1. Glossy photographs or pages _____
2. Colored illustrations, paper or print _____
3. Photographs with dark background ✓
4. Illustrations are poor copy _____
5. Pages with black marks, not original copy _____
6. Print shows through as there is text on both sides of page _____
7. Indistinct, broken or small print on several pages ✓
8. Print exceeds margin requirements _____
9. Tightly bound copy with print lost in spine _____
10. Computer printout pages with indistinct print _____
11. Page(s) _____ lacking when material received, and not available from school or author.
12. Page(s) _____ seem to be missing in numbering only as text follows.
13. Two pages numbered _____. Text follows.
14. Curling and wrinkled pages _____
15. Dissertation contains pages with print at a slant, filmed as received _____
16. Other _____

University
Microfilms
International

Solidification dynamics in binary alloy systems

by

Mark Alan Eshelman

A Dissertation Submitted to the

Graduate Faculty in Partial Fulfillment of the

Requirements for the Degree of

DOCTOR OF PHILOSOPHY

Department: Materials Science and Engineering
Major: Metallurgy

Approved:

Signature was redacted for privacy.

In Charge of Major Work

Signature was redacted for privacy.

For the Major Department

Signature was redacted for privacy.

For the Graduate College

Iowa State University
Ames, Iowa

1987

TABLE OF CONTENTS

NOMENCLATURE

A = Amplitude

a_c = κ_L/C_L

a_o = Linear stability coefficient

a_s = κ_s/C_s

a_1 = Nonlinear coefficient

C = Concentration

C_I = Concentration at the interface

C_L = Specific heat of liquid per unit volume

C_o = C_∞/K_o

C_s = Specific heat of the solid per unit volume

C_∞ = Concentration from advancing interface

D = Diffusion coefficient

G = Weighted average thermal gradient = $\kappa_s G_s + \kappa_L G_L/(\kappa_s+\kappa_L)$

G_c^b = Concentration gradient at interface at point of break up

G_c = Concentration gradient in the liquid at the interface

G_L = Thermal gradient in the liquid

g_L = $(\kappa_L/\kappa')G_s$

g_s = $(\kappa_s/\kappa')G_s$

$h(k)$ = As defined on page 27

K = Curvature

K_o = Partition coefficient

k = Wavenumber

k^* = $(V/2D) + [(V/2D)^2 + k^2]^{1/2}$

k_c = Critical wavenumber

l_c = $\Gamma/\Delta S K_o \Delta T_o$

l_s = $2\ D/V$

l_t = $K_o \Delta T_o / G$

m = liquidus slope (normally negative)

mG_c = $\Delta T_o V/D$

n = κ_s/κ_L

S = Supercooling

$S(k)$ = As defined on page 27

T = Temperature

T_E = Equilibrium freezing temperature of the advancing interface

T_L = Temperature in the liquid

T_m = Melting point of the alloy of composition C_∞

T_s = Temperature in the solid

t = Time

V = Velocity

V_b = Break up velocity

V_b^* = Break up velocity with dynamic considerations

V_c = Critical velocity

V_E = External, or drive velocity

V_m = Maximum velocity at which cells can exist

V_o = Critical velocity prior to an increase or decrease in velocity

V_t = Transition velocity of minimum cell spacing

v = Interface velocity

v_o = Velocity with respect to the zeroth order nonlinear problem

v_x = Velocity defined as parallel to the advancing interface

v_1 = Velocity with respect to the first order nonlinear problem

z = direction of directional freezing, or heat flow direction

Greek Symbols

α = $\gamma G/4\Delta S\Delta T_o^2$

β = $\gamma[m(K_o-1)]$

ΔH = Enthalpy of freezing

ΔS = Entropy of fusion per volume in units (for example, J/m^3)

Δs = Entropy of fusion per volume in units (for example, J/m^3K)

ΔT_o = $mC_\infty(K_o-1)/K_o$ = the freezing range of the alloy

ε = An interface perturbation

γ = Solid-liquid interfacial free energy

γ_o = Surface energy of the (100) plane

κ' = $1/2\ (\kappa_s+\kappa_L)$

κ_L = Thermal conductivity in the liquid

κ_s = thermal conductivity in the solid

ψ = Glickman's anisotropy parameter

δ = Small amplitude perturbation

$\dot{\delta}/\delta$ = Amplitude growth rate of a perturbation

Λ = Dimensionless parameter as defined on page 165

λ = $2\pi/k$ = wavelength

λ_1 = Primary spacing

λ_i = $10.58\ (l_s l_c)^{1/2}$

λ_j = $1.68\ (\lambda_i l_t)^{1/2}$

μ_c = Interface anisotropy property due to concentration considerations

μ_T = Interface anisotropy property due to thermal considerations

μ_x = Interface kinetic anisotropy term

τ_b = Time required for the occurrence of break up

ν = $V\Delta T_o/GD$

ν^+ = Dimensionless velocity at which experimental amplitude dropped sharply

ν_b = Dimensionless break up velocity

ν_b^* = Minimum value of ν_b

ν_c = Threshold value of the dimensionless velocity

ν_o = Dimensionless control velocity

ω = Wavenumber, is used in development of nonlinear model

ω_c = Critical wavenumber

GENERAL INTRODUCTION

Nature, with all its beauty and brillance, is sometimes simple, sometimes complex, but always fascinating. The simplicity of nature is often clouded when we investigate it with concepts and opinions already embedded in our minds. We must keep our minds open to see the beauty, the simplicity, and often, the complexity and intricacy of nature. Sometimes, the simple seems very complex, but more often, the complex appears very simple. A stunning example of both simplicity and complexity in nature is the snowflake. Mankind has consistently observed the six feather-like branches which emerge from the frozen droplet (Figure 1), but a precise understanding of how these branches form still remains elusive today. Do they form by pure chance? Are the branches totally determined by their growth environment? Are patterns determined at an early time in the growth and then, simply left to develop with time? These basic questions of pattern formation remain unanswered.

About three hundred years ago, Nicholas Steno (from reference [1a]) systematically studied crystal growth. He found that although crystals grow in a manner similar to plants and animals, there were some differences. Up until the time of Steno, men thought that crystals were a form of living thing. Steno showed instead, that growth conditions determine the structure which is formed. Today, there is again a desire to investigate the similarities which exist between crystal growth and other biological forms. This is because the general principles which

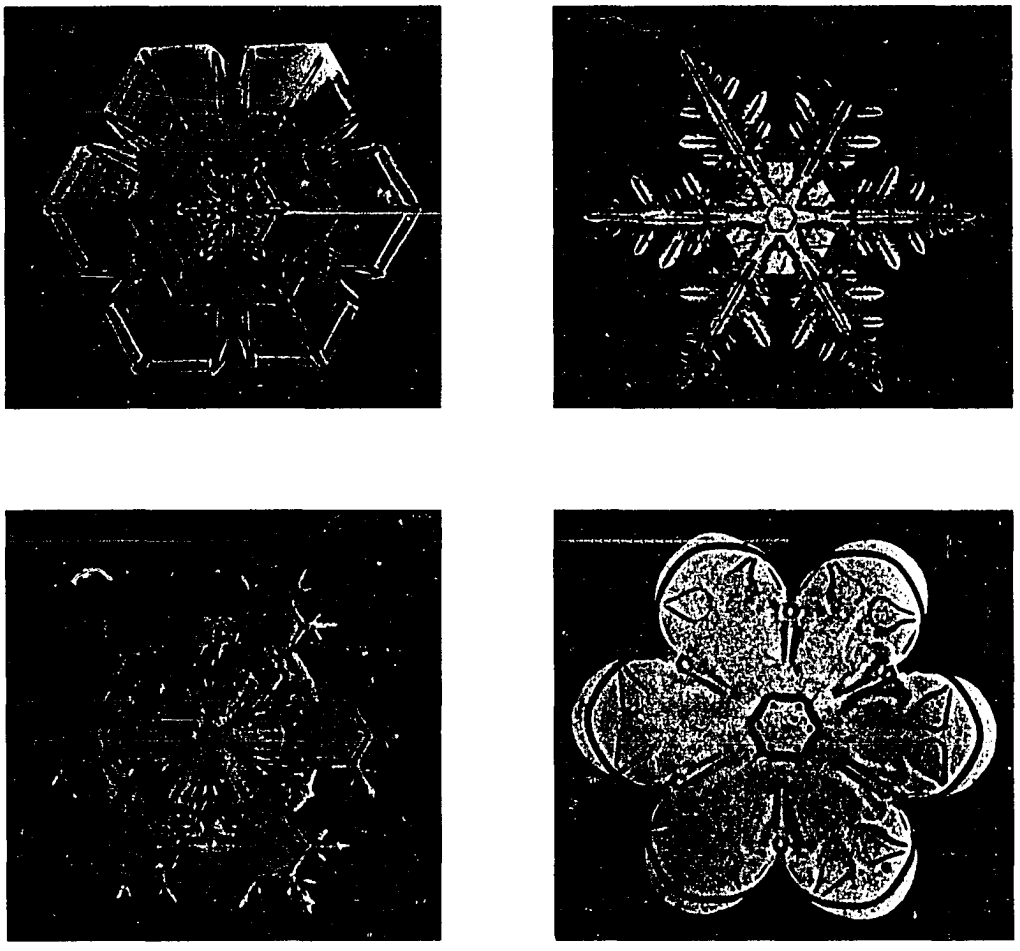

Figure 1. Actual snowflakes (from reference [1b]). There is similarity, and yet tremendous diversity

govern crystal morphologies may also apply to patterns which are formed in biological and other physical systems.

The concepts that have been used to describe crystal growth have become much more complex and detailed since the time of Steno. Great strides have been made in understanding many aspects of crystal growth. Theoretical models have been developed which produce structures that are similar to actual crystal growth structures, and experiments have been designed and carried out which shed light on some areas of crystal growth. We are beginning to understand what happens, but the most fundamental questions about pattern formation in crystal growth still remain unanswered. Specifically, we do not yet understand the principle which selects a specific pattern out of many possible patterns under given environmental conditions. Although the subject of pattern formation is fascinating to the theorist, and interesting to the pure scientist, discussion of utility of the study of such phenomenon seems to always arise. In the case of solidification, the value of studying the fundamental principles comes forth immediately. The reason for this is that all metallic parts in some stage of their processing have gone through the solidification process. The solidification conditions experienced strongly affect the microstructure which influences many physical and mechanical properties of the metallic part. Therefore, in the interest of improving properties of metallic objects, an understanding of the solidification phenomenon is very essential.

Some of the specific research areas where solidification has been studied recently are directionally solidified turbine blades, in situ

composite growth, laser processing of materials, and development of electronic materials. Each of these research areas is important in commercially manufactured products. One important aspect common to each of the research areas mentioned is directional solidification. It is for this reason that the broad topic of directional solidification was chosen as an area of study for this work.

During directional freezing, as velocity increases, three different morphologies predominate for an advancing solid-liquid interface. The morphologies are planar, cellular, and dendritic. Figure 2 shows these possible structures. Figure 2(c) shows elongated cells which are present near the cell dendrite transition. Elongated cells such as these raise the question of nomenclature because they are similar to dendrites in tip shape and overall length, but lack the side branches which are characteristic of dendritic structures. These elongated cells are referred to as dendritic cells. All four of the structures seen in Figure 2 are examined in this study.

All of the structures seen in Figure 2 have commercial importance. Planar interface solidification is important during the growth of single crystals because planar interface growth conditions give rise to single crystals of uniform composition. But in many practical situations, the slow growth rates required for planar interface stability are not economically desirable. For this reason, most casting and welding microstructures are formed under conditions which give rise to cellular and dendritic structures. Consequently, the study of cellular and dendritic growth is essential to determine processing

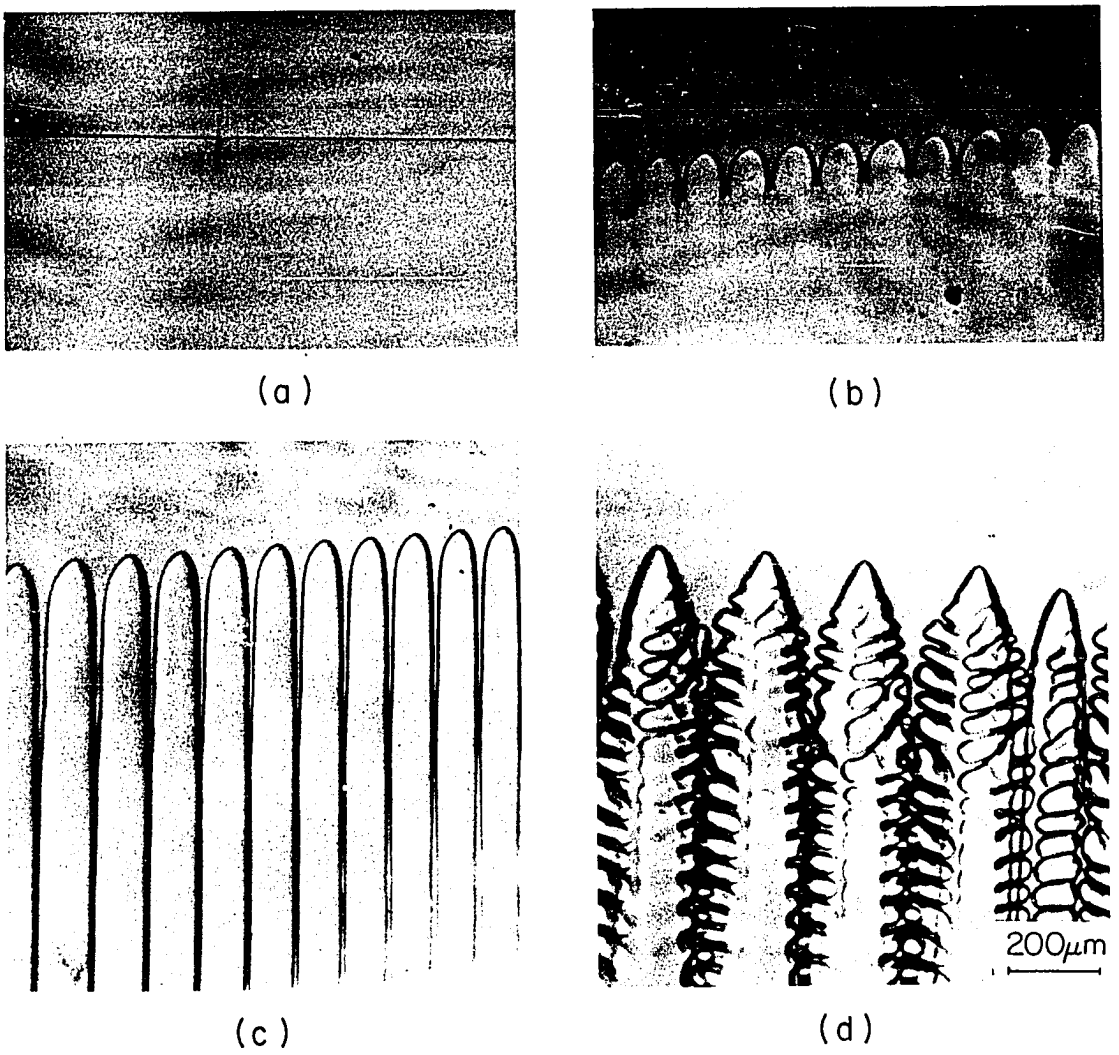

Figure 2. Interface structures observed during directional solidification of transparent metal analogs: (a) a planar interface, the solid is on the left, the liquid is on the right, (b) a cellular structure with solid cells growing out into the liquid, (c) cellular dendrites, and (d) dendrites

conditions which give optimum properties. These properties are largely influenced by the solute segregation pattern which depends on the cellular or dendritic spacings. The cellular-dendritic transition is also important in cast and welded objects because these different growth structures give different segregation patterns, thereby giving rise to different mechanical properties.

In this dissertation, an emphasis is placed on experimental studies. A detailed theoretical background is, however, presented so that the important principles which govern solidification microstructures can be clearly established. The analysis of theoretical models will also allow us to focus on critical information that is needed to further understand the pattern formation phenomenon. The theoretical background thus provides a direction for planning critical experiments to examine specific ideas.

Directional solidification was carried out experimentally on the apparatus shown schematically in Figure 3. Here, it is seen that a sample is moved at a specified externally imposed velocity through an externally imposed thermal gradient. The three possible solidification variables, the composition, growth velocity, and thermal gradient, can all be controlled accurately in these experiments. As mentioned above, there are very few physical systems in which all the variables important to the structure formed are completely controllable experimentally. For this reason, the results of directional solidification studies are of interest not only to materials science, but also to numerous other disciplines (such as physics or biology)

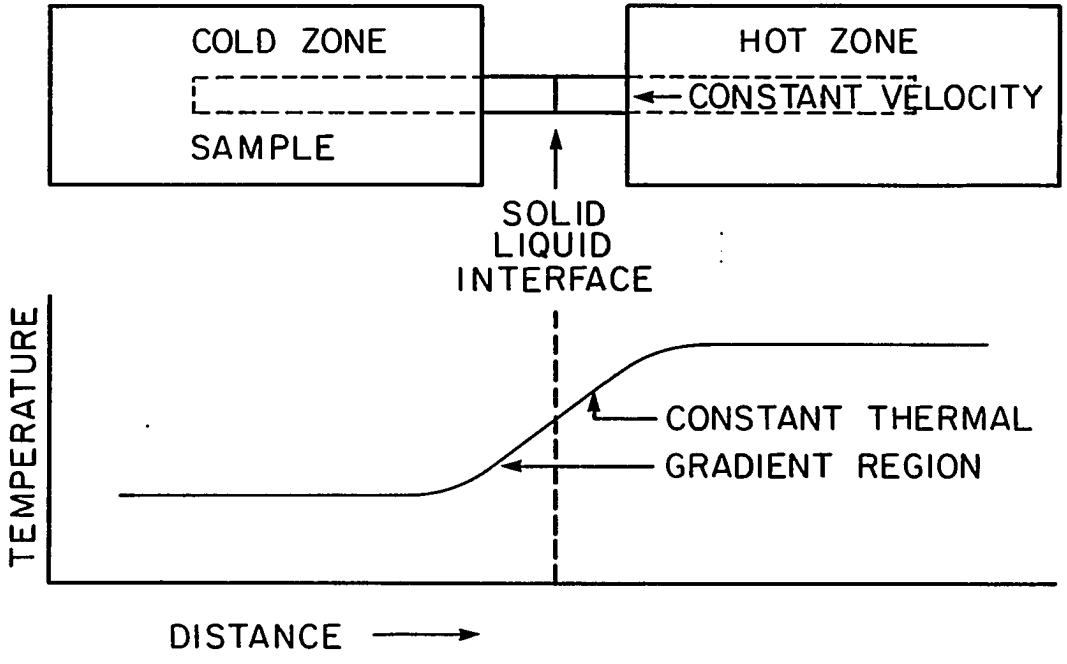

Figure 3. Schematic diagram of a directional solidification device

where the system variables are not completely controllable experimentally, but where a similar pattern formation does occur. There is, therefore, both scientific and commercial interest in the study of directional solidification microstructures.

The major questions which will be addressed in this work are:

(1) What are the physical principles which govern the transitions in interface shapes, i.e., the planar to cellular and cellular to dendritic transitions?

(2) What physical principles select or determine periodicity and amplitude of cellular or dendritic structures?

(3) If the steady-state spacing of the system is perturbed, what mechanisms are important to the system for regaining a steady-state?

(4) How does the periodicity of the pattern depend on the experimental variables?

In order to examine these questions as completely as possible, in situ studies have been performed in transparent, metal analog systems. The systems selected for the present studies are the succinonitrile-acetone, the pivalic acid-ethanol, and the carbontetrabromide-hexachloroethane systems. For these organic systems, physical properties have been determined precisely. These systems also freeze with structures which are similar to metals. In addition, they are transparent, and therefore, are ideal for establishing answers to the above questions.

The major conclusions which emerge from this study, and which are covered in detail in the appropriate sections of this work are:

(1) The experimental conditions at which a planar interface just becomes unstable are found to match accurately with the predictions of the linear stability analysis [2]. The wavelengths observed, however, at the occurrence of break up are significantly smaller than those predicted by the linear stability analysis.

(2) Cells of a finite length (amplitude) exist below the threshold velocity predicted by the linear stability analysis if the interface is perturbed to large amplitudes. The planar to nonplanar bifurcation is, therefore, subcritical. This shows that nonlinear effects are important during the planar to nonplanar transition.

(3) After the planar interface breaks up, the pattern formed starts at a small wavelength and progresses toward the longer wavelength until the final cellular steady state is developed. Development of the pattern is shown to occur when nonlinear effects become important. These nonlinear effects have been shown to occur at very early times following the break up. Both the time evolution of the steady-state pattern and the mechanisms which allow the adjustment in spacing are determined.

(4) Dynamics were found to be very important to cell spacing selection. This means that care must be taken to achieve steady state. The system may be locked into nonsteady-state growth spacings by time spent previously under different growth conditions. Stable and metastable spacings can also be produced, depending on the path taken to establish the spacing. A large experimental noise is required for nonlinear effects to induce the changes required for the steady-state

spacing to be established.

(5) The cellular state has three distinct spacing and cell length regions as the velocity increases above the threshold velocity. These are (a) a region where the cell length and spacing decrease with an increase in velocity, (b) a transition region where the cell spacing and cell length increase sharply, and (c) a region where the cell spacing decreases with increasing velocity.

(6) The cell-dendrite transition is not a sharp transition. It can occur over a range of velocities. Dendrites can occur below the normally observed cell-dendrite transition. There is no theory which predicts this, but the occurrence is similar to the hysteresis effect observed in our studies of the planar to cellular interface transition.

Explanation of Dissertation Format

This dissertation has been written in the alternate format. In the first section, the planar to cellular interface transition during the directional solidification of a binary alloy has been studied in the succinonitrile-acetone system. The interface velocity at which the planar interface becomes unstable and the wavenumbers of the initially unstable interface have been precisely determined and compared with the linear stability analysis. Critical experiments have been carried out to show that the planar to cellular bifurcation is subcritical so that a finite amplitude perturbation below the critical velocity can also give rise to planar interface instability.

In the second section, the pattern formation problem is addressed. The perturbations which form on an unstable planar interface are studied by average spacing, average amplitude, and spatial Fourier analysis. It was found that anisotropy plays a role in both interface instability and perturbation growth. It was also found that specific transient wavenumbers exists during the planar to cellular pattern formation process.

In the third section, directional solidification studies were carried out in the succinonitrile-acetone and pivalic acid-ethanol systems in order to study the variation in average cellular spacing with velocity. Three distinct behaviors were observed under steady-state growth conditions. For velocities near the critical velocity for planar interface instability, cellular spacing decreased with an increase in velocity. However, at velocities near the cell-dendrite transition, the cell spacing increased sharply. Beyond this transition region, the cell or dendrite spacing decreased with further increases in velocity. These experimental observations have been explained by using the current theoretical models of cell-dendrite growth. In addition, a finite band of velocities was identified in which both cellular and dendritic structures were found to be stable. A hysteresis effect was observed in the cell-dendrite transition indicating that the cell-dendrite bifurcation is subcritical.

In the fourth section, directional solidification experiments were carried out in model transparent systems to establish the dynamical processes by which an unstable planar interface restabilizes into a

periodic array of cells. In the succinonitrole-acetone system, where the interface properties are nearly isotropic, the cells increase their spacings by the cell elimination process and decrease their spacings by the tip-splitting mechanism. In the pivalic acid-ethanol system, the significantly anisotropic interface properties prevent the tip-splitting phenomenon. In this case, the cell spacing is decreased by going through either the cell-dendrite-cell or the cell-planar-cell transition. Dynamical studies of the variation in cellular spacing with changes in growth rate show that the spacing does not alter until a significantly large change in growth rate is imposed. When a change in spacing occurs, two distinctly different configurations are observed depending on whether the perturbation which leads to the change is localized or nonlocalized.

In the fifth section, the effect of anisotropy on cell growth is studied. It was found that anisotropy causes cells to facet both during the pattern formation process and in the steady state. It is also found that anisotropy causes cells to translate down an advancing solid-liquid interface. In addition, a schematic diagram of the interface kinetic anisotropy is constructed.

THEORIES OF PATTERN FORMATION

The models of pattern formation which have addressed directional solidification have come in stages. The first stage is essentially the zeroth order approximation to the problem. It merely addresses the problem of critical conditions beyond which a planar interface becomes unstable. This analysis was developed by Tiller et al. [3] in 1953. The first order model of linear stability analysis was done in 1964 by Mullins and Sekerka [2]. This model gave not only the critical conditions for planar interface instability, but also the wavenumbers of the patterns which should be observed at instability. The third stage was a second order nonlinear analysis. This was done in 1970 by Wollkind and Segel [4]. This nonlinear analysis predicts new types of effects not possible in the linear theory. An extension of the second order nonlinear analysis has been made recently by a number of authors into higher order systems. These models extend into the steady-state cellular growth region and have predicted structures which look like actual physically observed cells. The main disadvantage with higher order analysis is that the calculations are necessarily numerical. Therefore, direct comparison of models with experimentally observed structures is lengthy and difficult. All of these stages will be discussed below. Experimental work relevant to each area is also presented.

In review of the work done so far, it is found that although the models are quite well-developed, the experiments relevant to the models

have lagged behind. For this reason, critical experiments in the area of pattern selection were identified and carried out here. Experiments were designed to give insight into the physics of the problem so that theories might be developed which more accurately describe the phenomenon of pattern formation.

A number of assumptions were made throughout this work, both in the theoretical sections and in the experimental sections to simplify the problem. These are:

(1) No convection exists in the liquid ahead of the advancing solid-liquid interface. Convection in the liquid does occur during the solidification process. However, neglecting convection allows simplification of the already very complex situation so that the fundamental ideas which control the stability of a planar interface can be established. Convection can be thermally induced or it can be induced by solute density, but in either case, the driving force is differences in the density.

(2) A constant value for the partition coefficient was assumed in all the models.

(3) The value of the liquidus slope was kept constant.

(4) Diffusion in the solid is neglected.

In order to examine the theories, experimental studies which eliminate or minimize these effects are required. Transparent organic, metal analog systems generally hold well to these assumptions when studies are done in thin sample cells. That is an important reason why transport organic, metal analog systems were used in this study.

In this chapter, the three models described above for the break up of a planar interface are discussed. The three models are:

(1) The constitutional supercooling theory proposed by Tiller et al. [3]. This model includes the thermal gradient and the solute field in the liquid in its prediction of planar interface instability. It assumes that a planar interface will be unstable if a positive gradient of supercooling exists at the interface.

(2) The linear stability model developed by Mullins and Sekerka [2]. This model examines the rate of the growth or decay of an infinitesimal sinusoidal perturbation on a planar interface. Mullins and Sekerka include all that Tiller et al. [3] include, but also consider the effect of surface energy and the temperature gradient in the solid.

(3) The weakly nonlinear model developed by Wollkind and Segel [4]. This model expands on and develops the work of Mullins and Sekerka [2], specifically into the nonlinear regime.

In addition to these models, there is a discussion of higher order theoretical models, and an analysis of critical experiments needed.

The Constitutional Supercooling Criterion

It was within the steady-state directional solidification conditions that Tiller et al. [3] first proposed the possibility of a change in the interface morphology when the velocity was increased in differential amounts above some critical velocity. The most important principle that is discussed and quantified by Tiller et al. [3] is the

constitutional supercooling criterion.

If the thermal gradient in front of the advancing interface has a negative slope, then normal supercooling will exist in front of the interface. Supercooling can also exist in the region in front of the interface even though the thermal gradient is positive. This can happen by solute pile-up in front of the interface (Figure 4). Solute caused supercooling is called constitutional supercooling. The existence and the range of this supercooling will now be examined.

Constitutional supercooling is, therefore, supercooling that exists due to solutal concentrations near the moving interface. The existence of constitutional supercooling can be seen by examining the solute concentration field in front of the advancing interface. For steady-state planar growth, the concentration field in the liquid is given by:

$$C = C_\infty + C_\infty\left(\frac{1-K_o}{K_o}\right) \exp[-Vz/D] \qquad (1)$$

where C is the concentration, C_∞ is the concentration far from the interface, K_o is the partition coefficient, V is the velocity and D is the solute diffusion coefficient. The equilibrium temperature is a function of concentration so that the equilibrium temperature will vary with distance in front of the interface in the following way:

$$T_E = T_m + mC_\infty - \Delta T_o \exp(-Vz/D) \qquad (2)$$

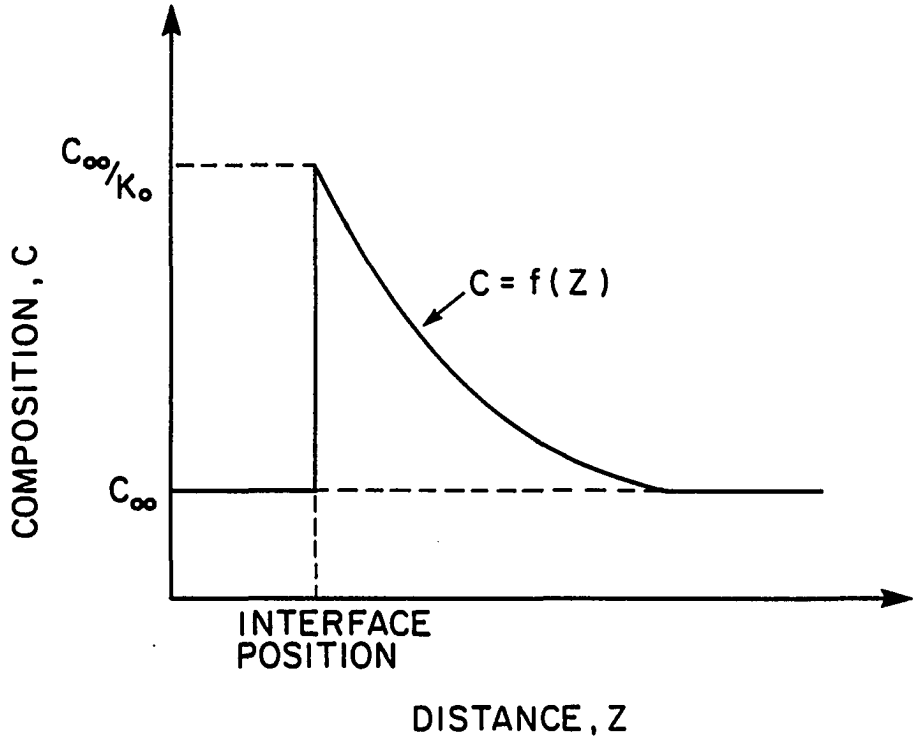

Figure 4. The concentration field which exists in the region near a steady-state growing solid-liquid interface

where T_E is the equilibrium temperature, T_m is the melting point of the pure material, m is the slope of the liquidus (which is normally considered negative), $\Delta T_o = mC_\infty(K_o-1)/K_o$ is the freezing range of the alloy, V is the velocity, D is the diffusion coefficient, and z is the distance ahead of the interface. The imposed temperature gradient in front of the interface can be expressed by the following equation:

$$T = T_m + mC_\infty/K_o + G_L z \qquad (3)$$

where T is the temperature at the distance z, and G_L is the thermal gradient. If T_E and T are plotted as a function of z, the schematic results appear as seen in Figure 5.

The shaded region denotes the region of constitutional supercooling. Note that constitutional supercooling exists only for a finite distance in front of the interface, and the supercooling increases with distance near the interface.

When Eqs. (2) and (3) are plotted as in Figure 5, the point of intersection other than at z = 0 gives the length of the constitutionally supercooled zone. This constitutional supercooled zone is given by $T_E - T$ from Eqs. (2) and (3). Tiller et al. [3] proposed that the interface will be unstable if a positive gradient of supercooling exists at the interface. If S is defined as supercooling, then,

$$S = T_E - T = \Delta T_o[1 - \exp(-Vz/D] - G_L z \quad . \qquad (4)$$

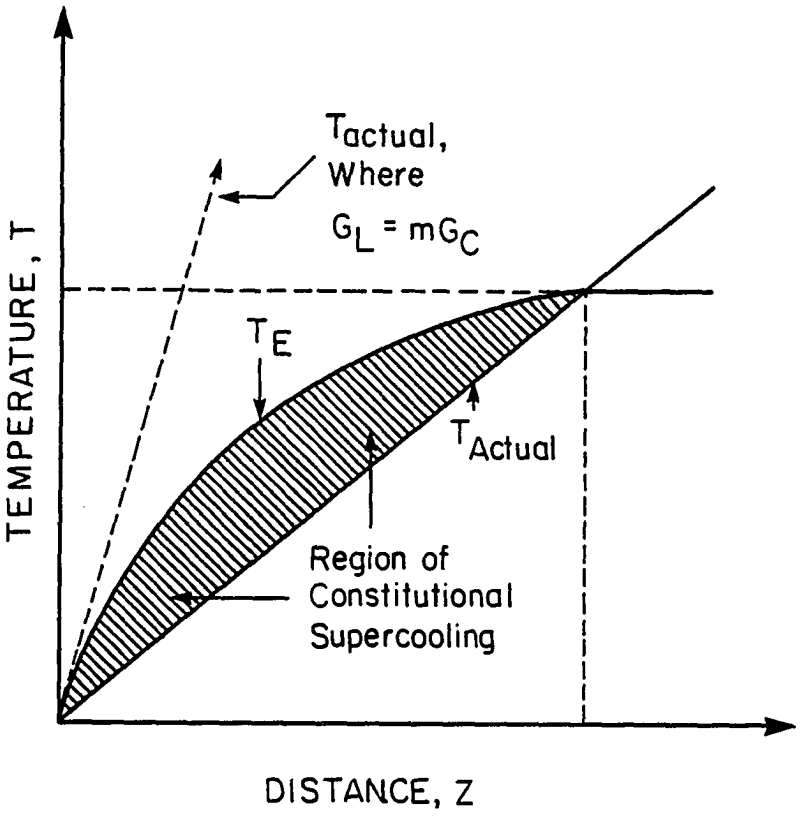

Figure 5. A schematic diagram of possible thermal field with equilibrium concentration dependent solid-liquid interface temperatures superimposed. The shaded region is the region in which constitutional supercooling exists

The interface will be unstable if $\partial S/\partial z \geq 0$ at $z = 0$, or

$$(\partial S/\partial z)_{z=0} \geq 0 \quad . \tag{5}$$

The critical point of stability, or neutral stability condition, is given by the condition $\partial S/\partial z = 0$ at $z = 0$, which gives

$$V = G_L D/\Delta T_o \quad . \tag{6}$$

This expression is the general expression for the limits of constitutional supercooling. If the limits of constitutional supercooling are exceeded, interface instability will occur, and the new structure will advance into the constitutionally supercooled region in front of the interface. Note that $\Delta T_o V/D = mG_c$, where G_c is the concentration gradient in the liquid at the interface. Thus, the neutral stability condition for a planar interface can also be written as

$$mG_c - G_L = 0 \quad . \tag{7}$$

There are three possible ways to study planar interface instability at the threshold values. These are to vary one of V, G_L, or ΔT_o while keeping the other two variables constant. Varying V or G_L is quite commonly done, but it is also possible to vary ΔT_o by changing concentration or crystallographic orientation [5]. The process of

orientation dependence on interface stability can be seen in Figure 6. Notice in this figure that the different grains break up differently due to the difference in orientation of the grains as can be seen in the final photomicrograph. Orientation can be obtained from inspection of the dendrites growth direction, and by knowing that dendrites grow in the [001] direction. The effective K_o, which is a function of orientation, is lowest when the growth orientation is along the [001] crystallographic direction. This means that the orientation most closely aligned with the [001] direction will break up first, since ΔT_o is highest when K_o is lowest.

Linear Stability Analysis

The interface instability model of Tiller et al. [3] gives a good basic background to the problem of interface instability, but there are several areas in which it is not complete. The three important aspects that are not included in their theory are as follows:

(1) It only considers the thermal gradient in the liquid ahead of the advancing interface. Neither the thermal gradient in the solid, nor the latent heat generated by freezing are considered.

(2) It does not take into account the stabilizing effect of the solid-liquid surface energy.

(3) It gives only the threshold conditions, it tells nothing of what the wavelength of the profile will be when these conditions are exceeded.

There is, therefore, a need to consider other models which can take into

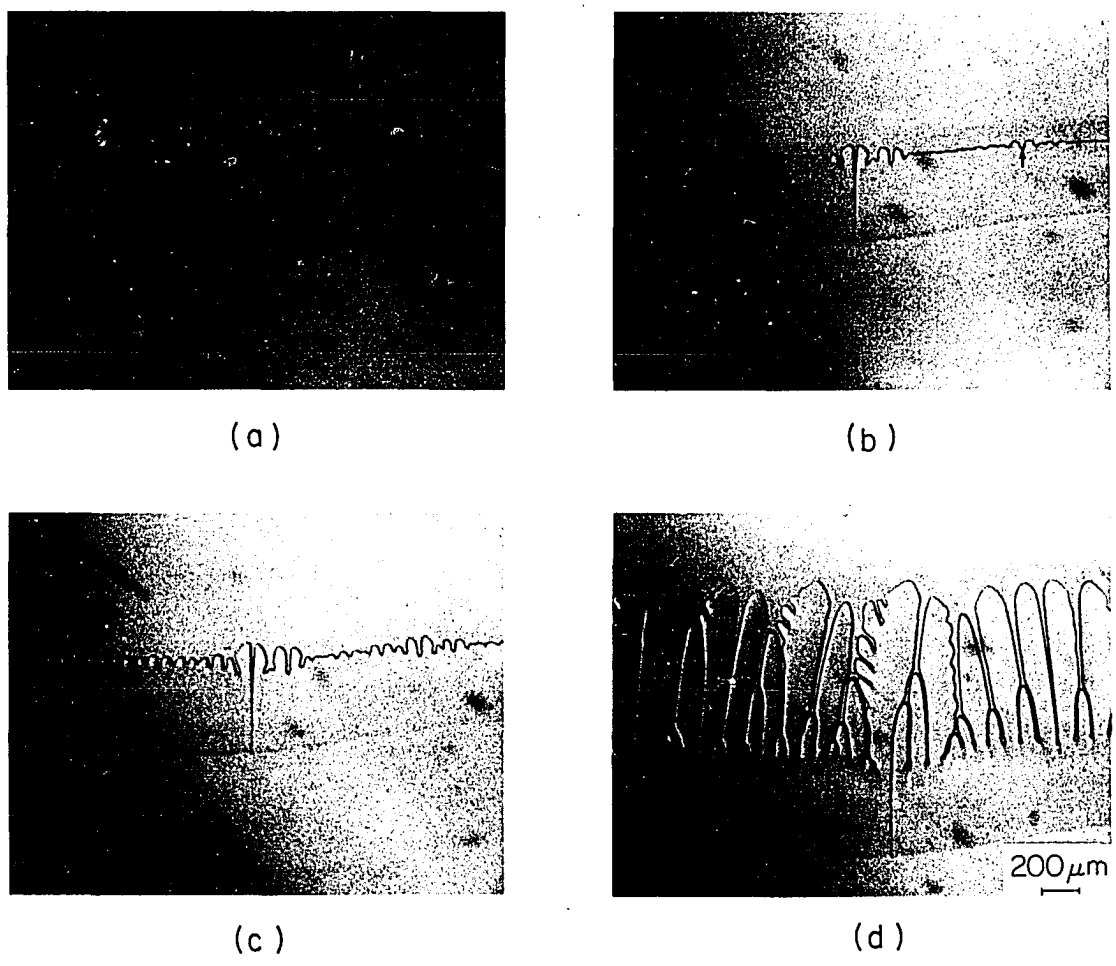

Figure 6. Planar interface break up in two grains with slightly different orientations. Notice that the right-hand grain breaks up slightly earlier than the grain on the left. This shows the importance of crystallographic orientation on interface stability. Times increase from a → d

account some or all of these three major points. Such an analysis was first carried out by Mullins and Sekerka [2].

Mullins and Sekerka [2] consider the thermal gradient in the solid and the liquid. They also considered the stabilizing effect of surface energy for an isotropic interface, and they predicted the wavelengths of the perturbations which will form and grow just beyond threshold conditions. The coordinate system and the interface perturbation used by Mullins and Sekerka is shown in Figure 7.

The analysis of Mullins and Sekerka [2] is known as linear stability analysis, since the boundary conditions were linearized in order to obtain solutions. The transport equations governing the thermal and solute profiles are as follows [2]. In the liquid,

$$\nabla^2 C + (V/D_L)(\partial C/\partial z) = 0, \tag{8}$$

$$\nabla^2 T_L + (V/a_L)(\partial T_L/\partial z) = 0, \tag{9}$$

and in the solid,

$$\nabla^2 T_S + (V/a_S)(\partial T_S/\partial z) = 0, \tag{10}$$

where L and s denote liquid and solid, respectively. It was assumed that diffusion in the solid was negligible. The variables are C = the concentration of the solute in the liquid, z = the direction orthogonal to the advancing interface, V = the constant velocity of

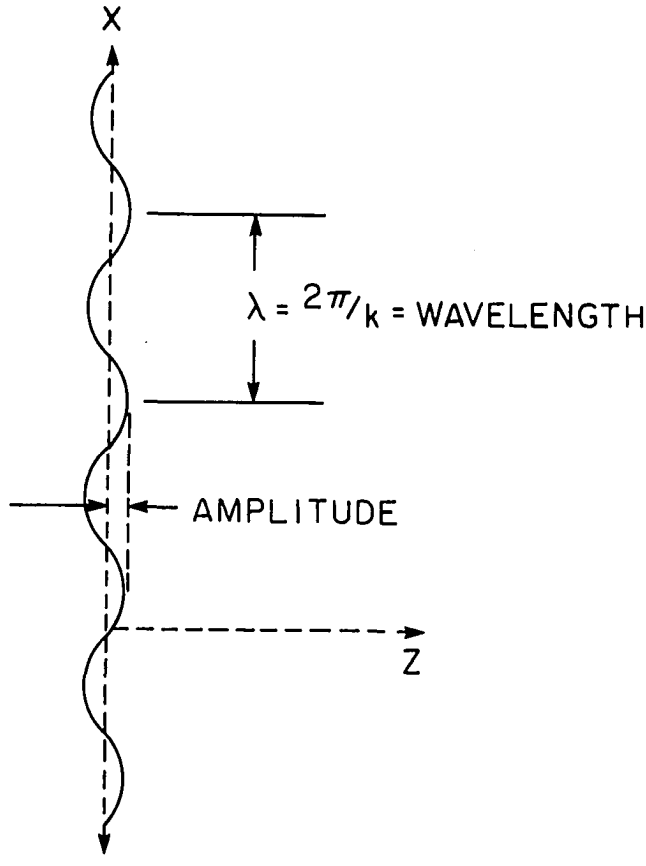

Figure 7. A schematic diagram of a perturbed solid-liquid interface. Axis are defined consistent with the models explained in this dissertation

the planar interface, D_L = the diffusion coefficient of solute in the liquid, T_L = the temperature in the liquid $a_L = \kappa_L/C_L$ = thermal diffusivity of the liquid, with κ_L = the thermal conductivity in the liquid and C_L = the specific heat of the liquid per unit volume, T_S = the temperature in the solid, $a_S = \kappa_S C_S$ = the thermal diffusivity of the solid, with κ_S = the thermal conductivity of the solid and C_S = the specific heat of the solid per unit volume. These equations are for the steady state at constant velocity. They consider an infinitesimal perturbation of the interface, as is shown in Figure 7. The interface profile was considered to be given by $z = \delta \sin kx$, where $k = 2\pi/\lambda$ and λ is the wavelength.

It should be noted that although Mullins and Sekerka [2] defined the problem in terms of the transport equations (8-10), they revert back to Laplace's equation for the thermal field when they enter into the solution stage. Laplace's equation is given by $\nabla^2 T_S = \nabla^2 T_L = 0$.

The boundary conditions at the perturbed interface are as follows:

$$T_I = T_m + mC_I = \Gamma \delta k^2 \sin kx, \qquad (11)$$

where $\Gamma = \gamma/\Delta S$ = the capillary constant, γ = the solid-liquid interfacial free energy, ΔS = the latent heat of the solvent per unit volume, T_m = the absolute melting temperature of a flat interface, K = the average curvature at a point on the solid-liquid interface, and $\delta k^2 \sin kx$ is the curvature of the perturbed interface. The interface velocity, v(x), at any point on the interface is then given

by the thermal or solute flux balance at the interface as:

$$v(x) = \frac{1}{L}\left[K_S\left(\frac{\partial T_S}{\partial z}\right)_I - K_L\left(\frac{\partial T_L}{\partial z}\right)_I = \frac{D}{C_I(k-1)}\left(\frac{\partial C}{\partial z}\right)_I\right], \qquad (12)$$

where K_S = the curvature of the solid, K_L = the curvature of the liquid, $C_I(K_o-1)$ = the difference in concentration between the solid and liquid sides of the interface, and K_o is the equilibrium partition coefficient.

These equations are linearized by using the following:

$$T_I = T_o + a\delta\sin kx = T_o + aW \qquad (13)$$

and

$$C_I = C_o + b\delta\sin kx = C_o + bW, \qquad (14)$$

where T_o and $C_o = C_\infty/K_o$ are the values for the flat interface and the second terms in each expression are the first order corrections for an infinitesimal perturbation on the interface. This, then, is linearization of the problem. The central result of Mullins and Sekerka's analysis [2] is as follows:

$$\frac{\dot{\delta}}{\delta} = \frac{Vk\{-2\Gamma k^2[k^*-(V/D)(1-K_o] - (g_S+g_L)[k^*-(V/D)(1-K_o] + 2mG_c[k^*-V/D]\}}{(g_S-g_L)[k^*-(V/D)(1-K_o] + 2kmG_c} \qquad (15)$$

where $\dot{\delta}/\delta$ = the amplitude growth rate of the perturbation, $k = 2\pi/\lambda$ with λ = the wavelength, $k^* = (V/2D)+[(V/2D)^2 + k^2]^{1/2}$, $g_s = (\kappa_s/\kappa')G_s$ with $\kappa' = 1/2(\kappa_s+\kappa_L)$, and G_s = the thermal gradient in the solid at the interface, $g_L = (\kappa_L/\kappa')G_L$ with G_L = thermal gradient in the liquid at the interface, and $G_c = VC_o(K_o-1)/D$.

This result is significant because it describes the critical conditions where the amplitude growth rate $\dot{\delta}/\delta$ becomes positive, and therefore, the interface becomes unstable, as a function of the wavelength $\lambda = 2\pi/k$. The result can be used to determine variation in k_c, the critical k for different G, V, and ΔT_o values, where G is given by $G = \kappa_s G_s+\kappa_L G_L/(\kappa_s+\kappa_L)$. It also gives the range of possible k values for a given G, V, and ΔT_o for which an interface is unstable, or stable. One can, therefore, predict the wavenumbers in the pattern that should be seen under given conditions.

Equation (15) can be rewritten in terms of two functions of k as follows:

$$\dot{\delta}/\delta = S(k)h(k), \tag{16}$$

where

$$S(k) = -\Gamma k^2 - (g_s+g_L)/2 + mG_c\{[k^*-V/D]/[k^*-(1-K_o)V/D]\} \tag{17}$$

and

$$h(k) = 2Vk/\{(g_s-g_L) + 2kmG_c/[k^*-(1-K_o)V/D]\}. \tag{18}$$

Of these two functions, only one, S(k), causes $\dot{\delta}/\delta$ to change sign. This is because h(k) is always positive and therefore, always favors stability. Therefore, stability depends on S(k) alone. Inspecting S(k) reveals that the first term arises from capillarity, and since it is negative for all values of V, G, ΔT_o and k, it promotes stability by damping out any existing perturbation. The second term in S(k) arises from thermal gradients. It is also always negative and thus, it will damp out all perturbations and favor stability. The third term in S(k) arises from solute diffusion. It is always positive and hence, favors interface instability. The stability of the interface is, therefore, determined by the relative magnitudes of the three S(k) terms. Instability occurs when the third term (solute diffusion) becomes larger than the sum of the first two terms (capillarity and thermal gradient).

If S(k) is set to zero, then the neutral stability condition is given by:

$$G - mG_c\{[k^*-V/D]/[k^*-(1-K_o)V/D]\} = -\Gamma k^2 \ . \qquad (19)$$

If surface energy effects are neglected, i.e., $\Gamma = 0$, then for $V\lambda \ll 1$, the above condition simplifies to

$$G - mG_c = 0 \ . \qquad (20)$$

This result is similar to the constitutional supercooling criterion proposed by Tiller et al. [3]. The major difference between Eqs. (20) and (7) is in the thermal gradient term. Thus, if the temperature gradient in the liquid, G_L, in Eq. (7) is replaced with the conductivity weighted average temperature at the interface, the constitutional supercooling criterion and the results of the linear stability are equivalent. Equation (20), with the conductivity weighted average thermal gradient, is known as the modified supercooling criterion.

In order to facilitate a better understanding of stability and instability, a figure is given below for each of the possible variables in Eq. (15). This equation was used to generate the information by computer. In Figures 8 to 11 below, all the variables other than the velocity were kept constant. The values of the solidification variables used in these calculations were G = 100°C/cm, ΔT_o = 10°C, D = 1.27 E-9 m^2/s, K_o = .103, ΔH = 4.49 E7 mJ/kg, and Γ = 6.62 E-8 Km, unless otherwise specified.

If the value of $\dot{\delta}/\delta$ is examined for possible unstable wavenumbers as a function of velocity are examined, then it is found that three possibilities exist. These three possibilities are shown in Figure 8. The first possibility is that all wavenumbers are stable at the given velocity, $\dot{\delta}/\delta<0$ for all V and k. The second possibility is that only one wavenumber is stable at the given velocity, that being the critical wavenumber, k_c, where $\dot{\delta}/\delta = 0$. The third possibility is that a range of wavenumbers is possible at a given velocity, $\dot{\delta}/\delta > 0$, for a finite range of V and k. In order to examine the variable effect on the

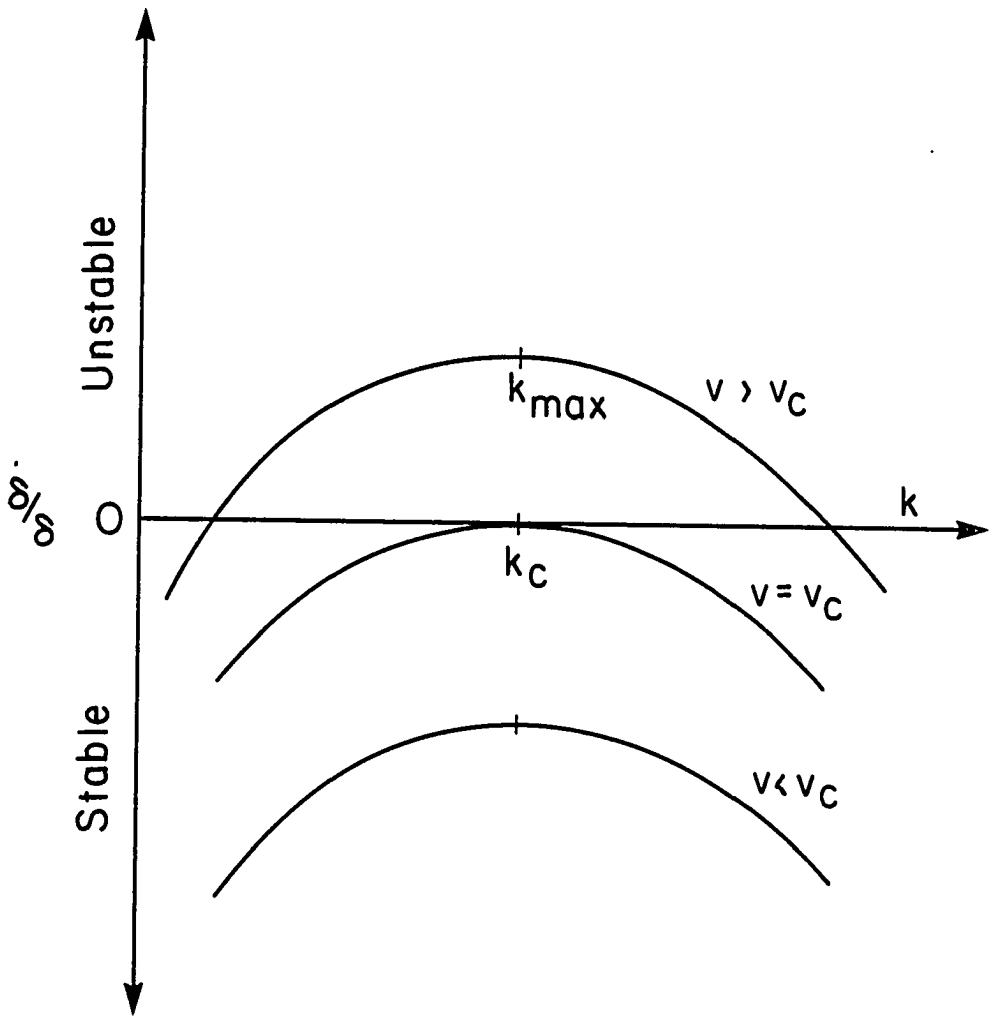

Figure 8. A schematic diagram of unstable wavenumbers, k's. The region above the k axis is the region of instability, the region below the k axis is the region of stability. The three possible situations for unstable wavenumbers as a function of velocity are: (a) $V < V_c$ resulting in stability for all k, (b) $V = V_c$ resulting in only one unstable wavenumber, k_c, (c) $V > V_c$ resulting in a region of unstable wavenumbers with the fastest growing wavenumber k_{max}

velocity-wavenumber relationship, calculations are carried out for two cases. The cases are where the temperature gradient is varied, and where the composition (or ΔT_o) is varied. The results are shown in Figures 9(a) and 9(b).

Figure 9(a) shows the variation of the unstable wavenumbers ($k=2\pi/\lambda$) as a function of velocity for different thermal gradient values. The stable region is outside the loop, and the unstable region is inside the loop. This is true for Figures 9 to 11. Figure 9(a) shows that raising the value of G stabilizes the interface for a given velocity. It also shifts the unstable ks to higher k values. Finally, it also shows that at low G values and low velocities, the unstable wavenumber spectrum expands as the velocity decreases. This occurs at small k values. The first observation, that of stabilizing the interface at higher G values, follows from the equation of Tiller et al. [3], which is $V = G_L D/\Delta T_o$. The other two observations are new results from Mullins and Sekerka's analysis [2].

Figure 9(b) shows that raising ΔT_o, which in some systems is the same as raising the concentration, moves the unstable region to lower velocities. There is also a dramatic increase in the width of the spectrum as ΔT_o is increased, which corresponds to a wide range of possible unstable wavenumbers. Here, as in Figure 9(a), the equation of Tiller et al. [3] explains the shift of the unstable region to lower velocities, but the increase in the width is only explained in the Mullins and Sekerka [2] linear analysis.

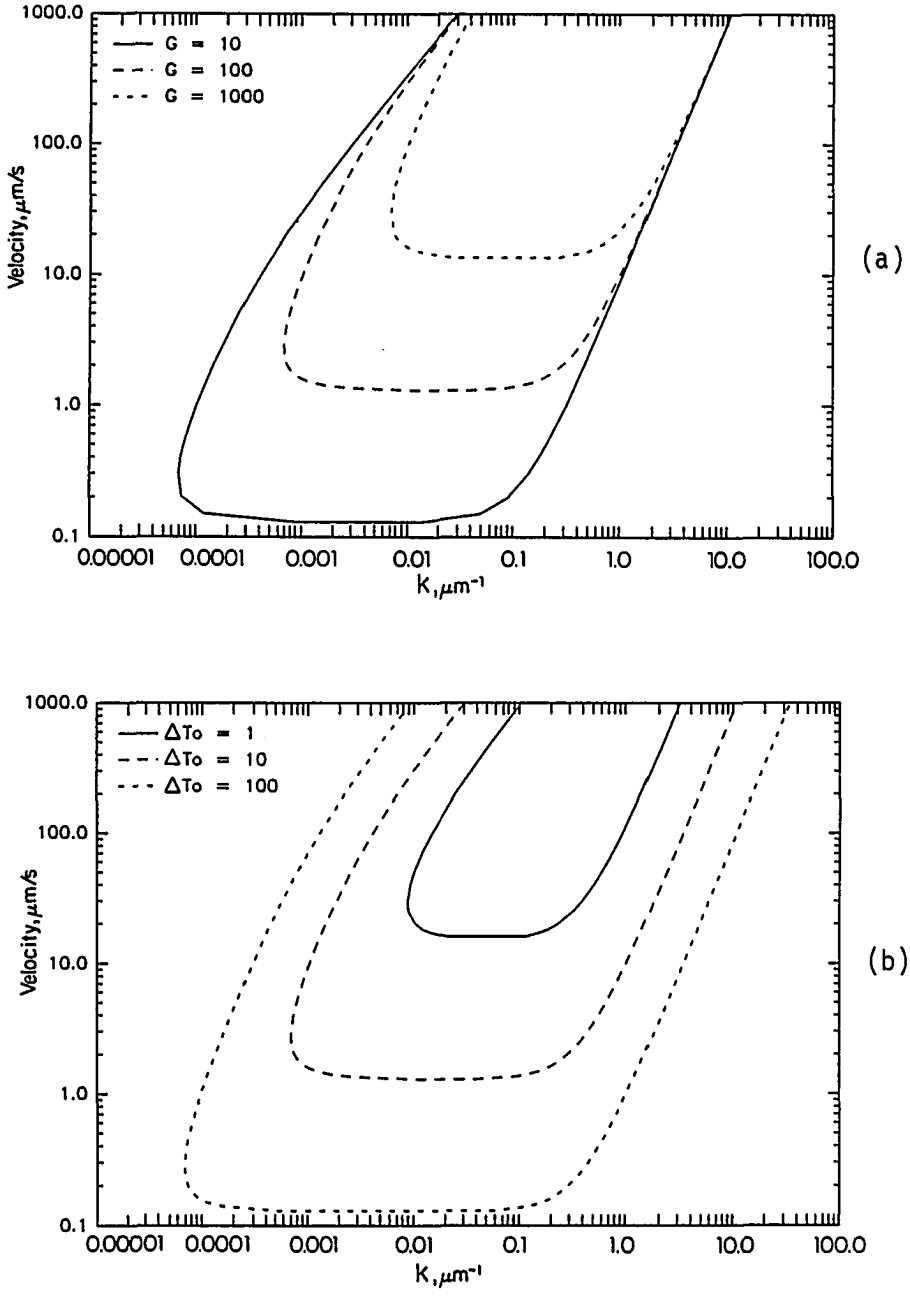

Figure 9. Variation of the unstable wavenumbers with changing experimental variables: (a) with a change in the thermal gradient, G, and (b) with a change in the concentration variable, ΔT_0

Figure 10(a) shows the variation of the instability spectrum as a function of the surface energy term. The effect of increasing Υ is uniform with velocity, but occurs only at the large wavenumber end of the spectrum. This is logical since surface energy effects are short range effects. The reason is because surface energy effects are a function of curvature, and as the radius of the arc of any curve goes up, the local curvature goes down.

Figure 10(b) shows the variation of the instability spectrum with changing ΔH, the latent heat term. Higher values of ΔH cause a narrower unstable region. The latent heat term only affects the short wavenumber instabilities, and then, only at high velocities. It is logical that the latent heat term should be velocity related since the amount of heat generated and pumped into the interface is velocity related.

The variation of Υ and ΔH do not appreciably change the critical velocity of planar interface instability, as shown in Figures 10(a) and 10(b). Consequently, the modified supercooling criterion, given by Eq. (20), which neglects the effects of the surface energy and the enthalpy of fusion, gives the critical velocity which is very close to the critical value predicted by the linear stability analysis in Eq. (19). The value of V_c increases slightly when the surface energy term is taken into account. Linear stability analysis, therefore, predicts a V_c value which is only slightly larger than that predicted by the modified supercooling criterion. Although the change in V_c is small, the unstable wavenumber spectrum increases significantly as the

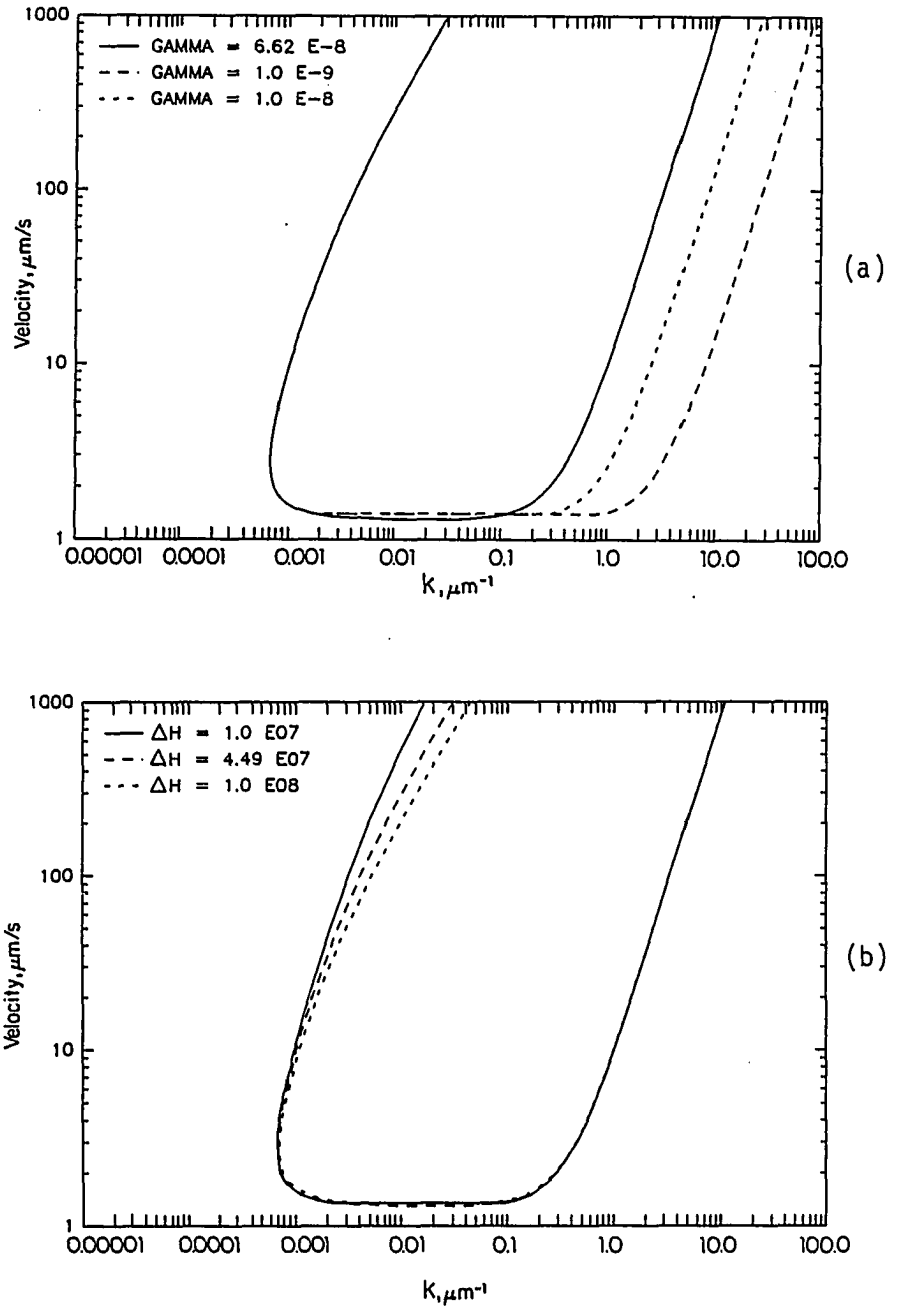

Figure 10. Variation of the unstable wavenumber region with a change in the system variables: (a) with a change in the surface energy, Υ, and (b) with a change in the enthalpy of freezing, ΔH

surface energy value is increased. Surface energy, therefore, is important, but in respect to the wavenumbers observed, and not in respect to the observed critical velocity.

Figures 11(a) and 11(b) show the response of the stability to a change in system parameters. The response of stability to a change in K_o will be examined first. Equation (19) shows that K_o affects the solute term only. The effect of K_o in the solute term comes in two places. The major effect is to change ΔT_o and therefore, the value of mG_c. The second effect is to change the value of the bracket in the solute term. When K_o is increased, ΔT_o is decreased, which causes V_c to increase (see Figure 9(b)). The second effect does not change V_c appreciably, but it does cause the low wavenumber branch to shift to slightly higher values. This is shown in Figure 11(a) where ΔT_o is artificially kept constant so that the shift in the low wavenumber branch can be clearly seen.

Figure 11(b) shows the effect of the diffusion coefficient on the stability. As the diffusion coefficient increases, the critical velocity increases. The wavenumber spectrum also shifts to lower wavenumbers as the diffusion coefficient increases at a given velocity.

These results clearly show that the value of the critical velocity depends very strongly on G, ΔT_o, and D. The effects of Υ and ΔH in V_c are quite small. Therefore, the linear analysis can normally be simplified to the modified supercooling criteria when examining the critical velocity. The difference in the value of the critical velocity between these two models is generally less than 10%.

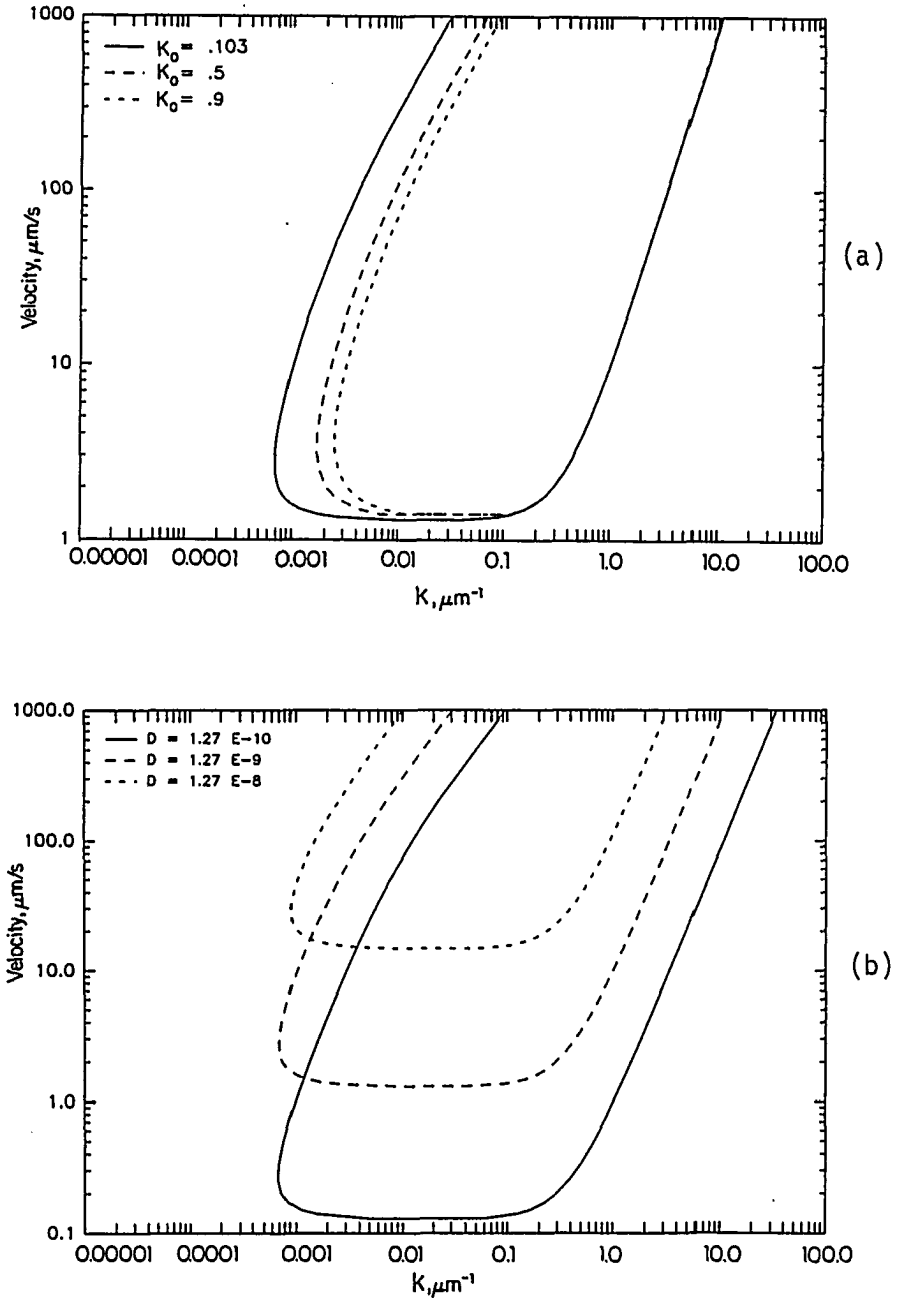

Figure 11. Variation of the unstable wavenumber region with a change in system parameters: (a) variation with a change in the partition coefficient K_O, and (b) variation with the diffusion coefficient D

Even though the critical velocity is not seriously affected by the surface energy, the values of the unstable wavenumbers are affected. In addition, the wavenumber spectrum near the critical velocity is extremely broad. This makes it very difficult to experimentally characterize the initial wavenumbers of the perturbed interface. A slight error in the velocity will allow the unstable interface to select from a wide range of wavenumbers. Experimentally, only G and ΔT_o can be controlled for a given system. Consequently, to reduce the error in wavenumber measurements, it is best to work at high thermal gradients and low solute concentrations. This can be seen in Figures 9(a) and 9(b), where the spectrum is narrower when G is large and when ΔT_o is small. Since large constant thermal gradients are difficult to obtain and sustain, it is important to select very dilute solutions. This is the best way to experimentally control the variables to minimize uncertainty in measured critical wavenumbers.

Absolute Stability

At growth conditions far into the unstable region, the capillarity term becomes very important, primarily because the solute and thermal fields become small. At very high velocities, the capillarity term dominates and stability is regained. This is the growth region called the region of absolute stability. The concept of the existence of an absolutely stable planar interface growth region at high velocities was a peculiarity in the time of Mullins and Sekerka, but today has been shown to be a reality by the high velocity experiments which are

possible by using laser or electron beam scanning techniques. Mullins and Sekerka [2] developed an absolute stability condition as

$$V > D\Delta T_o/\Gamma k \quad . \tag{21}$$

Great care must be taken when applying this stability condition since the conditions for which it is derived are the local equilibrium conditions. There is little doubt that at very high rates, the local equilibrium conditions are not satisfied. This was, however, the first prediction of a velocity beyond which a material would freeze without any segregation.

Limitations and extensions of Mullins and Sekerka's linear stability analysis

There are several limitations to Mullins and Sekerka's [2] linear stability analysis. The most severe limitation is that of the linear approximation. This means that at times very shortly after break up, the theory does not hold. It cannot, therefore, take into account the dynamic events which occur at times after break up. Some of the other limitations of the theory are neglecting anisotropy of surface properties and not considering problems which arise at high thermal peclet numbers.

Since the first linear stability analysis, there has been a considerable number of studies [6-14] which have extended the original analysis to include some parameter which Mullins and Sekerka assumed constant. With the exception of the effect of anisotropy, which is

reviewed in Section V, a brief reference to the work done in this area is given here. An excellent review of this material is given by Coriell et al. [15].

The effects of convection on stability have been studied by Coriell and Sekerka [6], Hurle et al. [7], and Favier and Rouzand [8]. Hurle [9] studied the effect of Soret diffusion and concentration dependence of both the liquidus slope and the partition coefficient. Wollkind and Maurer [10] and Sriranganathan et al. [11] studied the surface energy as a function of temperature and concentration. Wheeler [12] showed the effect of a periodic growth rate on the growth structures. Huggins and Elwell [13] established a stability criterion for electrocrystallization of molten salts. Finally, Shewmon [14] has included the effect of stress and the effect of interface diffusion on planar interface instability in solid-solid phase transformations.

Experimental studies on planar interface instability

The experimental attempts at checking Mullins and Sekerka's theory have been numerous [16-23]. Two major predictions of the theory, which have been tested experimentally are the critical velocity and the wavenumber of the unstable pattern at the critical velocity.

Morris and Winegard [16] studied Pb with Sb as a solute. Their work indicates that the perturbations begin at defects. Since the role of defects on interface instability will not be considered in this study, and was not considered by Mullins and Sekerka, this adds no special insight.

Davis and Fryzuk [17] worked with dilute In in Sn. Their work indicates that there was no stabilizing effect from the surface energy. Here, the system parameters and variables are not well enough established to consider this result as a test of the theory.

Work similar to Davis and Fryzuk [17] was done by Hecht and Kerr [18]. Hecht and Kerr worked with Sn-Bi alloys. They found that the interface was more stable than predicted, either by the constitutional supercooling criterion or by the linear stability analysis. There are several possibilities for this result. First, there may have been etching problems which made the observations erroneous. Second, bismuth solidifies with an interface which is faceted. Therefore, there may have been stabilization due to interface kinetic effects and anisotropic interface properties. Consequently, this does not appear to be a quantitative test of the theory.

Sato and Ohira [19], Sato et al. [20] and Shibata et al. [21] have recently studied Al-Cu, Al-Ti, and Al-Cr alloys. Sato and Ohira's results showed that initial perturbations were randomly distributed throughout the interface. Their work showed a wide range of frequencies at the critical point. They concluded from this that they must have been far from the critical point. In a later work, Sato et al. [20] showed that small segregation coefficients allow a large range of wavelengths. They were, thus, uncertain just how close they were to the critical conditions. Scatter in the results precludes any definitive statements from this work. As discussed earlier, a slight uncertainty in the velocity can give rise to a wide range of possible

unstable wavenumbers. Since the velocity was not precisely measured, the results reported for the wavenumbers are not reliable.

Shibata et al. [21] used the result of the linear stability analysis to establish the surface energies of Al-Ti and Al-Cr. Their work yields surface energies that are reasonably close to other methods of measuring the surface energy. However, there is sufficient uncertainty in the measured surface energy values to preclude this study from being considered as a quantitative proof of the linear stability analysis.

Jamgotchian et al. [22] have used a dilute alloy of Bi-Sb. This work is exceptional because they have taken care to eliminate convection in experiments which were designed to test Mullins and Sekerka's theory. The work of Jamgotchian et al. [22] indicates that Mullins and Sekerka's stability criterion gives a more accurate result of the critical velocity than does the expression of Tiller et al. [3] given in Eq. (7). Jamgotchian et al. obtained critical velocity values which range from 61-86% of the theoretical values. This work is by far the most complete and accurate work in this area, and yet, three problems exist which warrant further study. These are (1) the material studied was opaque and therefore, an accurate determination of the interface velocity at the time of break up could not be determined, (2) there is a considerable margin of error in the system parameters, especially the surface energy, and (3) the wavenumber of the unstable interface was not measured.

Kim [23] has taken a novel approach to the problem of the uncertainty of the interface velocity resulting from the opaque nature of metals. Kim pulsed the interface electronically at regular intervals and thereby produced markers showing the interface position in time revealing both the interface structure at that time and the interface velocity. The alloy used by Kim was In-Sb. This alloy should not experience convection since the density and melting points of In and Sb are similar. In addition, solidification was induced by changing the thermal field rather than by mechanical motion. There should not, therefore, have been mechanical vibrations in these experiments. The results reported are 27% lower than the theoretically predicted values for the threshold conditions. This was compared through the $\dot{\delta}/\delta$ function in Eq. (15). The wavelengths reported at these conditions are approximately two times larger than the predicted values.

Although this work is significant, there are still some problems. One of these is that the freezing interface was observed to facet shortly after break up. Once it faceted, the amplification rate of the perturbed interface increased sharply. This shows that there may have been dynamic factors involved with the formation of perturbations, which are at present unexplained. Facets also show surface anisotropy properties are present. Surface anisotropy properties were not considered by Mullins and Sekerka. The effects of anisotropy will be discussed in a later chapter of this work where it is shown that anisotropy does have an effect on interface instability at the threshold of instability formation.

An overview of the experimental evidence seems to indicate that experimentally determined critical velocity and corresponding wavenumber agree with the theory to within about 15-30% and a factor of two, respectively. In most of the experiments, the precise interface velocity at the time of instability was not measured. Furthermore, precise values of the system parameters are not available. Therefore, critical experiments are needed in a system for which all physical constants are well known. It is also important that the material studied be transparent so that the interface velocity at the time of instability can be precisely measured. This is important because a small error in the measured velocity will yield a large error in the possible wavenumbers theoretically predicted.

Interface Instability: Nonlinear Stability Analysis

Introduction to nonlinear analysis

It has been shown above that the linear theory of instability is useful in predicting threshold velocities for the planar to cellular transition. It should be noticed, however, that the linear assumptions break down very early after the onset of instability. For this reason, it is desirable to extend the analysis into the nonlinear regime in order to understand the principles which govern the reorganization of an unstable interface into a periodic array of cells. The extent to which linear analysis is valid can be seen in Figures 12 and 13. Figure 12 shows an unstable interface as it is just breaking up. In Figure 13, the amplitude of the unstable interface profile is

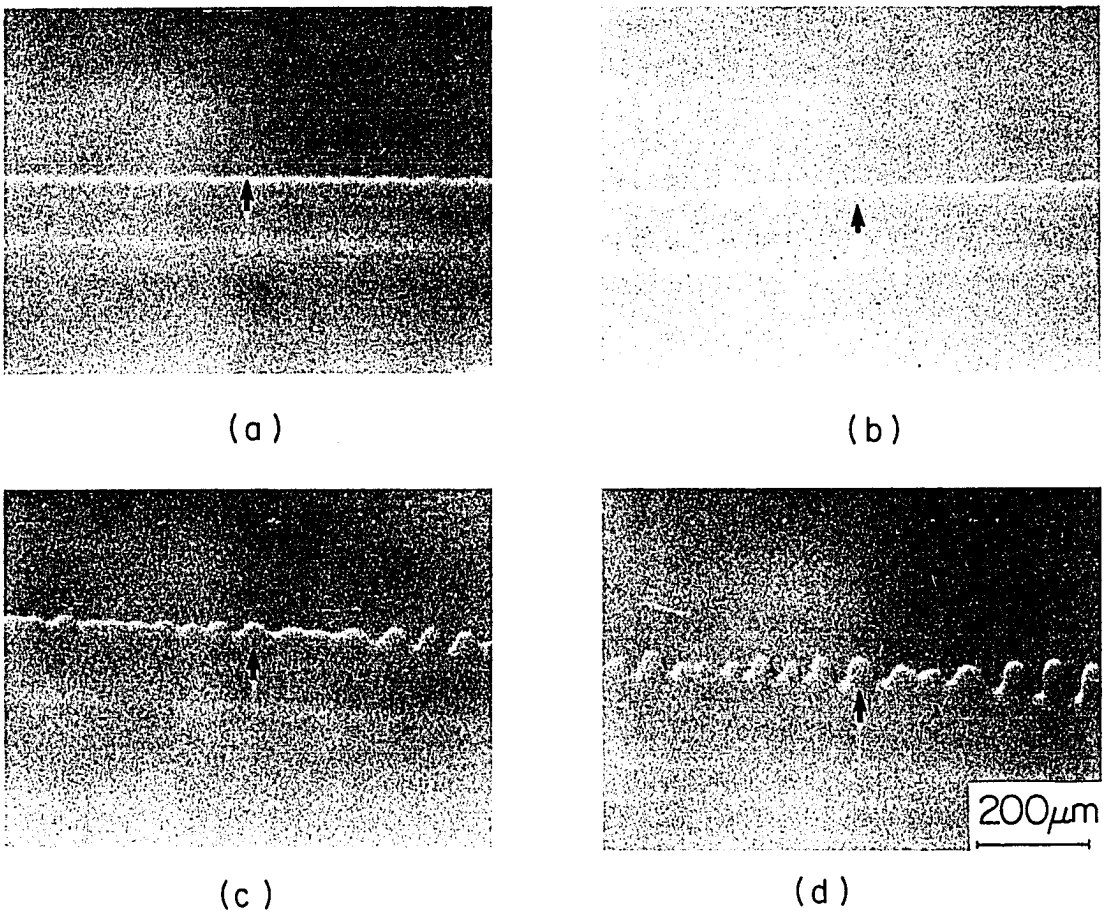

Figure 12. Break up of a planar interface. Succinonitrile 0.1 w/o acetone, G = 3.82 K/mm, V = 1.25 μm/s, (a) at time = 0 s, (b) at time = 15 s, (c) at time = 30 s, (d) at time = 45 s, mag. = 70X

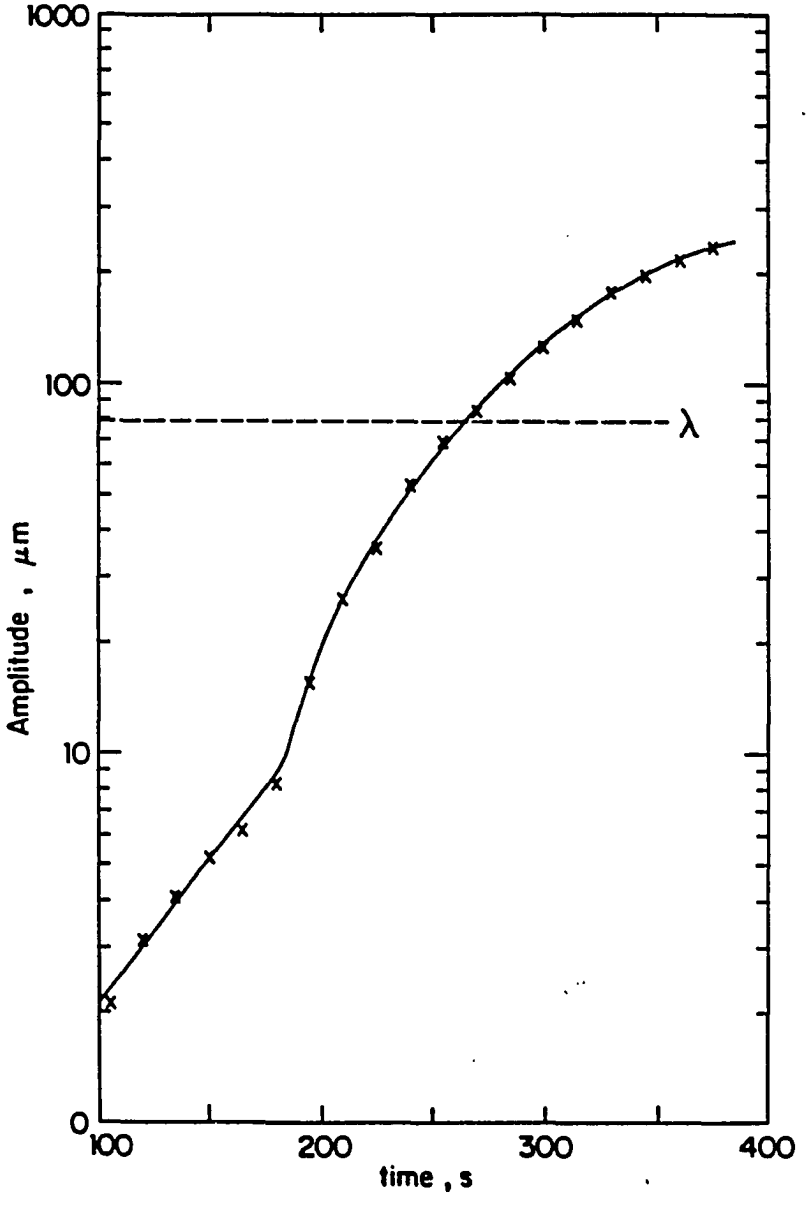

Figure 13. The variation in the amplitude of perturbation with time

plotted versus time, for the succinonitrile-acetone system. It can be readily observed that linear amplification exists for only about 170 seconds. After this, the instability amplifies in a nonlinear manner. The onset of this nonlinearity corresponds to interface shape shown in Figure 12(c). The early advent of nonlinearity shows that a nonlinear analysis is required to understand the development of cellular structures.

Nonlinear perturbations were observed in fluids by Reynolds [24] in 1883, but were not addressed theoretically until 1909 by Bohr [25]. Subsequently, Noether [26] and Heisenberg [27] used nonlinear theory to describe turbulent flow in fluids. The problem was further addressed in 1944 by Landau [28] who again worked with turbulent flow of fluids. A key equation in nonlinear theory was developed by Landau and is expressed as follows:

$$(1/A)(dA/dt) = a_0 - a_1 A^2 \tag{22}$$

where $|A|$ is the amplitude of the dominate mode, t is the time, a_0 is the linear coefficient, and a_1 is the nonlinear coefficient, which now bears the name Landau constant. The stability or instability is determined by the signs of the coefficients a_0 and a_1. The left-hand side of Eq. (22) is essentially equivalent to $\dot{\delta}/\delta$ from Mullins and Sekerka's analysis [2]. When $a_1 = 0$, this result will be equivalent to Mullins and Sekerka's result. In general, there are four possibilities, as will be presented and discussed in the analysis of

Wollkind and Segel's [4] work below. The four possibilities are generally plotted in terms of $d|A|/dt$ versus $|A|$ and are termed bifurcation plots. One might intuitively suspect that Landau's equation (22) is a truncated series with higher order terms neglected. This was not expressed by Landau, but is definitely the case, as will be seen in the nonlinear analysis of Wollkind and Segel. If $a_1 = 0$, the Landau equation becomes equivalent to the linear analysis model. Consequently, the Landau equation merely is a one-order higher correction of the linear model.

Nonlinear stability analysis is developed by using the same equations as the linear stability analysis with the exception that linearization of the boundary conditions is not imposed. The nonlinear stability analysis, therefore, attempts to answer the same questions as those answered by the linear stability analysis, i.e., pattern formation and solidification morphologies under given growth conditions. There are, as with most complex mathematical models, fundamentally two approaches to solve the problem, viz. the analytical solution and the numerical solution. There also exists a body of work which is analytical in the beginning, but shortly becomes untractable, except by numerical methods.

Those who have presented analytical models are Wollkind and Segel [4], Caroli et al. [29], and Wollkind and Notestine [30]. Those who have used numerical techniques for solution of the nonlinear equation include Kerszberg [31-33], McFadden and Coriell [34], Unger and Brown [35-37], Unger et al. [38], Karma [39] and McCartney and

Hunt [40]. Those who have held to the analytical approach as long as possible before using numerical techniques are Langer and Turski [41], Langer [42], Dee and Mathur [43], and Ben-Jacob et al. [44-45].

Analytical models of nonlinear stability extend the limits of the linear stability analysis to weakly nonlinear conditions. Weakly nonlinear analysis, which is the highest order analysis that is analytically tractable, does not go very far beyond the linear limit. In contrast, nonlinear models using numerical techniques have been able to extend the analysis out into the steady-state cellular region.

Nonlinear analysis

Wollkind and Segel [4] were the first to consider solidification problems using nonlinear stability analysis. Their analysis offers some interesting predictions which can be tested experimentally.

The model of Wollkind and Segel is two-dimensional in the moving frame of reference with (x,z) as the axis (see Figure 7). The x axis coincides with the mean interface position at time = 0. For all time greater than zero, x satisfies the equation $z = Vt + W(x,t)$, where $W(x,t)$ describes the interface. This means that the frame of reference is actually a moving frame of reference, which at steady state is stationary in the (x,z) coordinate system. The solidifying sample is assumed to move through a thermal gradient at a constant velocity. Solute diffusion in the solid is neglected, and the expression $C_S = K_O C_L$ is assumed. In addition to this assumption, Wollkind and Segel [4] also assume equal solid and liquid thermal diffusion

coefficients, and isotropic interface properties.

Although one could assume that the linear stability analysis of Mullins and Sekerka [2] leads directly to the nonlinear analysis of Wollkind and Segel [4], this is not quite true. The reason for this is that the method of solution used by Mullins and Sekerka is not identical with that used by Wollkind and Segel. Mullins and Sekerka's analysis, which was not covered in detail above, uses time derivatives of Fourier coefficients. On the other hand, Woolkind and Segel use a sequence of solutions starting from the zero order case and building on each other. The differences are not readily apparent, but are thoroughly discussed by Wollkind and Segel [4]. The two main differences are (1) Mullins and Sekerka implicitly assume an "exchange of stabilities" between real and imaginary components. Wollkind and Segel develop a proof to show that the assumption is correct. This comes out of the more general linear analysis of Wollkind and Segel. (2) In Mullins and Sekerka's analysis, the time derivatives are all neglected except for the amplitude growth rate time derivative. They used the steady-state approximation for the solute distribution, even when the amplitude is changing with time. In general, time derivatives cannot be neglected in the diffusion equations. If D/a (a = the thermal diffusion coefficient) is small, the error in the temperature equation is not serious, but neglecting time derivatives in the concentration equation is not rigorously valid. To Mullins and Sekerka's credit, their analysis is correct in the marginally stable case. Once an instability is formed, however, the analysis breaks

down immediately.

Since the nonlinear model of Wollkind and Segel builds on itself going from the steady-state planar case to the nonlinear case, and since it is long and quite detailed, it will not be fully developed here. We shall, instead, go through the physics of the analysis and the solutions obtained rather than present the analysis in detail.

Under the physical conditions described above, solutions for the thermal field and concentration field for the steady-state planar interface situation are directly determined. This is the zero order analysis and it is identical conceptually to the analysis of Tiller et al. [3]. An analysis of the stability of the solutions is carried out as time $\to \infty$. It is found that there are three possible situations. These are a stable interface for all time, an unstable interface, and an interface which sets up a finite amplitude pattern which persists as time $\to \infty$. What will be obtained depends on the growth conditions.

Wollkind and Segel proceeded by scaling and nondimensionalizing their variables. This prepares the way for their linear analysis.

The linear analysis uses terms of first order and considers the velocity dependence of the interface at any point on the interface. The general expression is as follows:

$$v(x,z,t;\varepsilon) = v_0(z) + v_1(x,z,t;\varepsilon), \tag{23}$$

where v is the interface velocity at any point on the interface, v_0 is the zero order problem, v_1 is the first order problem, and ε is a

perturbation on the interface. This expression is solved for the simultaneous equations arising from the interface shape, the concentration in the liquid, the temperature field in the liquid, and the temperature field in the solid. Perturbations are of the $\varepsilon[\cos(kx)\exp(a_o t)]$ type.

This is an eigenvalue problem, with the eigenvalue a_o. Here, as with the planar interface problem, stability, instability, or neutral stability are possible as $t \to \infty$. Neutral stability is stability given by a finite amplitude waveform which persists on the interface as time $\to \infty$.

These results are similar in form to Mullins and Sekerka's [2], but are more general. It is at this point that Wollkind and Segel examine the "exchange of stabilities" for the real and imaginary components, and find that the imaginary components are zero for all time and conditions. This means that there should be no wave translation along the interface. Note here that this result is for isotropic interface properties.

General nonlinear analysis considers perturbations of the type ε^n, and velocities of the type $v_n(x,z,t)$ where n goes from $1 \to \infty$. One realizes immediately that only one new order of terms is ultimately going to be considered, but the analysis proceeds as if the entire series is possible in the solution.

Solutions are examined of the cos(kx) type. Immediately, one can recognize that this is much more limited than the corresponding linear analysis case, since only one wave component can be examined. Wollkind

and Segel make the best of this by considering the threshold, or critical wave component, k_c. As in the linear case, the first question addressed is what will happen as time $\to \infty$? The second, and major point of interest, is the amplification rate equation. The amplification equation is the time derivative of the nonlinear solutions. Solvability conditions show that only odd powers exist. Therefore, the general solution to the amplification expression is:

$$\varepsilon dA(t)/dt = \varepsilon A(t) = a_0 \varepsilon A(t) - a_1 \varepsilon^3 A^3(t)$$

$$+ \sum_{n=2}^{\infty} a_n [\varepsilon A(t)]^{2n+1} \quad . \tag{24}$$

This amplitude equation is the central result of the nonlinear theory of Wollkind and Segel, and is commonly called the Landau equation with a_0 and a_1 as the two constants. As in the introduction to this section, the second constant, a_1 (except for the ε^2 term), is the Landau constant. Generally, only first and third order terms in ε are retained, and therefore, the equation appears as follows:

$$\dot{\varepsilon A}(t) = a_0 \varepsilon A(t) - a_1 \varepsilon^3 A^3(t) \tag{25}$$

or

$$\dot{A}(t)/A(t) = a_0 - a_1 \varepsilon^2 A^2(t) \quad . \tag{26}$$

Wollkind and Segel derive the values of the constants. The important physics of this problem depend upon the signs of the a_0 and a_1 coefficients. There are four possible cases that arise for the combination of a_0 and a_1: (a) $a_0<0$, $a_1<0$; (b) $a_0>0$, $a_1<0$; (c) $a_0<0$, $a_1>0$; and (d) $a_0<0$, $a_1<0$. Figure 14 shows these four possibilities graphically.

In Figure 14, instability is exhibited where the curve is above the axis, and stability where the curve is below the axis. The stability or instability pictured in the above graphs is for perturbations which vary in wavelength as a function of $(\varepsilon A)^2$. The above cases predict the following physical situations.

(a) $a_0>$), $a_1>0$. In this case, linear theory (i.e., using the a_0 term only) predicts instability. Nonlinear theory which includes the a_1 terms predicts finite amplitude stable equilibrium solutions.

(b) $a_0>0$, $a_1<0$. Here, no finite amplitude equilibrium solutions exist. The interface is destabilized by both linear and nonlinear elements. This is called supercritical bifurcation.

(c) $a_0<0$, $a_1<0$. In this case, linear theory predicts interface stability, while nonlinear theory introduces the destabilizing effect. The result is that for low values of $(\varepsilon A)^2$, there is stability, while for higher values, instability exists showing that above the threshold conditions finite amplitude waves will exist. Finite amplitude waves can also exist below the threshold velocity if they are formed either

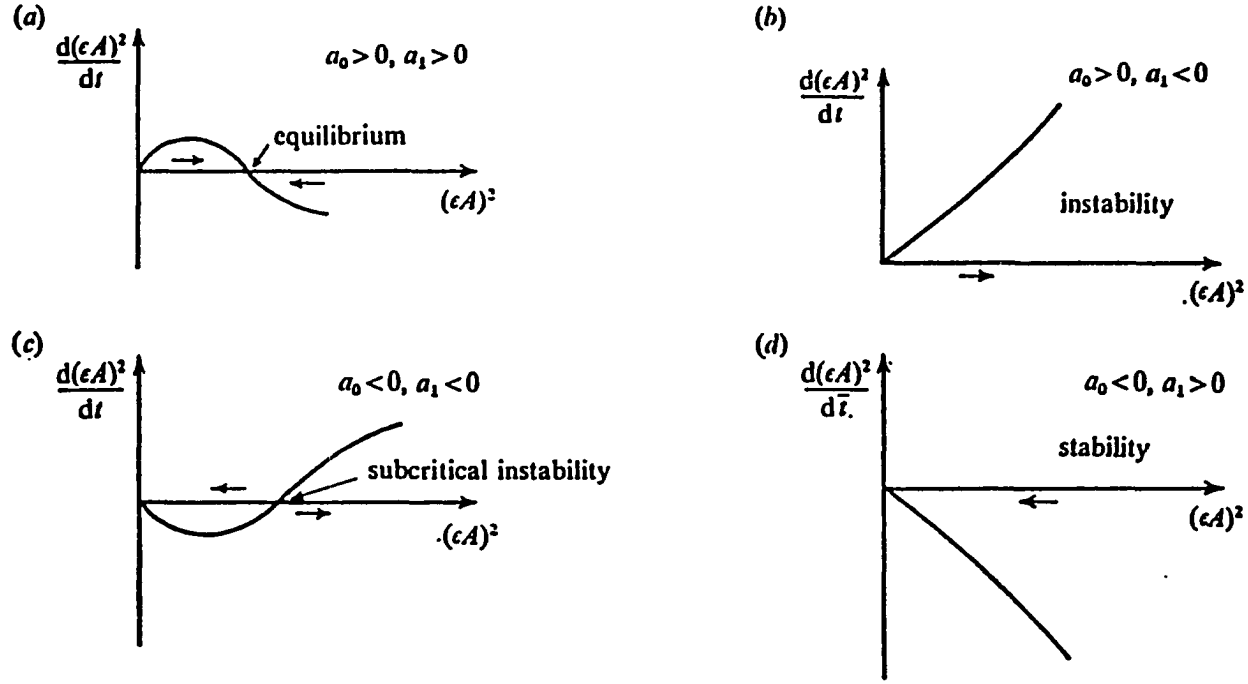

Figure 14. The four possibilities for an interface when nonlinear effects are included (from reference [4]). Instability exists above the horizontal axis, and stability exists below it. The possibilities are: (a) $a_0 > 0$, $a_1 > 0$, nonlinear effects stabilize a perturbed interface; (b) $a_0 > 0$, $a_1 < 0$, supercritical bifurcation, instability is always present for these conditions; (c) $a_0 < 0$, $a_1 < 0$, giving subcritical bifurcation, nonlinear effects destabilize the interface; (d) $a_0 < 0$, $a_1 > 0$, stability is always present for these conditions

by large perturbations, or by time spent above the threshold velocity prior to a reduction in the rate to a velocity below the threshold value. This situation is called the subcritical bifurcation.

(d) $a_0<0$, $a_1>0$. This situation yields total stability within the limits of this analysis.

Figure 15 shows Wollkind and Segel's speculation as to what occurs in different regions of G and Υ. To facilitate understanding of Figure 15, one can note that generally, $G = f(1/V)$ and $\omega_c = f(\Upsilon)$, where ω here is equivalent to the wavenumber k used throughout this work. As shown in Figure 15, Wollkind and Segel predict that cells will be seen in region (a) and dendrites will be seen in region (c).

Caroli et al. [29] have recently reviewed the work of Wollkind and Segel. They found that Wollkind and Segel made an error in their analysis which affects the magnitude, but not the sign of a_1. The value of a_1 is examined and simplified by Caroli et al. so that it can be compared to experimental work. It was found that for a small β expansion of the neutral stability equation, at low velocities, the value of a_1 can be given approximately as

$$a_1 \cong -\frac{(n-1)}{(n+1)}\frac{1}{8\beta} + (4K_0/\beta)^{2/3}[K_0^2+4K_0-2]/4K_0 + \ldots \qquad (27)$$

where $\beta = \Upsilon/[m(K_0-1)]$, and $n = \kappa_S/\kappa_L$. Under normal conditions, the first term will dominate. If, however, $n \cong 1$, then, the first term will vanish and the second term will dominate. This is the case when

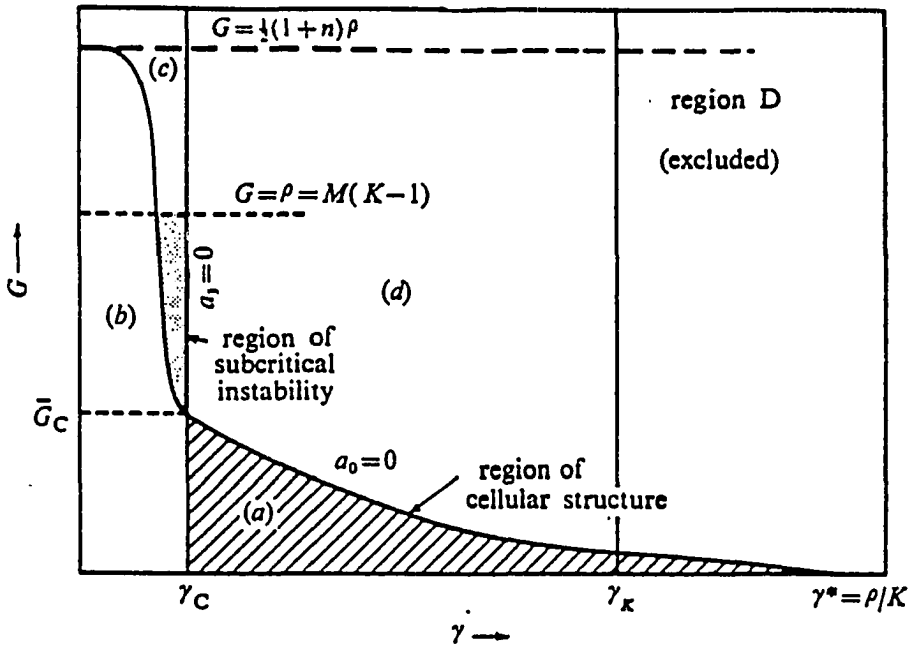

Figure 15. A schematic diagram from reference [4]. Conjectured regions of subcritical instability and cellular structures, as indicated

$\kappa_S = \kappa_L$, i.e., for succinonitrile-acetone alloys. In this case, at low velocities, the sign of a_1 will change (become positive) when $K_o > 0.45$. Remembering that this analysis is an expansion done at neutral stability, the bifurcation will change when a_1 changes sign.

In review, the key elements that can be understood from Wollkind and Segel's analysis [4] are as follows:

(1) If the bifurcation present is supercritical bifurcation, then nonlinearity does not significantly influence either the threshold velocity, or the threshold wavenumber. This would be type (b) bifurcation above. Nonlinear effects could, however, show up after the interface has broken down.

(2) Nonlinear theory could, according to Wollkind and Segel [4], also be used for predicting cells of a stable finite amplitude. This is given as possibility (a) above. Although cells are observed, and although the cellular region is nonlinear, the degree of nonlinearity in experimental cellular structures is far greater than that considered by Wollkind and Segel. Wollkind and Segel's analysis is presently termed weakly nonlinear, since it extends only to the first nonlinear term. Higher order analysis is necessary to be more accurate in the cellular region.

(3) Nonlinear analysis predicts the possible existence of subcritical bifurcation. This is a new possibility which was not addressed by linear theory. Subcritical birfurcation is situation (c) above. It should be noticed that during subcritical bifurcation, the interface may still form a pattern which begins in a linear manner.

This is true because the linear terms will dominate for very small amplitudes. The cellular growth region observed in Figures 12 and 13 is of this kind. This is because a linear region exists for a short time after which nonlinearity takes over. From Figures 12 and 13, it can be seen that the amplitude growth rate is more than weakly nonlinear. It is, therefore, of interest to consider the region beyond the weakly nonlinear region. For this reason, higher order analysis must be used to model cellular structures. Higher order analysis is done by numerical techniques.

Nonlinear stability analysis: The numerical approach

Whereas the analytical approach to nonlinear theory stability analysis is valuable only in the region near the onset of instability, the numerical approach allows the time evolution of interface structure to occur. Several different researchers have approached the problem and the results are encouraging, especially by comparison to experimental work done in metal analog systems.

An iterative approach to the nonlinear problem was taken by McFadden and Coriell [34]. They use the same equations and conditions as Wollkind and Segel [4], and input a guess for the initial interface position and morphology. Iterations are then made until a steady state is reached. The results model the general characteristics of cells fairly well, as can be seen in Figures 16-18. Although the results show the characteristics of a cellular structure rather nicely, the method is somewhat suspect since the final structure is a function of the input structure.

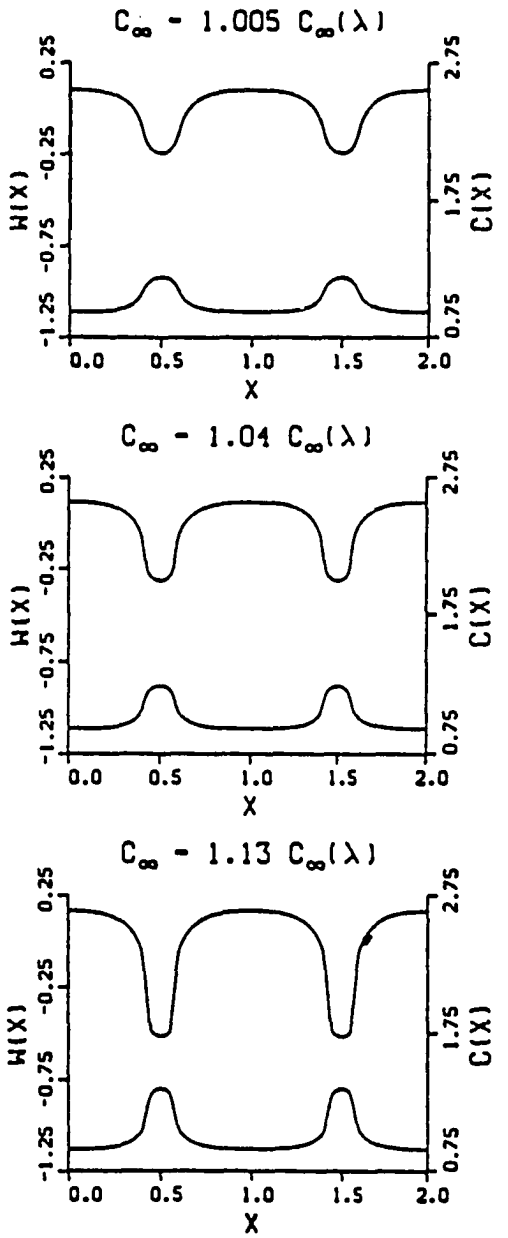

Figure 16. Predicted concentration profiles across two cells. Graphs show change with solute concentration far from the interface, C_∞. Figures are from reference [34]

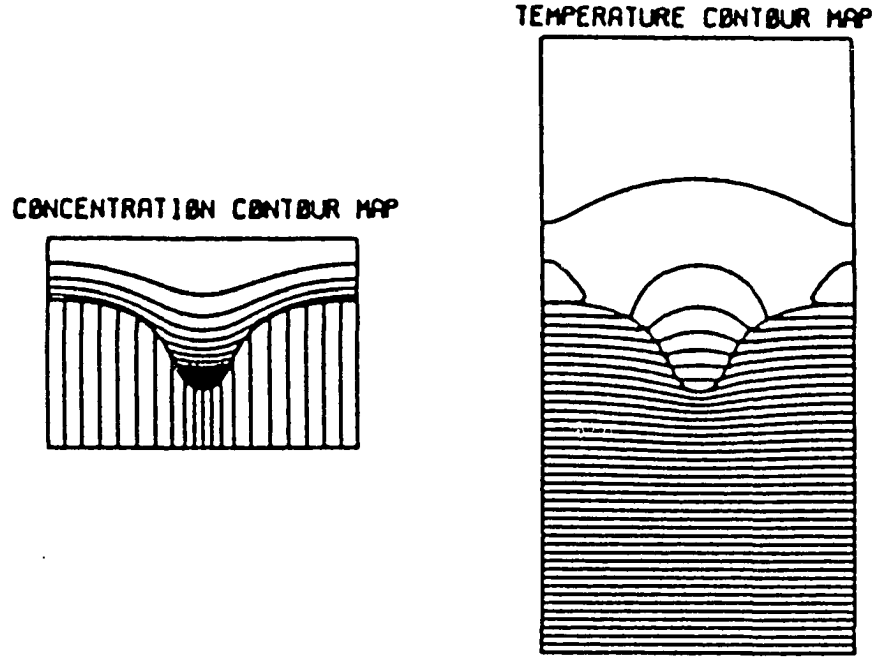

Figure 17. Concentration and temperature profiles for a single cell. Figures are from reference [34]

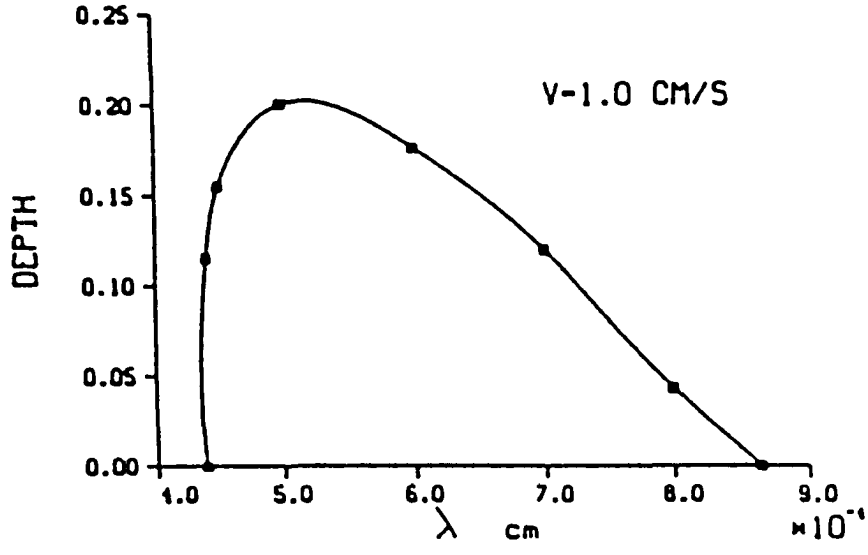

Figure 18. Cell groove depth as a function of velocity. Figure is from reference [34]

There are several numerical papers dealing with nonlinear pattern selection presented by Kerszberg [31-33]. In these papers, Kerszberg uses numerical integration and a very new method of expansion of terms to solve the nonlinear time dependent problem. He begins with the concepts of linear theory and then, expands these to nonlinear theory. Kerszberg's linear analysis gives the curve shown in Figure 19. This curve is very similar to those developed by Mullins and Sekerka [2] and also Wollkind and Segel [4]. Kerszberg then, expands his analysis into the nonlinear regime, and after doing so, presents Figure 20 which shows that the wavelengths selected by the nonlinear analysis are identical with those selected by the linear stability analysis at the threshold velocity. This graph given by Kerszberg is similar to the experimental results shown in the next section, but the variation in the cell wavenumbers with velocity increases rather than decreases.

The numerical analysis of Kerszberg also shows that the final pattern is a function of the initial choice for the input pattern. However, when white noise is introduced, a definite cellular spacing is produced. White noise is introduced because, as Kerszberg suggests, white noise exists in all solidification experiments due to mechanical vibrations or fluctuations in thermal gradient. Figures 21-24 are from reference [31]. These figures show the dynamics of cell adjustment with time. Processes such as these have been observed in organics [46]. Small amplitude cellular structures as shown in the figures were not seen in low concentration alloys of succinonitrile-acetone in the experiments. Small amplitude cells were

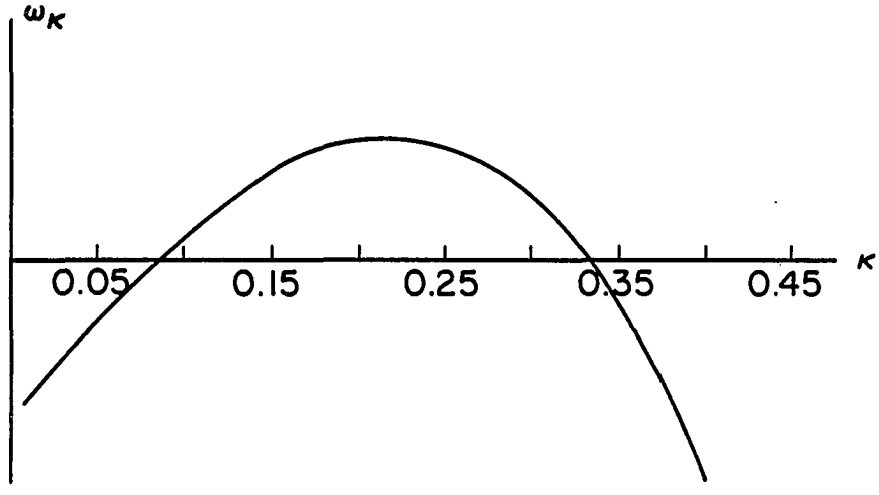

Figure 19. The linear stability coefficient as a function of wavenumber, k. Instability exists above the k axis and stability below it. Figure is from reference [32]

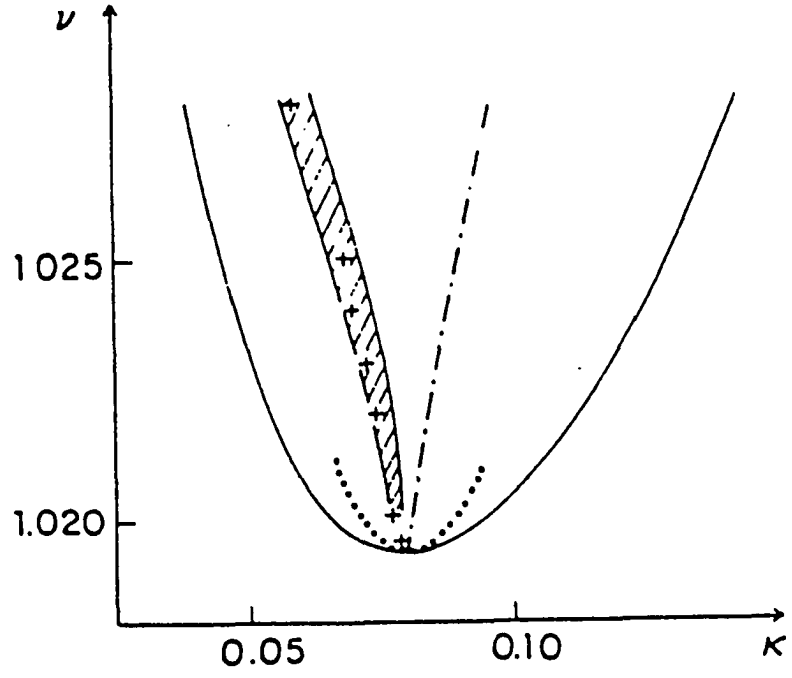

Figure 20. Unstable wavenumbers, k, as a function of velocity. The unstable wavenumbers are within the parabola. The dashed dot line marks the most favored growth wavenumber from linear stability analysis. The crosses and shaded areas are the points predicted from the nonlinear analysis in reference [33] and the error margin, respectively. Figure is from reference [33]

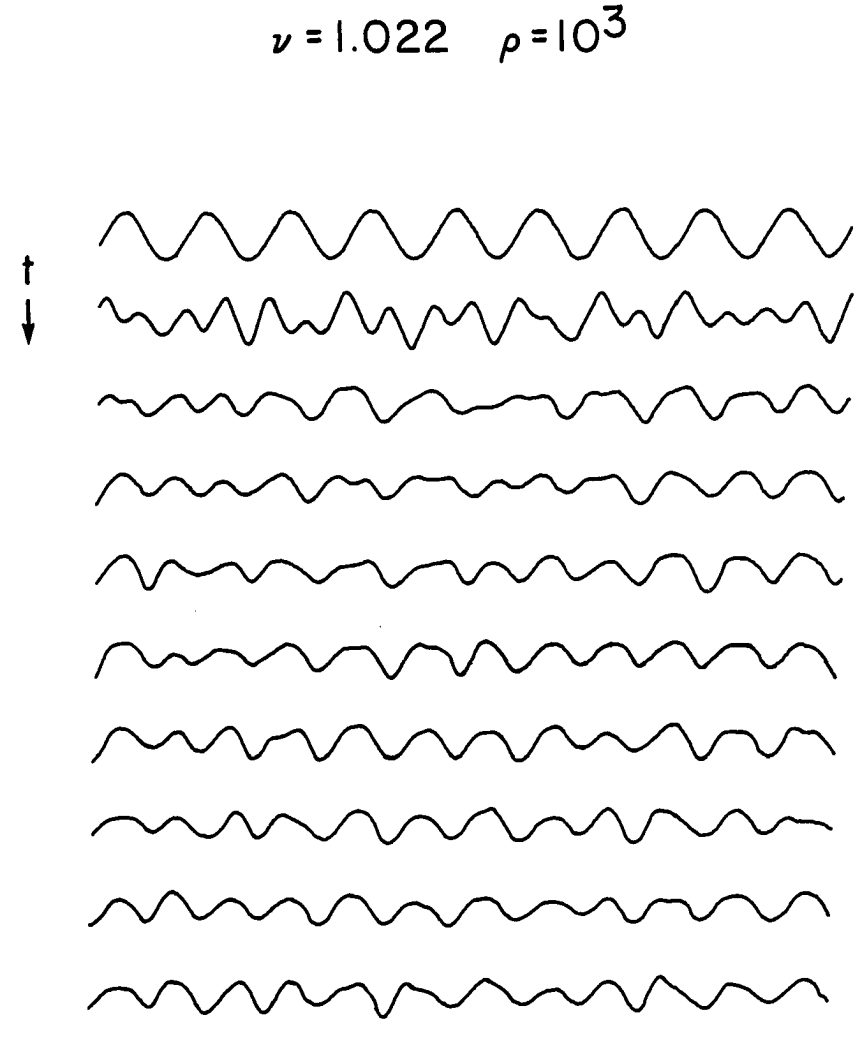

Figure 21. Development of a cellular structure as a function of time given an input structure and periodic white noise. This figure was constructed using the model described in reference [33]. Figure is from reference [33]

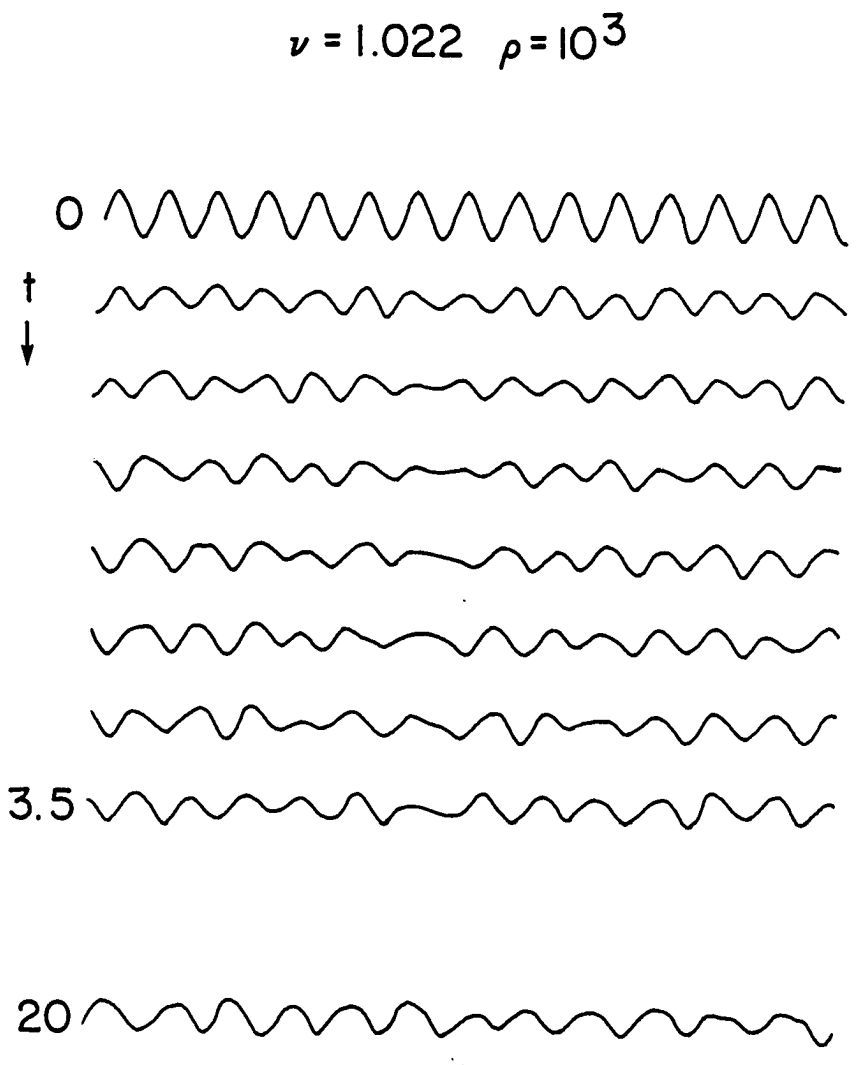

Figure 22. Development of a cellular structure as a function of time given an input structure and periodic white noise. This figure was constructed using the model described in reference [33]. Figure is from reference [33]

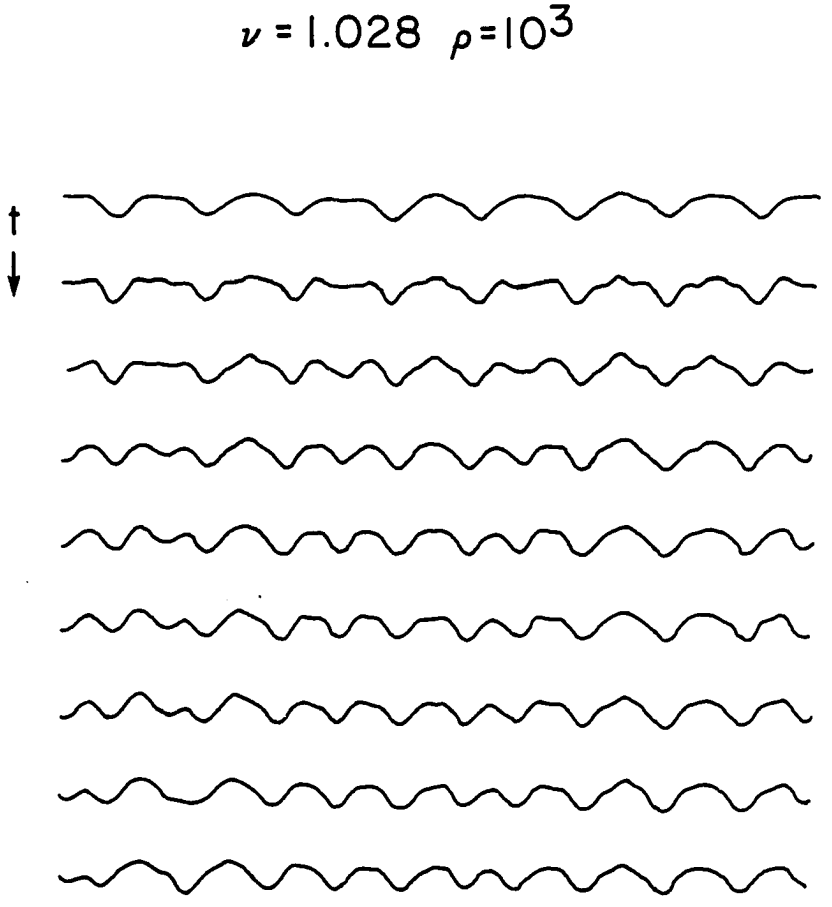

Figure 23. Development of a cellular structure as a function of time given an input structure and periodic white noise. This figure was constructed using the model described in reference [33]. Figure is from reference [33]

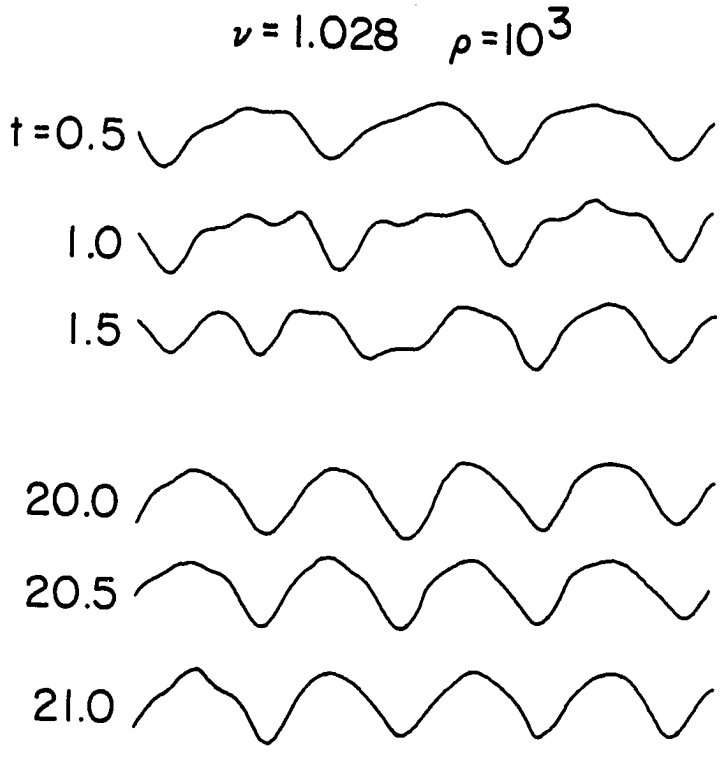

Figure 24. Development of a cellular structure as a function of time given an input structure and periodic white noise. This figure was constructed using the model described in reference [33]. Figure is from reference [33]

observed in pivalic acid-ethanol and carbontetrabromide-hexachloroethane alloys in this work and by de Cheveigne et al., respectively [47, 48].

Unger and Brown [35-36] have also done considerable work in the area of nonlinear stability analysis of solidifying planar and cellular structures. Their work focuses on the question of subcritical versus supercritical bifurcation in solidification pattern formation. There is nothing fundamentally different done by Unger and Brown that was not predicted by Wollkind and Segel [4], with the exception that Unger and Brown predict that the wavelength will experience halving of the cell spacing [35] at velocities near the threshold velocity. This has been observed by the author and is reported in Section I.

Nonlinear stability analysis: Analytical/numerical techniques and models

As mentioned above, in numerical nonlinear stability analysis, there are several types of analytical/numerical analyses in which the analytical elements are retained as long as possible for understanding before numerical solutions are used. Although there are a considerable number of such analyses, there are none that have yet been developed that maintain analytical aspects and comes even remotely close to physical reality. Very recently, a review of this type of analysis has been published by Langer [49]. This review offers insight into Langer's work, and also to related works in the area. The results given by Langer show that there are no generalized models that have yet been developed that solve the pattern formation problem. It is for this reason that work is currently being done on localized (versus

generalized) models [35-39]. This new concept in modeling has shown some promise. Solidification structures similar to cells and dendrites have been predicted by these models.

Considering the generalized models first, it is found that there are a number of avenues that could be followed in order to find workable realistic models. These possibilities are reviewed by Langer [49] and are given here.

(1) The first possibility for wavelength selection is that of boundary conditions in a small system. If the system is small enough that only one stable wavelength is possible, then wavelength selection is automatic. This occurs due to boundary condition constraint. If the boundary conditions are expanded a little to include other modes, then mode competition occurs, and wavelength selection will depend upon the systems' sensitivity to the starting conditions.

(2) The second possibility is that an important role is played by some variational principle. In this case, one imagines that the system optimizes around some principle, such as that of maximum growth rate, or minimum tip undercooling. Although this approach is popular, it has never been proven to be generally valid. If such a principle were true, one could imagine a minimization of free energy as such a criteria. Although this is a particular tempting principle, wavelength selection appears not to work on this principle in the case of pattern formation [49].

(3) A third possibility is that of noise-driven selection. Such a process has been derived by Kerszberg [31-33]. This process of

noise-driven wavelength selection would not induce selection of a unique value. It also requires externally induced perturbations in order to induce selection. Langer sees this as an unlikely possibility since no minimization of free energy principle has been found to occur, for noise-driven wavelength selection. It is this author's opinion that noise in the system accelerates wavelength selection, even though it may not ultimately determine the wavelength.

(4) The fourth possibility is that the wave selection mechanisms are dynamic. This is the concept of the propagation of a wave, or wave packet, from an already existing source. It may also be the case of a continuous developing wavelength as a function of time. Until recently, this was considered by Langer to be a plausible principle, but he has abandoned this in favor of localized models. Langer no longer holds this as the correct principle because dendrites are known to have a very definite and unique selection mechanism. A family of wavelengths is not observed for dendrites, but rather a unique value of the spacing is selected under given growth conditions.

Experimental studies by Somboonsuk [46] and Esaka [50], however, do show a small, but definite spectrum of dendrite spacings under given experimental conditions. It will be shown later in this work that there is also a finite spectrum of wavelengths that exists for steady-state cellular structures. The statement made by Langer is, therefore, not totally correct.

(5) The final possibility proposed by Langer is that there is no selection. This means that the selection which is observed is a

function of history, and a weak function of the boundary conditions. This possibility allows for a vast number of final wavelengths which are different and not related in any simple way. Although this is not satisfying, this appears to be Langers best guess at the generalized wavelength selection process.

The results of this analysis of pattern selection are not satisfying, and it is clear that considerable work still remains to be done in this area. Perhaps the inclusion of parameters which are currently neglected, such as the surface anisotropy coefficients, would assist in making the models match reality more closely. There may yet be other possibilities which are not discovered, or a combination of the above five possibilities which may be possible as a solution to the problem. It does appear, however, that some critical experiments are now needed to guide further theoretical developments.

Models

The models which are normally used for solidification are the symmetric model, the one-sided model, the string model, and the boundary layer model. These models will be described briefly here. The symmetric model and the one-sided model are generalized models, and the string model and the boundary layer model are localized models. The five possibilities for pattern formation discussed above were for generalized models. Although generalized models are preferred for modeling solidification because dendrites and cells exist in arrays in nature, localized models are more promising at present, as

will be discussed below.

The symmetric model considers the situation where both the solid and the liquid have similar thermal diffusion coefficients. This is the reason that the model is called the symmetric model. Besides the symmetry in the thermal diffusion coefficient, the model considers the interface to be a line heat source. This model is used for solidification of pure materials where only thermal diffusion needs to be considered.

If solute diffusion is considered, the symmetric model is still sometimes used, but since the diffusion coefficients of the solute often differ by two orders of magnitude between the solid and liquid, the symmetric model is not very accurate when solute is present. Therefore, when solute is present, the one-sided model is more generally used. The one-sided model is similar to the symmetric model with the exception that diffusion of heat and solute is considered to occur only in the liquid.

The string model is one of the local models. What is meant by local is that the immediate section of interface is modeled as being dependent only on its two end values. In other words, the interface is considered as a freely moving string which is chopped into incremental units that move together via the fact that their end points are attached. When using the string model, either symmetric or nonsymmetric conditions can be used.

The last model considered here is the boundary layer model. This model is similar to the string model, but the string has a memory of

what has gone on in the past. This memory is produced by using a finite length diffusion layer in the liquid, into which the heat and solute diffuse. The heat and solute generated by the moving boundary are collected in the boundary layer. The boundary layer then, imposes itself onto the interface by changing the growth conditions. This model produces structures that are similar to cells and dendrites and therefore, is a very promising model. Some of the structures produced, for pure undercooled melts, are shown in Figures 25-27.

Nonlinear stability: Higher order analysis

There has been some recent work [51, 52] in third and higher order systems that shows unusual properties. These higher order systems are a class called attractors. There are, of course, many types of these higher order attractors, but two that may be of interest here are the horseshoe attractor and the Lorenz attractor. These two are unique in that although they appear to be random in some of their properties, they are entirely deterministic. This means that once set into motion, the end is determined from the beginning. This concept of a deterministic solution is a different concept of pattern formation than is usually considered.

Experimental work by Trivedi and Somboonsuk [53] shows that there are two characteristic wavelengths observed in pattern formation of real solidifying structures. They label these wavelengths as λ_i and λ_j. These are connected together and to the thermal and solute length, respectively, by scaling laws. The scaling laws are as follows:

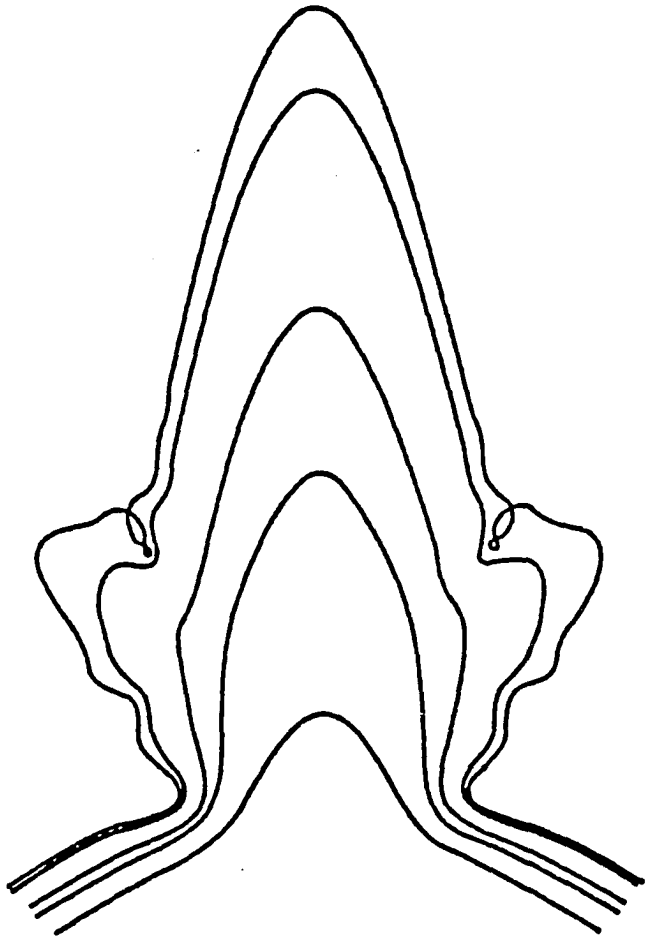

Figure 25. Development of a parabolic tip as a function of time using a localized boundary layer model. Figure is from reference [49]

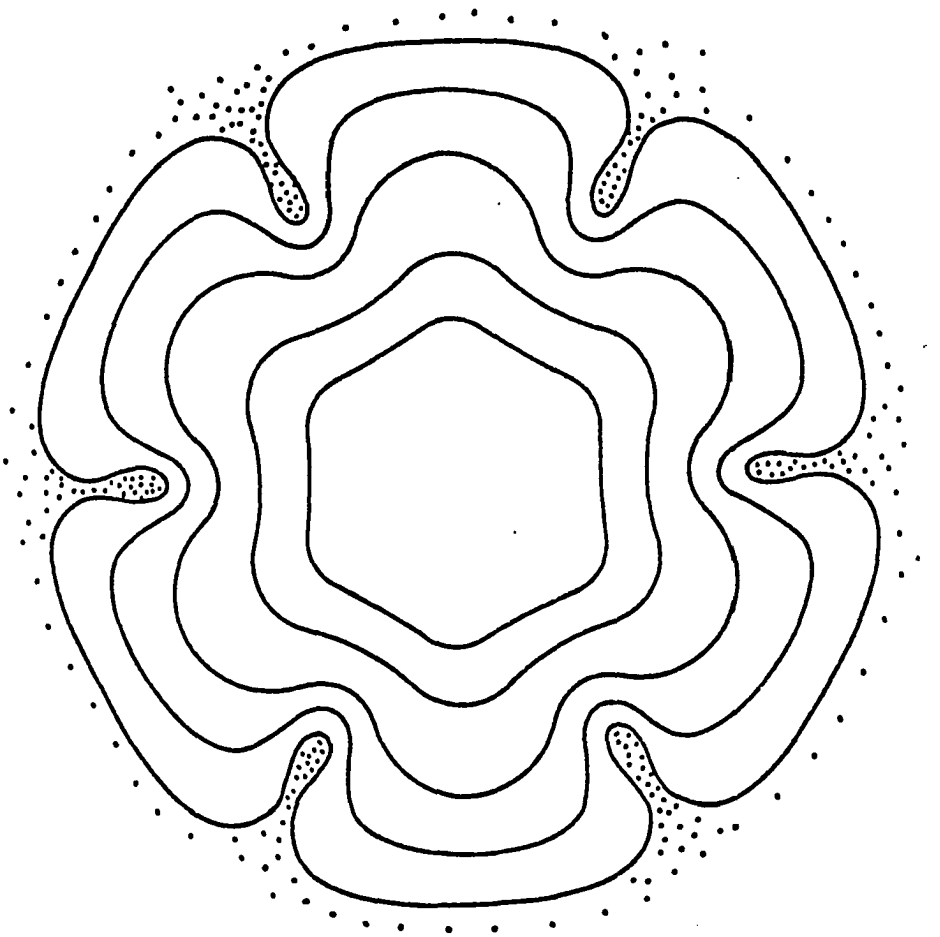

Figure 26. Development of a sixfold cellular structure as a function of time using a localized boundary layer model. Figure is from reference [49]

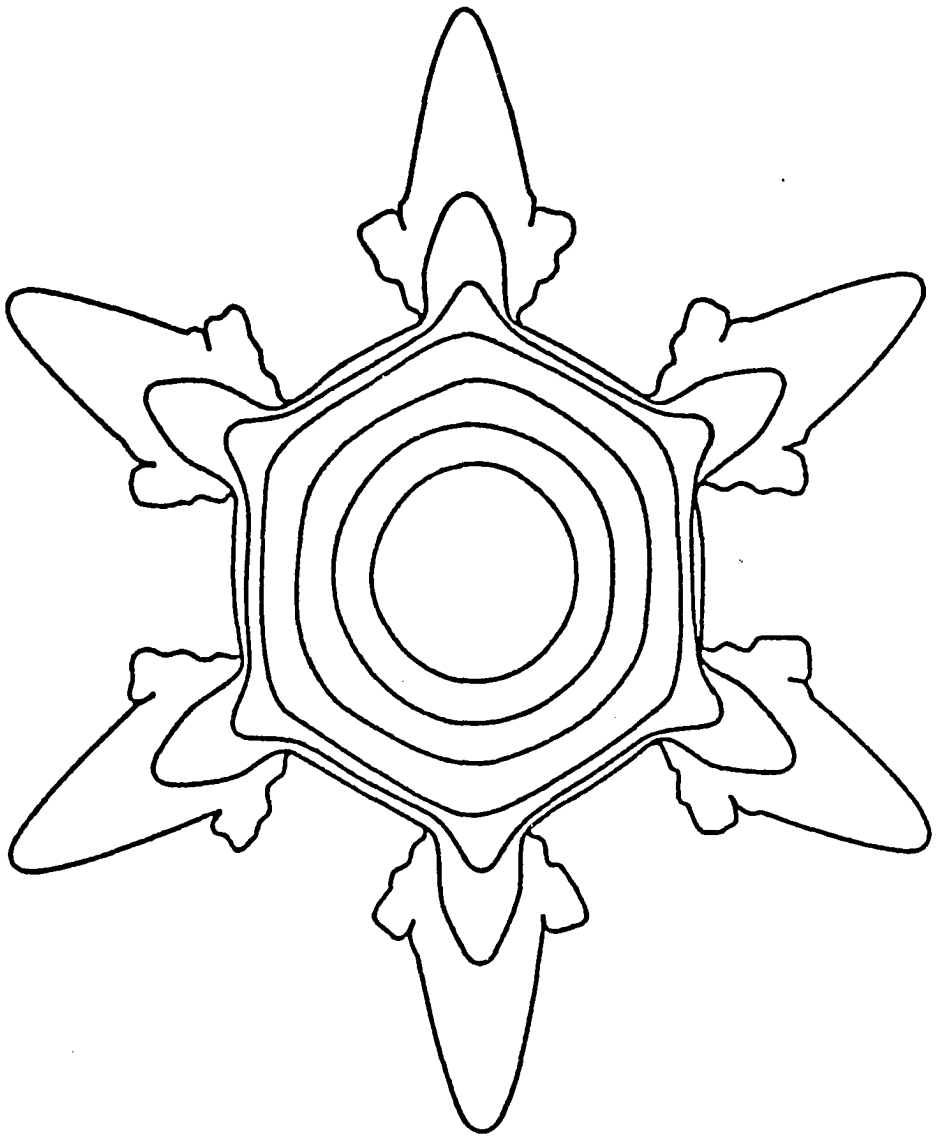

Figure 27. Development of a sixfold dendritic pattern as a function of time using a localized boundary layer model. Figure is from reference [49]

$$\lambda_i = 10.58\ (l_s l_c)^{1/2} \tag{28}$$

and

$$\lambda_j = 1.68\ (\lambda_i l_t)^{1/2}\ , \tag{29}$$

where $l_s = 2D/V$, $l_t = K_o \Delta T_o / G$, and $l_c = \Gamma / \Delta S K_o \Delta T_o$. The interest here is not to interprete the scaling laws, but to point out that they do exist. The present work also shows that the two characteristic wavelengths exist even at velocities extremely close to the critical velocity. The existence of these scaling laws indicates that the problem of pattern selection is not entirely chaotic. It is, rather, determined very distinctly by parameters of the system. Perhaps strange attractors should be considered in future pattern selection modeling.

Critical Experiments Needed

In review, we see that although there has been considerable work done on planar interface instability, there are several inherent problems that have largely been overlooked. There are, therefore, reasons why the experimental studies remain incomplete. One of the most common experimental problems is the problem of convection. This becomes particularly important at very low rates, where the stability work is generally done. A second problem is that of unknown system parameters. In most cases, accurate values of the system parameters simply do not exist. A third problem is velocity stability and accuracy at low rates. Very few investigators have established the

linearity of the velocity which occurred during the experimental run. Another reason why the studies are incomplete is the opaque nature of most sample materials. Due to the opaqueness of the samples, in situ experiments cannot be made. This allows for a considerable margin of error in the actual interface velocity at the time of break up since the interface velocity is assumed to be the externally imposed velocity. This may not be the case, as is shown in the next chapter.

As can be seen, there remains a need for a carefully controlled examination of both Mullins and Sekerka's [2] linear stability analysis and Wollkind and Segel's nonlinear analysis [4]. These examinations should be done in well-characterized transparent alloy systems. For these reasons, the succinonitrile-acetone system and the pivalic acid-ethanol system are ideal for such a study. The necessary parameters are well-known and the systems are transparent. These, therefore, were the experimental systems which were used in this quantitative study.

With the background given in the literature review, there are a number of critical experiments which could be done to test the accuracy and validity of the currently accepted theories. Some of these critical tests are given here. These tests give this work a purpose and a goal.

(1) A definitive test should be made to check the accuracy of Mullins and Sekerka's [2] linear stability analysis. Two points should be checked. These are, the accuracy of the critical velocity prediction, and the accuracy to which the theory predicts the wavelengths at the critical velocity. These tests can be made by

increasing the velocity just past the critical velocity slowly, and then, observing the wavelengths of the perturbations present.

(2) A check should be made to see if Wollkind and Segel's [4] prediction of subcritical bifurcation exists. The theory can be checked by observing the amplitude of the waves present at a velocity near to the critical velocity. A positive proof of subcritical bifurcation would be obtained if waves formed at a velocity above V_c persist at a velocity below V_c.

(3) Experiments which observe and measure the dynamic process of pattern formation would be extremely valuable for those doing theoretical modeling since the theory of pattern formation, in many respects, requires experimental input to guide further development. Theory would, thus, benefit greatly from a careful study of actual observations of the time evolution of a steady-state pattern. The path taken by the system toward steady state can be plotted in wavevector space, and the mechanisms of pattern evolution can be established.

(4) Theoretical models of cells are based on the assumption that the cellular patterns formed are steady state and are of a unique wavelength. It is important to determine experimentally the uniqueness of the wavelength selection criterion. Experimental studies are needed to examine the statistical distribution of spacing and to see if this distribution is sharp or broad.

(5) A careful study of the cellular range, and the cell-dendrite transition would be valuable because there is, presently, confusion in the literature. The confusion exists both in the theory and in

interpretation of experimental microstructures observed at different growth rates.

(6) The observance of anisotropic interface properties, and their affect on interface instability would check the linear stability theory of Coriell and Sekerka [54], which is presented in detail later. Measurements of the interface kinetic anisotropy would be the first measurements of this parameter in a solidifying material. The importance of kinetic anisotropy is not known at present, but theoretical models show that anisotropy may play an important part in pattern formation.

EXPERIMENTAL PROCEDURE

In directional solidification studies, there are three control variables after an alloy system has been chosen. The three variables are velocity, thermal gradient, and solute concentration. In this study, velocity was the variable which was used to cause changes in the growth structures. The thermal gradient and solute concentration remained constant throughout each experimental run.

The experiments done here used low concentration alloys. This was done because the threshold velocity for the planar-cellular transition goes up as the concentration goes down. By using low concentration alloys and therefore, achieving high threshold velocities, the deviations in the velocity, even though they were already small, were minimized. This is an important experimental consideration because velocities below 0.1 μm/s are extremely difficult to maintain with any accuracy. Problems such as building vibrations, etc., become important at these very low rates. For this reason, the threshold velocity was also kept above 0.4 μm/s. In addition, the most important experiments were done at times when the building was sparsely used. The entire experimental apparatus was placed on a shock absorbing base.

The Solidification Equipment

The solidification equipment is similar in principle to that described by Jackson and Hunt [55]. A number of modifications were, however, necessary to achieve higher accuracy and precision required

for the present studies. The modifications which were made to improve the linearity of the velocity are as follows:

(1) A stepper motor with 50,000 uniform steps per revolution was used in place of a DC motor and gears.

(2) A precision ground ballscrew was used in place of a threaded nut and bolt.

(3) No gears were used in the entire system. A tension V-belt was used to connect the motor to the ballscrew.

(4) Special alignment devices were made to align the ballscrew with the glide bars. It was found that this improvement took the linearity in the velocity from $\pm$ 0.25 μm/s to better than $\pm$ 0.05 μm/s.

(5) Precision bearings were used on the ends of the ballscrew in place of normal bearings. These were later replaced by teflon bushings. The teflon bushings reduced mechanical noise because there are no moving parts.

The present apparatus with modifications is shown in Figure 28. Schematic diagrams of the apparatus are shown in Figure 29. A detailed discussion of the various components of the apparatus is given by Mason and Eshelman [56].

Establishing the thermal gradient

Directional solidification was induced by moving a sample between fixed hot and cold chambers. The hot and cold chambers were held at a fixed distance apart with a machined lexan block. The lexan block below

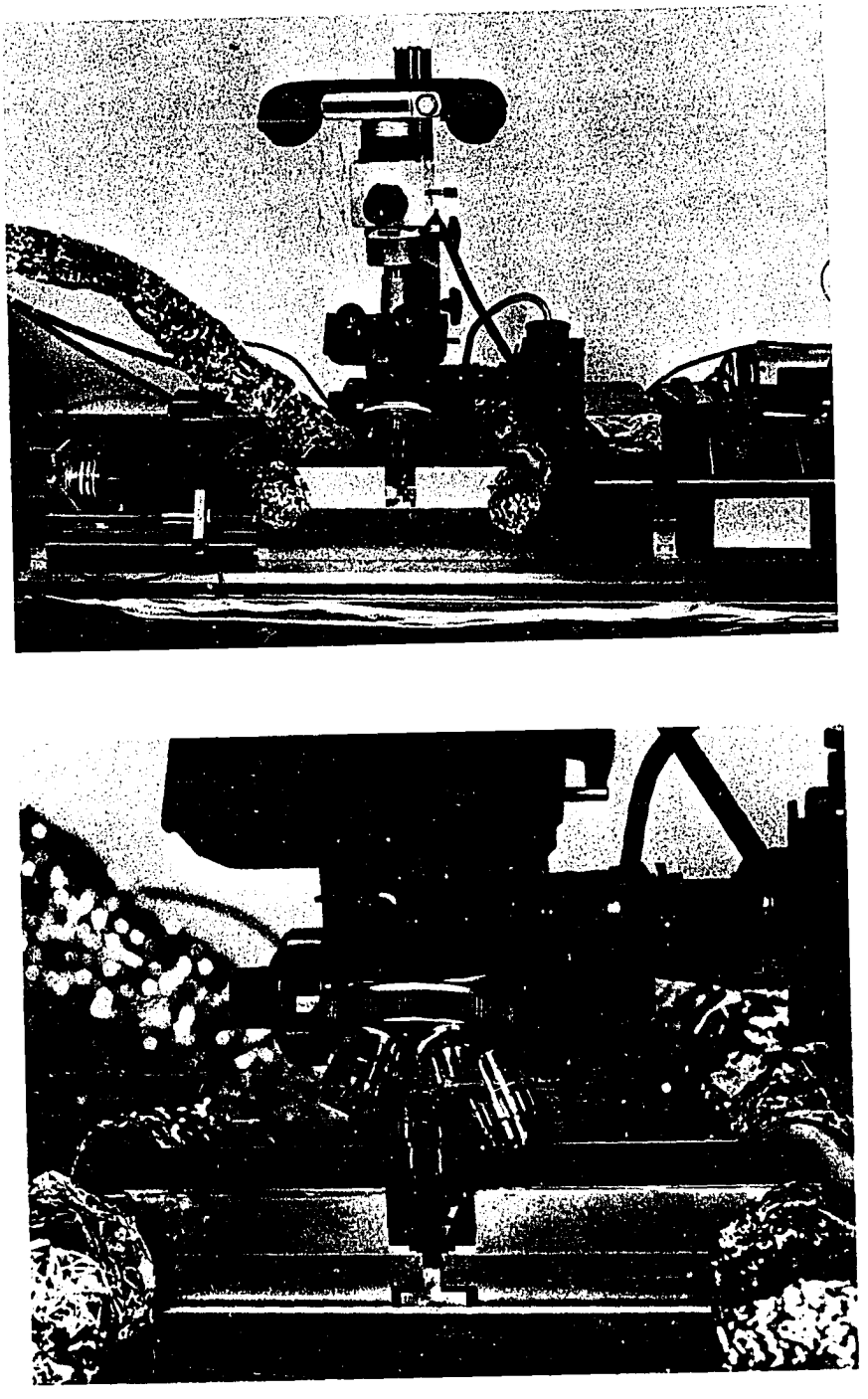

Figure 28. Photograph of the model transport apparatus. Top: Entire apparatus. Top insulator sheets removed for clarity. Bottom: Close up of hot and cold plate gap area

Figure 29. Schematic top and side view diagrams of the solidification apparatus. The labeled parts are:

1. Bottom plate
2. End shaft and bearing plate
3. Side wall, left and right
4. Position bearing for ball screw
5. Solid case shafts
6. Bearings for shafts
7. Sample carriage
8. Ball screw
9. Hex jam nut
10. Shaft and bearing plate
11. Bottom insulator plate
12. Center insulating block
13. Bottom hot plate
14. Top hot plate
15. Hot oil connect tube
16. Hot oil inlet and outlet
17. Bottom cold plate
18. Top cold plate
19. Top cover plate hot and cold
20. Bottom cover plate hot and cold
21. Cold water connect tube
22. Cold water inlet and outlet
23. Side cold insulator
24. Top cold insulator
25. Sample holder
26. Transducer rod
27. Transducer block support
28. Transducer block
29. Transducer
30. Pulley for ball screw
31. Side hot insulator
32. Top hot insulator
33. Motor front brace
34. Motor bottom brace
35. Motor side brace
36. Motor mount block
37. Bearing end plug adjustor
38. Pulley for motor

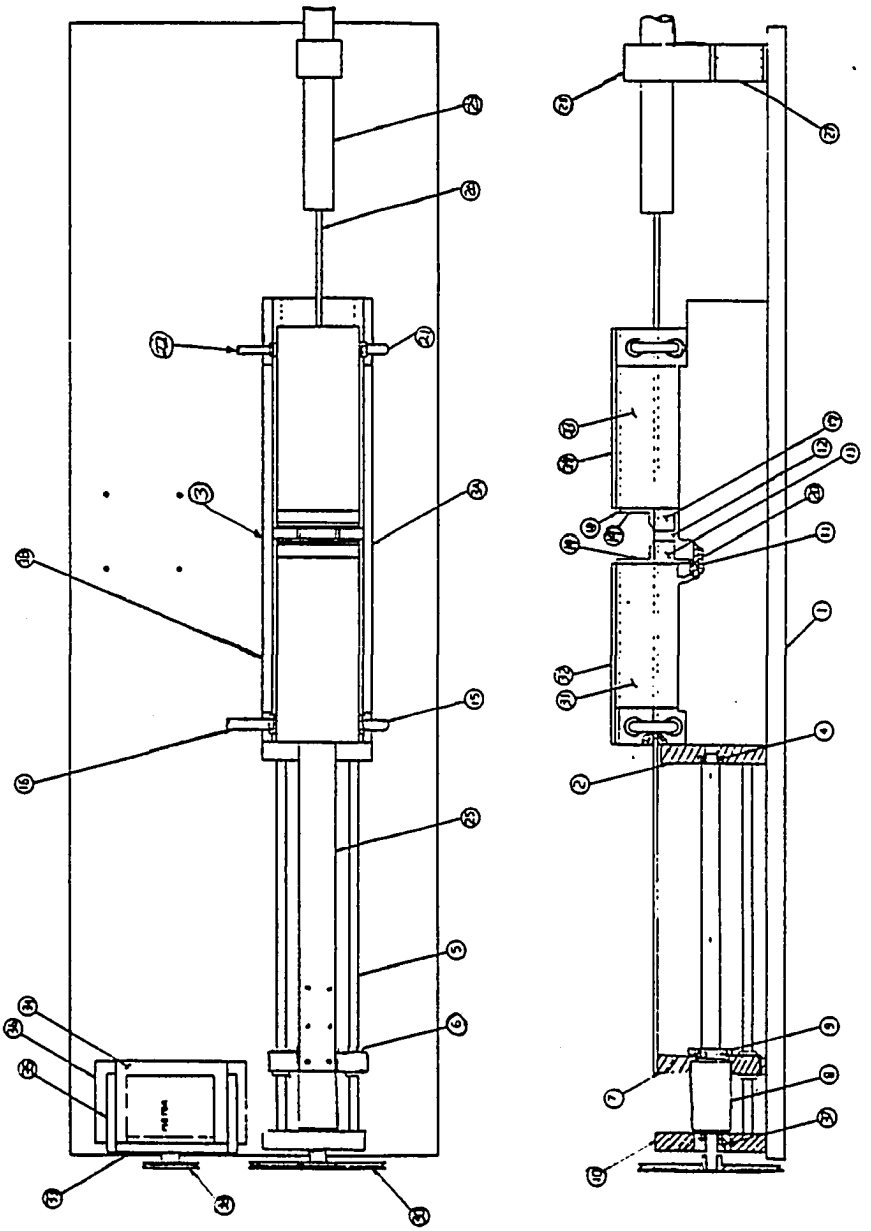

the sample between the hot and cold plates established a constant thermal gradient, and also reduced thermal convection due to air flow below the sample. There was also a 150 μm thick glass cover slip over the sample and between the hot and cold chamber. This thin glass cover slip reduced air convection from the top.

The cold chamber was controlled by passing a water/ethalene glycol mixture through it at a constant temperature. The fluid temperature was controlled by a Neslab Instruments, Inc., Portmouth, NH, Endocal refrigerated bath circulator model RTE-4. The temperature range available was -30 to 100°C, and the stability was specified to be ± 0.01°C within the temperature range from 20 to 60°C. The cold chamber was tested for stability and was found to hold a constant temperature of ± 0.03°C or better in the temperature range 10-40°C for periods of 1-2 days.

Two different types of hot chambers were used in these experiments. The first one used a resistance furnace. The power supply was a constant amperage DC power supply (Harrison model 6286A, Hewlett Packard, Skokie, IL). This furnace was found to maintain a constant temperature (about ± 0.5°C) for periods of several hours, but was found to drift with the room temperature by 1-2°C over a period of a day.

In order to improve the long-term stability of the thermal gradient, an oil bath hot chamber was developed for use on the system. The hot chamber oil was regulated and circulated by a Neslab Instruments, Inc. (Portsmouth, NH), Exacal model 250HT constant

temperature bath circulator. With this system, the hot chamber stability was tested and found to be ± 0.05°C or better, at 150°C, over a period of 24 hours.

Establishing a constant velocity

The drive mechanism was built around a precision ground ballscrew. The drive motor was a stepping motor with 50,000 steps per revolution. The motor was model M57-51-R14, by Compumotor Corporation, Petalumn, CA. The motor was controlled by a Commodore 64 computer made by Commodore Business Machines, Inc., Wayne, PA. With this system, the velocity was reproducible within ± 0.02 °C over long distances.

The motion of the sample was measured with a linear variable differential transformer, LVDT (type 3000 HR, Schaevitz Engineering, Pennsauken, NJ). Real time velocities were attained by electronically differentiating the LVDT output. A schematic diagram of the electronic differentiator is shown in Figure 30. The motion of the sample moving inside the system was measured and the instantaneous velocity was found to be linear to ± 0.02 μm/s at submicron per second velocities. A trace and scale of the velocity profile during an experimental run are shown in Figure 31.

The temperature of the interface and the thermal gradient were measured during the runs with calibrated thermocouples placed inside the sample cells. The thermocouples were calibrated against a NBS certified mercury thermometer in a large dewar apparatus, which is shown in Figure 32. The thermocouples were calibrated to accuracies of ± 0.03°C using this method.

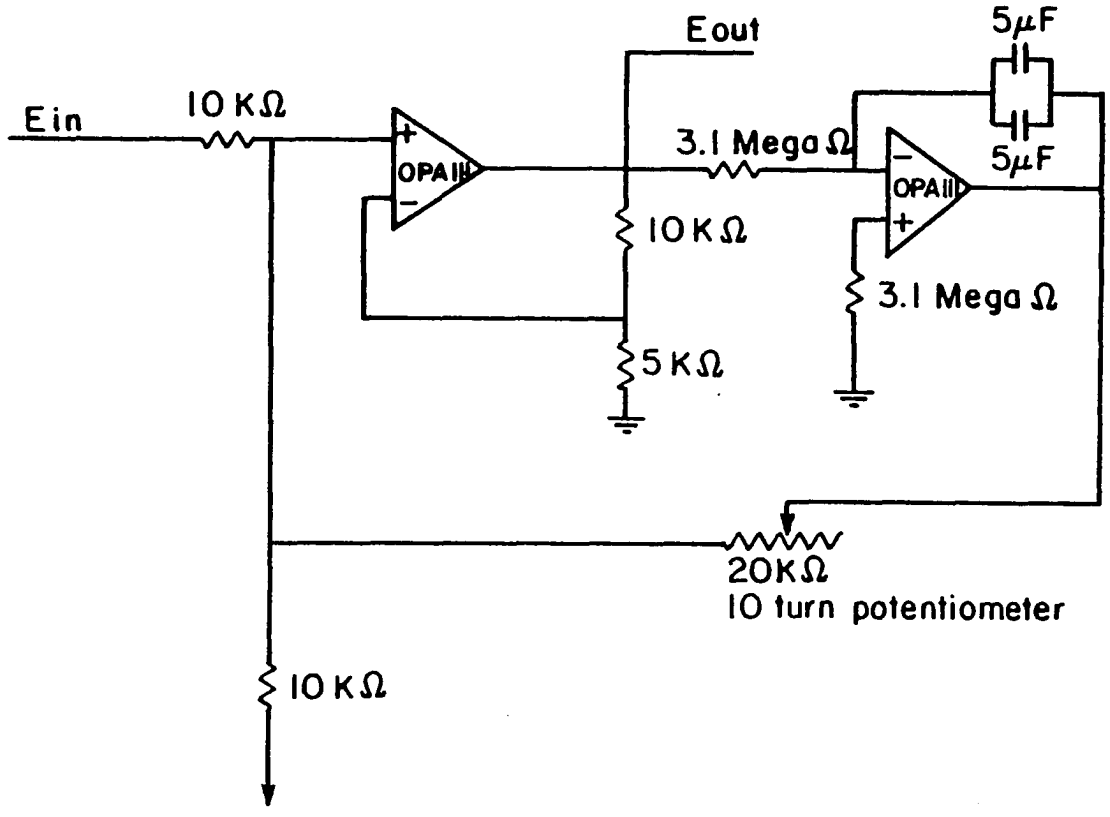

Figure 30. Schematic diagram of the electronic differentiator used in this work

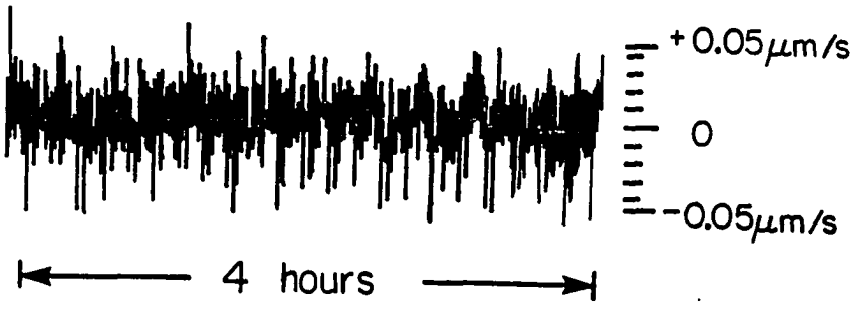

Figure 31. Output from the electronic differentiator during an experimental run showing the change in the velocity as a function of time. The small time scale variations are due to electronic noise generated by the differentiator. The larger time scale variations are actual variations in the velocity

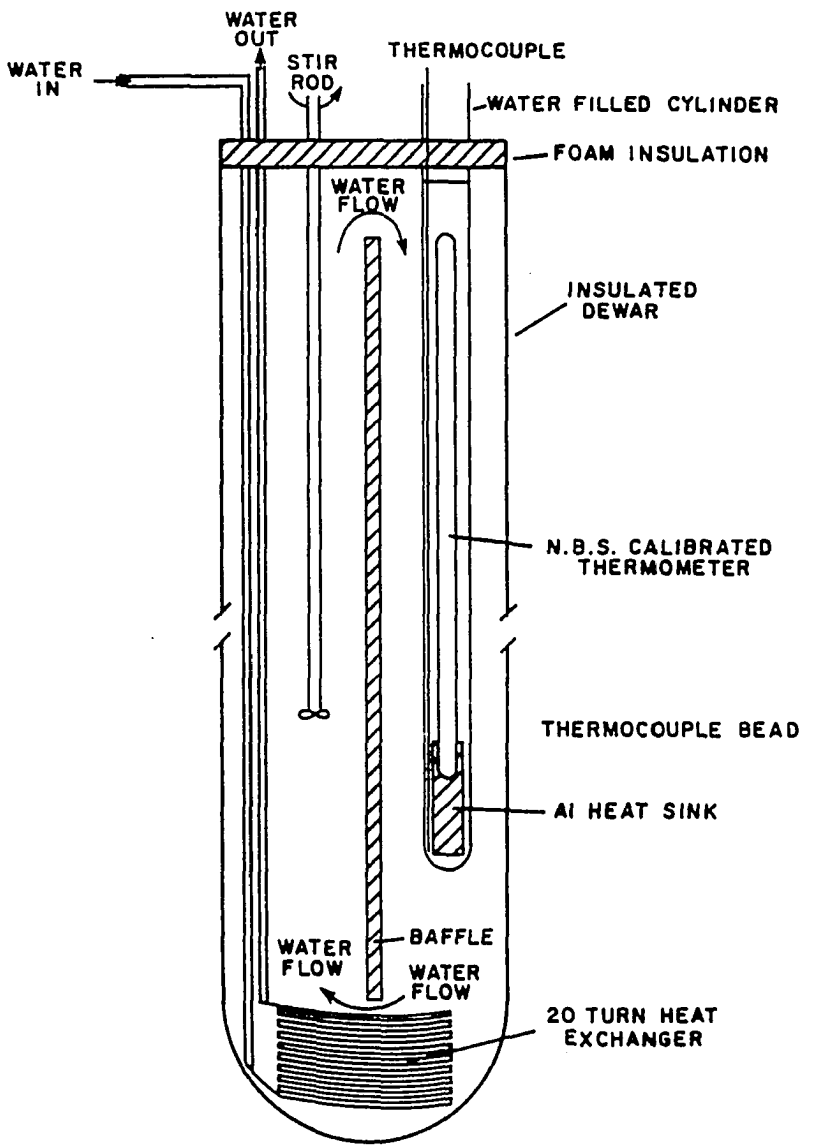

Figure 32. Apparatus used for thermocouple calibration. The water incoming to the apparatus was thermally controlled using the Neslab Endocal refrigerated bath circulator model RTE-4

Sample cell preparation

The sample cells were made by using two 75mm x 25mm microscope slides held at a constant distance apart with 150 μm thick brass shim stock. The slides and shims were preheated in a meeker burner between two stainless steel plates. After about five minutes of preheating, two sides and the end of the glass slides were fused with an oxygen-propane torch. The slides were then, placed in a tube furnace for post weld annealing. The furnace temperature was about 600°C. Figure 33 shows the sample cells in various stages of preparation. In order to easily fill the sample cell, a hole was cut in the end opposite to the open end using a rotary cut-off wheel. Following the cutting, the sample cell was thoroughly cleaned and baked in an oven at 100°C for a few hours to drive off any retained moisture.

A 75 μm calibrated chromel-alumel thermocouple was introduced into the sample slide through a small hold cut in the side of the slide. The thermocouple was inserted on the side of the slide to minimize the disturbance of the thermal field inside the slide. A cell with a thermocouple in place is shown in Figure 33.

Sample cells were filled in a dry box under a dry nitrogen environment with a small pressurized chamber, as shown in Figure 34. When this method was used for sample filling, the sample cells had to be preheated in order to ensure complete filling. After filling, the cell was placed on a copper block to induce solidification as quickly as possible. This was done to avoid macro-segration in the alloy. The cell was then, sealed with chemically inert epoxy. The epoxy used was

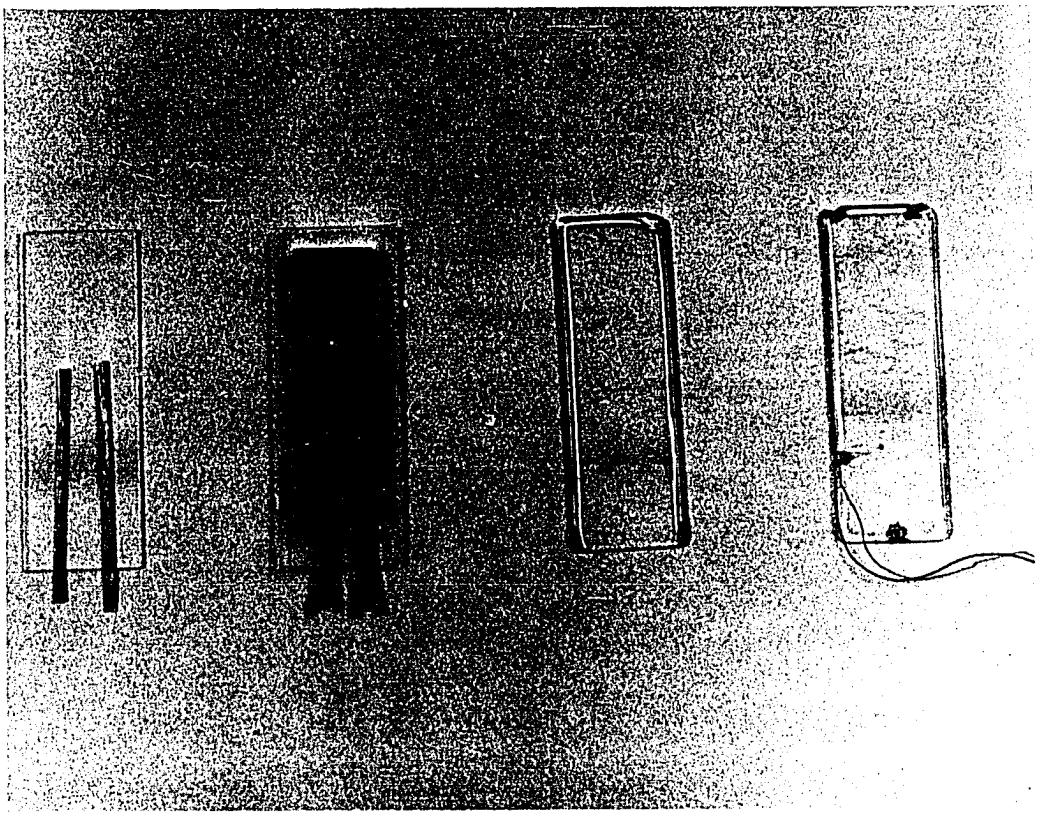

Figure 33. Sample cells. Left to right: Glass slides with spacers, cell with stainless steel heat sinks ready to fuse, fused cell, finished sample cell with thermocouple

Figure 34. Loading equipment. Left to right: cell holder, cell holder with cell inserted, pressurized loading jar

Epoxi Patch, from Dexter Corporation, Olean, NY.

Since all modeling generally neglects the effects of convection, it was important to ensure that convection could not occur in the samples. Convection was prevented by using sample cells with sample thicknesses of 150 μm. Somboonsuk [46] has shown that convection does not occur in transparent, metal analog systems in cells of this thickness. Somboonsuk's experiments to check convection effects used silica beads with sizes between 20 μm and 100 μm. The silica beads were never observed to move during solidification when the sample thickness was 200 μm or less.

In addition, the sample cell was chosen with a thickness large enough that the effects of the cell walls on the motion of the interface in the vertical direction were negligible. Caroli et al. [57] and de Cheveigne et al. [48] have shown that in sample cells with thicknesses greater than 50 μm, there is no effect of the cell wall on solidification processes.

A third reason for choosing sample cells with thicknesses of 150 μm was that the solidification structures operate in a two-dimensional manner at these thicknesses. Thicker samples show three-dimensional effects, and thinner samples change the growth characteristics of the solidifying structures [46].

Materials Preparation

Three transparent alloy systems were used in this study: Succinonitrile-acetone, pivalic acid-ethanol, and carbontetrabromide-

hexachloroethane. As-received material purity and the material purification techniques were different for each of the six materials. The as-received succinonitrile (SCN) had a three degree melting range. It was purified by standard zone refinement. In some cases, the SCN was double zone refined, or distilled prior to zone refinement. As discussed by Pfann [58], the final purity of the material is exponentially related to the tube length in which it is prepared. For this reason, the longest available (120 cm long and 8mm outer diameter) tubes were used. The total number of zone passes was 50-70. The purified SCN was found to have a melting range of $\pm$ 0.03 K.

The as-received acetone was 99.9 mol% pure. It was further purified by distillation and subsequent treatment with anhydrous $CaSO_4$. The acetone was stored in a dry environment when not in use.

The as-received pivalic acid contained about 10% water. It was, therefore, necessary to sublimate it prior to zone refinement. After sublimation, zone refinement was done in the same manner as described for SCN. The purified material had a melting point of 308.7 K. The highest melting point reported in the literature is 308.8 K.

The ethanol was used as received since reagent grade absolute ethanol was available. The purity level was reported to be 99.95 mol% pure.

The as-received carbontetrabromide (CBr_4) was purified by vacuum sublimation. This was repeated twice. Both times, the initial and final fractions were discarded. The final product was found to solidify with a planar interface at velocities of up to 25 μm/s in a thermal

gradient of 3.6 k/mm.

The as-received hexachloroethane (CCl_6) was purified by normal sublimation. The initial and final fractions were discarded.

Since the experiments in this work were critical experiments, the succinonitrile-acetone and pivalic acid-ethanol systems were used almost exclusively. The carbontetrabromide-hexachloroethane system was only used for comparative purposes, and then, only when anisotropic properties were studied.

The physical properties of the materials studied are shown in Table 1. The phase diagrams of the materials studied are shown in Figures 35-37.

A variety of alloys were used in the experiments done in this work. These are listed in Table 2.

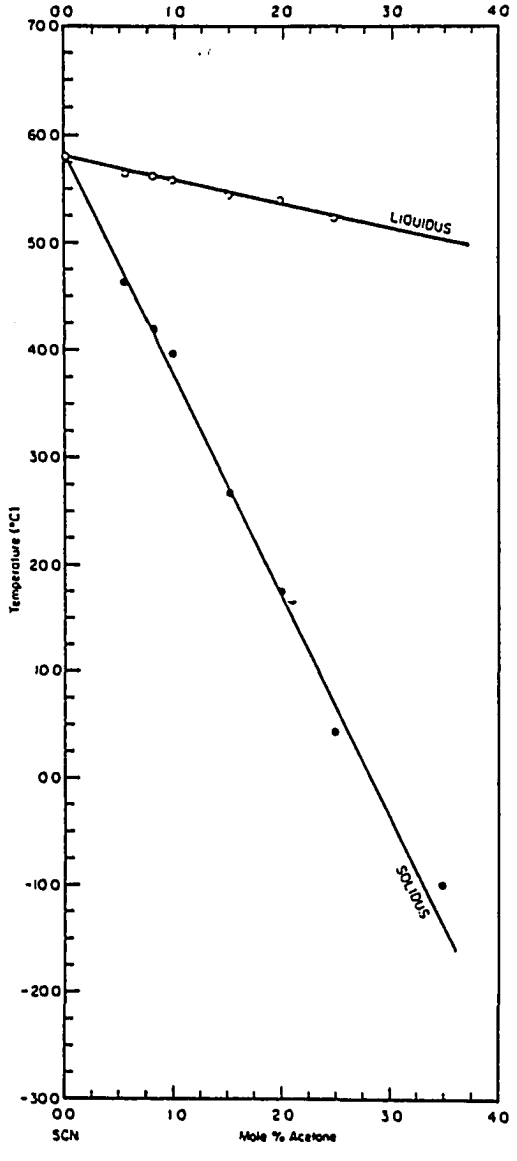

Figure 35. Phase diagram for the succinonitrile-acetone binary alloy system. Figure is from reference [59]

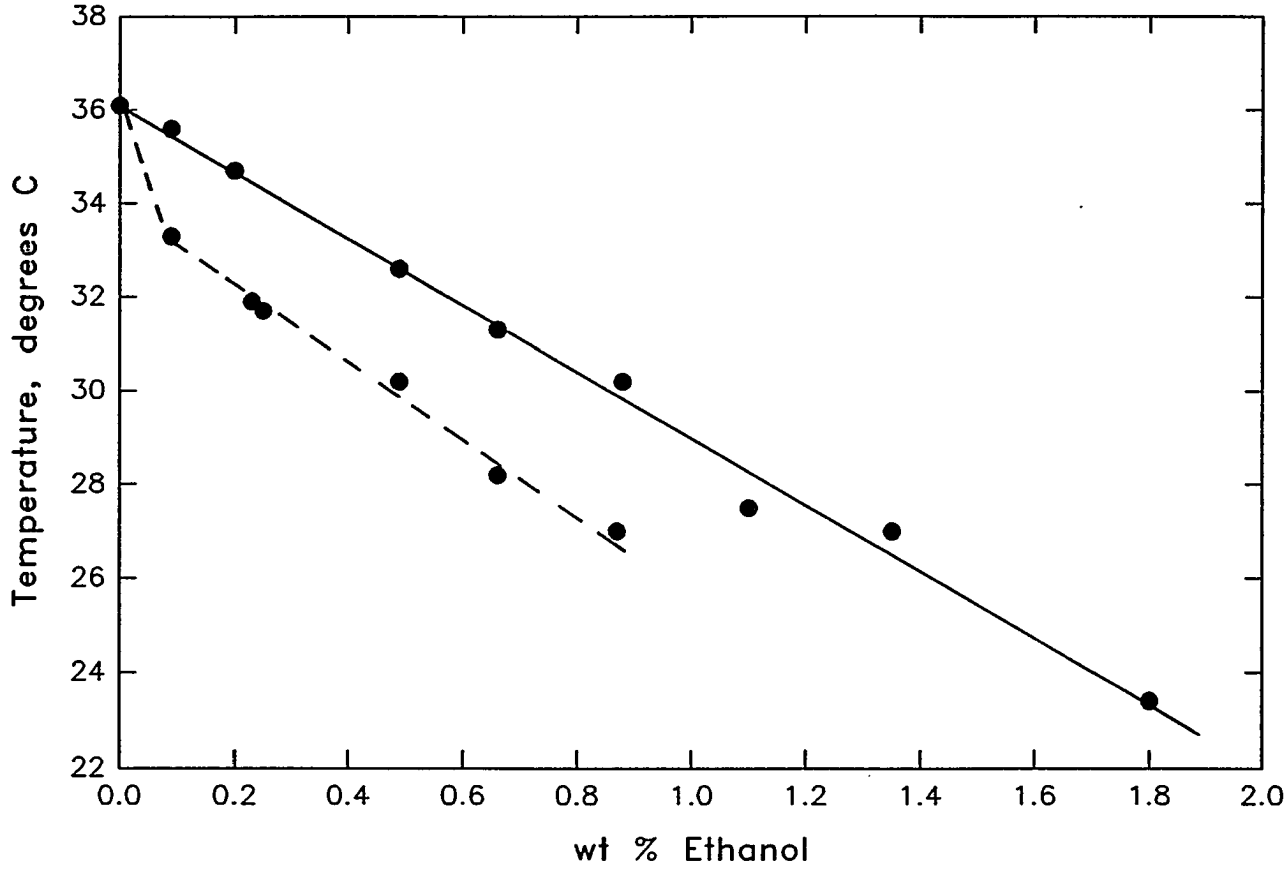

Figure 36. Phase diagram of the pivalic acid-ethanol binary alloy system. Figure is from reference [60]

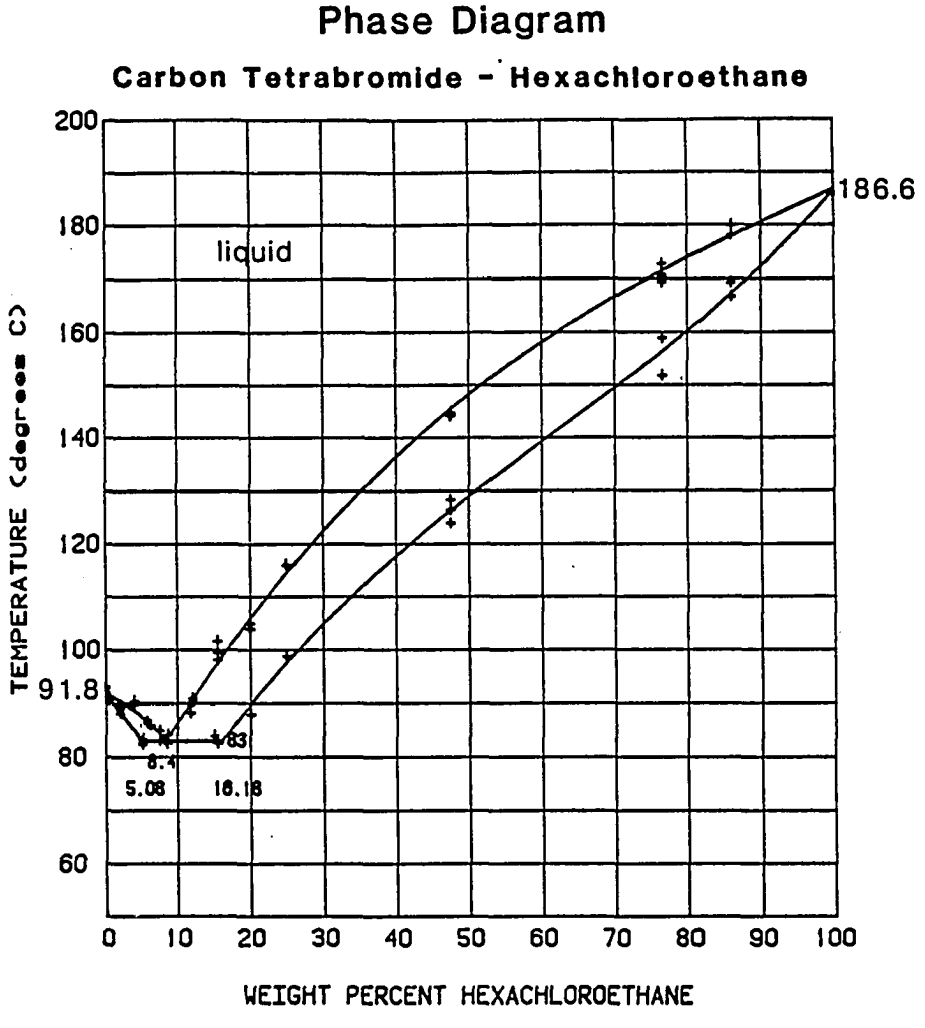

Figure 37. Phase diagram of the carbontetrabromine-hexachloroethane binary alloy system. Figure is from reference [61]

Table 1. Material and alloy properties of the experimental alloys used

	Succinonitrile	Pivalic acid	Carbontetra-bromide
Melting point, K	331.24	308.7	363.2
Entropy of fusion, J/mol-K	11.21	7.4	10.88
Density of solid, kg/m^3	1.016×10^3	0.905×10^3	3.26×10^3
Density of liquid, kg/m^3	0.907×10^3	-	-
Thermal conductivity of solid, J/msK	0.224	0.49	-
Thermal conductivity of liquid, J/msK	0.223	-	-
Surface energy, J/m^2	8.95×10^{-3}	2.81×10^{-3}	8.0×10^{-3}
Alloy properties	Succinonitrile-acetone	Pivalic acid - 0.2 wt% ethanol	Carbontetra-bromide - 0.2 w/o hexachloroethane
Diffusion coefficient, cm^2/s	1.27×10^{-5}	2.0×10^{-6}	1.5×10^{-5}
Liquid slope, K/wt%	-3.02	-7.14	-0.6
Equilibrium partition coefficient	0.103	0.4	0.43

Table 2. Alloy compositions used in this work

Alloy	Range of compositions
Succinonitrile-acetone	0.1 - 2.8 w/o acetone
Pivalic acid-ethanol	0.076 - 0.2 w/o ethanol
Carbontetrabromide-hexachloroethane	0.2 w/o hexachloroethane

SECTION I. THE PLANAR INTERFACE INSTABILITY

INTRODUCTION

The major aims of this work are to test the predictions of the linear and weakly nonlinear stability analyses by carrying out detailed experimental studies of the planar interface instability in a well-characterized system. Although a number of experimental studies in metal systems has been carried out to examine the conditions for the planar interface stability [1-7], the precise velocity of the interface break up, V_c, could not be determined because the interface break-up velocity was associated with the externally imposed velocity. Somboonsuk and Trivedi [8] have shown that there is a sufficiently long transient before the actual velocity of the interface approaches the externally imposed velocity so that a precise measurement of V_c requires not only the measurement of the actual interface velocity at the time of break up, but also the dynamical values of the thermal and solute gradients at the interface. In this paper, we shall report the results of directional solidification experiments in succinonitrile-acetone system in which the actual interface velocities at the time of the planar interface instability were measured. These dynamical velocities were then correlated with the critical velocities predicted under steady-state growth conditions.

Two major predictions of the linear stability analysis which will be examined in this study are the critical velocity and the associated wavenumbers for which a planar interface becomes unstable. For small velocities, the Mullins-Sekerka result can be simplified to give the

critical velocity, V_c, by the relationship [9]

$$\nu_c = 1 + 3(K_0 2\alpha)^{1/3} \nu_c^{1/3}, \quad \alpha\nu \ll 1 \tag{1}$$

where ν_c is the threshold value of the dimensionless velocity, $\nu = V \Delta T_0/GD$, and the parameter α is given by

$$\alpha = \Upsilon G/4\Delta S \Delta T_0^2 \quad . \tag{2}$$

Note that $\nu_c = 1$ represents the modified constitutional supercooling criterion. At the critical velocity, the Mullins-Sekerka analysis predicts the unstable wave number, k_c, to be [9]:

$$k_c \simeq (G/2\Delta T_0)(K_0/\alpha)^{1/3} \nu_c^{2/3}, \quad \alpha\nu \ll 1 \quad . \tag{3}$$

Experiments were also carried out to test the prediction of a weakly nonlinear analysis presented by Wollkind and Segel [10]. They concluded that the planar to nonplanar bifurcation can be subcritical so that a planar interface, if subjected to large amplitude deformations, could become unstable at $\nu < \nu_c$. Thus, the second aim of this study is to present experimental results which examine the nature of this bifurcation. Our results confirmed the existence of subcritical bifurcation and showed that large amplitude cells remained stable when the interface velocity was slowly changed from $V > V_c$ to $V < V_c$. Also, very small amplitude perturbations were not observed at

V just above V_c. The amplitude of the interface increased from zero at $V < V_c$ to a finite value when V was increased just above V_c. Furthermore, when the interface was maintained just below V_c for a long time, long amplitude perturbations with large wavelengths were also observed which gave rise to an unstable interface.

EXPERIMENTAL

Directional solidification studies on the succinonitrile-acetone binary alloy system were carried out in the system described in the Experimental Procedure Section of this dissertation. Special care was taken to ensure that all the experimental variables were controlled and measured accurately. In these studies, the temperature gradient and the composition were kept constant and the interface instability was examined as a function of velocity. In order to observe any change in temperature gradient which may occur during the interface instability, experiments were carried out with two thermocouples in the cell which were positioned such that the first thermocouple traced the temperature profile of the steady-state planar interface growth at $V < V_c$ and the second thermocouple traced the temperature profile after the interface just became unstable at $V > V_c$. No significant change in the temperature gradient at the interface was observed prior to and after the break up.

The concentration of acetone was varied between 0.10-0.35 wt.%. Initially, the composition was controlled by mixing appropriate weights of the components. However, the exact concentration of acetone in the cell was subsequently determined by measuring the planar interface temperature with a calibrated thermocouple during a steady-state run at $V < V_c$.

Three sets of experimental studies were carried out. For a given composition and temperature gradient, the critical velocity was

calculated from Eq. (1). The sample was then solidified at velocity V_o, which was below V_c, where a planar interface growth was observed. After a steady-state growth was established at V_o, the external velocity was changed rapidly to V_E, where $V_E > V_c$. The subscript E denotes the externally applied velocity. The interface location and shape were photographed continuously at 1 second intervals, and Figure 1 illustrates the interface break-up phenomenon. The velocity of the interface with time was then calculated from the distance vs. time measurements, and this is shown in Figure 2. The interface velocity, as well as the time at which the interface just became unstable, as seen from the photographs, were then marked on this plot. Since the break up was observed before the interface velocity coincided with V_E, a series of runs was made with different V_E values, and the interface velocity, V_b, at which break up occurred was measured for each V_E run. These experiments are shown in Figure 2. The critical velocity, V_c, was then taken to be equal to the smallest V_b value where the break up was observed. A second set of experiments was also carried out in which the external velocity was changed from V_o to $V > V_c$ in small velocity steps. At each velocity, the run was made for a sufficiently long time to observe any sign of instability. The velocity at which the first break up was observed was then noted. Since the change in velocity was sufficiently small, about 0.05 μm/s near V_c, the external velocity at which the break up was observed was taken to be equal to the V_c.

The third set of experiments was designed to study the planar to cellular bifurcation. In this study, a planar interface was first

(a)

(b)

(c)

Figure 1. Break up of a planar interface. Succinonitrile 0.15 w/o acetone, G = 3.76 K/mm, V = 0.8 μm/s, (a) at time = 0 s, (b) at time = 570 s, (c) at time = 870 s, mag. = 43X

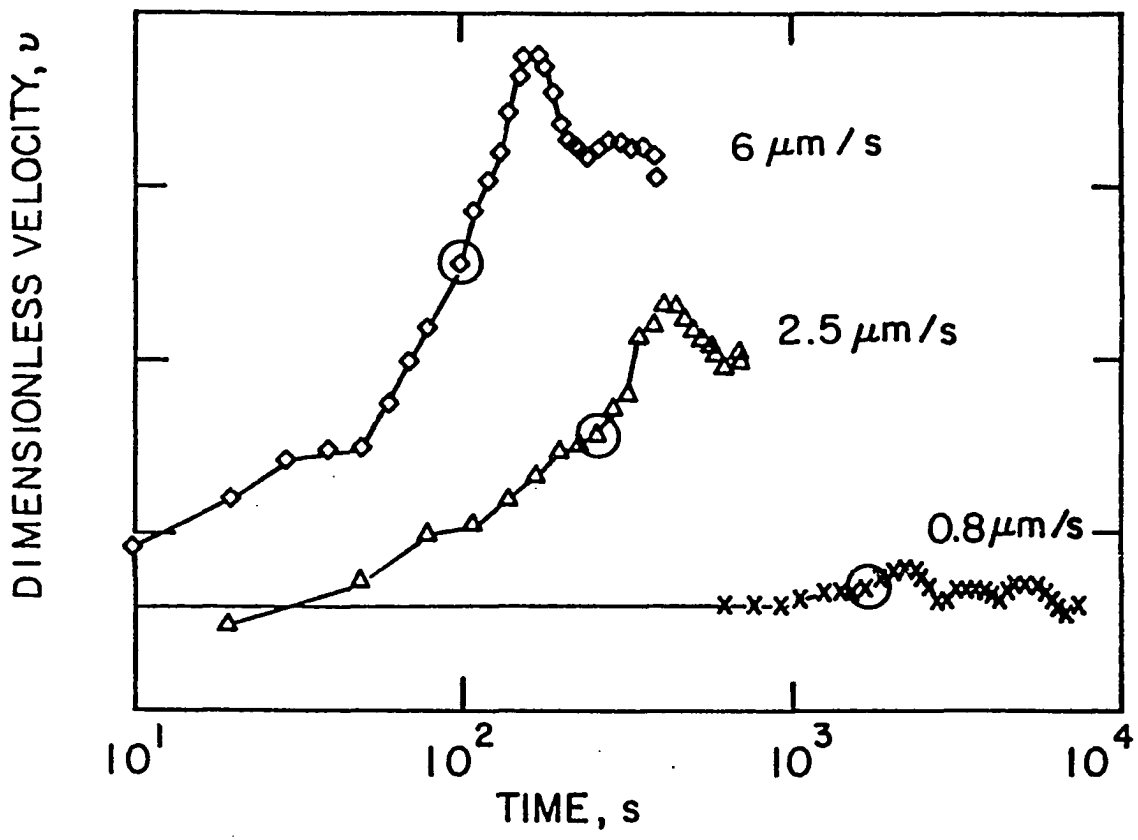

Figure 2. The variation in the dimensionless interface velocity, ν, with time when the external velocity was changed from ν_0 to ν_E. The circles denote the interface velocity and the corresponding time at which the planar interface became unstable

stabilized at $V < V_c$. The velocity was then increased in small steps until the first sign of break up was observed. At each velocity step, a constant velocity was maintained for at least 15 minutes or more to see if the interface became unstable. When a velocity was found at which the planar interface just became unstable, the sample was run at that velocity for a sufficient time to form a periodic cellular structure. The amplitude and wavenumber of this periodic structure were then measured. Next, the velocity was decreased in steps to see if the interface became planar below V_c. A velocity was determined, which was significantly less than V_c, where the cellular to planar transition occurred. Since the cellular structure was found to be stable below V_c, another experiment was carried out in which a planar interface was held just below V_c for a long time. A large amplitude fluctuation in the shape was observed after about three hours. The stability of the interface in the presence of these large amplitude fluctuations was then examined.

RESULTS AND DISCUSSION

Planar Interface Instability

The theoretical analysis of the planar interface instability examines the stability of a planar interface which is initially moving at a constant rate. Experimentally, the study of planar interface instability requires the velocity to be changed from $V = V_o$ to $V = V_E$, where $V_o < V_c < V_E$. Figure 2 shows the actual change in interface velocity when the external velocity was changed from V_o to V_E. Both the interface velocity, V_b, at which the break up was observed and the time, τ_b, required to reach the break-up velocity were found to be functions of V_E.

To examine the critical velocity at which an instability is observed, it is important to keep the sample at a given velocity for a sufficiently long time for the solute and thermal fields to readjust. Thus, when no interface break up is observed, the time of run must be sufficiently long for the interface velocity to equal the external velocity. When a break up of the interface is observed, the time taken by the interface to reach V_b is a function of V_E. This variation in τ_b as a function of V_E was measured, and is shown in Figure 3. The time taken for the interface to reach the break-up velocity was found to be inversely proportional to V_E.

The variation in ν_b as a function of $\nu_E-\nu_o$ is shown in Figure 4, where $\nu = V\Delta T_o/GD$. Although there is a significant scatter in the data, ν_b was found to increase as $\nu_E-\nu_o$ was increased. The lowest

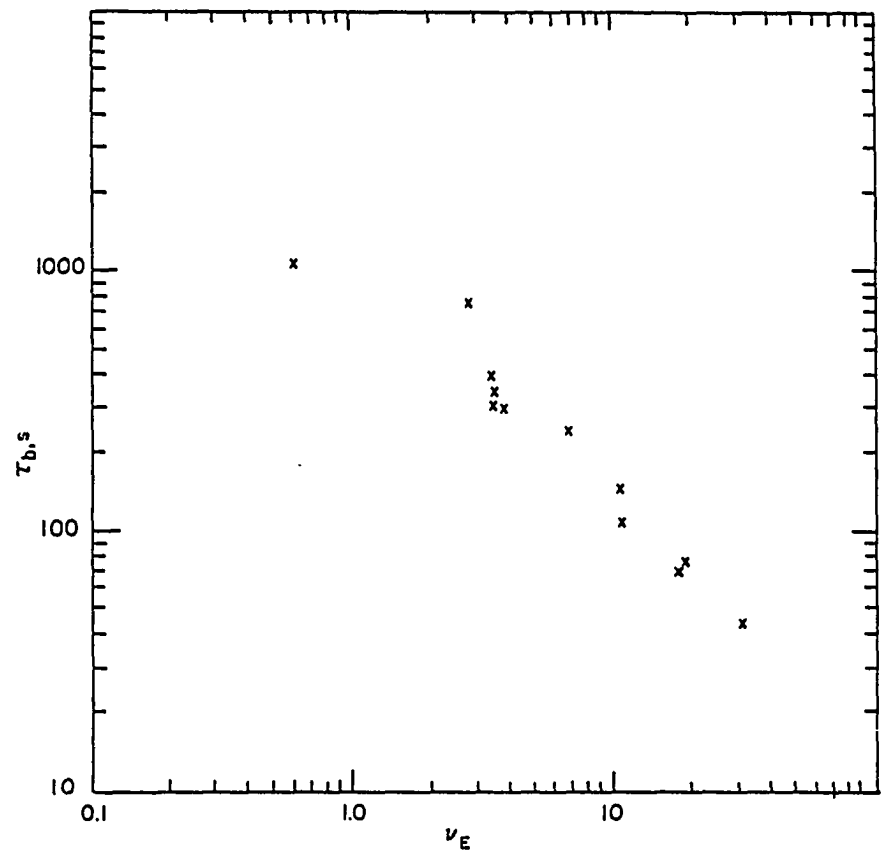

Figure 3. The variation in the time τ_b required for the interface to break up versus dimensionless external velocity, ν_E. The external velocity was changed from ν_0 to ν_E

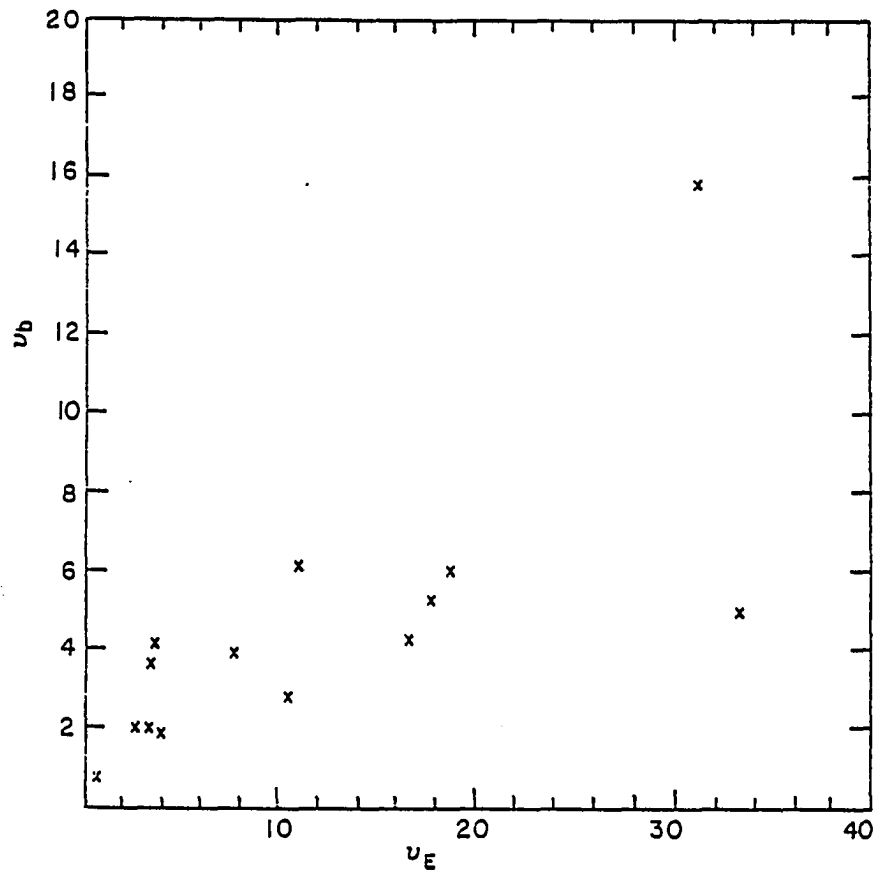

Figure 4. The relationship between the dimensionless velocity, v_b, at the break up and the dimensionless external velocity, v_E

velocity, ν_b, where the break up was observed will be close to the ν_c value. This minimum value of ν_b will be denoted by ν_b^*.

The theoretical value of V_c is obtained under the assumption of a steady-state solute profile that is characteristic of the velocity V_c. Experimental values of the critical velocity, however, were measured under nonsteady-state conditions since the interface velocity was changing when the interface became unstable. When V_E and V_o are close to V_c, this dynamic effect may be negligible. To gain some insight into the difference between the critical values obtained during the steady-state (V_c) and during the dynamic (V_b^*) conditions, we shall now briefly examine the factors that could influence the difference between V_c and V_b^*.

There are three important physical factors that could influence the magnitude of V_b. First, the destabilizing influence of the solute field depends on the composition gradient, G, at the interface. When an appropriate value of G_c is reached, the interface can potentially become unstable. However, a finite time is needed for the perturbed profile to develop and during this time, the interface velocity can increase beyond V_c. For this reason, the value of V_b is found to increase as the value of V_E-V_o is increased.

A second factor which could also influence the value of V_b at large V_E-V_o values is the change in the thermal gradient. Since thermal conductivities of the solid (K_s) and the liquid (K_L) are nearly equal in the succinonitrile system, the thermal balance at the interface would show that the change in thermal gradients in the liquid (G_L) and

in the solid (G_S) at the interface are related by the equation

$$\delta(G_S-G_L) = (\Delta H/K_L)(V_b-V_o) \ , \qquad (4)$$

where δ indicates the change in gradients. Since additional heat of fusion due to an increase in interface velocity needs to be dissipated through the solid, one can obtain an upper limit on the change in average gradient by assuming that the liquid gradient changes negligibly. The maximum change in the average gradient is then given by

$$\delta G = (\Delta H/2K_L)(V_b-V_o) \ . \qquad (5)$$

Thus, for large (V_b-V_o), the weighted average value, G, also increases slightly, which would stabilize the interface to slightly higher values. This effect, however, is small since for $V_b-V_o \simeq 1$ μm/s, the change in gradient is only about 0.1 K/mm. Thus, the maximum change in gradient was less than 3% in our experiments, so that the thermal effects can be readily ignored.

The third factor observed was V_E-V_o small. When this was the case, the change in interface velocity with time was found to be a very slowly varying function, as seen in Figure 2, so that one would not expect a significant change in interface velocity during the time it took to form observable perturbations in the interface shape. However, the interface velocity was still changing so that the concentration gradient in liquid at the interface, G_c, was not equal to

that for a steady-state interface growth at V_b. This difference in G_c at the interface could give rise to some deviation between V_b^* and V_c values. Smith et al. [11] have shown that when the velocity of the interface is suddenly increased, the concentration in the liquid and in the solid at the interface suddenly increases from the steady-state values of C_∞/K_o and C_∞, respectively, where C_∞ is the average composition of the alloy. This increase occurs because the total mass of solute ahead of the planar interface decreases as the velocity is increased. Therefore, solute concentration in the solid must increase from its steady-state value of C_∞. The solute concentration in the liquid will first increase, then go through a maximum, and finally, decrease to its steady-state value of C_∞/K_o. This variation in interface composition will change the value of G_c in the transient regime. If C_L is the concentration in the liquid at the interface when the interface velocity is V_b, then the concentration gradient, G_c^b is given by

$$G_c^b = -(V_b/D)C_L(1-K_o)$$

or

$$mG_c^b = (V_b\Delta T_o/D)(K_oC_L/C_\infty) \ , \qquad (6)$$

and linear stability analysis shows the condition for the planar interface stability (Eq. 19) in the general literature review as

$$-G + mG_c \left[\frac{k^* - V/2D}{k^* - V/2D\ (1-K_o)}\right] - (\Gamma)k^2 = 0 \quad . \tag{7}$$

For low velocities and for $K_o = 0.1$, the term in the large bracket will be nearly unity, so that one may estimate the change in critical velocity by substituting mG_c^b in place of mG_c for the dynamical conditions. This will relate V_c and V_b^* by the following equation:

$$V_c = V_b^* \ (K_o \ C_L/C_\infty) \quad . \tag{8}$$

The actual determination of V_c thus, requires the measurement of C_L. Experimentally, we have determined the displacement Δx of the interface, in a reference system attached to the interface, from its steady-state position to its location at V_b^* when the break up occurred. From this displacement, the change in interface temperature was calculated and the value of C_L was then calculated from the phase diagram. This gave the relationship

$$K_o C_L/C_\infty = 1 - (K_o G\Delta x/m_L C_\infty) \quad . \tag{9}$$

By substituting the above result in Eq. (8), and using the dimensionless velocity ν, one obtains

$$\nu_c = \nu_b^* \ [1 - (K_o G\Delta x/m_L C_\infty)] \quad . \tag{10}$$

For our experimental results, K_o = 0.1, G = 3.76 K/mm, m_L = -3.02 k/wt%, C_∞ = 0.15 wt%, Δx = 0.26 mm, and V_b^* = 0.84, we obtain

$$\nu_c = 1.02 \ . \tag{11}$$

The theoretical value of ν_c from the modified supercooling criterion is given by ν_c = 1, and for the linear stability analysis of Mullins and Sekerka [12], ν_c = 1.03. The experimentally determined value of ν_c is thus, very close to that predicted by the linear stability analysis.

Another experiment was carried out for G = 3.82 k/mm and C_∞ = 0.10 wt% acetone in which a planar interface was established below V_c. The velocity was then increased in steps of 0.05 μm/s, and at each velocity, a sufficient time was allowed to establish the steady-state condition. The planar interface was found to be stable at V = 1.55 μm/s, but it became unstable at V = 1.60 μm/s. This experimental value corresponds to ν_b = 0.87, and it will be close to the theoretical value of ν_c = 1.065 if dynamical effects, as described earlier, were taken into account. These experimental results thus, clearly establish the validity of the linear stability analysis in predicting the critical velocity for the planar-nonplanar bifurcation.

For the experiments described in Figure 2 and a number of other experiments, the initial wavenumber of the perturbation was also determined. To eliminate the effect of grain boundaries, the wavenumbers were measured at interface locations far from any boundaries. The

variation in initial wavenumbers with velocity V_b are shown in Figure 5. It was found that the wavenumbers increased with an increase in the velocity at which the instability was observed. The variation in the critical wavelength, λ_c, with composition and thermal gradient is shown in Figures 6(a) and 6(b), respectively. The experimental value of the wavelength observed at V_b^* is also shown in Figure 6(a) for comparison. The experimental value of the wavelength was found to be significantly smaller than that predicted by the linear stability analysis. The difference between the theoretical and experimental values is so large that it cannot be justified by the dynamical effects discussed previously. A more detailed discussion on the wavenumber selection is given in Section IV of this dissertation.

Planar-Cellular Bifurcation

The stability of a planar interface for finite amplitude perturbations was first examined by Wollkind and Segel [10]. Their results can be expressed by the Landau equation, valid in the immediate vicinity of the bifuraction, which is given by

$$\frac{dA_k}{dt} = a_o(k)A_k - a_1 A_k^3 \quad . \tag{12}$$

The condition, $a_o = 0$, gives the bifurcation point, as predicted by the linear stability analysis. The parameter a_1 is known as the Landau constant. From the Landau equation, it is predicted that a planar interface becomes unstable when $dA_k/dt > 0$, so that it is possible to have an unstable planar interface if $a_o < 0$ and $a_1 < 0$, such that

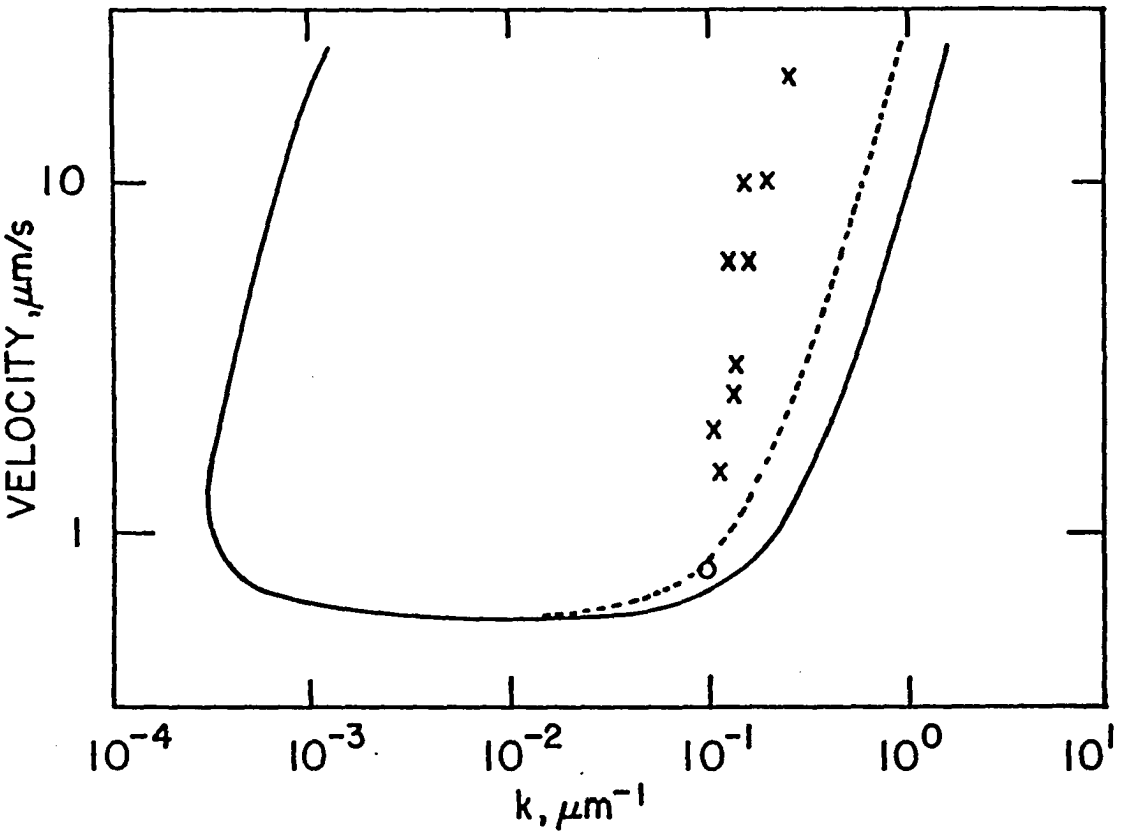

Figure 5. The variation in the initial wavenumbers of an unstable interface with the break up velocity V_b. The solid line is the marginal stability curve and the dotted line represents the wavelengths with maximum amplification rate as predicted by the linear stability analysis of a planar interface. Experimental results are for G = 4.28 K/mm and C_o = 0.35 wt.% acetone. The open circle value is for C_∞ = 0.15 wt.%

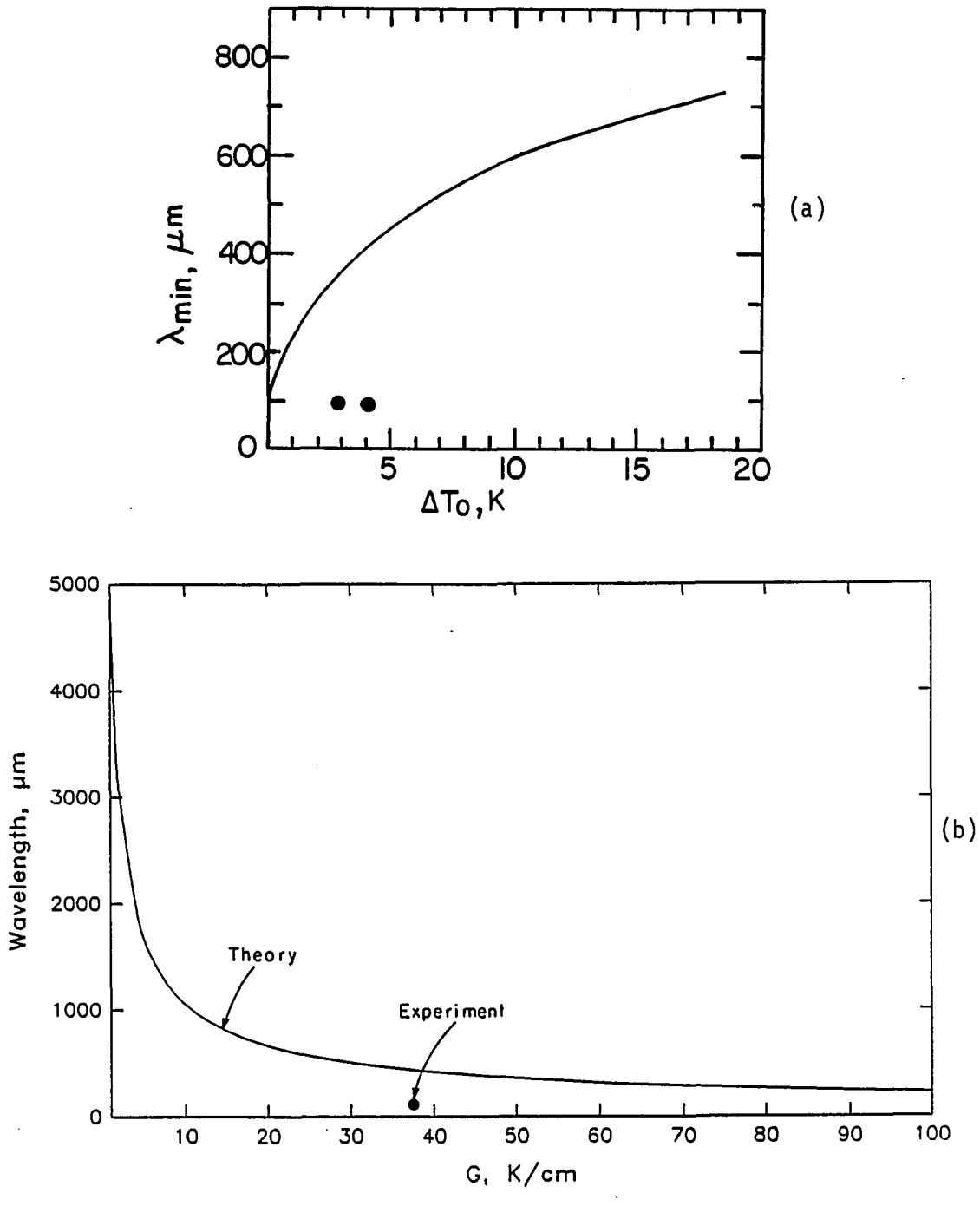

Figure 6. A comparison of the theoretical and experimental values of the wavelength at critical velocity (a) variation with composition and (b) variation with thermal gradient

$dA_k/dt > 0$. This condition is known as the subcritical bifurcation. Subcritical bifurcation means that a planar interface will become unstable at $\nu < \nu_c$ if large amplitude perturbations are present. It also shows that for $\nu > \nu_c$, there is no continuous transition from planarity to small amplitude deformations. Such a continuous transition would, however, be observed if $a_1 > 0$, a condition known as the supercritical bifurcation. For supercritical bifurcation, a planar interface is unstable only for $\nu > \nu_c$.

In order to examine the type of bifurcation that is present in the succinonitrile-acetone system, experiments were carried out in which a planar interface was first established at $V < V_c$. The experimental conditions were as follows: $G = 3.82$ K/mm, $C_\infty = 0.10$ wt% acetone and a steady-state planar interface was established at $V = 0.5$ μm/s. The external velocity was then increased in steps of 0.75, 1.0, 1.25, 1.325, 1.40, 1.45, 1.50, 1.55, and 1.60, and at each velocity, sufficient time was allowed to obtain a steady state. It was found that at $V = 1.60$ μm/s, the planar interface became unstable after 4 minutes. When the first instability was observed, the sample was solidified for a long time until a steady-state cellular array was established. It was found that the amplitude of cells was quite large. The amplitude, thus, increased discontinuously at ν just above ν_c. This indicates that the planar-to-cellular bifurcation is subcritical in the succinonitrile-acetone binary alloy system. For subcritical bifurcation, the large amplitude cells should also remain stable for $\nu < \nu_c$. Consequently, once the cell structure was established at ν just above

ν_c, the velocity was decreased slowly in steps. At each velocity, sufficient time was allowed for the cell amplitude to change. For some velocity range, $\nu < \nu_c$, the cell structure did not change to a planar interface, but remained stable with a slightly different amplitude. The variation in the amplitude with $\nu > \nu_c$ is shown in Figure 7. The cell structures up to $\nu = \nu^+$ had strong cusps, where ν^+ is the subcritical velocity at which the amplitude dropped sharply, i.e., 1.0 μm/s. However, at $\nu < \nu^+$, the cusps disappeared and the amplitude decreased quite sharply. At the lower velocities, $\nu < \nu^+$, the sample was run for about 15 minutes at each velocity. This time was not sufficient for the small amplitudes to decay so that the actual behavior could be more accurately indicated by the dotted line. A similar subcritical bifurcation has recently been reported by de Cheveigne et al. [13, 14] for the planar interface instability in an impure carbon tetrabromide system.

Figure 8 shows the variation in wavelength with velocity. Note that the wavelength increased initially as the velocity was decreased. However, at V = 1.4 μm/s, a tip instability was observed which significantly reduced the wavelength. This tip-splitting continued until V = 1.3 μm/s. Below this velocity, the wavelength again increased as the velocity was decreased until V = 0.9 μm/s. This increase in wavelength occurred by the process of elimination of some of the cells. At V < 0.9 μm/s, the cusps were removed and the wavelength decreased by cell elimination until a planar interface was again established.

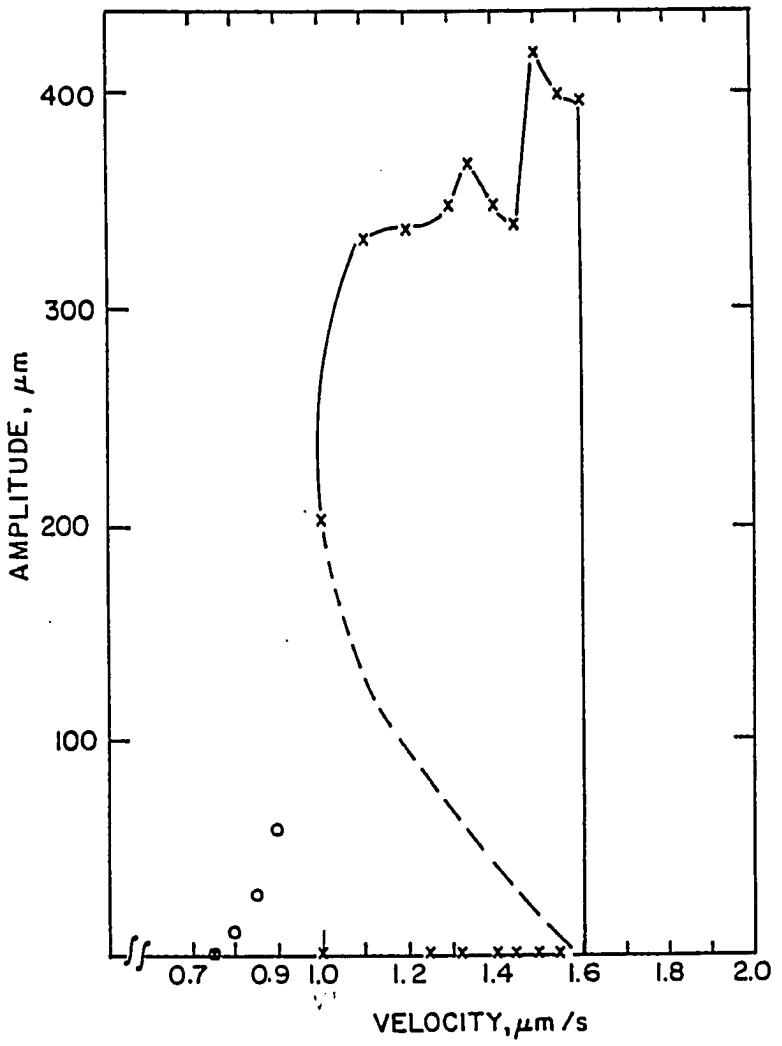

Figure 7. The variation in cell amplitude with velocity for the directional solidification of succinonitrile - 0.10 wt.% acetone at G = 3.82 K/mm. The velocity was initially increased in steps from 0.5 to 1.6 μm/s. After the interface became unstable, the velocity was decreased in steps from 1.6 to 0.7 μm/s. Circles denote smooth interface shapes, without cusps, which were unstable. The dotted line indicates a possible lower amplitude in the subcritical bifurcation curve

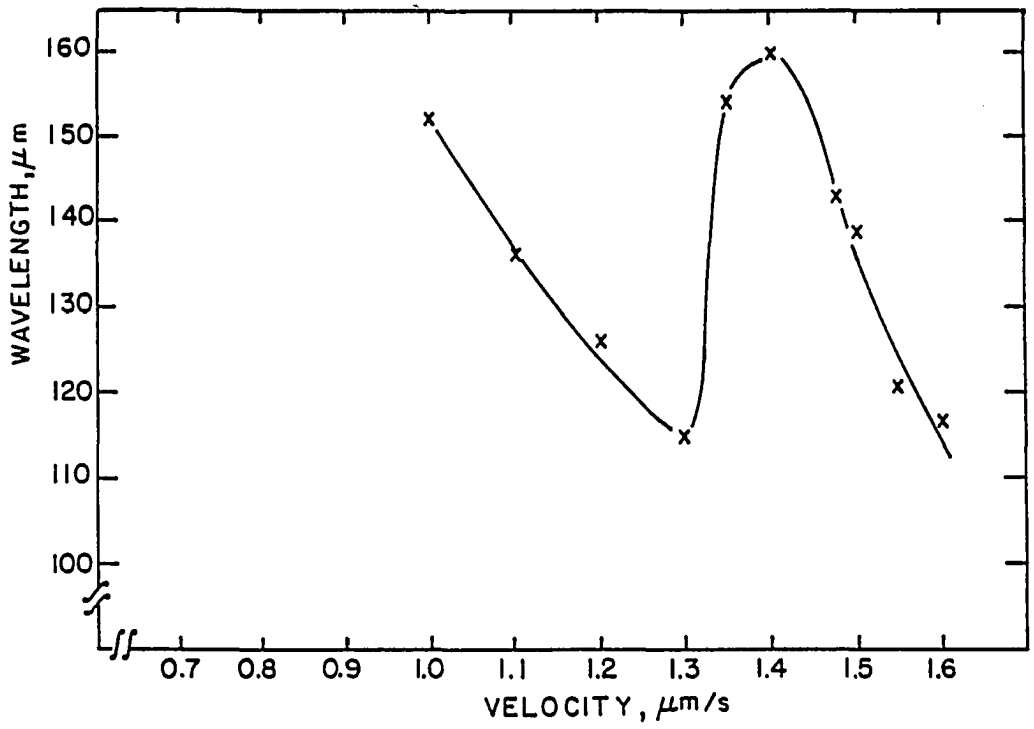

Figure 8. The variation in wavelength with velocity during the subcritical bifurcation of Figure 7

We shall now examine the nonlinear stability analysis of Wollkind and Segel [10] to see the condition for the existence of the subcritical bifurcation. Caroli et al. [15] have given the expansion for a_1 under the condition of small velocities. For equal thermal conductivities of the solid and liquid, the sign of a_1 can be determined from the relationship [15]:

$$a_1 = (4K_o\Delta T_o D\ \Delta S/\gamma V)^{2/3}\ [(K_o^2 + 4K_o - 2)/4K_o] \quad . \qquad (13)$$

Since all the parameters in the first bracket on the right-hand side are positive, the sign of a_1 will be determined by the value of the second bracket, which becomes negative when $K_o < 0.45$. Since $K_o = 0.1$ in the succinonitrile-acetone system, this theory predicts the existence of subcritical bifurcation. In order to check the theory further, it would be desirable to study another solute in succinonitrile in which $K_o > 0.45$. The existence of a subcritical transition has also been predicted by the numerical simulations of McFadden and Coriell [16] and Unger and Brown [17]. Unger and Brown [17] also predicted a second bifurcation close to the V_c where the wavelength suddenly becomes half. Our experimental results show that at $V \simeq 1.3$ μm/s, such a change in wavelength is observed (see Figure 8).

Since our results indicated the presence of subcritical bifurcation, an experiment was carried out in which the sample was held close to, but just below V_c, where a planar steady-state interface was established. For this experiment, the theoretical critical velocity

was 0.55 μm/s, and the experimental velocity was kept constant at 0.50 μm/s where a planar interface was present. After about three hours at this velocity, a finite amplitude perturbation with large wavelength was observed. This perturbation could either be due to fluctuations over a long period of time or due to the cell being a finite width. However, when the amplitude of perturbation became large, the interface became unstable, as shown in Figure 9. The perturbation initiated at the low temperature part of the interface and then, propagated along the interface. Note that the leading part of the interface was always stable.

One may examine this result by considering a very simple model which assumes that for long, large wavelength, the depressed part of the interface could be considered planar with little influence from the interface at a distance from it. At the location where the interface became unstable, the interface temperature was lower so that the equilibrium interface concentration was higher. By measuring the displacement, Δx, the temperature and the composition of the interface were calculated from the equilibrium phase diagram. By using a localized model, the critical velocity for this composition condition was calculated and was found to be 0.41 μm/s, which is slightly below the experimental imposed velocity of 0.5 μm/s. Therefore, instability of the interface was actually to be expected. This long wavelength interface perturbation was predicted by Sivashinsky [18].

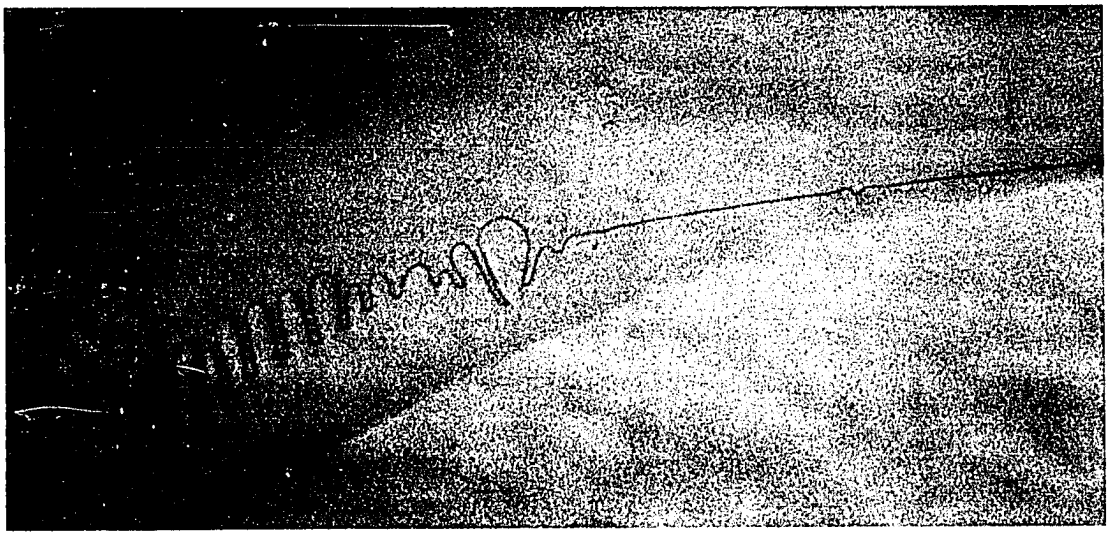

(b)

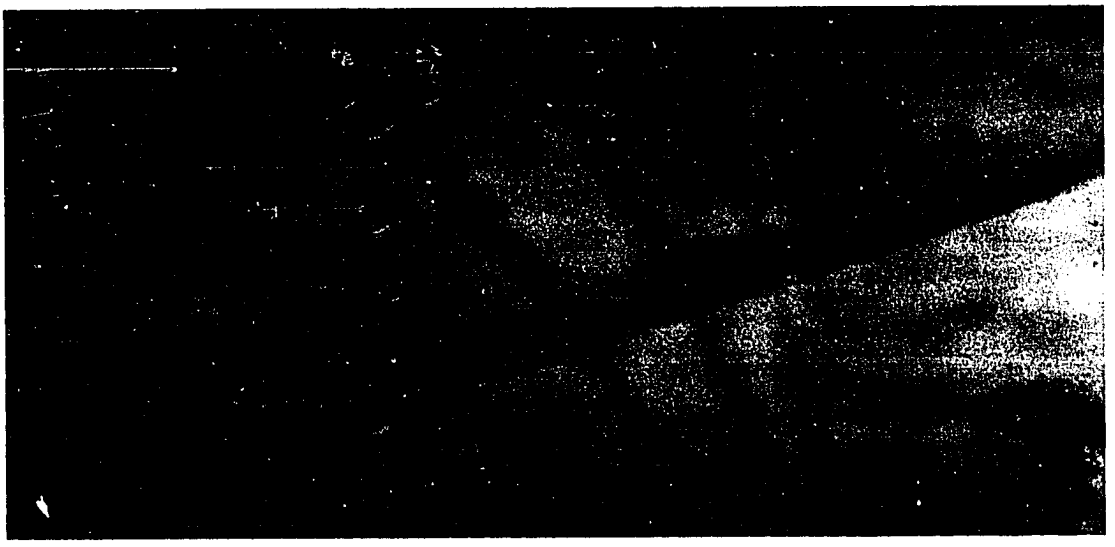

(a)

Figure 9. Long wavelength interface break up. Succinonitrile 0.35 w/o acetone, G = 4.0 K/mm, V = 0.5 μm/s, (a) after 3.6 hrs., (b) after 4.5 hrs., mag. = 57X

CONCLUSIONS

Directional solidification experiments in the succinonitrile-acetone system were carried out under conditions close to the critical conditions for the planar interface instability. It was found that the critical velocity of the interface agrees with that predicted by linear stability analysis. The initial wavenumbers of the unstable interface were significantly larger than those predicted by the linear stability analysis. The planar-to-cellular bifurcation was shown to be subcritical. Due to this large amplitude, perturbations were found to give rise to a nonplanar interface below the critical velocity.

REFERENCES

1. Chalmers, B. "Principles of Solidification"; John Wiley and Sons, Inc.: New York, 1964.

2. Flemings, M. C. "Solidification Processing"; McGraw-Hill: New York, 1974.

3. Sato, T.; Ohira, G. J. Crystal Growth 1977, 40, 78.

4. Shibata, K.; Sato, T.; Ohira, G. J. Crystal Growth 1978, 44, 419.

5. Jamgotchian, H.; Billia, B.; Capella, L. J. Crystal Growth 1983, 62, 539.

6. Kim, K. M. J. Crystal Growth 1978, 44, 403.

7. Holmes, D. E.; Gatos, H. C. J. Appl. Phys. 1981, 52, 2971.

8. Somboonsuk, K.; Trivedi, R. Acta Metall. 1985, 38, 1051.

9. Langer, J. S. Rev. Mod. Phys. 1980, 52, 1.

10. Wollkind, D.; Segel, L. Phil. Trans. Roy. Soc. London 1970, 268, 351.

11. Smith, V. G.; Tiller, W. A.; Rutter, J. W. Canadian J. Phys. 1956, 33, 723.

12. Mullins, W. W.; Sekerka, R. F. J. Appl. Phys. 1964, 35, 444.

13. de Cheveigne, S.; Guthmann, C.; Legrun, M. M. J. Crystal Growth 1985, 73, 242.

14. de Cheveigne, S.; Guthmann, C.; Legrun, M. M. J. de Physique 1986, 47, 2095.

15. Caroli, B.; Caroli, C.; Roulet, B. J. Physique 1982, 43, 1767.

16. McFadden, G. B.; Coriell, S. R. Physica 1984, D12, 253.

17. Unger, L. H.; Brown, R. A. Phys. Rev. 1984, B29, 1367.

18. Sivashinsky, G. I. Physica 1983, 8D, 243.

SECTION II. PATTERN FORMATION: DYNAMIC STUDIES

INTRODUCTION

The phenomenom of pattern formation in systems which are driven far from thermodynamic equilibrium has received an increasing amount of theoretical interest in a variety of scientific disciplines [1-8]. The places where pattern selection is of interest include advancing fronts of redox reactions in metaorites [1], muscle tissue [2, 3], supersonic jets [4], hydrodynamics of turbulent flow [5], and solidification in metallurgical systems [6-8]. The system that will be considered here is the directional solidification of a two-component alloy system. At low velocities, a planar solid-liquid interface exists. As the velocity is increased above some critical value, V_c, the planar interface becomes unstable and reorganizes into a periodic array of cells. If the velocity is increased further, a transformation from a cellular to a dendritic pattern occurs.

When a planar interface is driven just beyond the critical velocity, experimental studies [9-14] show that the steady-state cellular structure which emerges has a definite wavelength and amplitude whose magnitudes depend on the value of the steady-state velocity. Theoretical models, based on the solvability condition, predict a discrete set of wavelengths [15]. The principle which selects a particular wavelength from a set of possible wavelengths is not yet established. It is generally found that the selection process occurs in a highly nonlinear manner [16], which allows the elimination or creation of cells to reach a final spacing.

The process of the evolution of a pattern to the final spacing is what will be studied here. The analysis of interface pattern formation is done by inspection of average amplitude and spacing development with time, and by spacial Fourier analysis of interface profiles observed at progressing times.

EXPERIMENTAL

The alloys used for this study were succinonitrile 0.15 w/o acetone and pivalic acid 0.2 w/o ethanol. The compositions, the growth velocities, and the thermal gradients were carefully controlled and measured in each experimental run. Growth orientations were determined after the run by increasing the growth velocity into the dendrite growth regime. In the dendrite growth regime, the [001] direction is given by the dendrite tip growth direction.

The onset of instability was induced by solidifying the sample at a subcritical velocity for several hours and then, increasing the velocity from a value just below the critical velocity to a value slightly above the critical velocity. Photomicrographs were taken with automatic photographic equipment at 30-second intervals for 120 minutes. The general characteristics of the structures were observed and determined by direct measurements. Spacial Fourier transforms were obtained by digitizing the photomicrographs and inputting the data sets into a VAX computer for analysis. The data sets were smoothed with a 3-point center weighted smoother and the Fourier transform was then preformed using the complete transform. Smoothing of the Fourier transform was done for trend analysis.

RESULTS AND DISCUSSION

The experimental results will be presented in two parts. The first section will present a general examination of the dynamical evolution of the steady-state cell spacings. The second part will examine the Fourier analysis spectrum produced.

Cellular Spacing Evolution, General Characteristics

Figure 1 shows the time-evolution of the interface profile in the succinonitrile-acetone system when an initially planar interface was subjected to V = 0.8 μm/s which is greater than V_c. The initial cellular spacing was small (Figure 1(a)), but it increased with time by eliminating some cells such as those marked "E" in Figure 1(b). During the process of spacing adjustment, the system over-eliminated the cells, and thus, needed to decrease its spacing. This was achieved by the tip-splitting mechanism, indicated by "S" in Figure 1(c), which created additional cells and thus, reduced the spacing. These mechanisms of cell elimination and tip-splitting were also observed earlier by Jackson and Hunt [17].

The variations in the average cell spacing and cell amplitude with time are shown in Figure 2. Average cell spacing was measured at the leading front and the average amplitude was taken as the average distance between the cellular front and the base of the cells. The adjustment of the cell spacing, first by the cell elimination process and then by the tip-splitting process, is quite evident in this figure.

Figure 1. A sequence of micrographs showing the time-evolution of a cellular structure in the succinonitrile - 0.15 wt.% acetone alloy directionally solidified at G = 3.76 K/mm and V = 0.8 μm/s: (a) 11 min., (b) 49.5 min., (c) 59.5 min., and (d) 74.5 min.

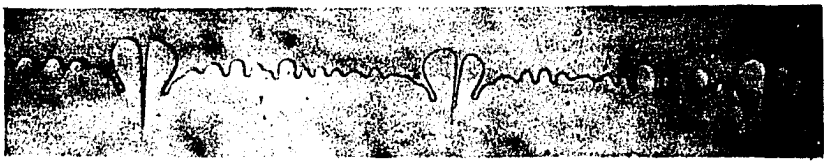

(a)

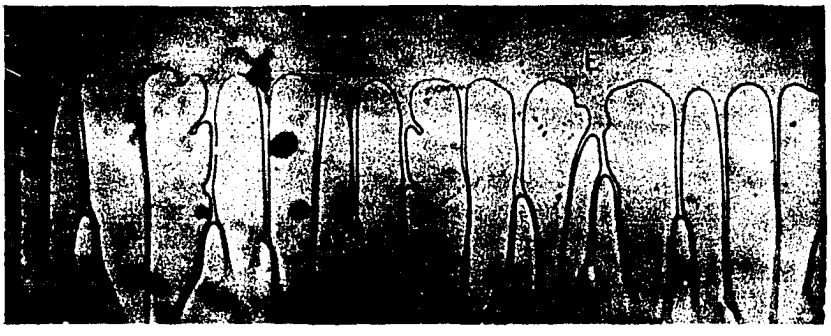

(b)

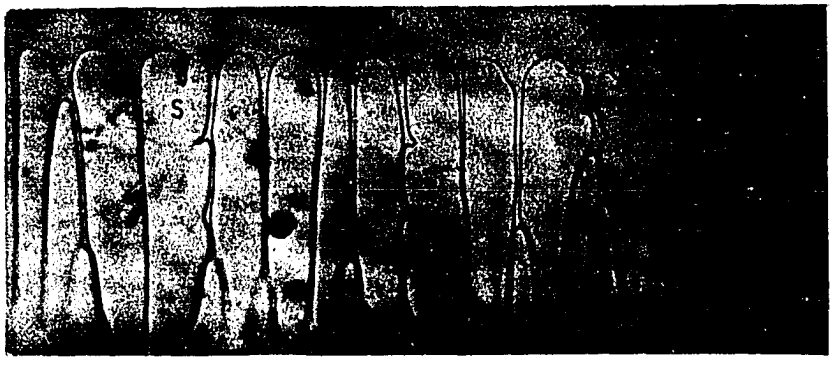

(c)

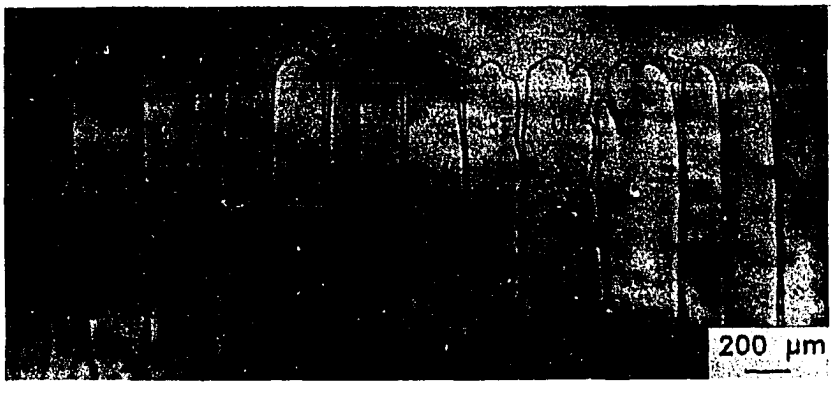

(d)

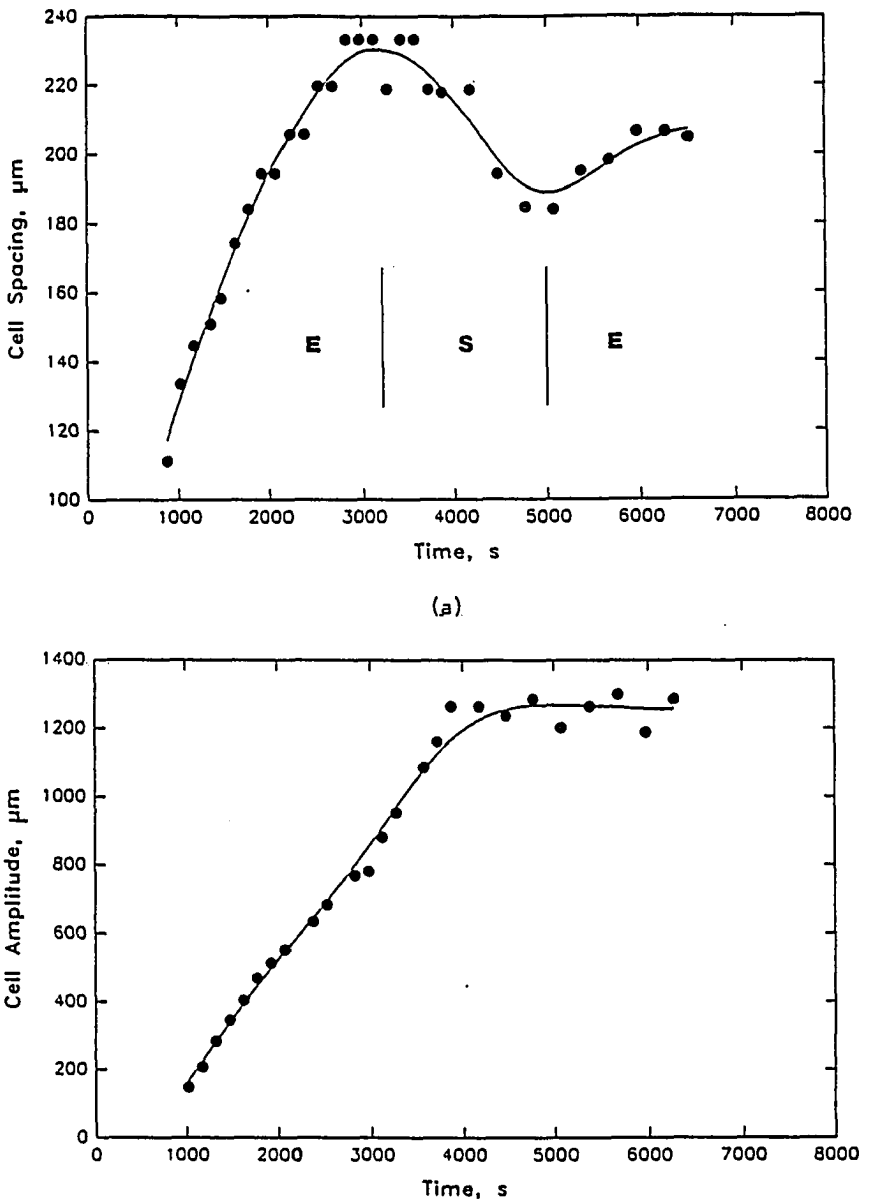

Figure 2. Variations in the average (a) cell spacing, and (b) cell amplitude with time. Alloy composition and solidification conditions are the same as in Figure 1

Note that the dynamics of the tip-splitting process again created more cells so that further cell-elimination occurred, as indicated by the second region "E" in Figure 2. These dynamic processes of cell-elimination and tip-splitting caused a continuous adjustment of spacing even after long times.

Often, one observes a nearly steady-state cell spacing in a given array, except at some locations where a specific cell will show an oscillating pattern. This occurs when the local spacing is only slightly larger than the steady-state spacing. In this case, the system attempts to lower the spacing by tip-splitting. However, the new spacing created by the additional cell is smaller than the steady-state spacing so that one of the cells gets eliminated, which again gives rise to a slightly larger spacing. Thus, the processes of tip-splitting and elimination continue giving rise to an oscillatory growth pattern for that cell, as shown by the letter O in Figure 1(d).

Figure 2(b) shows the variation in amplitude with time. Initially, as the cell spacing increased by the cell-elimination process, the amplitude of cells also increased. The amplitude reached its final value and remained unaltered, while the spacing continued to adjust by tip-splitting and cell elimination.

Figure 3 shows the dynamics of cellular array formation in the pivalic acid-ethanol system. In this system, we shall report the time-evolution of only those cellular arrays in which the growth direction of cells coincided with the heat flow direction for reasons that are discussed below. The initial evolution of the cellular array

Figure 3. A sequence of micrographs showing the time-evolution of cellular structures in the pivalic acid - 0.2 wt.% ethanol alloy solidified at G = 2.98 K/mm and V = 0.5 μm/s. (a) 38 min., (b) 50 min., (c) 60 min., and (d) 125 min.

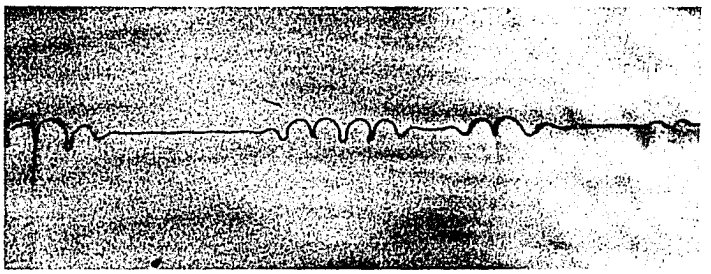

(a)

(b)

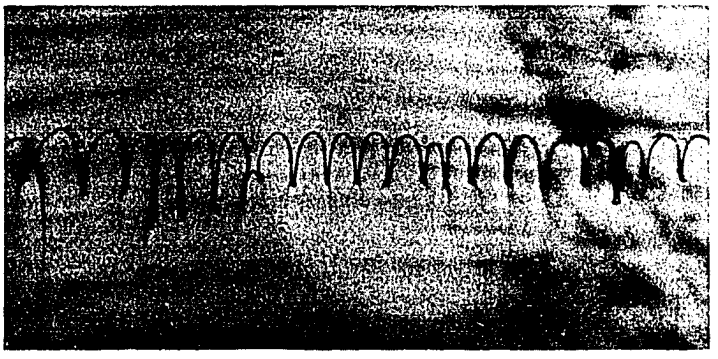

(c)

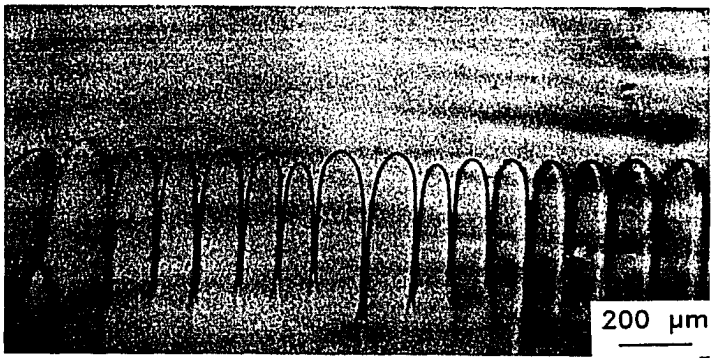

(d)

was very similar to that observed in the succinonitrile-acetone system, i.e., fine spacings observed initially coarsened with time by the cell-elimination process. However, no tip-splitting mechanism was observed in the pivalic acid-ethanol system. This is due to anisotropy of the interfacial energy and the interface kinetics effect which exist in this system [18]. These anisotropy effects make it difficult for the tip to split since it requires the tip orientation to deviate from the favorable growth orientation. In other words, the anisotropy effects stabilize the tip, and thereby, prevent the tip-splitting phenomenon. This observation is reflected in the variation in the average cell spacing and cell amplitude with time, shown in Figure 4. Both cell spacing and cell amplitude increased with time until they reached their steady-state values.

The variation in the cell amplitude with time showed two plateaus. The first plateau occurred when the initial instability, observed at a few locations of the interface, propagated laterally until the entire interface became cellular, as seen in Figures 3(a) and 3(b). Once a uniform cellular pattern was formed, the amplitude of cells increased slightly as the cell elimination began. The amplitude then, remained nearly constant as the unstable cells were being eliminated gradually. Once the initial cell elimination process was completed, further elimination of cells occurred rapidly which caused the amplitude to increase sharply. This cell-elimination process continued until a steady-state cellular spacing was established.

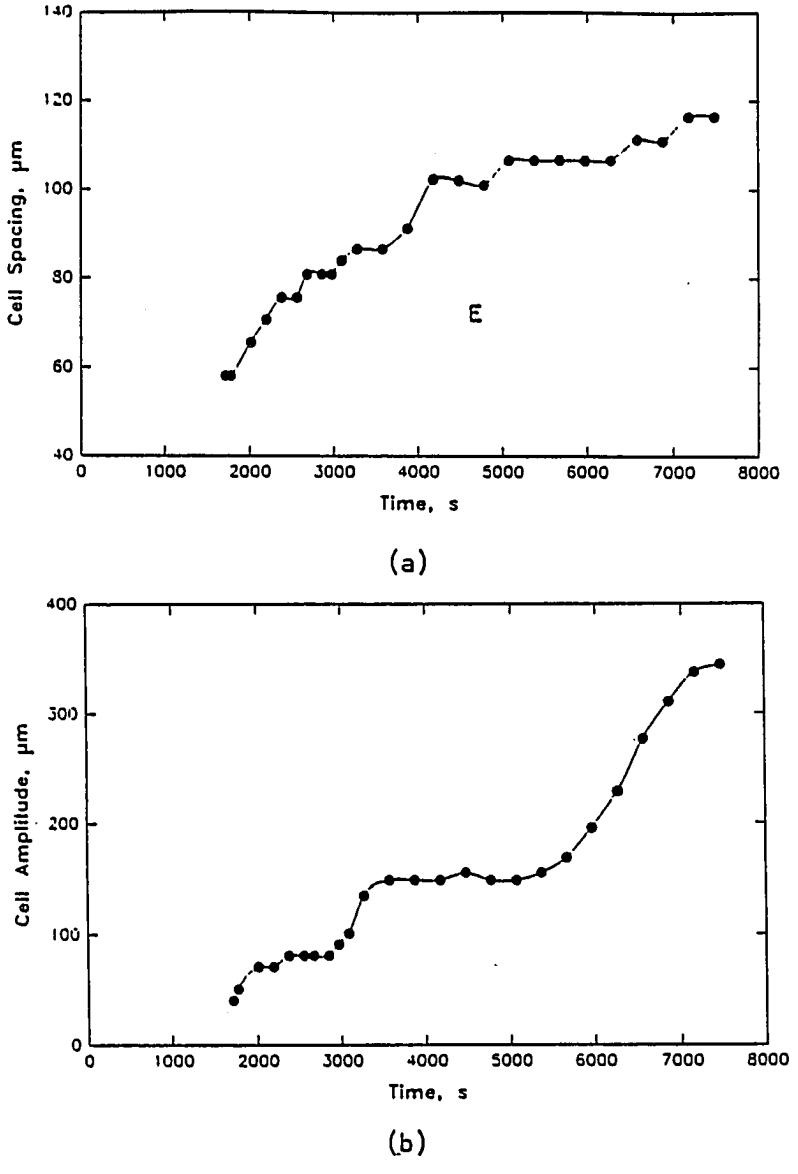

Figure 4. Variation in (a) the average cell spacing, and (b) the average cell amplitude as a function of time. The alloy composition and solidification conditions are those given in Figure 3

In order to examine the manner in which the cell amplitude increased with time, we have measured the location of the cell tips as a function of time. The distance of the cell tips from an arbitrary point in a moving coordinate system (or as viewed under a microscope) was measured, and the results are shown in Figure 5. The tip location, after some initial change, reached a fixed value long before the amplitude reached its steady-state value. This indicated that a further increase in amplitude occurred by the deepening of the cells with time while the tip position remained essentially fixed.

Analysis of Pattern Formation by Fourier Analysis

The above analysis shows that the interface breaks up with a spacing smaller than the final steady-state spacing. It also shows that anisotropy stabilizes a given pattern once the pattern is formed. To give more insight into the dynamics of pattern selection, the Fourier transformed digitized interface patterns will now be examined. The Fourier analysis of pattern formation observed here will be presented in two parts. First, the results observed in the succinonitrile-acetone alloy will be presented, and second, the results from the pivalic acid-ethanol system will be presented. The reason for separating the two studies in this manner is to investigate the effect of anisotropic interface properties on cellular pattern formation. Since succinonitrile has much smaller anisotropy, it is examined first.

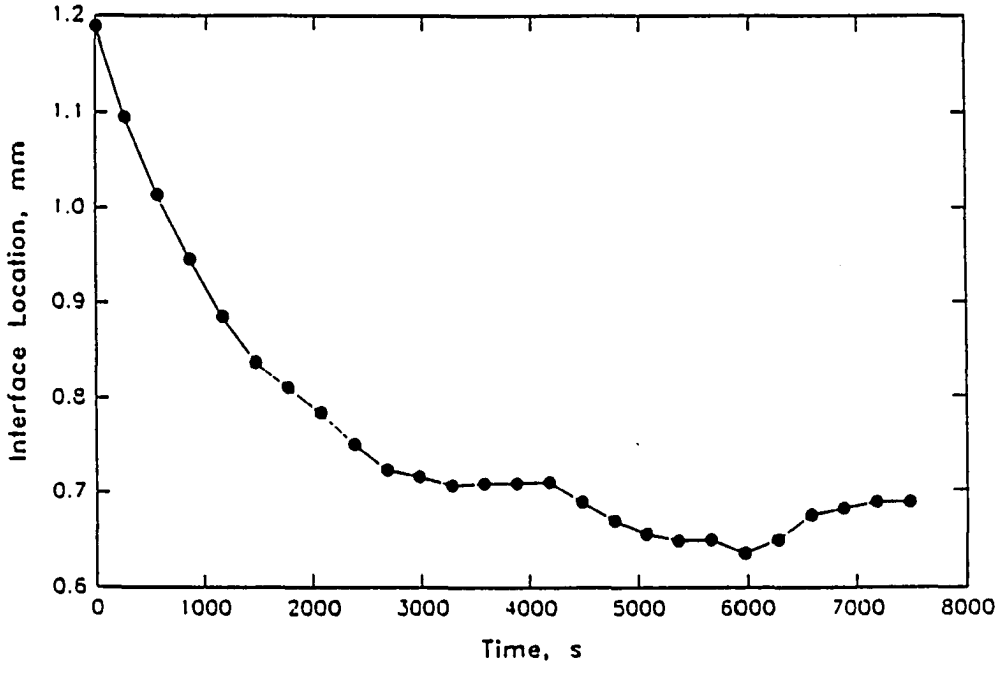

Figure 5. Variation in the location of the interface as a function of time. The alloy composition and solidification conditions are those given in Figure 3

Pattern formation in the succinonitrile-acetone system

The digitized interface patterns are shown in Figure 6. Spacial Fourier transforms of the digitized interface patterns are shown in Figure 7. The initial instability occurs with a peak at the wavenumber of 0.0708 μm^{-1} under the growth conditions stated. There is also a peak at the wavenumber 0.003 μm^{-1}, but it is difficult to track since it is under the bias near the origin. This second peak corresponds to the long wavelength perturbation which can be seen in Figure 1(a). The existence of two characteristic wavenumbers for the initial instability of the interface was also discussed by Trivedi and Somboonsuk [19]. Since the low wavenumber peak disappears in the cellular growth region once the interface is uniformly perturbed, it will not be discussed further here.

In general, the characteristics of the spectrum do not change significantly between 0 and 2 minutes, except that the peak at 0.0708 μm^{-1} shifts to the left. This shift responds to the slight increase in spacing which occurs between the pair of perturbations shown in Figure 1(a). In addition to the shift, small peaks begin to appear at lower wavenumber values. A sharp change in the spectrum occurs between 2 and 3 minutes. It will be shown later that this time corresponds to the onset of nonlinear effect.

Figure 7(b) shows the continued growth of the major peaks from 6 to 10 minutes after the onset of instability. There is some shifting of the peaks, but generally, only peak growth is occurring.

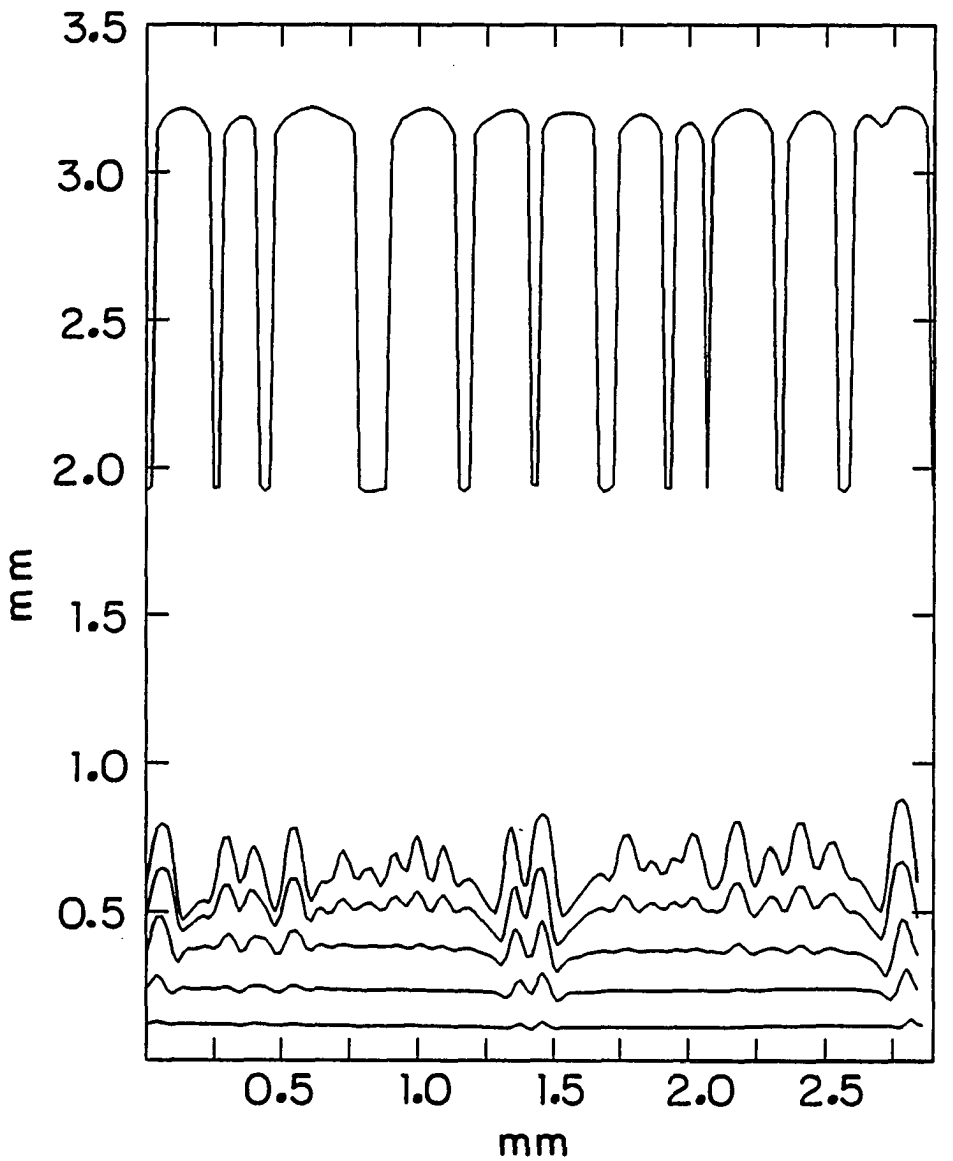

Figure 6. Digitized interface profile as a function of time. Times are 0, 5, 10, 15, 20, and 50 minutes after break up of a planar solid-liquid interface. The break up occurred in succinonitrile 0.15 w/o acetone, with G = 3.76 K/mm and V = 0.8 μm/s

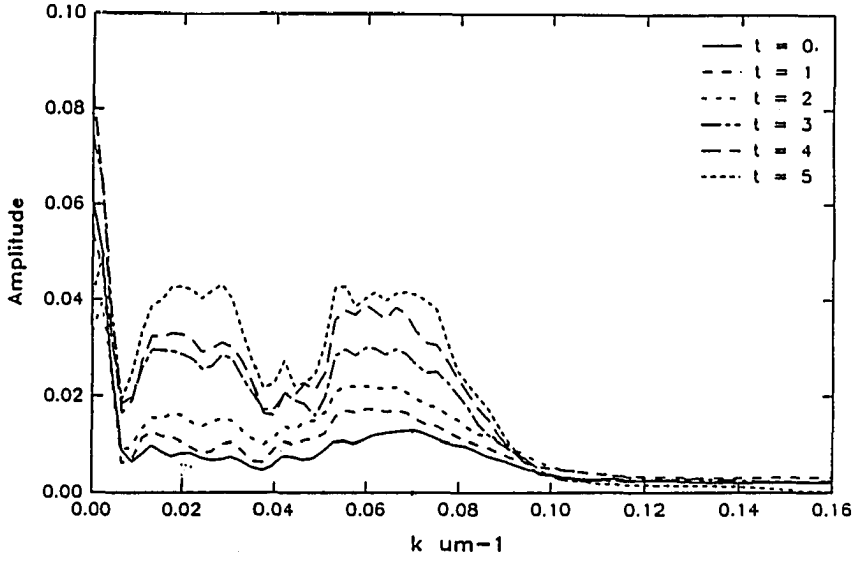

(a)

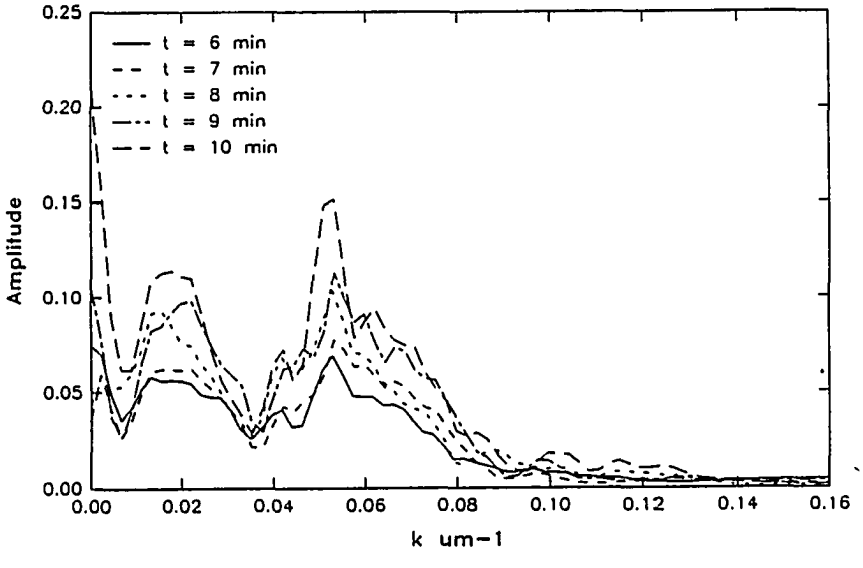

(b)

Figure 7. Fourier transforms of digitized interface profiles. Times are (a) 0, 1, 2, 3, 4, and 5 minutes after planar interface break up, and 6, 7, 8, 9, and 10 minutes after planar interface break up. Alloy and solidification conditions are those given in Figure 6

Figure 8(a) shows the Fourier spectra for t = 0, 5, 10, 15, and 20 minutes after the onset of interface instability. Two important observations can be made from this figure: (1) a finite number of peaks is observed, and (2) the peak which corresponds to the lowest wavenumbers begins, after time to amplify at the largest rate. Figure 8(b) shows the spectra after 50 minutes. Note that one peak is prominent, indicating that the pattern is approaching the steady-state wavelength.

This analysis of the interface shapes gives insight into the dynamical nature of the pattern formation. The initial peak, which forms in the linear region, amplifies more slowly compared to the subsequent peaks which dominate in the nonlinear region. In order to examine the amplification rate of these various wavenumber peaks, the amplitude of particular wavenumbers was plotted as a function of time for three characteristic peaks, as shown in Figure 9. The three wavenumbers which were chosen represent the initial, intermediate, and final wavenumbers of the pattern.

The initial peak, which corresponds to $k = 0.0708\ \mu m^{-1}$, shows a linear behavior up to about 2 minutes. After 2 minutes, sharply nonlinear behavior occurs. At later times, this peak begins to grow more slowly and other peaks become dominate. The intermediate peak ($k = 0.0507\ \mu m^{-1}$) grows at a slower rate than the peak at $0.0708\ \mu m^{-1}$ initially, but then it competes with the final peak ($k = 0.0199\ \mu m^{-1}$) until about 20 minutes. The peak at $k = 0.0199\ \mu m^{-1}$ finally becomes predominate at about 20 minutes. The final peak has a significant

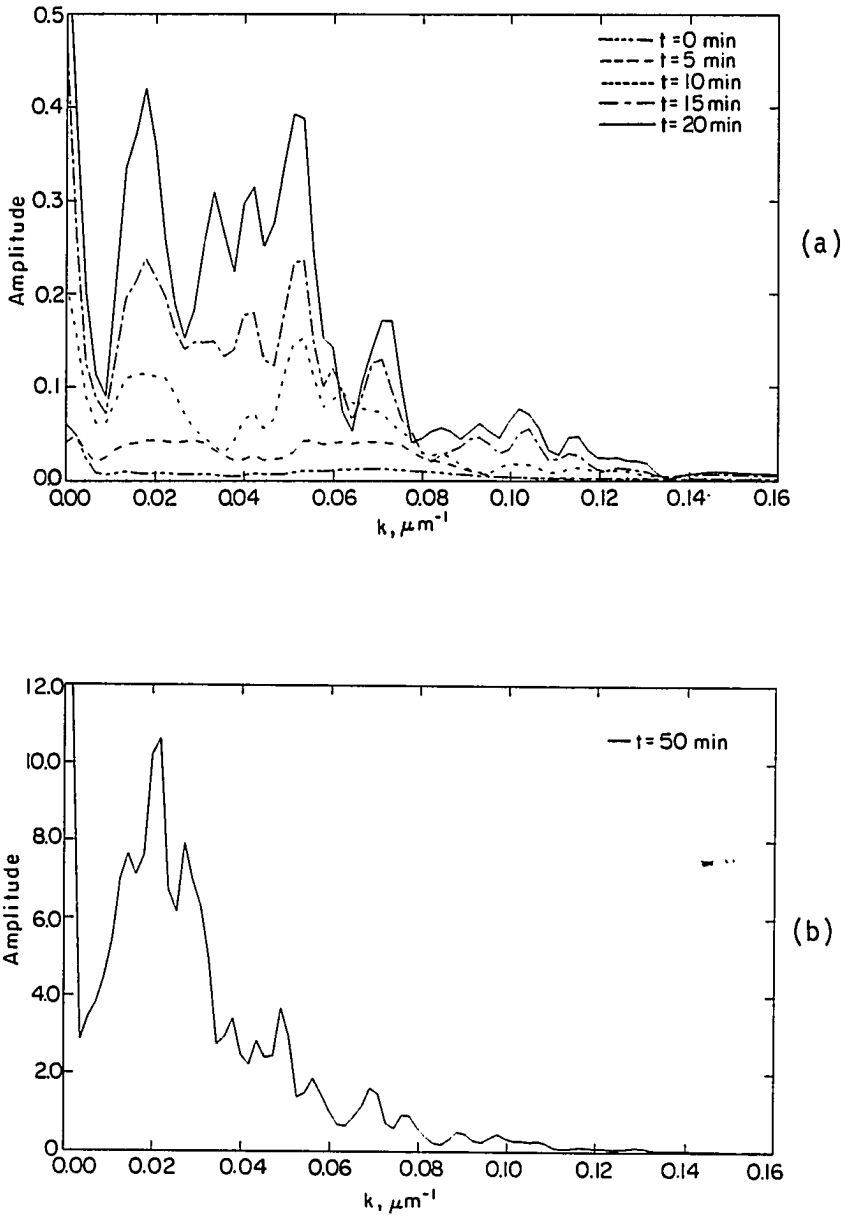

Figure 8. Fourier transforms of digitized interface profiles. Times are (a) 0, 5, 10, 15 and 20 minutes after planar interface break up, and (b) 50 minutes after planar interface break up. Alloy and solidification conditions are those given in Figure 6

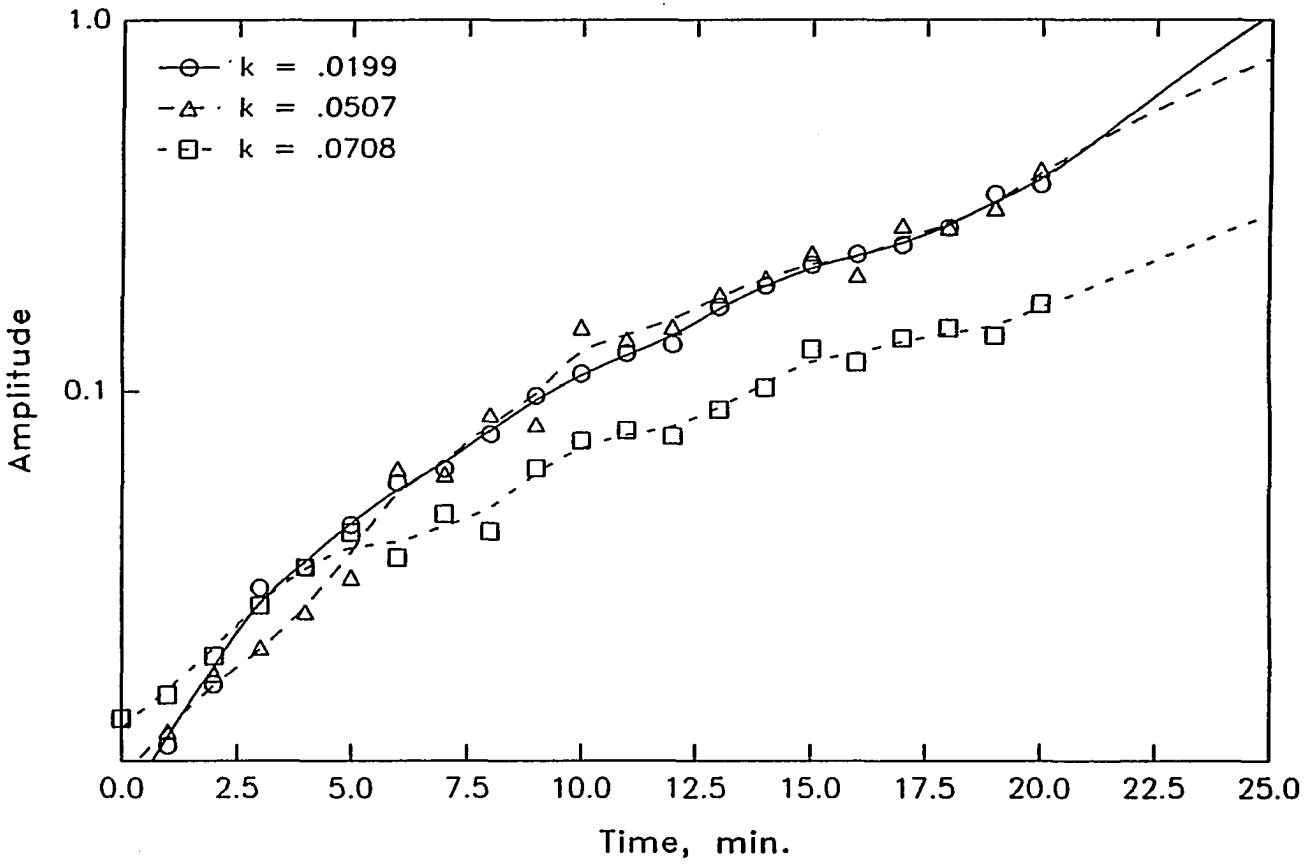

Figure 9. The amplitude of the specified wavenumbers as a function of time. The data was taken from the Fourier transforms generated from the digitized interface profiles. Alloy concentration and solidification conditions are those given in Figure 6

width (Figure 8(b)) which shows that the wavelength selection criterion is not extremely sharp.

The pattern selection process can, therefore, be divided into linear and nonlinear regions. In the linear region, the $k = 0.0708\ \mu m^{-1}$ peak predominates. An increase in the growth rate peaks at lower wavenumbers occurs when nonlinear effects become important. In the early nonlinear region, several peaks coexist for a period of time. At longer times, the lowest wavenumber peak begins to amplify sharply and dominates. This rapid amplification occurs when nonlinear effects allow cell elimination, as shown in Figures 1 and 3, which causes the pattern to decrease the value of the dominate wavenumber.

In these experiments, the initial instability was observed when the external velocity was changed from 0.7 to 0.8 μm/s. In Section I, it was shown that the instability occurs before the planar interface reaches the imposed velocity. Since the instability occurs during the transient period, it is not possible to compare the initial wavenumber observed experimentally here with the results predicted by the linear stability analysis [7].

Pattern formation in the pivalic acid-ethanol system

Figures 10(a) and 10(b) show computer reconstructions of the interface patterns observed in Figure 3. The first observation that is readily evident from these two figures is that the pattern which is formed is more regular than the pattern which was formed in succinonitrile-acetone in Figure 1. From Figures 11-13, it can be seen that at times

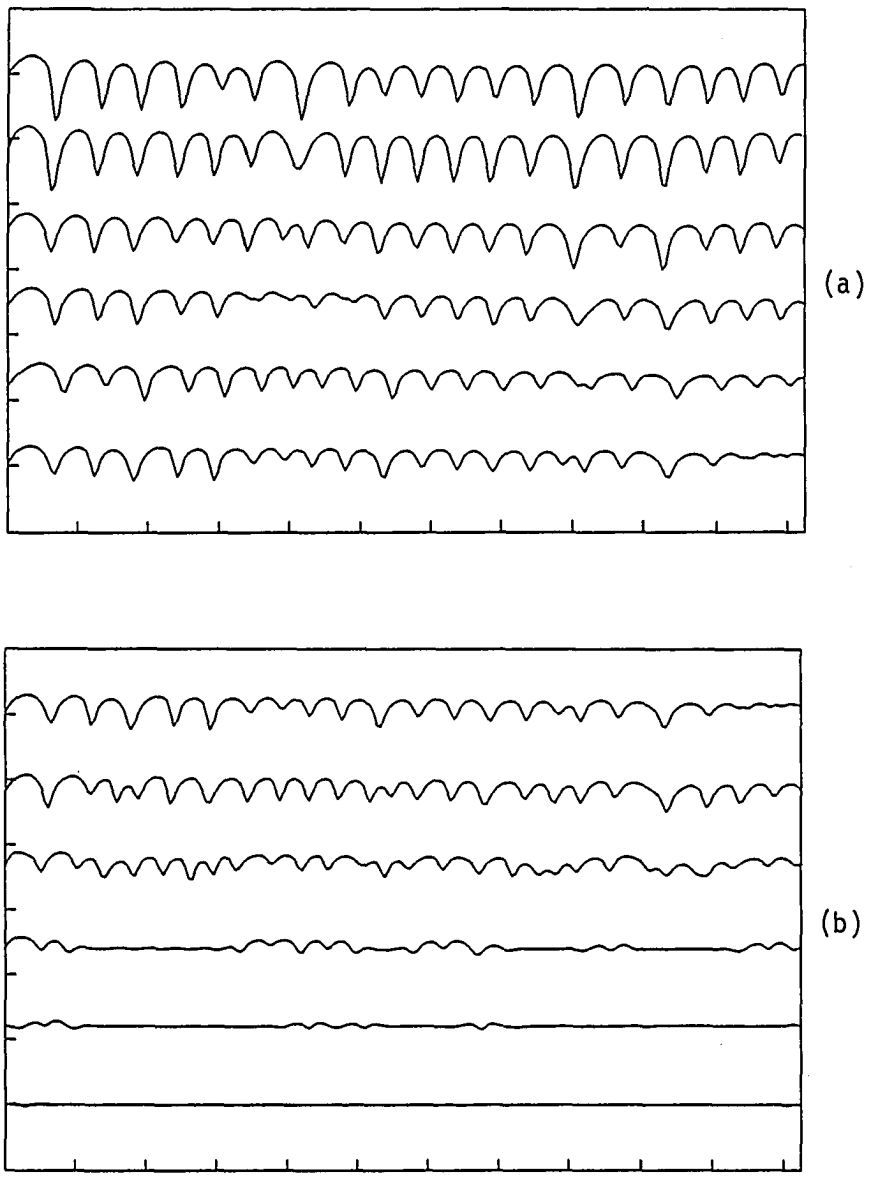

Figure 10. Digitized interface profiles in pivalic acid 0.2 w/o ethanol with G = 2.98 K/mm and V = 0.5 μm/s (a) at times of 0, 10, 20, 30, 40, and 50 minutes after planar break up, and (b) at times of 50, 60, 70, 80, 90, and 100 minutes after planar interface break up

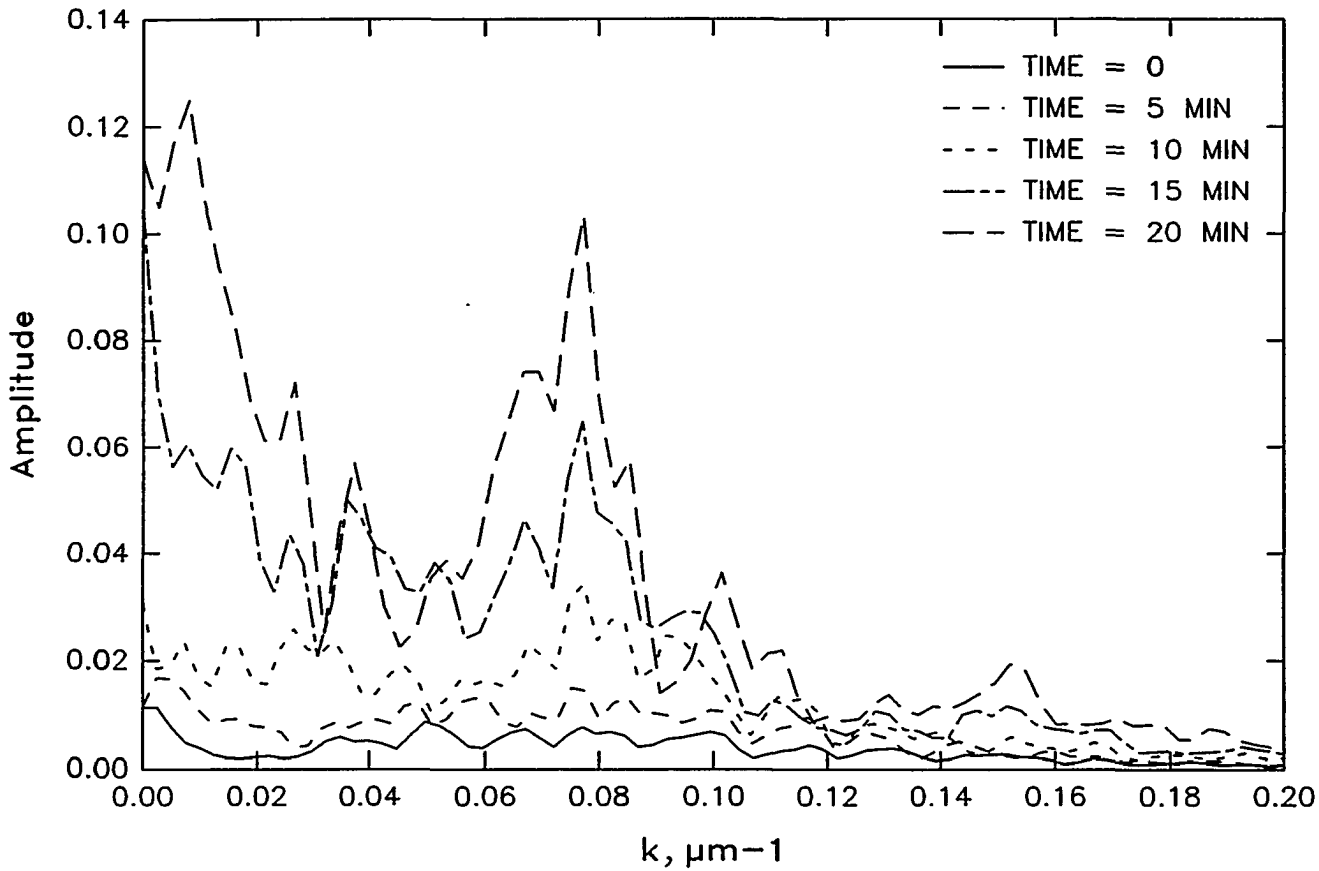

Figure 11. Fourier transforms of digitized interface profiles with the alloy composition and solidification conditions given in Figure 10. Times are 0, 5, 10, 15, and 20 minutes after planar interface break up

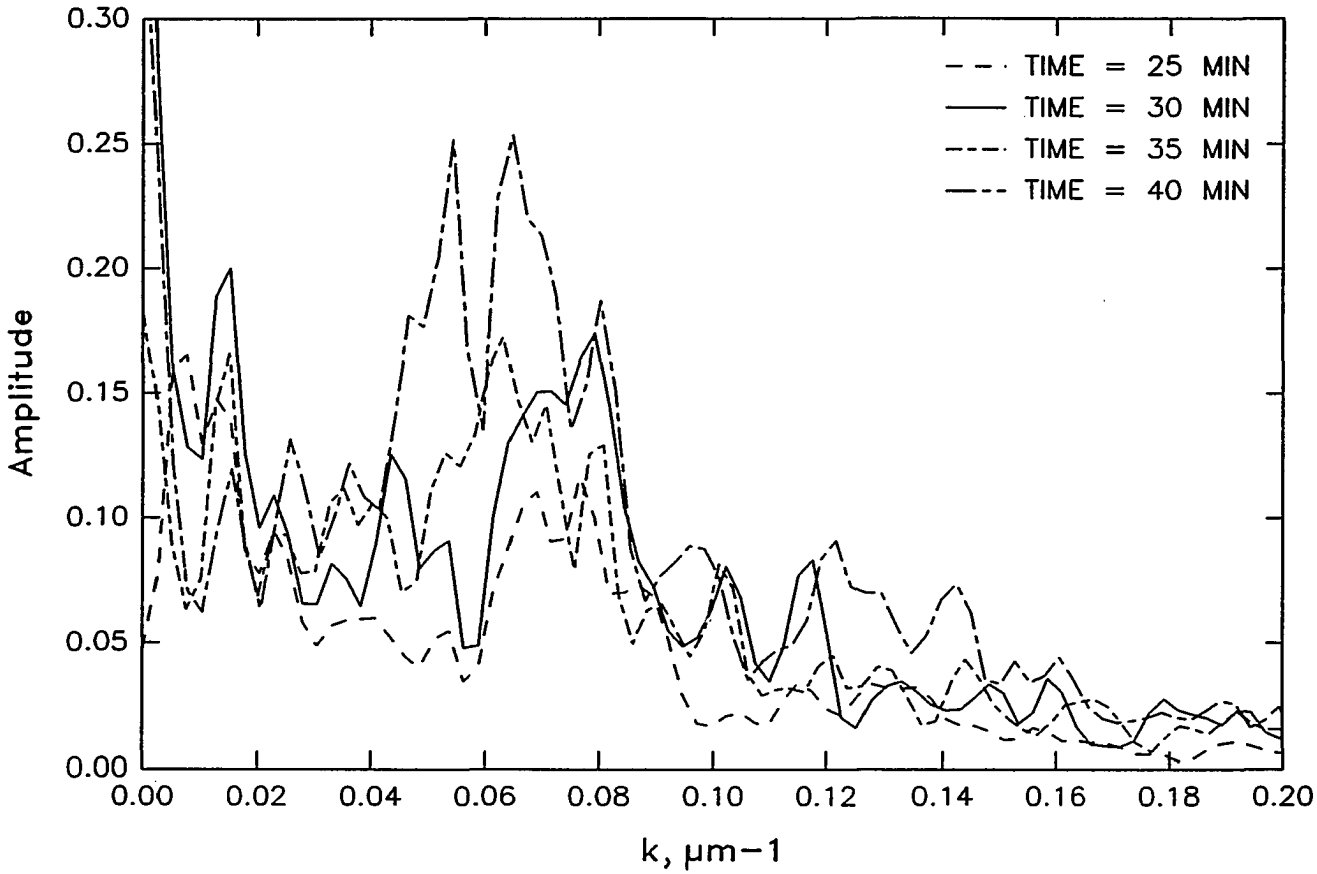

Figure 12. Fourier transforms of digitized interface profiles with the alloy composition and solidification conditions given in Figure 10. Times are 25, 30, 35, and 40 minutes after planar interface break up

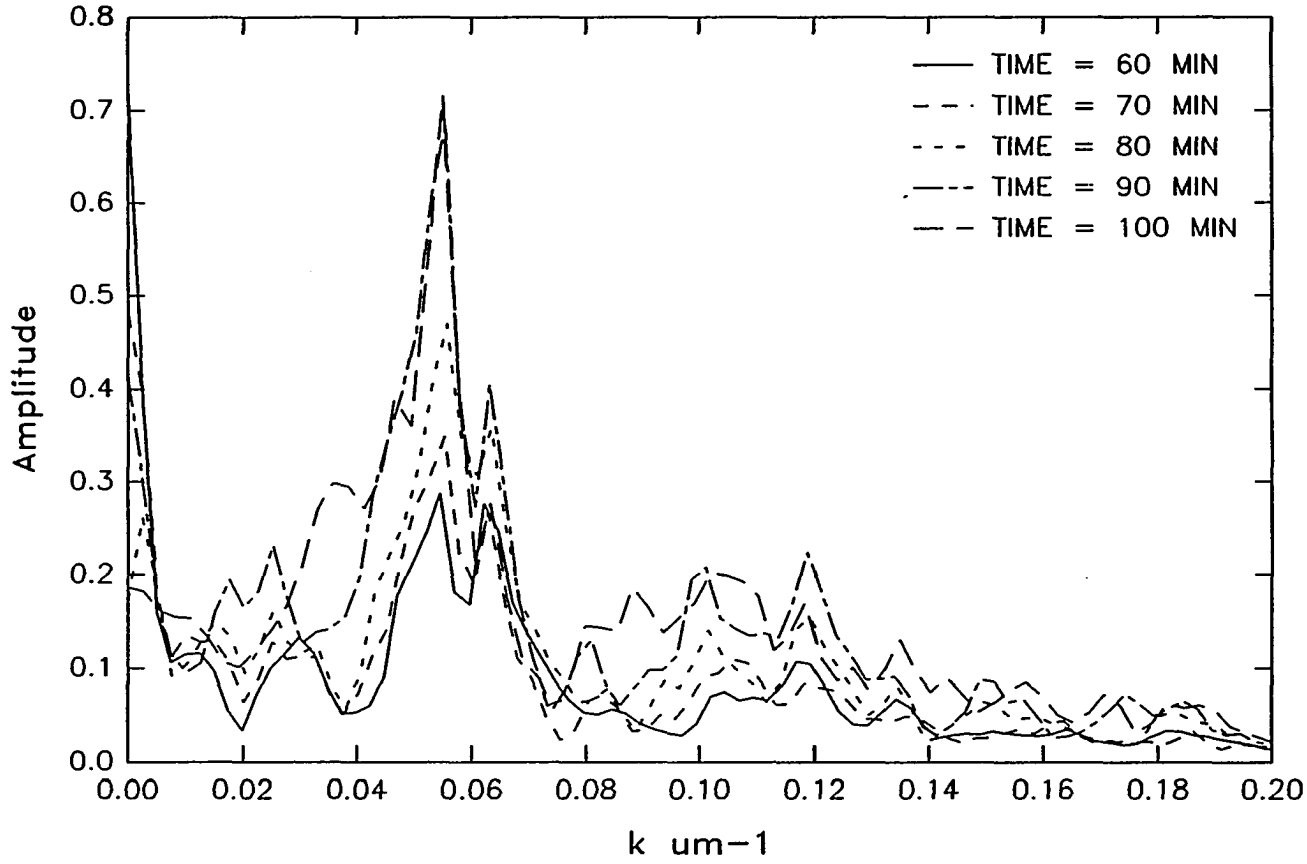

Figure 13. Fourier transforms of digitized interface profiles with the alloy composition and solidification conditions given in Figure 10. Times are 60, 70, 80, 90, and 100 minutes after planar interface break up

between 0 and 25 minutes, the dominant wavenumber is $k = 0.0774\ \mu m^{-1}$. From 25 to 40 minutes, the dominate wavenumber is $k = 0.0632\ \mu m^{-1}$, and for 60 to 100 minutes, $k = 0.0556\ \mu m^{-1}$ is the dominate wavenumber. The amplitudes of these three important wavenumbers have been plotted as a function of time in Figure 14. There are two important points shown in Figure 14. The first of these is the interaction of the three major wavenumbers, as discussed above. Here, as was the case for the succinonitrile-acetone system, the interface forms a pattern with wavenumbers higher than the final steady-state wavenumber. Over time, the interface adjusts to give one dominant wavenumber which amplifies faster than the other wavenumbers. This process was seen in Figures 10a and 10b. The result is a steady-state final wavenumber with a value much less than the initial dominant value. There is a transient region both for pivalic acid-ethanol and succinonitrile-acetone in which several wavenumbers are present. The final dominant wavenumber becomes prominant after some time.

It is important to note that even in the transient period, specific wavenumbers exist. There is not a broad band of transient wavenumbers. Rather, a discrete set of wavenumbers exists in the transient region. This is true for pattern formation processes in both the succinonitrile-acetone and pivalic acid-ethanol systems.

The second point that can be seen in Figure 14 is the length of the linear growth region. It can be seen that the weakly nonlinear growth region persists until about 25-30 minutes after interface break up. As can be seen from Figure 10a, the onset of sharp nonlinearity occurs when

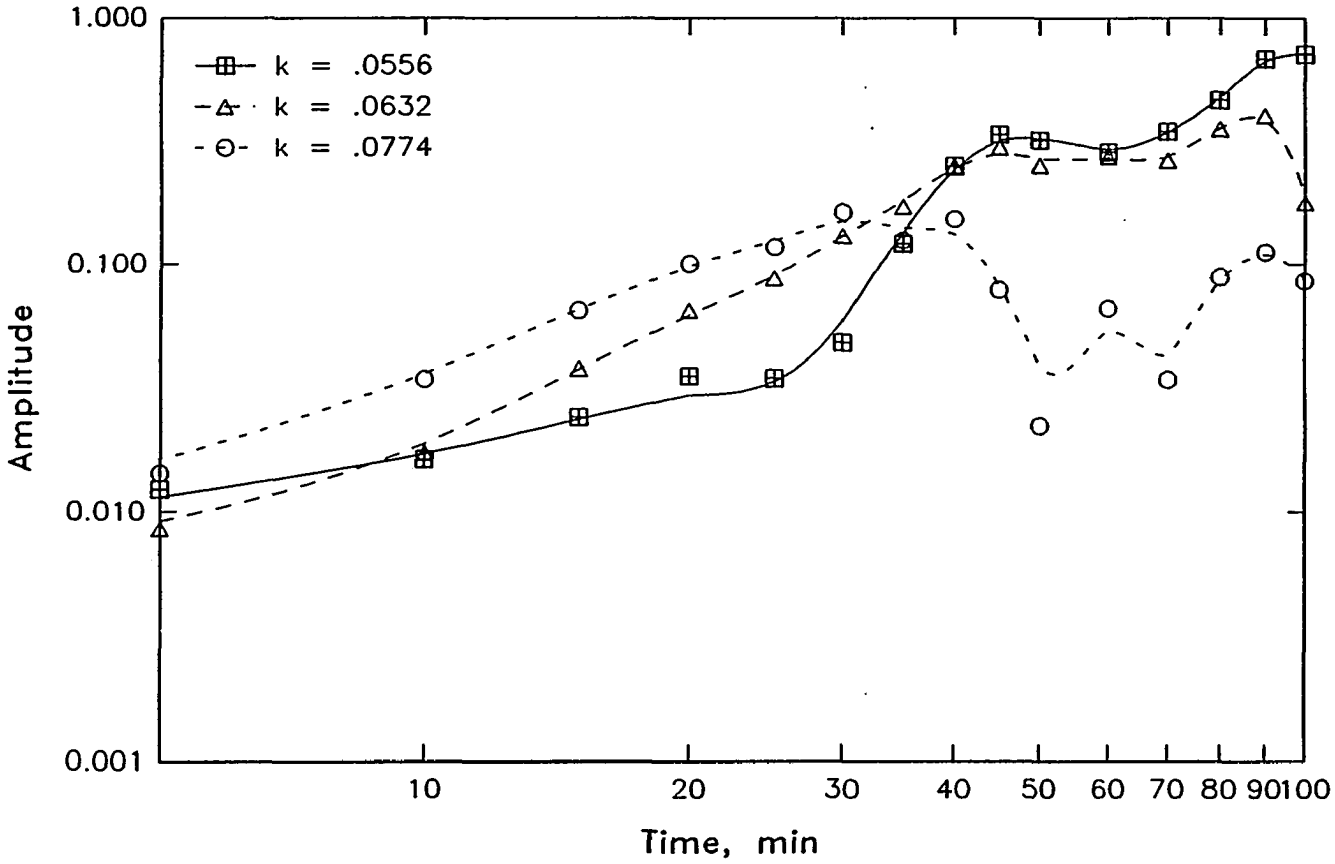

Figure 14. Amplitude variations as a function of time for the specified wavenumbers. Data is taken from the Fourier transforms of the digitized interface profiles with the alloy composition and solidification conditions given in Figure 10

the interface is uniformly perturbed. Once the interface is fully perturbed, then nonlinear effects become important.

As can be seen, the results for the pivalic acid-ethanol pattern formation are qualitatively very similar to those of succinonitrile. There are differences in the pattern formation processes, such as a longer length of a linear region in pivalic acid-ethanol, but the general characteristics in the two systems are very similar. Some of the other growth characteristics which are different between the two experimental systems studied here are discussed in subsequent sections of this work (see Sections IV and V).

CONCLUSIONS

The process of planar interface break up and the dynamical changes in pattern formation which lead to the selection of a steady-state cellular wavenumber were investigated. The time-evolution of a steady-state interface pattern shows that wavenumber selection process occurs in the nonlinear growth region. The spacing and wavenumber formed in the linear region amplifies slowly in the nonlinear region. Therefore, it is overtaken by other peaks. In the nonlinear region, a discrete set of wavenumbers are observed which ultimately leads to selection of a unique wavenumber as steady-state is approached. The final peak in both experimental systems shows a significant width meaning that the wavelength selection criterion is not extremely strong. The patterns formed in the two experimental systems experience similar dynamics in the process of pattern selection.

The effect of anisotropic interface properties on spacing adjustment shows that anisotropy does play a role in pattern selection. The Fourier analysis shows that anisotropy causes the linear growth region to be longer. In other respects, anisotropy did not play a major detectable role when the cell growth orientation was aligned with the [001] crystallographic orientation. In subsequent sections, anisotropy is shown to play a significant role when these two directions are not aligned.

REFERENCES

1. Ortoleva, P. Physica 1984, 120, 305.
2. Glass, L.; Guevara, M. R.; Belair, J.; Shrier, A. Phys. Rev. 1984, 29A, 1348.
3. Oster, G. F.; Odell, G. M. Physica 1984, 12D, 333.
4. Smarr, L. L.; Norman, M. L.; Wirkler, K.-H. A. Physica 1984, 12D, 83.
5. Sharp, D. H. Physica 1984, 12D, 3.
6. Trivedi, R. J. Crystal Growth 1980, 49, 219.
7. Mullins, W. W.; Sekerka, R. F. J. Appl. Phys. 1964, 35, 444.
8. Wollkind, D. J.; Segel, L. A. Phil. Trans. R. Soc. London 1970, 268, 351.
9. Somboonsuk, K. Ph.D. Dissertation, Iowa State University, Ames, Iowa, 1984.
10. Kurz, W.; Fisher, D. J. "Fundamentals of Solidification"; Trans Tech SA: Switzerland, 1984.
11. Trivedi, R. Metall. Trans. 1984, 15A, 977.
12. Somboonsuk, K.; Mason, J. T.; Trivedi, R. Metall. Trans. 1984, 15A, 967.
13. Trivedi, R.; Somboonsuk, K. J. Mat. Sci. Eng. 1984, 65, 65.
14. De Cheveigne, J.; Guthmann, L.; Lebrun, M. M. J. Crystal Growth 1985, 73, 242.
15. Caroli, B.; Caroli, L.; Roulet, B.; Langer, J. S. Phys. Rev. 1986, 33A, 442.
16. Kerszberg, M. Physica 1984, 12D, 262.
17. Jackson, K. A.; Hunt, J. D. Acta Metall. 1965, 13, 1212.
18. Glicksman, M. E.; Singh, N. B. ASTM Tech. Publ. 1986, 890, 44.
19. Trivedi, R.; Somboonsuk, K. Acta Metall. 1985, 33, 1061.

SECTION III. CELLULAR SPACINGS: STEADY-STATE GROWTH

INTRODUCTION

The instability of a planar interface and the subsequent reorganization of the interface shape into a periodic array of cells or dendrites are the key processes which characterize most microstructures of solidified alloys. Once the planar interface becomes unstable, the dynamic process leading to the evolution of a periodic array of cells is a nonlinear phenomenon [1, 2]. The theoretical criterion which determines the wavelength of such a periodic spatial structure has not yet been established. Furthermore, experimental studies in different systems have not yielded a consistent relationship between the steady-state cellular array wavelength and the growth velocity. The major aim of this paper is to present detailed experimental studies to precisely characterize the velocity-dependence of the steady-state cellular wavelength. In subsequent papers [3, 4], the dynamic processes which lead to wavelength selection will be discussed. The theoretical models and the experimental results available in the literature on cellular spacing will now be discussed.

Theoretical Models

Theoretical models on cellular spacings have been developed mainly for steady-state growth conditions and these models have been based on the solution of the steady-state transport equations.

There are three models for steady-state cell spacing: Hunt's model [5], Trivedi's model [6], and Kurz and Fisher's model [7].

Hunt's model [5] considers the sides of a cell to be modeled by the Scheil equation. Since solidification is a free boundary problem, the cells select shapes which are dependent on the immediate growth environment. The cellular shapes that are formed experimentally are somewhat flat behind the tip, but the curvature increases in the tip region. Since modeling using the Scheil equation requires uniform concentration in the direction perpendicular to the growth direction, Hunt's model is not valid near the tip. Thus, Hunt proposes a sphere for the tip. The necessity of replacing the tip with a sphere can be seen when the two-dimensional diffusion problem in the region near the tip is considered. Two-dimensional diffusion is present wherever the interface is curved. Since the curvature is large near the tip, two-dimensional diffusion must be considered.

Hunt's model [5] uses the radius equation of Burden and Hunt [8] to solve for the radius. As in all the models, the radius is not uniquely described unless a selection criterion is used. Hunt uses the principle of minimum tip undercooling as the principle by which the radius is selected. The solution for the primary spacing follows from the analysis after the radius is selected and is given by the following equation:

$$VG^2\lambda_1^4 = -(64\gamma D/\Delta s)[m(1-K_o)C_\infty + K_o GD/V] \ . \qquad (1)$$

Trivedi [6] modified Hunt's model by imposing a parabolic shaped tip rather than a spherically shaped tip. Trivedi also used the

marginal stability criterion as the criterion by which a particular tip radius and consequent spacing were chosen from a family of possible radii. The marginal stability criterion uses the wavenumber selection criterion of Mullins and Sekerka [9] at the point of neutral, or marginal, stability to determine the length of the wave, or radius, present under given conditions. The final spacing is given by Trivedi as

$$\Lambda = (\lambda_1^2 G/\rho K_o \Delta T_o) \tag{2}$$

where

$$\Lambda = 4\sqrt{2}\ \Lambda L/p^2 \ , \tag{3}$$

with

$$\Lambda = \gamma V/2\Delta S D K_o \Delta T_o \tag{4}$$

and $L = 1/2(l+1)(l+2)$ in which $l = 6$ is the harmonic found to be operative for dendrite growth. The value of λ_1 is determined by solving for the velocity at a given peclet number (p), and then, solving for the radius and subsequently, λ_1. It should be noted that this model is expressed by Trivedi [6] to be valid only in the region of the cell dendrite transition.

Kurz and Fisher [7] modeled cells assuming the cell to be fully described as an eliptical shape. Using this assumption for the cell shape and the marginal stability criterion, Kurz and Fisher solve for

the primary spacing in the high and low velocity region. The equations are:

$$\text{For low velocity,} \qquad \lambda_1 = \left[\frac{6\Delta T'}{G(1-K_o)}\left(\frac{\Gamma}{mG_c - G}\right)\right]^{1/2}, \tag{5}$$

$$\text{For high velocity,} \qquad \lambda_1 = 4.3\Delta T'^{1/2}\left(\frac{D\Gamma}{\Delta T_o K_o}\right)^{1/4} V^{-1/4} G^{-1/2}. \tag{6}$$

These three models are compared in Figure 1. As can be seen, all the models predict that the cell spacing will go to zero at the critical velocity. This is the case for all three models, since the radius of curvature, upon which λ_1 is inversely dependent, goes to infinity when a flat interface is approached. In this chapter, it is shown that the cell spacing goes to infinity in just discontinuity at V, the critical velocity.

Hunt's model predicts that the cell spacing first increases, then goes through a maximum and finally, decreases as the velocity is increased beyond the critical velocity, V_c, for planar interface instability. The maximum in cellular spacing can be shown to occur at $2V_c$. Trivedi's model predicts the maximum in cell spacing to occur near the cell-dendrite transition velocity, which is approximately equal to V_c/K_o, with K_o being the solute distribution coefficient. Kurz and Fisher's model is covered in relation to the length of the cellular region in the Results part of this section.

More detailed theoretical models on steady-state cell spacings have been based on an analogy with the nonlocal models of dendritic

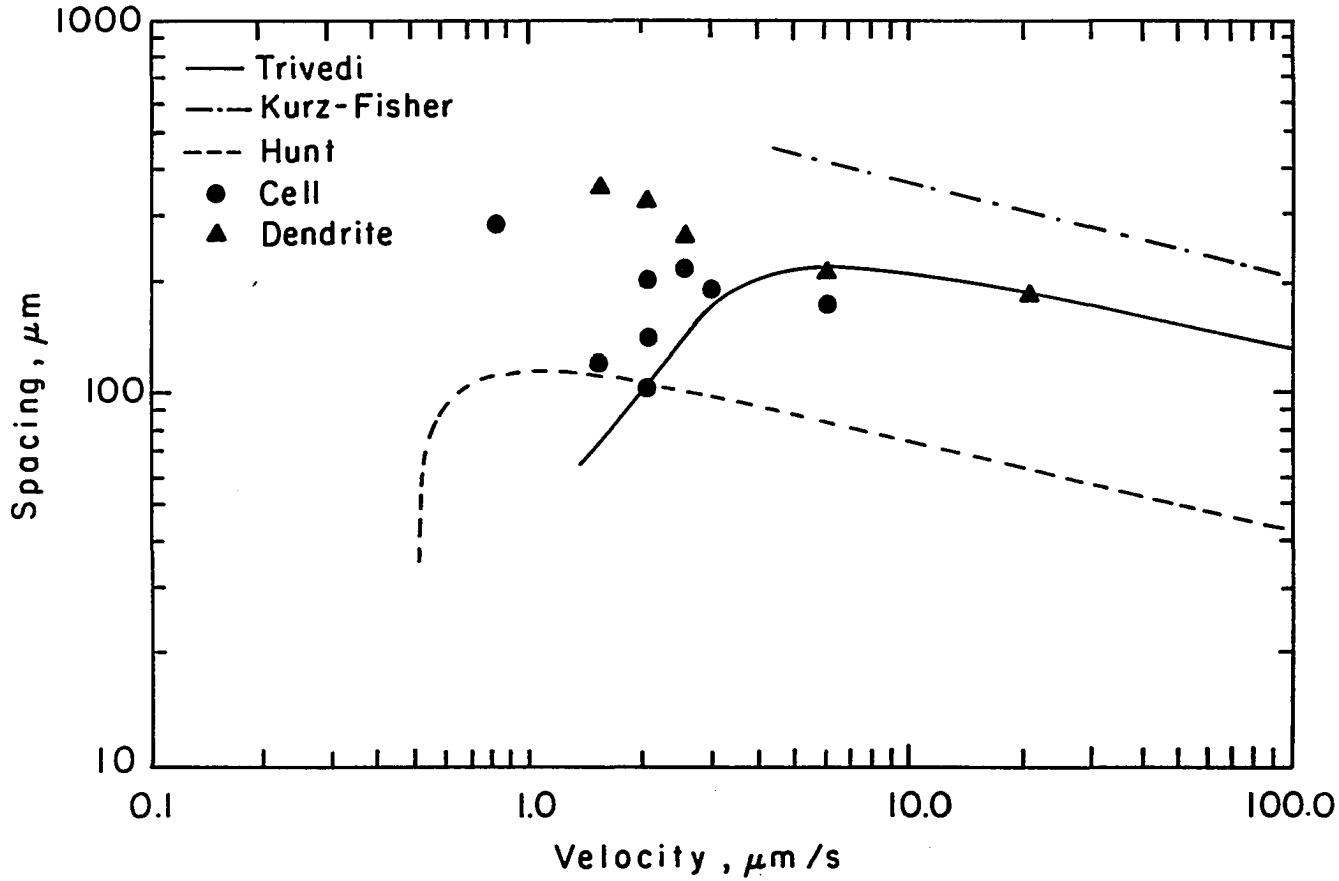

Figure 1. Comparison of the three available cell models. Experimental data from succinonitrile-acetone experiments are included for comparison

growth [10, 11] and with the analysis of viscous fingering in a Hele-shaw cell [12, 13]. These models show that the solvability condition is the key criterion by which the cellular wavelength is selected. By using this approach, Karma [14, 15] has developed a relationship which predicts the cellular and dendritic wavelength as a function of velocity. This relationship was derived for a specific phase diagram in which the solidus and the liquidus lines were parallel, and the actual determination of spacing required numerical calculations. Nevertheless, the general qualitative picture that emerged from this analysis showed that the cellular spacing decreases with an increase in velocity.

Experimental Studies

Experimental measurements of cellular spacings have been carried out by a number of investigators [16-25], whose results appear to show contradictory behavior. One can classify these results into five different groups:

(1) Venugopalan and Kirkaldy [18] reported that no steady-state cellular spacings were observed near V_c in the succinonitrile-salol system.

(2) Sharp and Hellawell [19] studied the variation in cell spacing with velocity in an Al-Cu system by changing the velocity in steps. They found that the cell spacing did not change appreciably as the velocity was increased near the critical velocity.

(3) By using the decantation technique, Rutter and Chalmers [20] and Tiller and Rutter [21] found that cell spacings decreased with an increase in velocity. A similar result was qualitatively reported by Jin and Purdy [22] in Fe-8 wt.% Ni alloys. de Cheveigne et al. [23, 24] and Venugopalan and Kirkaldy [18] studied the variation in cellular spacing with velocity in transparent organic systems, and they found a similar behavior at velocities larger than V_c, although in a very low composition alloy Venugopalan and Kirkaldy [18] observed the cell spacing to increase initially and then, decrease with velocity.

(4) Somboonsuk et al. [16], Mason et al. [25, 26], and Esaka and Kurz [17] found cell spacing to increase with velocity near the cell-dendrite transition velocity in the succinonitrile-acetone system. A similar variation in cell spacing was observed by Bechhoefer and Libchaber [27] in an impure pivalic acid system. Klaren et al. [28] also observed a similar variation in the Pb-Au alloys.

(5) Jamgotchian et al. [29] and Miyata et al. [30] reported that cellular, as well as dendritic spacings decreased with velocity. They, however, observed a sharp increase in spacing at the cell-dendrite transition. Similar results were obtained by McCartney and Hunt [31] who showed that the variation in cell and dendrite spacings with velocity were similar except that the dendrite spacings were higher than cell spacings.

In order to precisely characterize the velocity dependence of the steady-state cellular spacing, detailed experimental studies on cellular spacings were carried out over the entire range of velocities

where cellular structures exist. These experiments were also extended to examine the higher velocities at which dendritic structures readily form so that the changes in spacing at and above the cell-dendrite transition could be characterized completely. Succinonitrile-acetone and pivalic acid-ethanol systems were selected for these experimental studies since they are optically transparent. The existence of steady-state growth conditions can, therefore, be ascertained readily. These experimental results were then compared with the existing theoretical models and also with previously reported experimental results in other systems.

EXPERIMENTAL

Experimental studies were carried out on directional solidification equipment [32, 33] initially in the succinonitrile-acetone system since all the thermophysical properties of this system have been measured quite precisely [34]. Since the solid-liquid interfacial energy of succinonitrile is nearly isotropic [34, 35], experiments were also carried out in another system which exhibits significant anisotropy in the solid-liquid interfacial energy. For this purpose, the pivalic acid-ethanol system was chosen. Glicksman and Singh [35] have shown that pivalic acid has about 5% anisotropy in interfacial energy. Experiments shown later in Section V on cellular growth also show that a significant kinetic anisotropy was present in this system [4]. In order to compare the cellular spacing variation with velocity in succinonitrile-acetone and pivalic acid-ethanol systems, only those cells which grew along the heat flow direction were considered in this study.

The experimental conditions used for the directional solidification runs on the two systems are summarized in Table 1. The compositions and temperature gradients were selected such that the critical velocities for the planar interface instability were about 0.5 m/s for both the systems. In all these experiments, the initial velocity was first maintained at a constant value at which the planar interface was stable. The velocity was then increased rapidly to the desired value. The sample was solidified at this velocity for a sufficiently long time to ensure that steady-state conditions had been

Table 1. Conditions used for the directional solidification experiments

	Succinonitrile-acetone system	Pivalic acid-ethanol system
Solute content, wt.%	0.15, 0.35	0.076
Temperature gradient, K/mm	3.76	2.98
Initial velocity, μm/s	0.5	0.08
Velocity range, μm/s	0.8 - 20.0	0.5 - 20.0

established. This experimental approach is to be distinguished from the approach in which the velocity is increased continuously or in very small increments. This is an important consideration [3], which has generally been ignored, since these two types of approaches may yield an entirely different set of cell spacings at a given velocity [3, 28, 36].

RESULTS

Figure 2 illustrates the effect of velocity on the steady-state cellular structures in pivalic acid-0.076 wt.% ethanol system under a constant temperature gradient condition of 2.98 K/mm. As the velocity was increased above 0.5 μm/s, both the wavelength and the amplitude of the cells decreased. With further increase in velocity, the cellular spacing and amplitude increased sharply at some velocity, as seen in Figure 2c. After this sudden increase, the cell spacing again decreased gradually with an increase in velocity (Figure 2d). The variation in cell spacing with velocity is shown in Figure 3a. Similar results were also obtained in a succinonitrile-0.35 wt.% acetone binary alloy system and these results are shown in Figure 3b.

Figure 3 shows that both cellular and dendritic structures coexist within a finite band of velocities. In this region, when an experiment was repeated several times, cells were observed in some experiments and dendrites in other experiments. These cellular and dendritic structures were observed under identical experimental conditions, as shown in Figure 4. Frequently, cells and dendrites were observed to coexist in the same experiment, and these results are shown in Figure 5. For both these cases, the dendrite spacings were always larger than the cell spacings. A change in the shape of the tip was also observed as cells transformed to dendrites. Experiments were extended into the region where only dendritic structures were stable and Figure 6 shows such a dendritic structure in

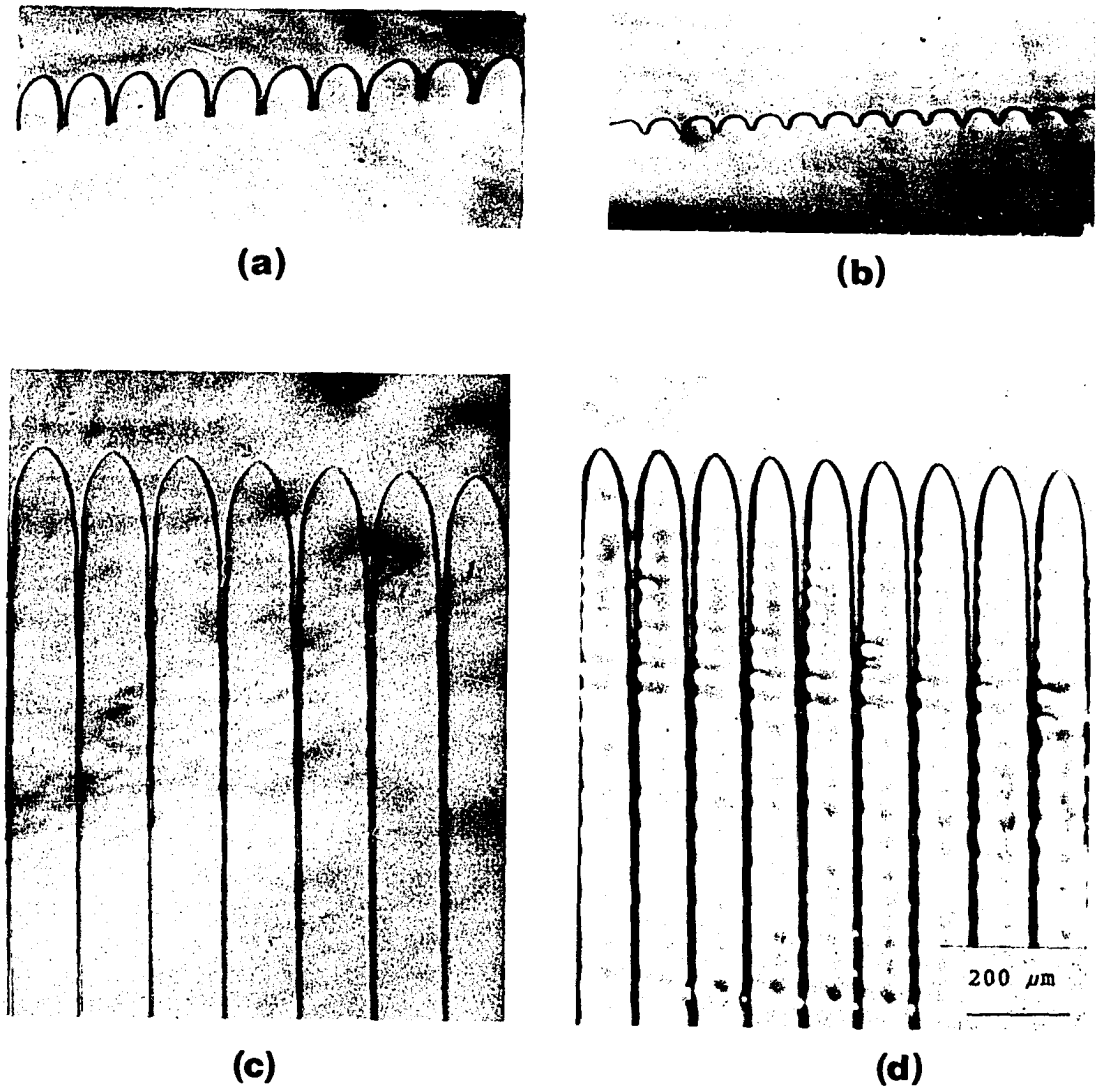

Figure 2. Steady-state cellular structures observed in the pivalic acid - 0.76% ethanol alloy at growth velocities of (a) 0.5, (b) 1.0, (c) 3.0, and (d) 7.0 μm/s

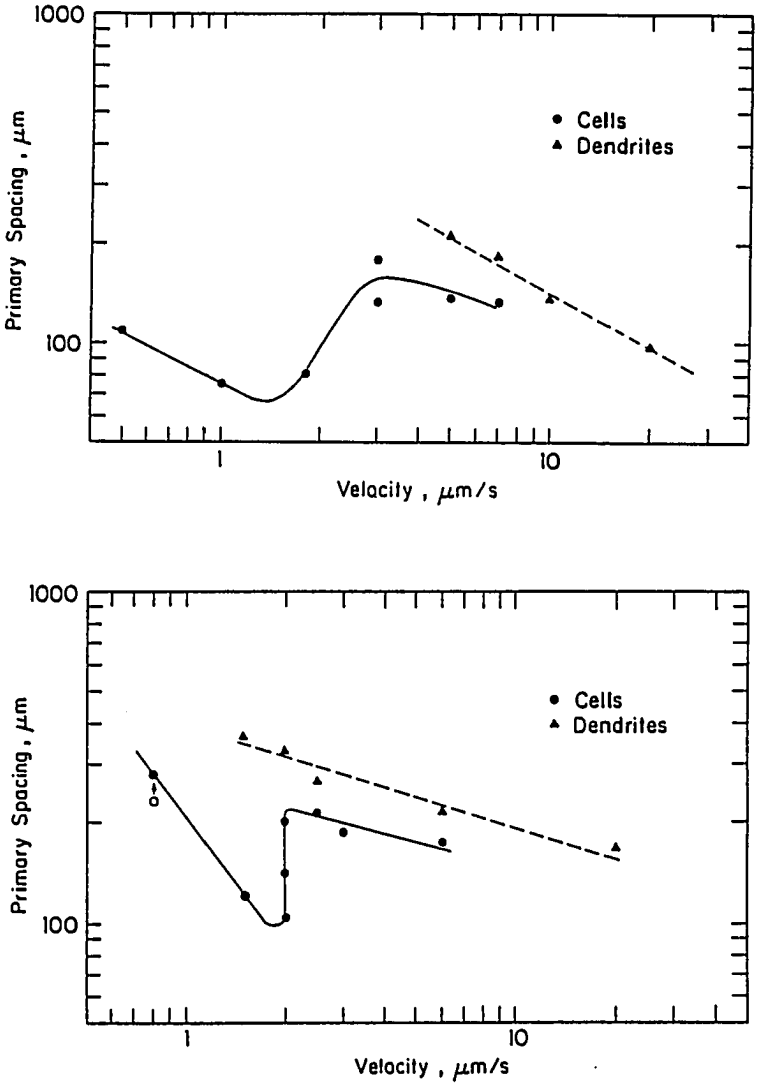

Figure 3. Variation in the intercellular and interdendritic spacing with the growth velocity. (a) Pivalic acid - 0.076 wt.% ethanol system at G = 2.98 K/mm, (b) succinonitrile - 0.35 wt.% acetone system at G = 3.76 K/mm. The open circle data point is for succinonitrile - 0.15 wt.% acetone, and the arrow indicates a correction to 0.35 wt.% acetone by using the relationship $\lambda \alpha C_s^{0.25}$, where C_s is the solute concentration

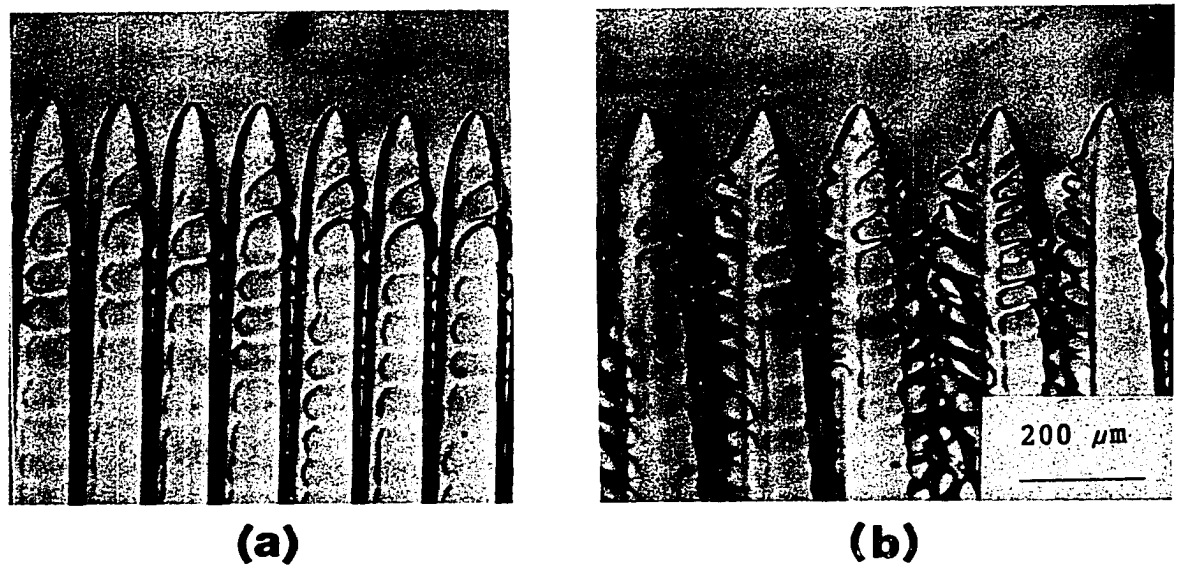

Figure 4. Duplicated experimental runs showing (a) cellular and (b) dendritic structures observed in two different experimental runs conducted under identical conditions of V = 7.0 μm/s and G = 2.98 K/mm in the pivalic acid - 0.076 wt.% ethanol system

Figure 5. Simultaneous occurrence of cellular and dendritic structures in the cell-dendrite transition regime: (a) pivalic acid - 0.076 wt.% ethanol alloy solidified at V = 5.0 μm/s, (b) succinonitrile - 0.35 wt.% acetone alloy solidified at V = 1.0 μm/s

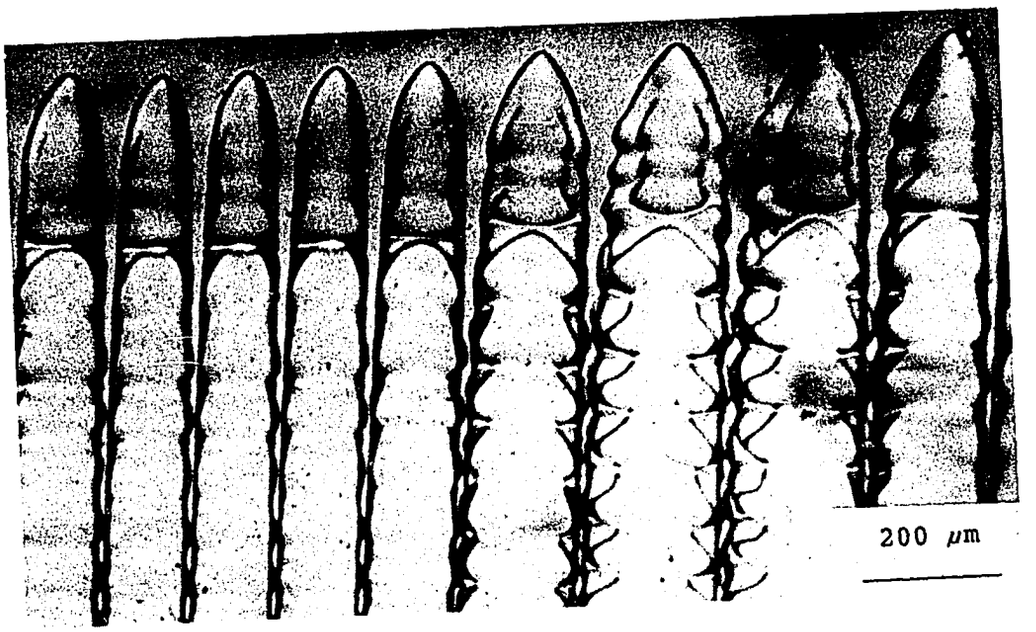

(a)

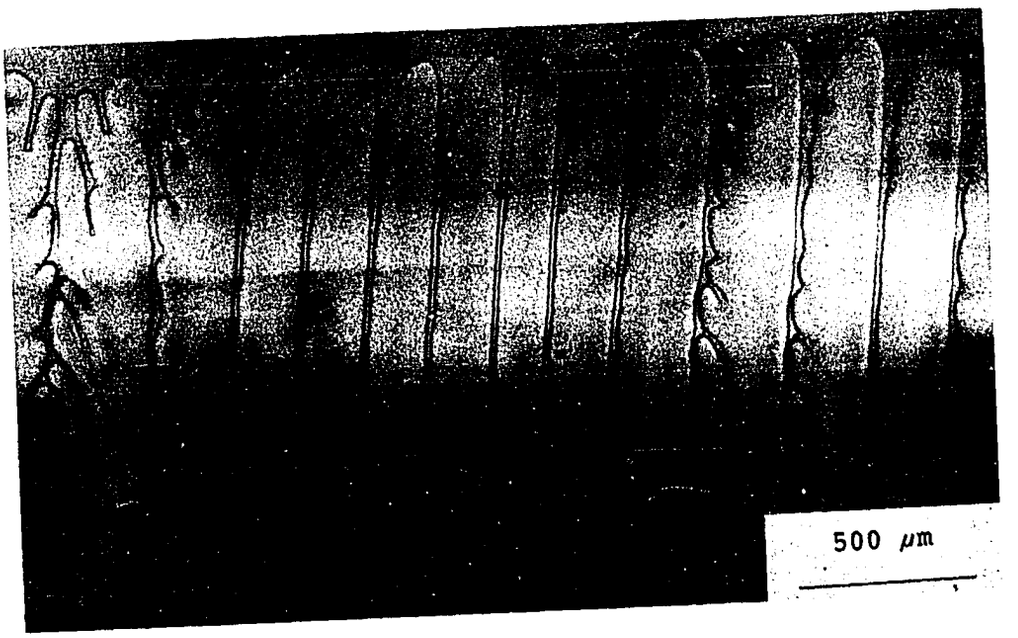

(b)

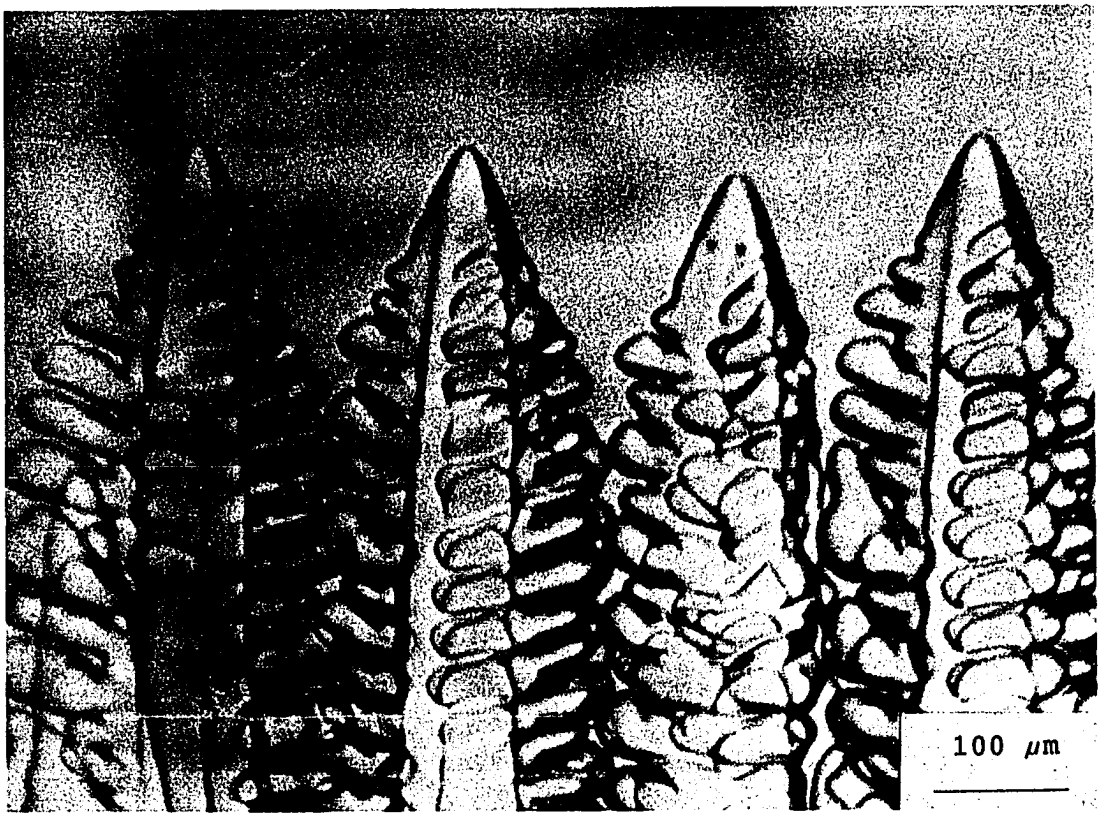

Figure 6. Steady-state dendritic microstructure observed in the pivalic acid - 0.076 wt.% ethanol system at V = 20 μm/s

the pivalic acid-ethanol system at V = 20.0 μm/s. The dendrite spacings within the transition velocity band and at higher velocities were found to fall on one line, as shown in Figure 3a.

In the pivalic acid - 0.076 wt% ethanol system, the critical velocity for the planar interface instability was estimated to be about 0.5 μm/s for a temperature gradient of 2.98 K/mm. An experiment was carried out in which a steady-state run was first made at 0.25 μm/s to establish a planar interface. When the velocity was increased to 0.5 μm/s, the interface reorganized into a periodic array of cells with a finite amplitude, as shown in Figure 2a. The existence of finite amplitude cells near the critical velocity indicates that the planar to nonplanar bifurcation in the pivalic acid-ethanol system is subcritical. Similar subcritical bifurcations have also been established in the succinonitrile-acetone system [2] and in the carbon tetrabromide-bromine system [23, 24].

Figure 3 plots the average cellular spacing with velocity. Since the mechanisms by which local cellular spacings adjust do not allow small changes in spacings, the selection of cell spacings is not very sharp. This weak spacing selection criterion is responsible for the long time needed to establish the steady-state profile, particularly near the threshold velocity for the planar interface instability. There is also a small but finite variance in the spacing at a given velocity even when steady-state growth conditions are attained after a long duration of the experiment. In order to study the distribution of spacings, a Fourier spectrum of the interface shape was calculated, and

the results are shown in Figure 7. A definite peak was obtained at a wavenumber of 0.063 μm^{-1}, and a small peak corresponding to the first harmonic was also observed. The width of the major peak was small, but finite.

Figure 7. Analysis of the wave pattern of cells in pivalic acid - 0.076 wt.% ethanol. (a) The structure at V = 0.5 μm/s, (b) the digitized interface structure, (c) spatial fast Fourier transform of the interface profile shown in (a)

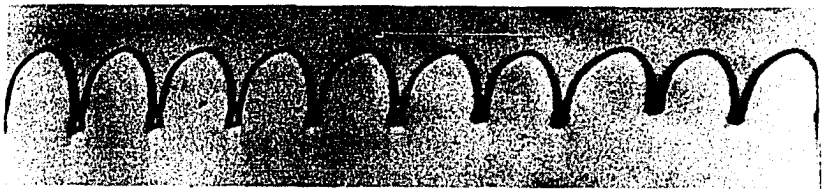

(a)

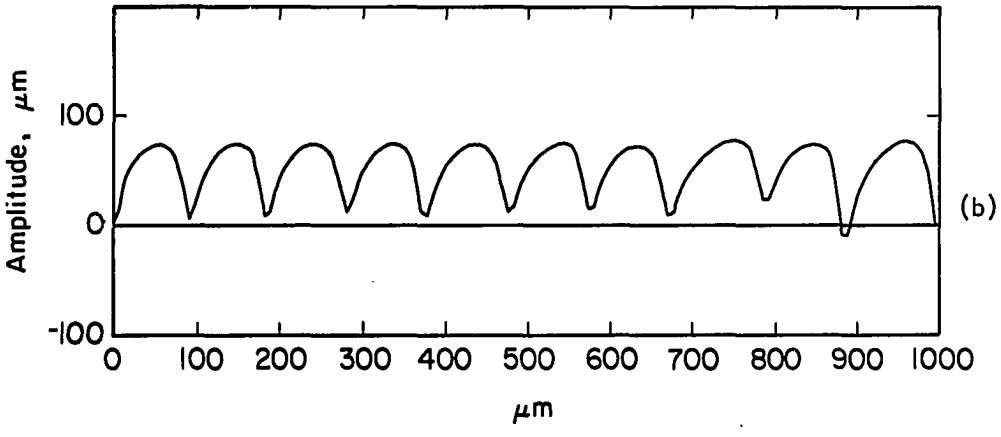
Amplitude, μm
100
0
-100
0
100
200
300
400
500
600
700
800
900
1000
μm

(b)

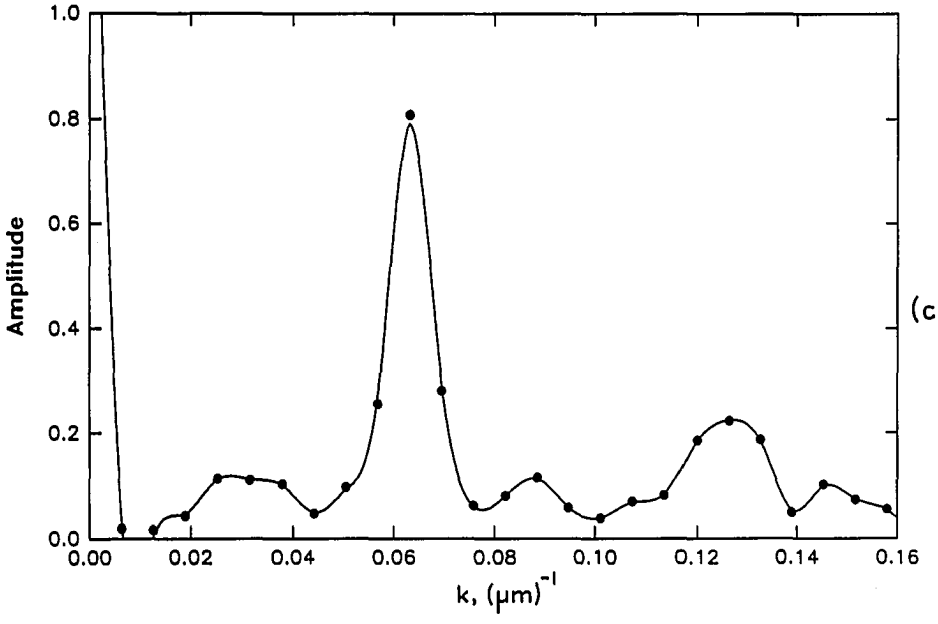
Amplitude
1.0
0.8
0.6
0.4
0.2
0.0
0.00
0.02
0.04
0.06
0.08
0.10
0.12
0.14
0.16
k, (μm)⁻¹

(c)

DISCUSSION

The variations in the cell and dendrite spacings will be discussed first, and second will be an examination of the reasons for the coexistence of cells and dendrites within a finite velocity band. Subsequently, the results will be compared with the existing theoretical models and with the available experimental results in other systems.

Cell and Dendrite Spacings

In view of the cell and dendrite spacing variation with velocity, shown in Figure 3, the experimental velocities studied in this paper will be divided into three parts: (1) the velocity range between V_c and V_t, where V_t is the velocity at which a local minimum in the cell spacing was observed, (2) the velocity range between V_t and V_m, where V_m is the largest velocity at which a cellular structure was found to be stable, and (3) the velocity range above V_m, where only dendritic structures were observed.

Significant differences in cell characteristics were observed between the cells which formed below V_t and those which formed above V_t. Within the first velocity range, $V = V_t - V_c$, the spacing and the amplitude of the cells decreased with an increase in velocity. The amplitude of the cells was also of the same order of magnitude as the cell spacing. When the velocity was increased above V_t, a significant increase in spacing and a very large increase in amplitude were

observed. In the velocity range above V_t, the cell amplitudes were at least an order of magnitude larger than the cell spacings. The tip region, which was somewhat blunt below V_t, became very sharp and assumed a nearly parabolic shape as the velocity was increased above V_t. Such cells are sometimes called the dendritic cells.

The second velocity range, between the velocities V_t and V_m, represents a range of velocities over which the cell-dendrite transition occurs. Several important observations were made in this region which give a clearer insight into the cell-dendrite transition phenomenon. (i) The cell-dendrite transition was not sharp, but it occurred over a range of velocities. (ii) Within this velocity band, either a stable cellular structure, or a stable dendritic structure, or a coexisting cellular and dendritic structure was observed for given experimental conditions. It was, therefore, concluded that two solutions for the steady-state growth problem exist in this region, one solution giving rise to a cellular structure, and the other to a dendritic structure. (iii) Above V_t, the cellular spacing variation with velocity exhibited a maximum. The dendritic spacing, however, decreased continuously with velocity. (iv) A hysteresis effect was observed in the cell dendrite transition. A cellular structure, obtained just above V_t, remained cellular as the velocity was increased. When the velocity exceeded V_m, a cell to dendrite transition occurred. This dendritic structure then remained stable when the velocity was decreased. In succinonitrile-acetone systems, the transition from dendrites to cells occurred slightly below V_t. These results indicate that the cell-dendrite

bifurcation is subcritical.

The general characteristics of the planar-cellular-dendritic transitions observed under directional solidification conditions can be represented by a bifurcation diagram shown in Figure 8. Subcritical bifurcation is observed for the planar to cellular transition. The finite amplitude of cells at V_c is then found to decrease as the velocity is increased up to V_t. Above V_t, a sharp increase in the amplitude occurs. At V_t, subcritical bifurcation is again observed for the cell-dendrite transition. In addition, between V_t and V_m, two steady-state solutions yielding cellular and dendritic structures are shown to exist. Finally, above V_m, only dendritic structures form for the velocity ranges examined in this work.

The factors which are critical in determining whether a cellular or a dendritic structure would be present in the velocity region between V_m and V_t, where both these structures were found to be possible, will now be examined. The actual selection of a cellular or dendritic structure depends on the dynamical processes which are operative as the interface reorganizes into a steady-state pattern. Although the detailed dynamic studies will be presented in Section IV, the aspects which are germane to the cell or dendrite selection process are briefly discussed here.

First, the process by which an unstable interface reorganizes into a cellular or a dendritic process will be examined. Figure 9 illustrates the pattern evolution with time for conditions where only a dendritic structure is stable. The unstable planar interface first

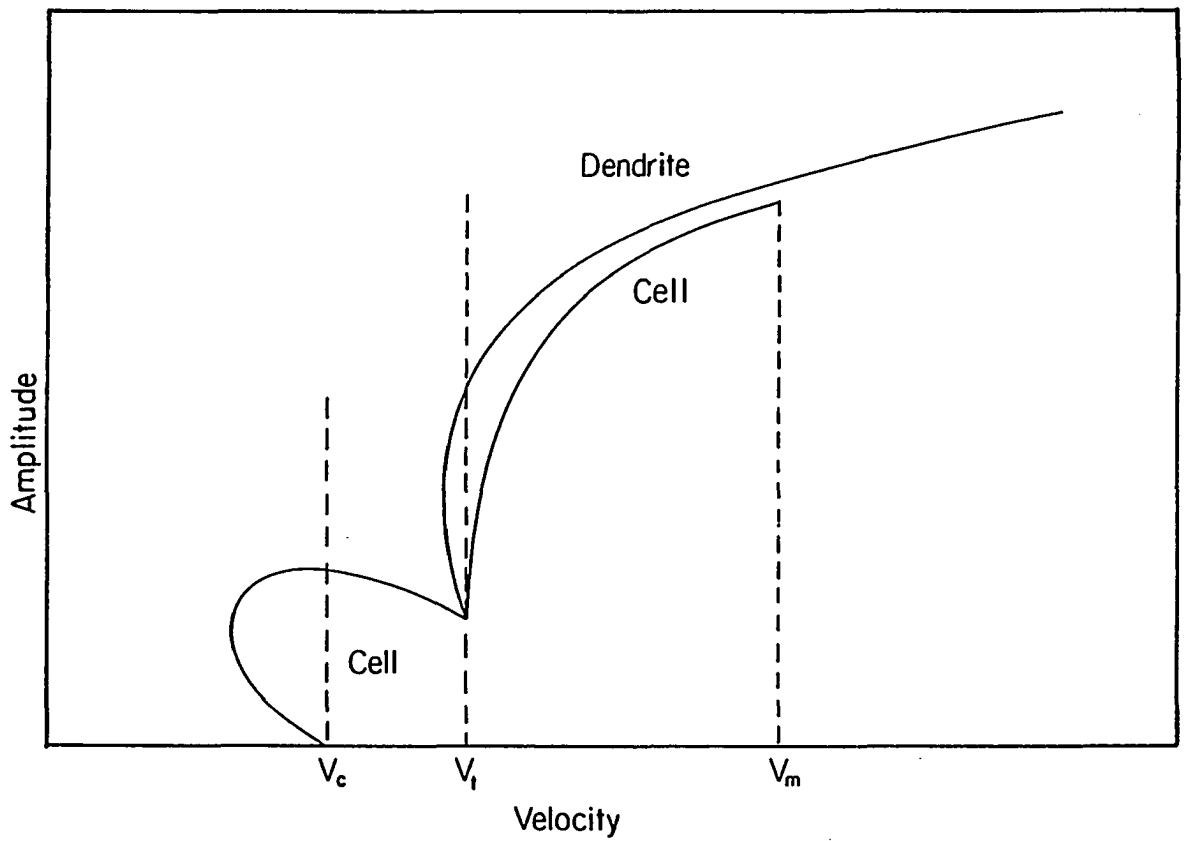

Figure 8. A schematic diagram showing the subcritical bifurcations for planar to cellular and cellular to dendritic transitions

Figure 9. Time evolution of solidification structures observed in the pivalic acid - 0.076 wt.% ethanol system at a constant growth rate of 7.0 μm/s. (a) t = 100 s, (b) t = 340 s, and (c) t = 1440 s

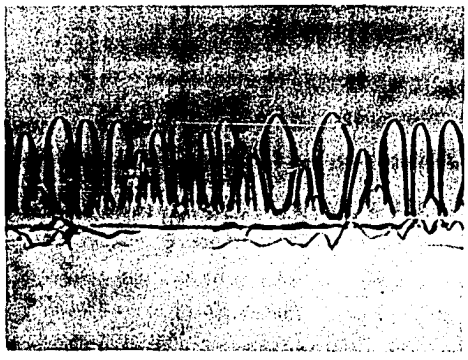

(a)

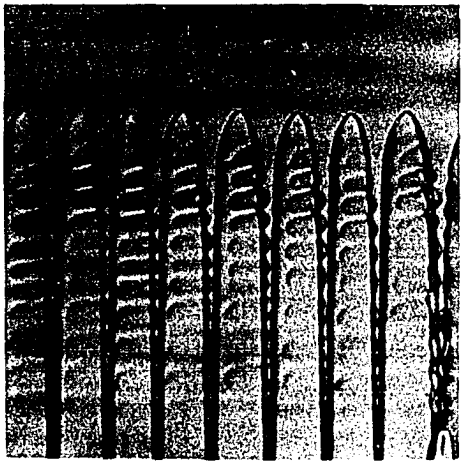

(b)

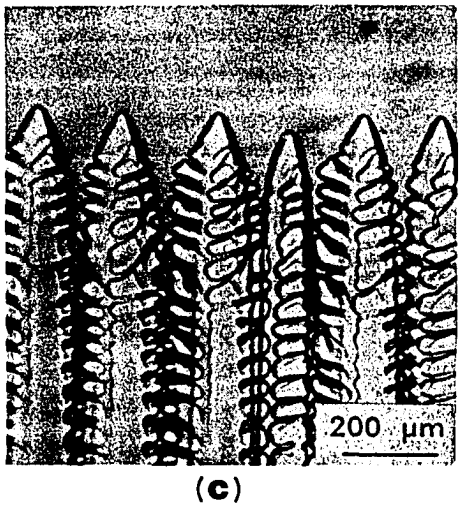

(c)

forms a cellular structure which then, transforms to a dendritic structure. The cellular spacing of the intermediate pattern is smaller than the final dendritic spacing so that some cell elimination is required for the transition from a cellular to a dendritic pattern. In the velocity range where both cellular and dendritic structures are possible, the difference in the cell and dendrite spacing is small. Consequently, once the interface forms a cellular array, it finds it difficult to increase the spacing of the entire array which is required for the formation of dendrites. Thus, in some cases, a cellular structure is retained. In other cases, a local change in spacing can be achieved by eliminating some cells, and a dendritic structure then, results in this area. Such coexisting structures are shown in Figures 4 and 5.

The dynamic studies on interface velocities, reported by Somboonsuk and Trivedi [36] and by Eshelman and Trivedi [2], have shown that when the external velocity is increased to a specific value, the interface velocity first overshoots and then, decreases to the value imposed by the external velocity. Consequently, during this velocity overshoot, some over-elimination of cells will occur which will increase the cell spacing sufficiently to form a dendritic structure. The difference in cell and dendrite amplitudes is small, whereas the difference in cell and dendrite spacing is more pronounced. A decrease in spacing is, therefore, required for a dendritic structure to transform to a cellular structure as the interface velocity decreases to match the external velocity. This spacing adjustment cannot be achieved

readily [3] so that dendritic structures will be retained.

Comparison with Theoretical Models

The first detailed model of cellular spacing, developed by Hunt [5], predicted that the cellular spacing would increase sharply from zero to a maximum as the velocity was increased from V_c to $2V_c$. At higher velocities, the cell spacing decreased with velocity and no discontinuity in spacing was predicted at the cell dendrite transition. Kurz and Fisher [7] assumed the cell shape to be elliptical and derived a relationship between the cell spacing and velocity. Their model gave results which were similar to the results of Hunt's model [5], except that a large decrease in cell spacing was predicted as the velocity was increased to the cell-dendrite transition. The experimental results reported in this paper do not agree with either of the two above-mentioned theories.

The theoretical model of Hunt [5] was subsequently modified by Trivedi [6] for dendrite spacings only. This modified Hunt model predicted a maximum in spacing near the cell-dendrite transition. This prediction is consistent with our observations, although this theory assumes a parabolic tip, which is valid only for dendrites and for cells near the cell-dendrite transition. Recently, theoretical models for cellular growth have been proposed by Billia et al. [37] and Karma [14, 15]. Both these models use the mathematical models of viscous fingering to determine the shape of the cells which develop during the directional solidification of alloys. The model developed by Billia

et al. [37] predicts a finite spacing near the critical velocity, V_c, for the planar interface instability. However, the spacing is found to increase first, then go through a maximum and finally, decrease without any discontinuity at the cell-dendrite transition. These predictions are again not validated by our experimental results.

Let us first examine the velocity region (ΔV) near the critical velocity for planar interface instability, in which the cellular spacing decreases with velocity. In this region, the model of Trivedi [6] cannot be applied since the shape of the cell tip deviates strongly from a parabola. In addition, Hunt's model [5] is based on the mass balance which uses the Scheil equation, to determine the cell shape far behind the cell front. In this model, the shape of the cell near the tip region was not determined, but was approximated as a sphere. However, Figures 2a and 2b show that the amplitude of cells is of the same order of magnitude as the wavelength so that the solute and thermal fields in the vicinity of the cell tip are critical in determining the cell spacing. Consequently, Hunt's model cannot be applied in this region. A more detailed model developed by Karma [15] takes the shape of the interface into account by using an analogy with the viscous fingering model. His model requires numerical calculations and it is proposed for a phase diagram which has a constant miscibility gap, i.e., parallel solidus and liquidus lines. Since the miscibility gaps in our systems are temperature-dependent, we cannot directly apply this theoretical model to study quantitatively the variation in spacing with velocity. Karma's model does, however, predict the spacing to decrease

with velocity in the velocity range close to V_c, which is consistent with our observation. The experimental results show that the spacing decreases as $V^{-0.5}$, as shown by curve 3 in Figure 10.

Figure 2 shows that the sharp increase in spacing that is observed experimentally can be correlated with a sharp change in cellular characteristics. The cell amplitude increases sharply and the ratio of amplitude to wavelength becomes very large. Furthermore, the cell tip approaches a parabolic shape. We may, therefore, apply the model developed by Trivedi [6] for $V > V_t$. Curve 1 in Figure 10 shows the result of this model which agrees reasonably well with the experimentally observed variation of the cell spacing with velocity.

The variation in dendrite spacing with velocity shows a linear relationship in Figure 10. If the marginal stability criterion for dendrite growth, proposed by the Langer and Muller-Krumbhaar model [1], is substituted in the spacing equation given by Trivedi, the theoretical results represented by curve 2 are obtained. These results agree remarkably well with our experimental observations. Thus, the interface structure, in a small velocity range, can either be cellular or dendritic depending on whether the tip dimension is affected by the thermal field or not. If both structures exist, the tip temperature should be higher for the dendrites than for the cells, in which case, the dendritic front will lead the cellular front by a very small distance. This is indeed observed experimentally (Figure 5).

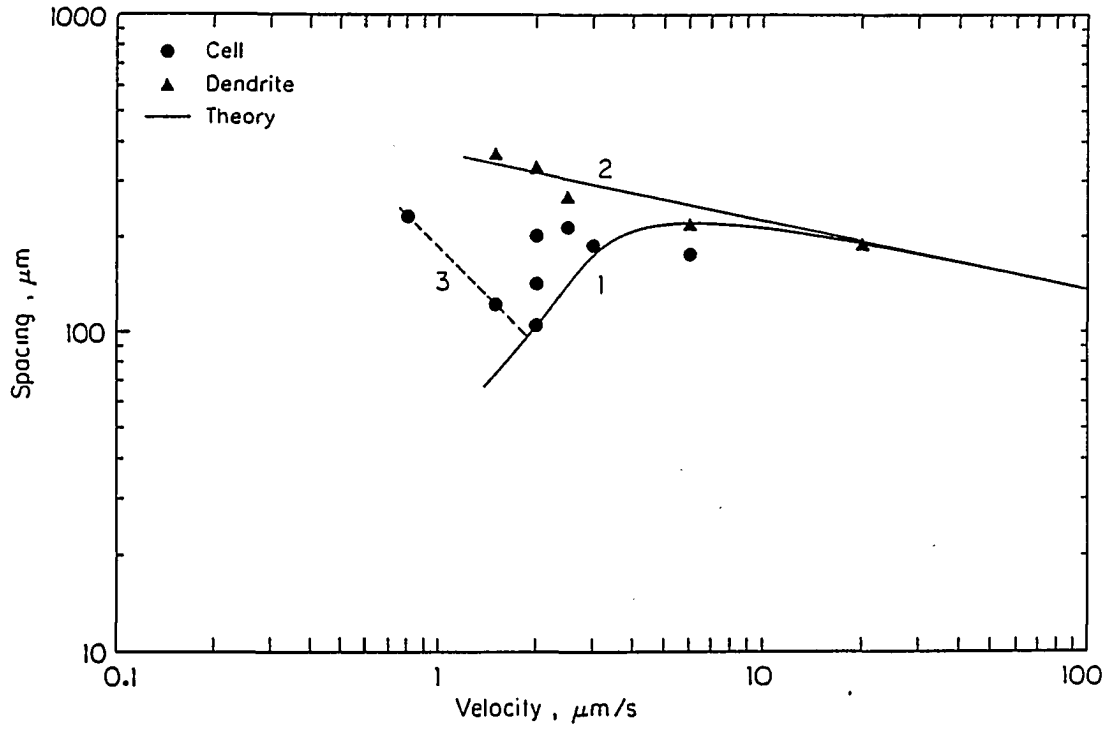

Figure 10. Comparison of the theoretical model with the experimental data on primary spacing in the succinonitrile - 0.35 wt.% acetone system. Line 1 is predicted by the general model of Trivedi [6]. Line 2 is the result of Trivedi's model when the Langer and Muller-Krumbhaar model of the stability criterion [1] for dendrite tip radius is used. Line 3 represents experimental results for which no satisfactory model is available

Comparison with Other Experimental Results

The detailed experimental studies shown here show that the spacings decrease with velocity, except for a sharp increase near the cell-dendrite transition in both the succinonitrile-acetone and the pivalic acid-ethanol systems. Such variations in spacings have also been found in a number of other systems, specifically in the Al-Tl system by Jamgotchian et al. [29], in the Al-Cu system by Billia et al. [37], and in the Al-Cu by Miyata et al. [30]. Cellular structures in metallic systems generally exist at very low velocities where thermosolutal convection effects become important. It is, therefore, necessary to examine experimental results in which convection effects were negligible. One such careful study was carried out by McCartney and Hunt [31] who showed that cell and dendrite spacings decrease with velocity except that the results for cells and dendrites could not be represented by the same line. In their experiments, a ternary alloy of Al-Si-Mg was designed in which the density driven convection effect was carefully eliminated. Although their results were given for different values of gradients, we have normalized their results by considering the spacing to vary as $G^{-1/2}$ (using Hunt's model [5]). These normalized results are shown in Figure 11. These results also show that there is a range of velocities over which dendritic and cellular structures can be present.

A number of experimental studies have been reported in the literature to characterize the variation in the cellular spacing with velocity. A decrease in cellular spacing with velocity was observed by

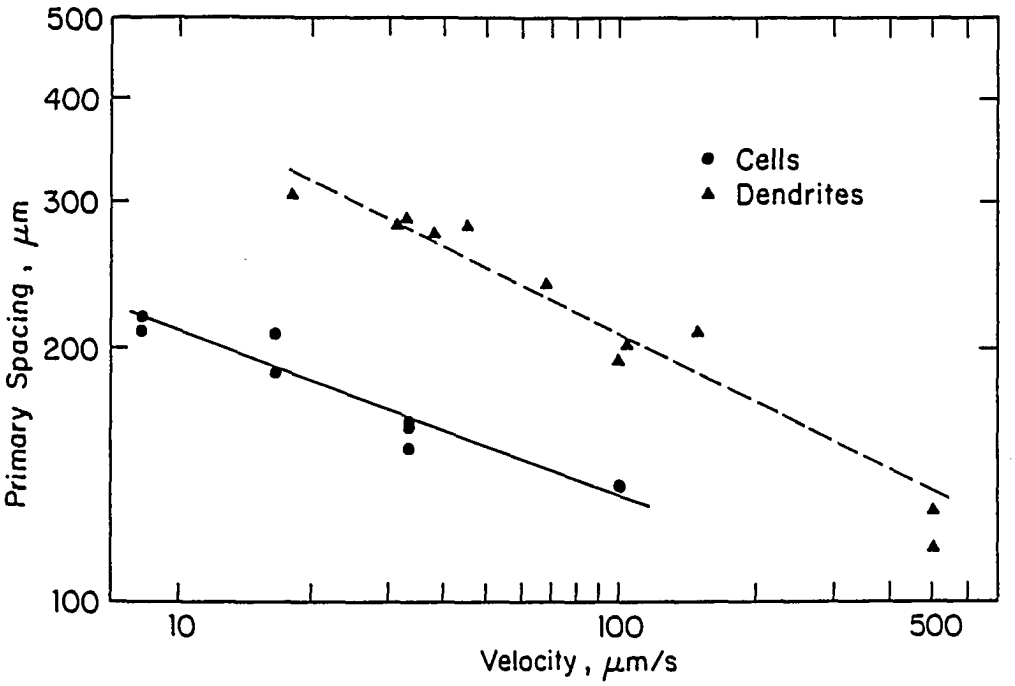

Figure 11. Variation in the primary spacing of cellular and dendritic structures with the growth rate in an Al-Si-Mg alloy. The data are taken from the work by McCartney and Hunt [31] and replotted by normalizing them to a constant temperature gradient of 3.0 K/mm

Rutter and Chalmers [20] and Tiller and Rutter [21] in the Pb-Sn system, Jin and Purdy [22] in the Fe-Ni system, de Cheveigne et al. [23, 24] in the carbon tetrabromide-bromine system, Sharp and Hellawell [38] in the Al-Cu system, and Venugopalan and Kirkaldy [18] in the succinonitrile-solol systems. These experiments, however, were carried out only in the cellular region so that the increase in spacing, which would have occurred near the cell-dendrite transition, was not observed.

The increase in cellular spacing with velocity was reported by Somboonsuk et al. [16] and Esaka and Kurz [17] in succinonitrile-acetone systems and by Bechhoefer and Libchaber [27] in an impure pivalic acid system. Similar results were also found by Klaren et al. [28] and Mason et al. [25, 26] in Pb-Au and Pb-Pd systems. All these studies were carried out near the cell-dendrite transition so that the observed increase in spacing is consistent with the observations reported in this paper.

Venugopalan and Kirkaldy [18] reported that no steady-state cellular structure was observed near V_c in the succinonitrile-solol system. However, detailed experimental studies in the succinonitrile-acetone [2] and the carbon tetrabromide-bromine [23, 24] systems have clearly shown the existence of steady-state cellular spacings near V_c. The time required to establish the steady state near V_c was found to be quite long [2, 23, 24] and it appears that Venugopalan and Kirkaldy [18] did not carry out their experiments for times sufficient to establish the steady-state configuration.

Sharp and Hellawell [19, 38] observed that there was no appreciable change in spacing with velocity near V_c, although spacings did decrease as the velocity was increased further. This observation of constant spacing with velocity is a dynamical effect which will be discussed in detail in Section IV.

The various experimental results on cellular and dendritic spacings can now be explained in terms of a general variation shown in Figure 12. Two important parameters are ΔV and $\Delta\lambda$ which are functions of the system parameters. As discussed by Kurz and Fisher [7], the value of V, i.e., $V_t - V_c$, depends on K_o and can be given by

$$\Delta V = V_c \, (1-K_o)/K_o \, K_o < 1 \quad . \tag{7}$$

In contrast, we still do not have a clear understanding of the parameters which control the magnitude of $\Delta\lambda$.

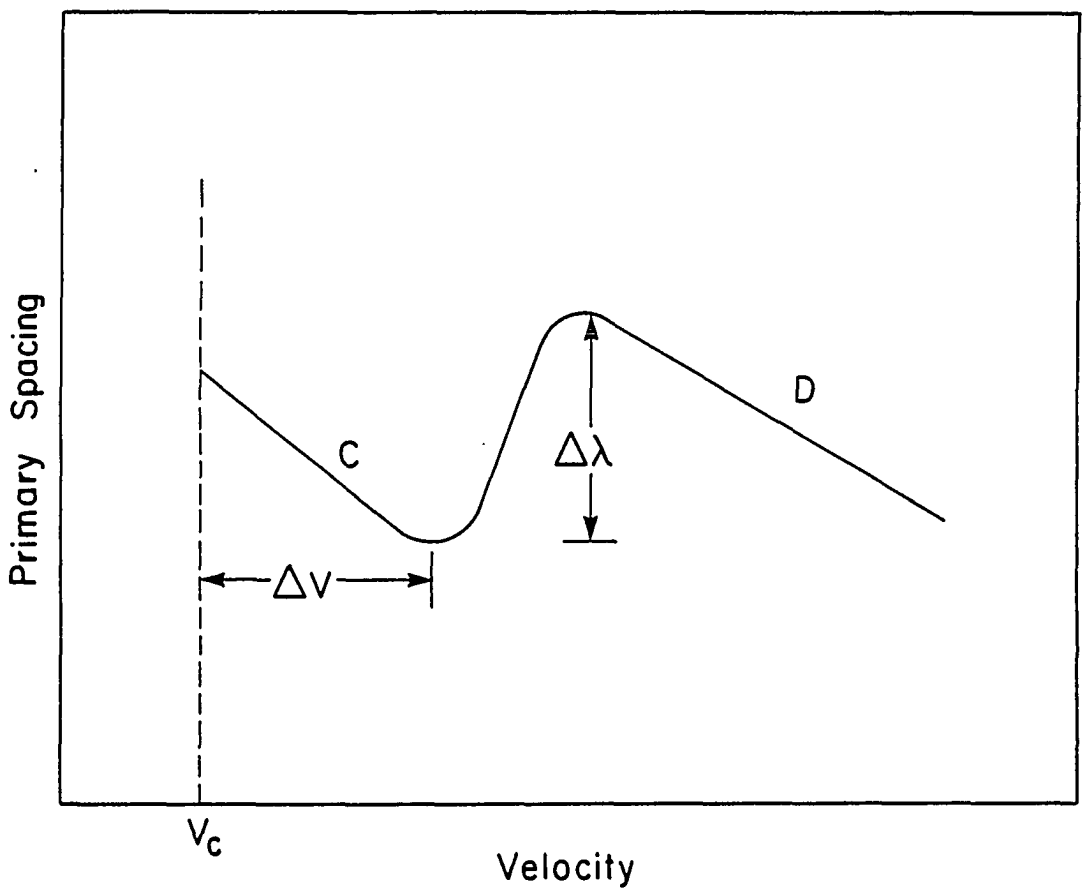

Figure 12. Schematic diagram showing the general variation in primary spacing with the growth velocity. ΔV represents the range of velocities in which steady-state cellular structures develop. $\Delta\lambda$ is the change in primary spacing which occurs near the cell-dendrite transition velocity

CONCLUSIONS

Experimental studies were carried out in the succinonitrile-acetone and pivalic acid-ethanol systems to characterize the variation in cell and dendrite spacings with velocity. The entire velocity range, for which stable cellular structures exist, was investigated. Both systems showed similar behaviors when the cells were oriented in the heat flow direction. The cellular spacing was found to decrease with an increase in velocity above the critical velocity for the onset of planar interface instability. However, a sharp increase in cell spacing was observed at velocities close to the cell-dendrite transition. With further increase in velocity, the cell or dendrite spacing again decreased steadily. The increase in cellular spacing was correlated with the sharp increase in the amplitude of the cells and with the sharpening of the cell tips.

Both cellular and dendritic structures were found to exist within a finite band of velocity. A small, but finite spectral width of cellular spacings was also observed and was attributed to the limitations of the dynamical processes which enable the cells to adjust their spacings.

The initial decrease in cellular spacing with an increase in velocity, near the critical velocity for planar interface instability, was qualitatively explained by using the theoretical model of Karma. In this region, the shape of the cellular front and the thermal and solute fields near the tip region are shown to influence the spacing

significantly. A detailed quantitative model of cellular spacing in this region is not yet available, although recent theoretical developments, based on the viscous fingering model, appear to be encouraging.

The sharp increase in cellular spacing with velocity near the cell-dendrite transition velocity and the subsequent decrease in cellular spacing with velocity were in reasonable agreement with the predictions of Trivedi's model [6]. Furthermore, when the temperature gradient effects on the tip radius were neglected, the theoretical spacing matched precisely with the observed dendrite spacing. It is, thus, concluded that within a narrow band of velocities, both cellular and dendritic structures can be stable. The development of a cellular or dendritic interface is a free boundary problem, and the interface would select the specific structure depending on the relative effects of the thermal and the solute fields on the tip radius. When the thermal effects on the tip radius are small, the interface assumes a dendritic structure with a slightly higher amplitude and a smaller tip radius. When the thermal effects on the tip radius are not negligible, a cellular structure with a slightly smaller amplitude and a larger tip radius is formed. A bifurcation diagram, which shows the existence of these two solutions in a finite velocity range, is proposed. Experimental results indicate that the cell-dendrite bifurcation is subcritical, although further experimental studies are required to quantitatively establish the cell-dendrite bifurcation.

REFERENCES

1. Langer, J. S. Rev. Mod. Phys. 1980, 52, 1.
2. Eshelman, M. A.; Trivedi, R. Acta Metall. (submitted).
3. Seetharaman, V.; Eshelman, M. A.; Trivedi, R. Acta Metall. (submitted).
4. Seetharaman, V.; Eshelman, M. A.; Trivedi, R. Acta Metall. (submitted).
5. Hunt, J. D. "Solidification and Casting of Metals"; The Metals Society: London, 1979; Book 192, p. 3.
6. Trivedi, R. Metall. Trans. 1984, 15A, 977.
7. Kurz, W.; Fisher, D. J. Acta Metall. 1981, 29, 11.
8. Burden, M. H.; Hunt, J. D. J. Crystal Growth 1974, 22, 109.
9. Mullins, W. W.; Sekerka, R. F. J. Appl. Phys. 1964, 34, 444.
10. Caroli, B.; Caroli, C.; Roulet, B.; Langer, J. S. Phys. Rev. 1986, A33, 442.
11. Kessler, D., University of Michigan, Ann Arbor, MI; Levine, H., Schlumberger Ltd., 277 Park Avenue, New York, NY (unpublished work).
12. McLean, J. W.; Saffman, P. G. J. Fluid Mech. 1981, 102, 455.
13. Pelce, P.; Pumir, A. J. Crystal Growth 1985, 73, 337.
14. Karma, A., Department of Physics, California Institute of Technology, Pasadena, CA, (unpublished work), September 1986.
15. Karma, A. Private Communication. California Institute of Technology, Pasadena, CA, September 1986.
16. Somboonsuk, K.; Mason, J. T.; Trivedi, R. Metall. Trans. 1984, 15A, 967.
17. Esaka, H.; Kurz, W. J. Crystal Growth 1985, 72, 578.
18. Venugopalan, D.; Kirkaldy, J. S. Acta Metall. 1984, 32, 893.
19. Sharp, R. M.; Hellawell, A. J. Crystal Growth 1970, 6, 253.

20. Rutter, J. W.; Chalmers, B. Canadian J. Phys. 1953, 31, 15.

21. Tiller, W. A.; Rutter, J. W. Canadian J. Phys. 1956, 34, 96.

22. Jin, I.; Purdy, G. R. J. Crystal Growth 1974, 23, 37.

23. de Cheveigne, S.; Guthmann, C.; Lebrun, M. M. J. Crystal Growth 1985, 73, 242.

24. de Cheveigne, S.; Guthmann, C.; Lebrun, M. M. J. de Physique 1986, 47, 2095.

25. Mason, J. T.; Verhoeven, J. D.; Trivedi, R. J. Crystal Growth 1982, 59, 516.

26. Mason, J. T.; Verhoeven, J. D.; Trivedi, R. Metall. Trans. 1984, 15A, 1665.

27. Bechhoefer, J.; Libchaber, A., University of Chicago, Chicago, IL. (to be published).

28. Klaren, C.; Verhoeven, J. D.; Trivedi, R. Metall. Trans. 1980, 11A, 1953.

29. Jamgotchian, H.; Billia, B.; Capella, L. J. Crystal Growth 1983, 64, 338.

30. Miyata, Y.; Suzuki, T.; Uno, J.-I. Metall. Trans. 1985, 16A, 1799.

31. McCartney, D. G.; Hunt, J. D. Acta Metall. 1982, 29, 1851.

32. Hunt, J. D.; Jackson, K. A.; Brown, H. Rev. Sci. Instrum. 1966, 37, 805.

33. Mason, J. T.; Eshelman, M. A., IS-4906, Ames Laboratory, Iowa State University, Ames, Iowa, 1986.

34. Huang, S. C.; Glicksman, M. E. Acta Metall. 1981, 29, 701.

35. Glicksman, M. E.; Singh, N. B., ASTM Tech. Publ. 1986, 890, 44.

36. Somboonsuk, K.; Trivedi, R. Acta Metall. 1985, 33, 1051.

37. Billia, B.; Jamgotchian, H.; Capella, L. J. Crystal Growth (to be published).

38. Sharp, R. M.; Hellawell, A. J. Crystal Growth 1970, 6, 334.

SECTION IV. CELLULAR SPACINGS: DYNAMICAL STUDIES

INTRODUCTION

Interface pattern formation during the directional solidification of alloys has recently received considerable theoretical attention [1-11]. In the directional solidification, a solid-liquid interface is driven externally at a constant velocity under fixed conditions of temperature gradient and composition. The interface shape undergoes a planar to cellular to dendritic transition as the velocity is increased. So far, only the critical velocity, V_c, above which a planar interface becomes unstable, has been well-established. This critical velocity has been predicted by the linear stability analysis of Mullins and Sekerka [12], and its validity has recently been confirmed by the experimental studies of Eshelman and Trivedi [13].

Once a solid-liquid interface is driven beyond V_c, the unstable planar interface reorganizes into a periodic array of cells. The development of this periodic interface profile is a free boundary problem and experimentally, under given conditions, the interface has been found to assume a steady-state shape with definite amplitude and wavelength [14]. In contrast, theoretical models which neglect surface energy effects predict a continuum of possible wavelengths. Furthermore, when surface energy effects are taken into account, the microscopic solvability condition gives rise to a discrete set of possible wavelengths rather than a particular wavelength. Thus, the critical aspect that is not yet well understood is the principle which governs the selection of a definite wavelength of cellular patterns

under a given set of experimental conditions.

Experimental studies [15-17] have shown that the steady-state cellular wavelengths are always significantly larger than the fastest growing wavelengths predicted by the linear stability analysis. Trivedi and Somboonsuk [15] have carried out experimental studies to examine the dynamical changes in interface pattern formation. They have shown that the initial wavelength of an unstable planar interface is significantly smaller than the steady-state cellular wavelength which emerges after a sufficiently long time. This dynamical evolution of the steady-state wavelength occurs in a nonlinear regime [13] so that the linear stability analysis cannot be used to predict the steady-state cellular wavelength. The nonlinear analyses, however, predict multiple solutions. Until now, most of the theoretical approaches and experimental studies have been aimed at characterizing the steady-state cellular profile. Only a few experimental studies on the development of a periodic cellular structure during the transient period have been carried out [15-20]. Langer [2] has suggested that the key to the wavelength selection may lie in the dynamics of the pattern evolution, and it appears that such studies are now needed to provide an insight into the cellular wavelength selection principle. This paper, therefore, reports experimental studies on the dynamics of cellular wavelength selection.

The dynamics of the cellular spacing evolution have been studied theoretically by Kerszberg [9-11] who has solved the nonlinear equation of motion by numerical techniques. This approach predicts periodic

steady-state cellular structures which resemble experimentally observed profiles. However, a range of steady-state spacings is obtained and the final spacing of the cellular array is found to depend on the initial profile assumed for the calculations. A unique spacing is observed only when a small, but finite white noise is imposed on the system. This noise is responsible for inducing the strongly nonlinear events which drive the profile to a unique wavelength by eliminating some cells or by creating new cells via tip-splitting [11, 19].

The theoretical model gives us some insight into the dynamics of the spacing selection process. However, a number of questions still remain unanswered. Kerszberg [10] has found that the solutions depended on the order of the expansion considered. Furthermore, the model assumes a phase diagram with a constant miscibility gap, i.e., parallel liquidus and solidus lines. When a more realistic phase diagram with a temperature-dependent miscibility gap is considered, no stationary solutions were observed. In contrast, experimental studies described earlier [14] show unique stationary solutions for systems with temperature-dependent miscibility gaps. In addition, Kerszberg has predicted that the spacing will increase with increasing velocity. This is contrary to the experimental observations which show that the cellular spacing decreases with increasing velocity near the critical velocity for planar interface instability.

In order to obtain a better understanding of the cellular array problem, some critical experimental studies are needed which can give clear insight into the dynamics of the spacing selection process. In

this section, such experimental studies will be reported, with an emphasis on the following aspects of the cellular growth: (1) the mechanisms of cellular spacing adjustment in the nonlinear regime of pattern evolution, (2) the effect of anisotropy in interface properties on the mechanism of wavelength selection, and (3) the response of the interface to both small and large changes in velocity.

EXPERIMENTAL

Directional solidification studies were carried out in an apparatus which is previously described by Somboonsuk et al. [21] and Mason and Eshelman [22]. All the experimental variables, viz. velocity, temperature gradient and composition, were controlled and measured precisely [22, 23]. Two systems, based on succinonitrile and pivalic acid, were selected for this study. Both these materials have low entropy of fusion which causes the solid-liquid interface to move by the continuous growth mechanism [24]. Furthermore, both of these materials solidify with cubic structures for which the preferred growth direction is <100>. The major difference between these systems is in the anisotropy of interface properties. Glicksman and Singh [25] and Huang and Glicksman [26] have measured the anisotropy in surface energy for these systems, and they have shown that the surface energy, γ, can be expressed as

$$\gamma/\gamma_0 = 1 + \psi \cos 4\theta \ , \qquad (1)$$

where γ_0 is the surface energy of the (100) plane and θ is the angle between the normal to a given orientation and the normal to the (100) plane. The anisotropy parameter, ψ, was reported to be 0.005 for succinonitrile and 0.05 for pivalic acid [27]. The factor of ten difference in the anisotropy coefficient should be sufficiently large to bring out the effect of anisotropy on the cellular morphology.

The presence of kinetic anisotropy in a given system can be studied by examining the direction of cell formation with respect to the heat flow direction. Coriell and Sekerka [28] have shown that the kinetic anisotropy does not affect the amplification rate of the perturbation on a planar interface. It does, however, translate the perturbation parallel to the interface. Consequently, if appreciable kinetic effects are present, a significant deviation in the cell shape will occur. In impure succinonitrile, a small deviation in the cell shape was observed by Heslot and Libchaber [20]. In order to examine the kinetic effect in the pivalic-acid ethanol system, we have carried out experiments on the formation of cellular structures. A significant displacement of cell tip region along the preferred crystallographic growth direction was observed, as shown in Figure 1. Careful examination of this figure also shows the definite presence of small faceted regions. Thus, kinetic anisotropy effects are quite significant in the pivalic acid-ethanol system. In order to obtain a meaningful comparison of the dynamical processes in the succinonitrile-acetone and pivalic acid-ethanol systems, only those cellular arrays which grew along the heat flow directions were considered in this study.

Two sets of experimental studies were carried out. In the first set, the system was solidified at a velocity below the threshold velocity, V_c, for the planar interface instability. Once the steady-state planar growth was established, the system was driven at a velocity $V > V_c$, and the time-dependent changes in the average spacing and the average amplitude were measured. These experiments were carried out

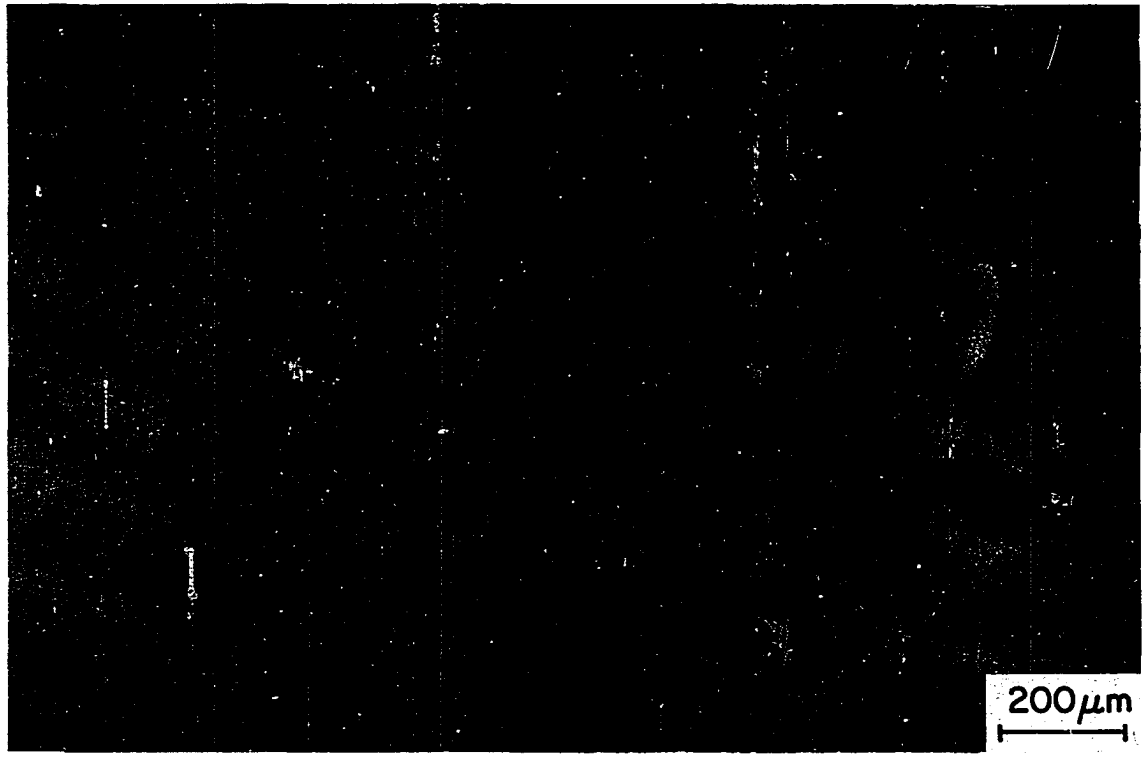

Figure 1. Steady-state cellular microstructure obtained in the pivalic acid - 0.2 wt.% ethanol system at V = 0.5 μm/s. Anisotropy in growth kinetics causes the translation of the cell tips along the solid-liquid interface and leads eventually to the growth of cells at an angle to the heat flow direction

for sufficiently long times during which steady-state cellular arrays were formed. The mechanisms by which the cellular spacings and amplitudes approached their steady-state values were then established. These experiments were carried out in both the succinonitrile-acetone and the pivalic acid-ethanol systems.

In the second set of experiments, a steady-state cellular array was first established at a velocity just above V_c. The velocity was then increased in small steps, and at each step, the system was allowed to solidify for 15 minutes. The response of the interface profile to these changes in velocity was then studied. The velocity of the system was then changed by larger steps to examine the dynamical changes in spacing which occurred when the system was subjected to larger perturbations. The compositions of the materials and the conditions used for these two sets of experiments are given in Table 1.

In addition to the time-dependent changes in the average cellular spacing, the distribution of spacing for a given steady-state profile was also measured. A correlation was observed between the local spacing and the local amplitude of the cell.

Table 1. Summary of the experimental conditions and the compositions of the materials used

Experiments	Materials used[a]	Temperature gradient G(K/mm)	Velocity (μm/s)
Evolution of cellular structure at constant velocity	SCN - 0.15 wt% acetone	3.76	0.8
	PVA - 0.2 wt% ethanol	2.98	0.5
Interface dynamics with changes in velocity	PVA - 0.076 wt% ethanol	2.98	0.5-2.0

[a]SCN = succinonitrile; PVA = pivalic acid.

RESULTS AND DISCUSSION

The experimental results will be presented and discussed in this section in two parts. First, will be consideration of the dynamical response of the cellular pattern to both small and large changes in growth conditions. Second, the relationship between the cell amplitude and cell spacing will be presented.

Interface Dynamics with the Change in Velocity

In this set of experiments, a steady-state cellular structure was first established in the pivalic acid-ethanol system at a velocity of 0.5 μm/s which was just above V_c. The velocity was then increased in steps of 0.1 μm/s and the system was directionally solidified for 15 minutes at each velocity. The velocity-time cycle is shown in Figure 2.

Previous experimental studies [14] show that the steady-state cellular spacing in this alloy decreases with an increase in velocity in the velocity range of 0.5-1.5 μm/s. Since the tip-splitting mechanism which is required to decrease the spacing does not operate readily in anisotropic systems, it is important to examine the alternative mechanisms by which a reduction in the cell spacing occurs. This was achieved by examining the response of the interface to a gradual increase in velocity. The cellular spacings which were observed at the end of each step are shown in Figure 3. The steady-state spacings measured earlier [14] are superimposed on this figure to

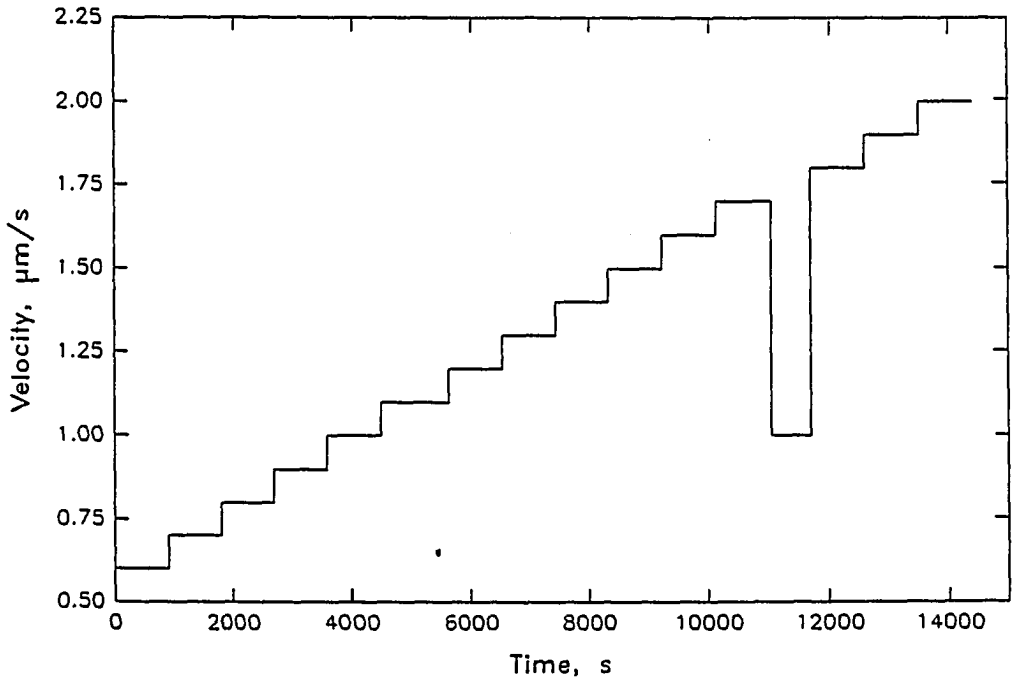

Figure 2. The velocity-time cycles used for studying the dynamic changes in the cell spacing and cell morphology

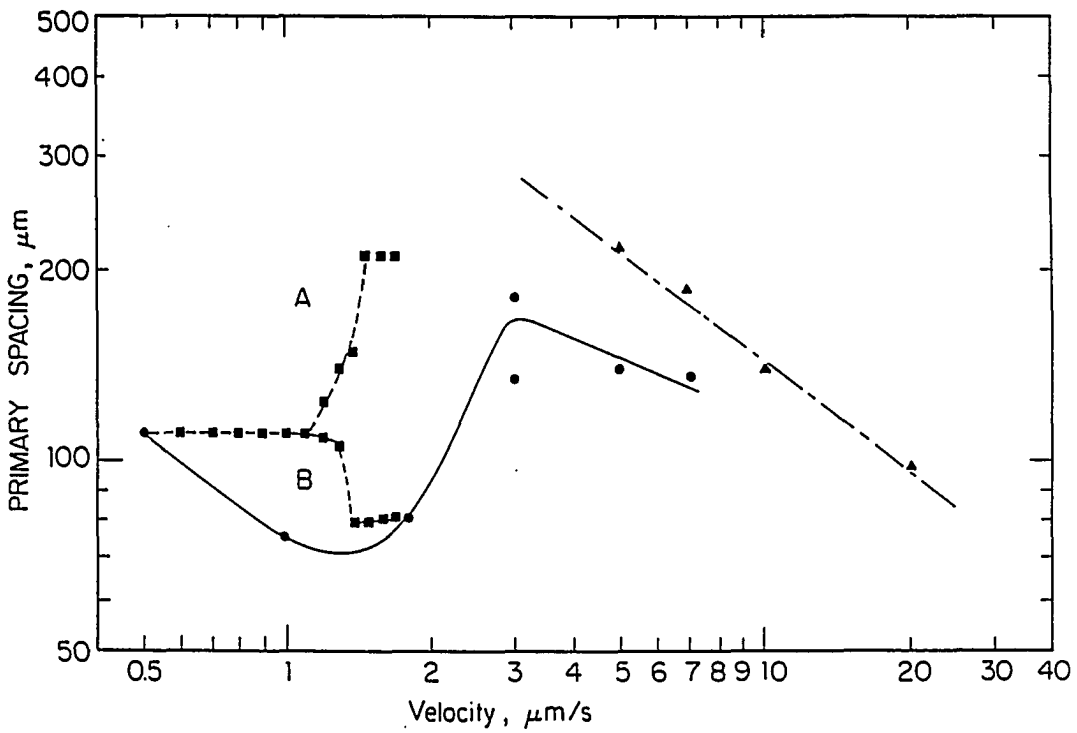

Figure 3. Variation in the average cell spacing with velocity when the velocity was increased from 0.5 to 1.7 μm/s in steps of 0.1 μm/s. Steady-state cellular-dendritic spacings are also included in the figure for comparison. ■ = dynamic cell spacing; o = steady-state cell spacing; Δ = steady-state primary dendrite spacing

provide a comparison between the steady state and the dynamical spacings of cellular structures.

When the velocity was increased from 0.5 μm/s, no change in cellular spacing was observed up to the velocity of 1.1 μm/s. The interface shape, however, changed significantly, as shown in Figure 4. The amplitude of the cells increased with an increase in velocity and the cells became thinner. Furthermore, the cell tips became sharper causing the radius of the cell tip to decrease with velocity. This observation is similar to that reported by Somboonsuk and Trivedi [27] for the dynamics of dendrite growth. They showed that, when the velocity was increased, dendrite spacings did not change, but the dendrite tip radius rapidly changed to its steady-state value. Thus, the system was able to adjust locally in the tip region, but the spacing change, which requires long-range interactions, did not occur readily.

As the velocity was increased from 1.1 to 1.4 μm/s, the cellular front became unstable. Two different regions of the interface followed two distinctly different paths to change the spacing. This bifurcation is shown in Figure 3. In one region (marked A), the spacing increased, whereas in the other region (marked B), the spacing decreased sharply.

In the region where the cellular spacings decreased, B, the change in the spacing was initiated by a localized perturbation which then propagated along the interface. This local perturbation occurred at a specific cell whose local spacing was slightly larger than the average spacing. As the velocity was increased to 1.4 μm/s, this cell

Figure 4. Cellular structures in pivalic acid. (a) Steady-state cellular structure obtained at V = 0.5 μm/s. (b) Cellular structures obtained dynamically (after 15 min. of growth) at V = 1.1 μm/s. Pivalic acid - 0.076 wt.% ethanol system directionally solidified at G = 2.98 K/mm

(a)

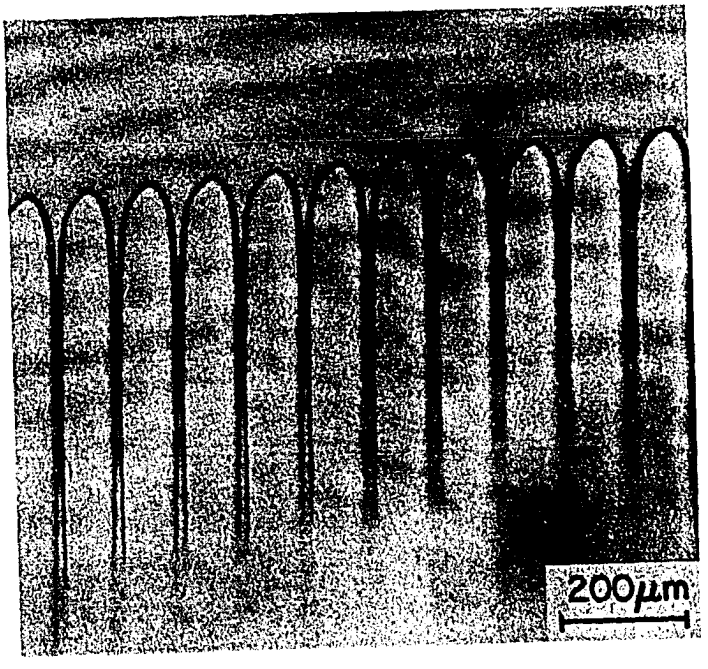

(b)

transformed into a dendrite, as shown in Figure 5. The dendrite side arm rotated and became a cell (Figure 5b). As this new cell was created, the diffusion field interaction with the neighboring cell caused the neighboring cell tip to become nearly flat (Figure 5c). This flat region then became unstable, thereby creating an additional cell (Figure 5d). This process of cell creation and interaction with the neighboring cell propagated the instability along the interface (Figure 5e), until an array of cells with a finer spacing was formed (Figure 5f). Thus, the cellular array decreased its spacing by going through a cell-dendrite-cell transition. When the velocity was further increased in steps to 1.7 μm/s, the cell spacing approached the steady-state spacing.

In the second region of the cellular structure, A, the cellular spacing increased sharply as the velocity was changed from 1.4 μm/s to 1.5 μm/s. Here, the perturbation was nonlocalized. The entire cellular front first became unstable, as shown in Figure 6. Each alternate cell was eliminated and a doubling of spacing was observed. Thus, instead of decreasing the spacing to achieve the steady-state value, the system underwent a sharp increase in the spacing. It is interesting to note that the high-velocity branch of the steady-state cellular spacing, if extrapolated, will pass through the point representing the large spacing formed at V = 1.7 μm/s under dynamical conditions. Thus, the bifurcation in spacing, which was observed over the velocity range of 1.4 - 1.5 μm/s, appears to be the result of the system moving toward the stable steady-state and the metastable

Figure 5. A sequence of micrographs showing the reduction in cell spacing through the cell-dendrite-cell transition. V = 1.4 μm/s, (a) 1 min., (b) 3 min., (c) 6 min., (d) 7 min., (e) 9 min., and (f) 15 min.

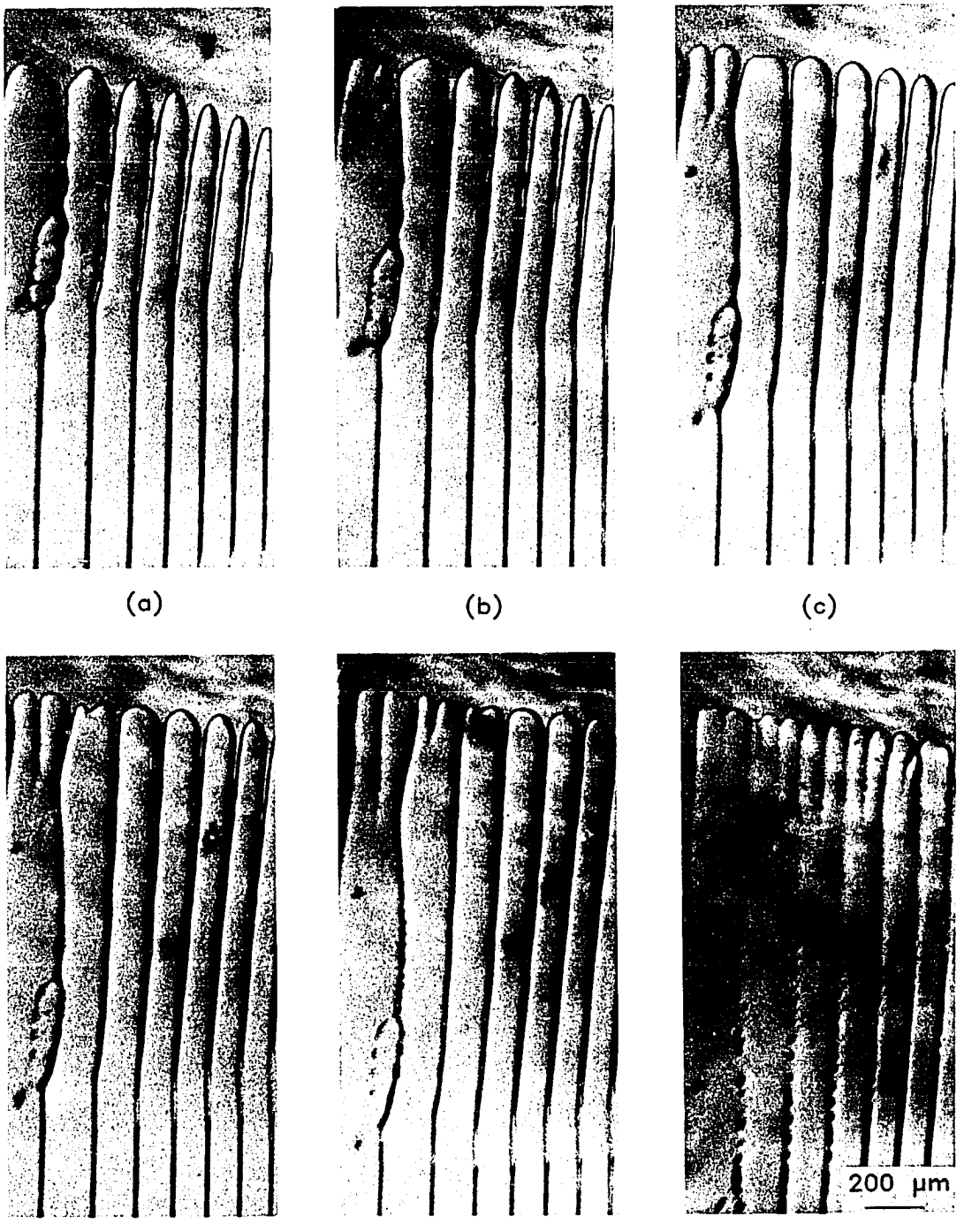
(a)
(b)
(c)
(d)
(e)
(f)
200 μm

Figure 6. Time sequence of cellular structures when the velocity was changed from 1.4 to 1.5 μm/s, illustrating the rapid coarsening of the cellular structures: (a) 1 min., (b) 4 min., (c) 7 min., (d) 15 min.

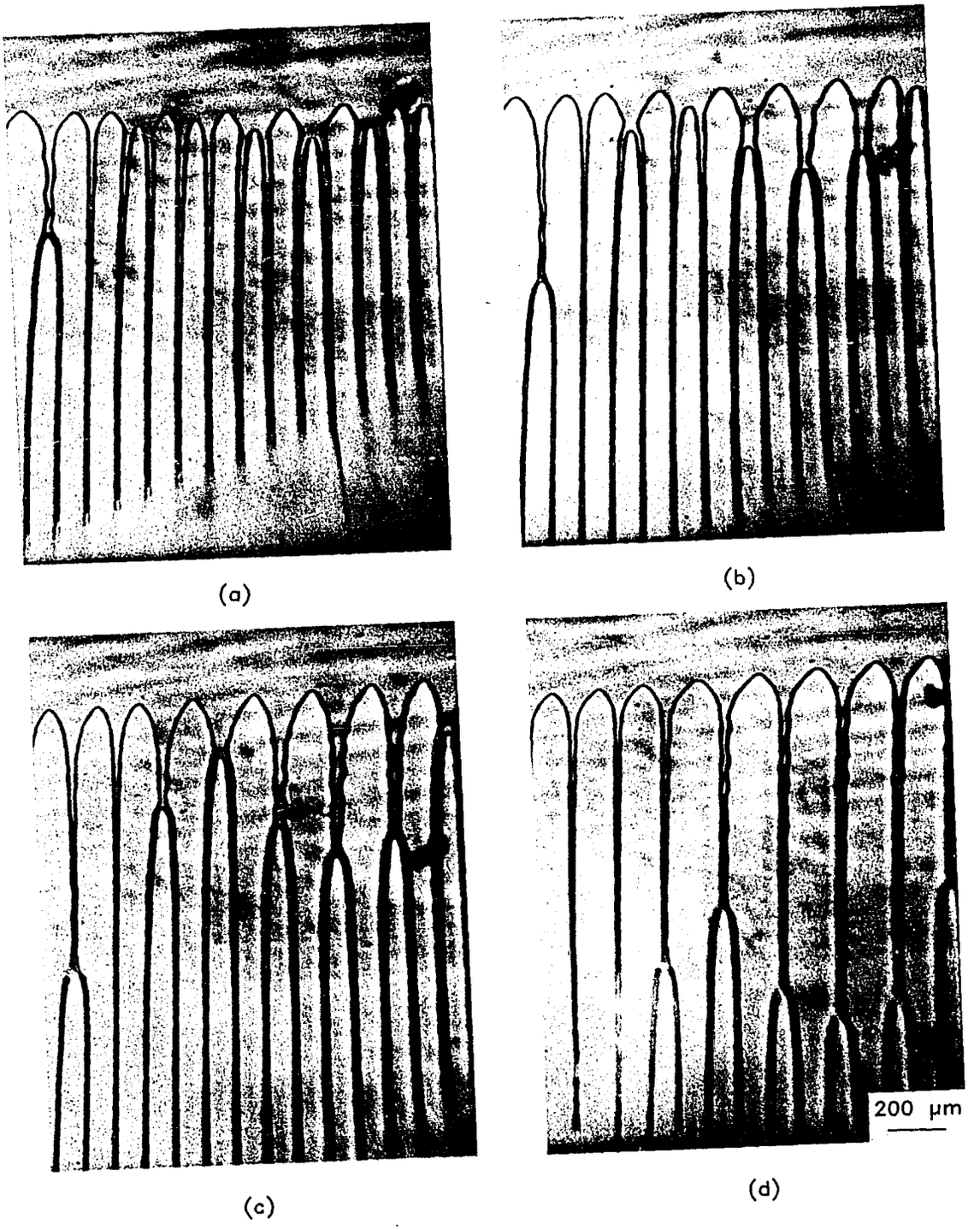

(a)

(b)

(c)

(d)

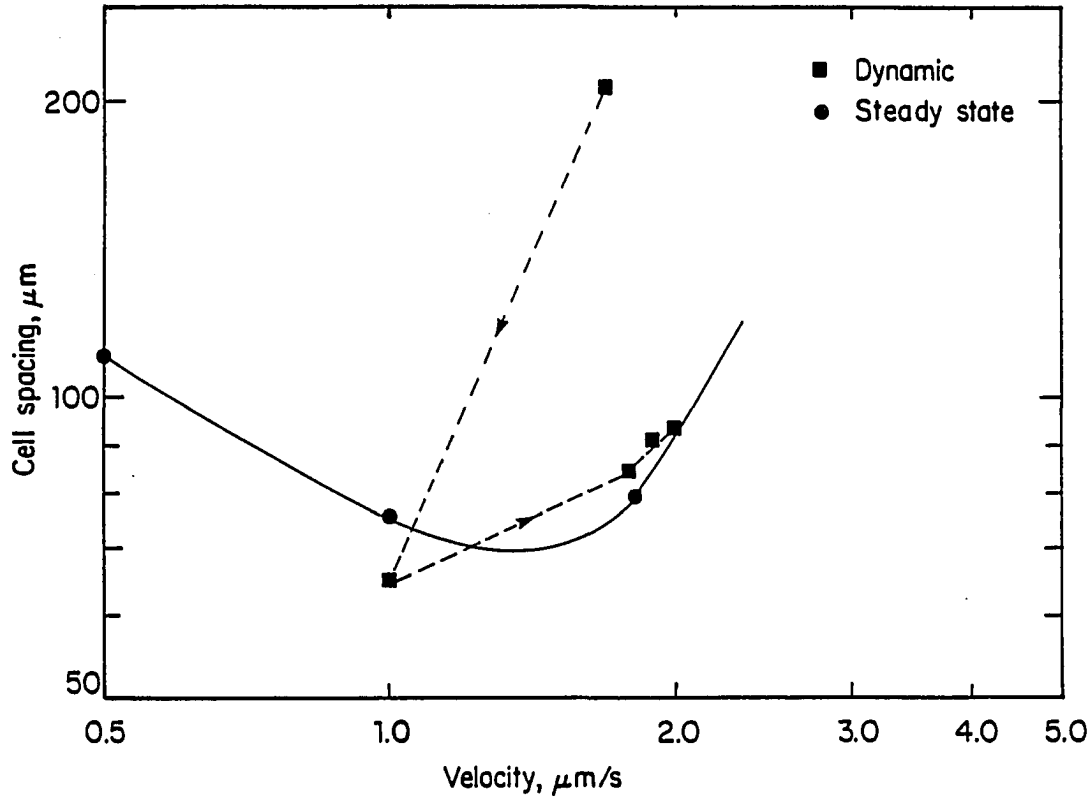

Figure 7. Variation in dynamic cell spacing with velocity. The velocity was changed suddenly from 1.7 to 1.0 μm/s and then to 1.8 μm/s. Further changes in velocity from 1.8 to 2.9 μm/s were in steps of 0.1 μm/s. The relevant portion of the steady-state cellular spacings vs. velocity plot is included for comparison

steady-state cellular spacing values.

Experimental studies, described above, clearly show that the cellular spacings do not respond quickly to the small changes in velocity. Further experiments were, therefore, carried out in which the velocity was changed significantly. The cellular structure, which was formed at a velocity of 1.7 μm/s, was first subjected to a sudden decrease in velocity from 1.7 to 1.0 μm/s and then, to a sudden increase in velocity from 1.0 to 1.8 μm/s. The cellular spacing was found to decrease sharply and approach the steady-state value, as the velocity was decreased from 1.7 to 1.0 μm/s and held at 1.0 μm/s for 11 minutes (Figure 7). The velocity was then increased sharply from 1.0 to 1.8 μm/s, and the cell spacing was found to increase to the steady-state value. Thus, a large change in the system, or a large noise, was found to drive the system toward the steady-state spacing quite rapidly.

The mechanisms by which the cellular spacing decreased as the velocity was decreased from 1.7 to 1.0 μm/s were also studied. Specifically investigated was the response of the large cell spacing branch observed at 1.7 μm/s to a sharp decrease in velocity. As the velocity was decreased rapidly from 1.7 μm/s to 1.0 μm/s, the amplitude of the cells decreased and the radius of the cell tip increased sharply, as shown in Figures 8a and 8b. The cell fronts then became nearly planar and the amplitude of the cells became very small, even though no change in the spacing occurred (Figure 8c). These flat cells then became unstable, breaking up into a finer cellular array

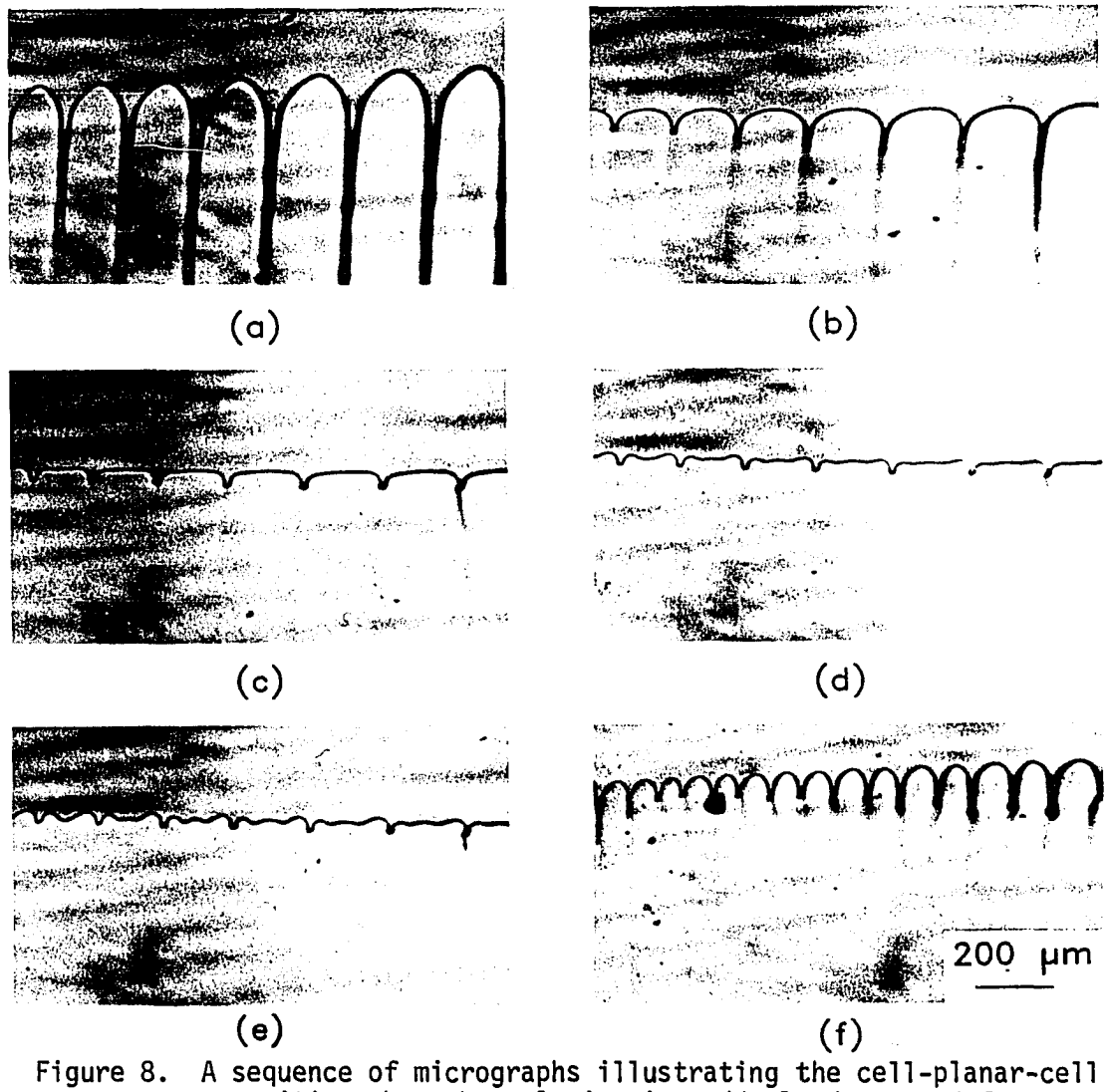

Figure 8. A sequence of micrographs illustrating the cell-planar-cell transition when the velocity is suddenly decreased from 1.7 to 1.0 μm/s and held at 1.0 μm/s for (a) 0 min., (b) 5 min., (c) 8 min., (d) 10 min., (e) 11 min. and (f) 15 min. after the change in velocity from 1.0 to 1.8 μm/s

spacing (Figure 8e). Thus, the cellular spacing adjustment occurred by the system going through a cellular-planar-cellular transition.

The velocity was now increased rapidly from 1.0 to 1.8 μm/s. Both the amplitude and the cell spacing increased to values which were characteristic of the steady-state condition, as seen in Figure 7. Thus, the system which was far from steady-state at V = 1.7 μm/s, achieved the steady-state configuration quite rapidly when it was subjected to a velocity-cycle of large magnitude, i.e., 1.7 → 1.0 → 1.8 μm/s.

The experimental results presented so far clearly show that dynamical effects are very important in systems with significantly anisotropic interface properties. Reproducible steady-state spacings were observed only when the system was driven from $V < V_c$ directly to the required velocity. Once a cellular structure forms, a significant driving force or large noise in the system is required to establish steady-state configurations. Thus, the results of many experimental studies in which a correlation between microstructure and growth rate is determined by changing the velocity in small steps should be viewed with caution.

Cell Spacing and Cell Amplitude

The steady-state cellular profiles, described in [14], showed that both the spacing and the amplitude of cells decreased with an increase in velocity. Furthermore, the dynamical studies, presented here, showed that as the velocity was increased, no change in spacing occurred up to a certain velocity. Thus, the difference between the actual

spacing and the steady-state spacing became larger with the increase in velocity. This was accompanied by an increase in the amplitudes of the cells. These observations suggest that some correlation may exist between the cell spacing and the cell amplitude.

In the previous section, it was shown that the cellular spacing selection criterion is not very sharp. A spatial Fourier transform gave a peak with a finite width. This indicated that the local cell spacing can deviate significantly from the average value. Therefore, the local cell spacing and the local cell amplitude (or the groove depth) were measured for the transient as well as the steady-state arrays of Figures 9c and 9d. The results, shown in Figure 10, clearly indicate that cellular amplitudes increased with an increase in cellular spacings.

Previous studies in metallic systems on cellular spacing variation with distance behind the tip indicated that cellular spacings increased with an increase in the distance behind the tip [28]. From this observation, it was concluded that cells coarsened with time. No coarsening of cells was, however, observed in our experiments. The apparent increase in the cell spacing is the result of the spectrum of groove depths which develop due to the fluctuations in cellular spacings. If cellular spacings in successive sections were measured, one would indeed observe an increase in spacing when the section passes the smallest groove length.

Figure 9. A sequence of micrographs showing the time-evolution of cellular structures in the pivalic acid - 0.2 wt.% ethanol alloy solidified at G = 2.98 K/mm and V = 0.5 μm/s: (a) 38 min., (b) 50 min., (c) 60 min., and (d) 125 min.

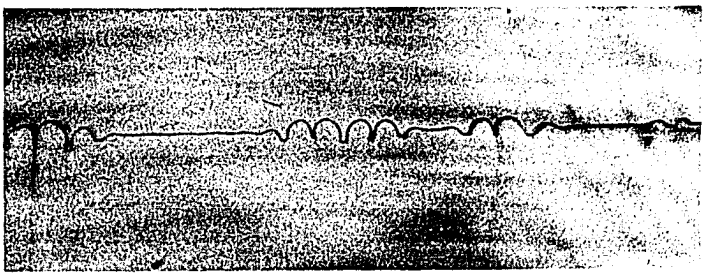

(a)

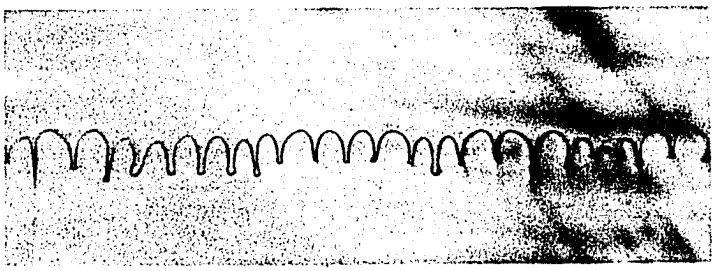

(b)

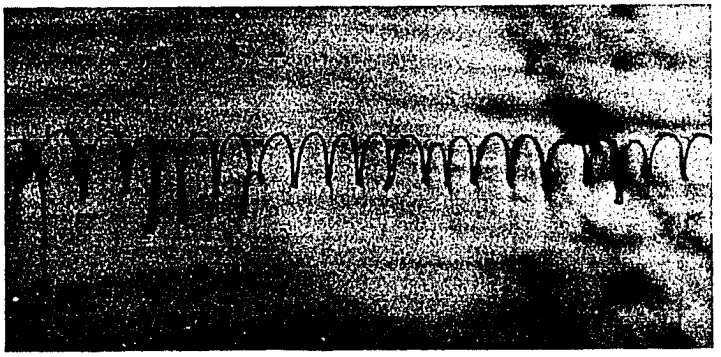

(c)

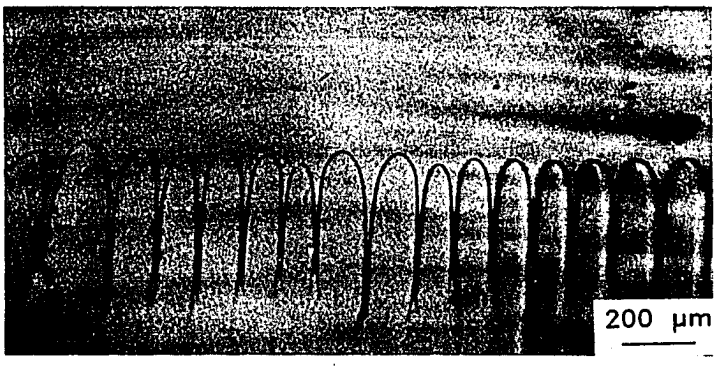

(d)

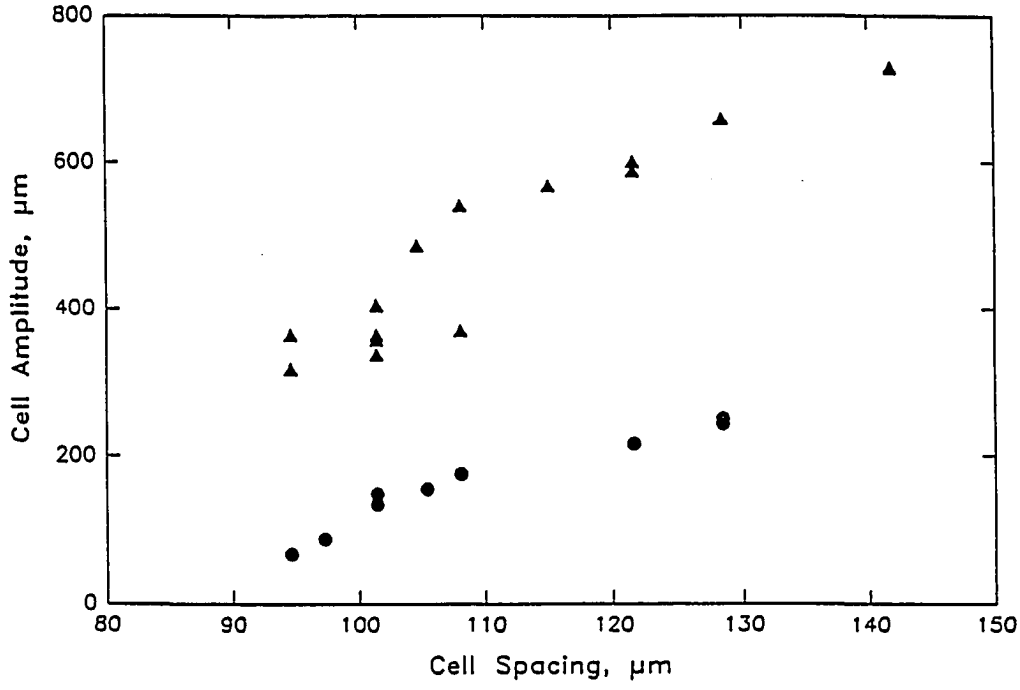

Figure 10. Relation between cell amplitude and cell spacing in the pivalic acid - 0.2 wt.% ethanol alloy, directionally solidified at V = 0.5 μm/s and G = 2.98 K/mm. Δ = steady-state morphology; o = transient morphology

CONCLUSIONS

One of the major unresolved questions in the theory of cellular growth is the principle which governs the selection of a specific cellular spacing under given experimental conditions. Anisotropy was found to play a significant role in spacing selection. As shown in Section II, cell spacing adjustment in isotropic systems occurs by cell elimination and tip-splitting. Dynamical studies in an anisotropic system show that no tip-splitting occurs at the cell tip unless the cell tip loses its sharp curvature. Thus, the creation of additional cells requires the system to go through the cellular-dendritic-cellular or the cellular-planar-cellular transition.

The spacing selection criterion in an anisotropic system has been found to be so weak that a cellular spacing formed at one velocity could be retained at significantly higher velocities. The amplitude and the radius, however, respond quickly to the changes in the velocity. These results indicate that the theoretical model to study the evolution of the steady-state spacing in anisotropic systems would be very complex and would require the presence of a very large noise which will allow the existing spacing to respond to the change. The shape of the cell front and the cell tip radius, however, respond quickly to the changes in growth conditions so that the tip shape and the tip radius selection criteria appears to be quite sharp. Furthermore, what happens near the tip region is found to play a key role in predicting the variation in the steady-state cellular spacing with velocity in the

cellular region close to V_c. Thus, additional theoretical and experimental studies are needed to understand the development of cellular profiles near the tip region.

REFERENCES

1. Langer, J. S. Rev. Mod. Phys. 1980, 52, 1.
2. Langer, J. S. Acta Metall. 1977, 25, 1121.
3. Meiron, D. Phys. Rev. 1986, A33, 2704.
4. Hong, D. C.; Langer, J. S. Phys. Rev. Lett. 1986, 56, 2032.
5. Coriell, S. R.; McFadden, G. B.; Sekerka, R. F., Ann. Rev. Mater. Sci. 1985, 15, 119.
6. Unger, L. H.; Brown, R. A. Phys. Rev. 1984, B29, 1367.
7. Unger, L. H.; Brown, R. A. Phys. Rev. 1985, B31, 5931.
8. Karma, A., Department of Physics, California Institute of Technology, Pasadena, CA (to be published), September 1986.
9. Kerszberg, M. Phys. Rev. 1983, B27, 6796.
10. Kerszberg, M. Phys. Rev. 1983, B28, 247.
11. Kerszberg, M. Physica 1984, 12D, 262.
12. Mullins, W. W.; Sekerka, R. F. J. Appl. Phys. 1964, 35, 444.
13. Eshelman, M. A.; Trivedi, R. Acta Metall. (submitted).
14. Eshelman, M. A.; Seetharaman, V.; Trivedi, R. Acta Metall. (submitted).
15. Trivedi, R.; Somboonsuk, K. Acta Metall. 1985, 33, 1061.
16. de Cheveigne, S.; Guthmann, C.; Lebrun, M. M. J. Crystal Growth 1985, 73, 242.
17. de Cheveigne, S.; Guthmann, C.; Lebrun, M. M. J. de Physique (to be published).
18. Bechhoefer, J.; Libchaber, A., University of Chicago, Chicago, IL. (to be published).
19. Jackson, K. A.; Hunt, J. D. Acta Metall. 1965, 13, 1212.
20. Heslot, F.; Libchaber, A. Physica Scripta 1985, T9, 126.

21. Somboonsuk, K.; Mason, J. T.; Trivedi, R. Metall. Trans. 1984, 15A, 967.

22. Mason, J. T.; Eshelman, M. A., IS-4906, Ames Laboratory, Iowa State University, Ames, Iowa, 1986.

23. Eshelman, M. A. Ph.D. Dissertation, Iowa State University, Ames, Iowa, 1987.

24. Jackson, K. A. "Solidification"; American Society of Metals: Metals Park, Ohio, 1971.

25. Glicksman, M. E.; Singh, N. B., ASTM STP 1986, 890, 44.

26. Huang, H. C.; Glicksman, M. E. Acta Metall. 1981, 29, 717.

27. Somboonsuk, K.; Trivedi, R. Acta Metall. 1985, 33, 1051.

28. Coriell, S. R.; Sekerka, R. F. J. Crystal Growth 1976, 34, 157.

SECTION V. THE ROLE OF ANISOTROPY ON SOLIDIFYING MICROSTRUCTURES

INTRODUCTION

When studying anisotropy and the role that it plays in solidification, it should be remembered that there are two kinds of anisotropy that may both be important. The two kinds of anisotropy are surface energy anisotropy, and anisotropy of interface solidification kinetics. Although these two may be related, they should be kept separate, both in mathematical modeling and in the consideration of the physics of solidification.

Surface energy anisotropy, which was first discussed by Gibbs [1], arises from a crystallographic dependence of the surface energy γ. It was following this concept that the Wulff theorem and Wulff plots arose (see Figure 1). Later, Hoffman and Cahn [2] and Cahn and Hoffman [3] modified the original analysis of Gibbs in vector form. The result of this is that previously unexplained problems of equilibrium shapes, such as the problem of discontinuity of interface energies at corners, are fully explained.

Surface energy anisotropy has, thus, been shown to give rise to deviations from a spherical shape in the case of equilibrium conditions for small solid spheres in a pool of liquid. Recently, Glicksman and Singh [4] have used the equilibrium shape concept to determine small surface energy anisotropies for succinonitrile and pivalic acid.

The second kind of anisotropy which is present is interface kinetic anisotropy. This kind of anisotropy exhibits itself in the interface mobility term. Glicksman and Singh [4] claim that surface

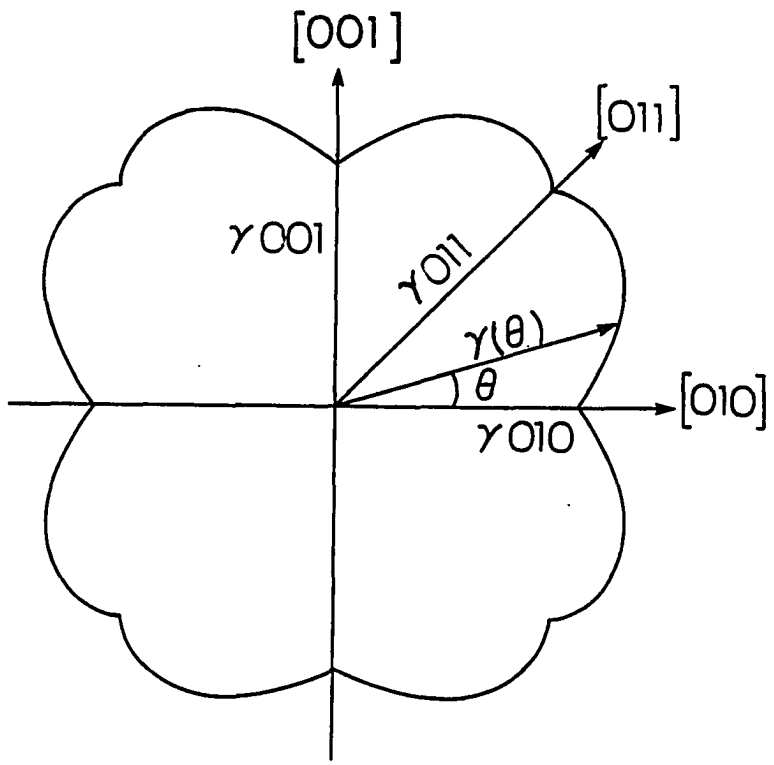

Figure 1. Schematic diagram of the variation in interface energy as a function of orientation

energy anisotropy stabilizes the dendrite tip, whereas Cahn [5] has shown that interface kinetics can also stabilize perturbations on paraboloids, to which dendrites match quite closely. Therefore, interface kinetic anisotropy should not be overlooked as an explanation for dendrite tip stability. Dendrite tip stability will not be discussed further here. The subject was introduced to illustrate the roles played by the different kinds of anisotropy in interface growth structures. The effect of anisotropic interface properties on shapes of interface structures formed after interface break up will be discussed in this section.

An additional theoretical prediction by Coriell and Sekerka [6] shows that while interface energy anisotropy contributes to a deviation from the shape observed in equilibrium conditions, interface kinetic anisotropy promotes wave translation during the growth of a perturbed planar interface. This translation effect is examined in the present work. From the theoretical work, it is not clear which kind of anisotropy is active, and when it is active. For this reason, critical experiments need to be done to clarify this problem and investigate the importance of anisotropic interface properties.

THEORY

An extension of the work of Mullins and Sekerka [7] on linear stability of an interface which included interface anisotropy was first carried out by Coriell and Sekerka [6]. They include the two possible types of anisotropy, i.e., the surface energy anisotropy and the interface kinetic anisotropy. A brief review of Coriell and Sekerka's work will be given here since the anisotropies which they discuss are important to the interpretation of the experimental work which will follow.

Coriell and Sekerka begin with the same basic assumptions that Mullins and Sekerka used with the exception of the inclusion of the two types of interface anisotropy mentioned. Their model considered variations in the surface energy and interface kinetic coefficients as a function of orientation in three dimensions. Since our experimental studies need to consider only one dimension along a surface, we shall simplify the model to the two-dimensional case. Furthermore, we shall assume constant liquidus and solidus slopes with the equilibrium partition coefficient equal to k and the slope of the liquidus equal to m. Coriell and Sekerka's model of planar interface instability is similar to that of Mullins and Sekerka, except that Coriell and Sekerka consider the effect of anisotropic kinetics on the interface. Coriell and Sekerka start with the same thermal and solute transport equations used by Mullins and Sekerka in the Theories of Pattern Formation Section of this Dissertation. The boundary

conditions are modified, and are as follows.

At the interface $$T_{sI} = T_{LI}, \tag{1}$$

$$C_{sI} = K_o C_I \ . \tag{2}$$

The velocity, v, of the perturbed interface is related to the imposed velocity, V, of the unperturbed interface by the following:

$$v = V + (\partial W/\partial t) \ , \tag{3}$$

where W is the shape of the perturbed interface. The velocity, v, is obtained from the thermal and solute flux balance at the interface:

$$v = (k_s/L_v)(\partial T_s/\partial z)_I - (k_l/L_v)(\partial T_L/\partial z)_I \tag{4}$$

and

$$v = -D(\partial C/\partial z)_I/C_I - C_{sI} \ . \tag{5}$$

The major difference between Mullins and Sekerka's model and Coriell and Sekerka's model is in the description of the temperature field along the interface. The local equilibrium condition of Mullins and Sekerka's model is relaxed by Coriell and Sekerka, and they consider the velocity to be proportional to the deviation from

equilibrium. Coriell and Sekerka [6] consider a general form for the velocity as:

$$v = f(T_e - T_{LI},\ C_I,\ W_x,\ W_{xx}) \tag{6}$$

where

$$T_e = T_m + mC_I - \Gamma K[1 + \gamma_{xx}/\gamma] \ , \tag{7}$$

and subscript x denotes partial differentiation with respect x, and K is the curvature.

The function f is expanded about the unperturbed values to give:

$$v = f[T_{eo} - T_{LIO}, C_{IO}] + \mu_T(T_{e1} - T_{LI1}) + \mu_c C_{I1} + \mu_x W_x + \mu_{xx} W_{xx} \ , \tag{8}$$

where $\mu_T = \partial f/\partial(T_e - T_{cI})$, $\mu_c = \partial f/\partial C_I$, $\mu_x = \partial f/\partial W_x$, and $\mu_{xx} = \partial f/\partial W_{xx}$ where partial derivatives are evaluated in the unperturbed state. The μ_x function is an interface kinetic anisotropy term. The first term on the right-hand side is equal to the unperturbed velocity, V.

Using these equations and boundary conditions, Coriell and Sekerka [6] obtain solutions for the interface shape and position by Fourier transformation and integration. The result is that for a perturbation of the form $\cos(k_x x)$, the solution is given by

$$W(x,t) = \cos(k_x x + 2jS_I t)\exp(2jS_R t) \tag{9}$$

or

$$W(x,t) = \cos\{k_x[x + 2J(k)(\mu_x/\mu_T)t]\}\exp[2J(k)S_R t] \ , \qquad (10)$$

where

$$S_R(k_x) = [-G + mG_c \frac{k^* - V/D}{k^*-(1-K_o)V/D} - \Gamma k_x^2]$$

$$- [\Gamma k_x^2(\gamma_{xx}/\gamma) - k_x^2\mu_{xx}/\mu_T$$

$$+ (\frac{G_c\mu_c}{\mu_T})(\frac{k^*-V/D}{k^*-(1-K_o)V/D})] \qquad (11)$$

with

$$k^* = (V/2D) + [(V/2D)^2 + k^2]^{1/2} \qquad (12)$$

and

$$J(k) = Vk/\{(G_s-G_L)[1+2K_o k/L_v\mu_T]$$

$$+ 2kG_c[m+\mu_c/\mu_T]/[k^*-(1-K_o)V/D] \ . \qquad (13)$$

$$S_I = k_x\mu_x/\mu_T \ . \qquad (14)$$

In Eq. (11), there are three main terms. The first of these main terms corresponds to Mullins and Sekerka's results. The second term contains three subterms. The first of these subterms corresponds to the surface energy anisotropy, the second corresponds to the interface mobility, and the third corresponds to the change in the

thermal gradient due to the anisotropy effect.

As can be seen, the amplitude of the perturbation is governed by the function $2J(k)S_R t$, where the subscripts R and I denote the real and imaginary components, respectively. The amplitude is controlled by the real part only. It also can be seen that an imaginary, or travelling wave component will be present when $S_I \neq 0$. This is an interesting result because it predicts that it is possible for the perturbations to travel down the interface. The velocity of the travelling wave is given by:

$$v_x = (-2j\mu_x/\mu_T) = [-2J(k)\mu_x/\mu_T] \quad . \tag{15}$$

In different terms, the initial perturbation will have a phase velocity which is inclined to the unperturbed interface normal by an angle θ. The angle θ is given by

$$\theta = \arctan [v_x/V] \quad . \tag{16}$$

Note that this is an experimentally measurable quantity. Such measurements are made in this chapter. It is possible to measure θ and in turn, estimate μ_T. Although the value of θ is measurable, it must be remembered that the conditions for which the analyses were done are conditions of linearity. This makes the measurement truly valid only at very small amplitudes. The linear stability analysis breaks down

when slopes of the order of 12-15 [8] degrees from a planar interface are present. Even though this is so, measurements still should offer some rough estimate for the interface kinetic anisotropy parameter, which up to now has been completely elusive.

The interface energy anisotropy also plays a role in interface stability, according to Coriell and Sekerka [6]. The degree to which the anisotropy affects stability is given by a parameter $Q(\omega_x)$, which is:

$$Q(k_x) = k_x^2[\gamma + \gamma_{xx} + (L_v T_m)(\mu_{xx}/\mu_T)] \quad . \tag{17}$$

The interface is most unstable where $Q(k_x)$ is a minimum. This $Q(k_x)$ term only plays a role at the point of instability. Once the interface has established a pattern, the growth rate of the pattern and the translation of the pattern are not affected by the surface energy anisotropy, according to Coriell and Sekerka [6].

EXPERIMENTAL

The material solidified in these experiments was pivalic acid 0.2 wt.% ethanol. In the experimental runs, the critical velocity was approximately 0.2 μm/s. The runs were, therefore, started at 0.1 μm/s for a period of several hours. The velocity was then increased to 0.2 μm/s for about half an hour. In this short time, the interface remained planar. The velocity was then increased to the final velocity of 0.5 μm/s, where interface break up and subsequent reorganization into a cellular pattern was observed.

The occurrence of break up was recorded photographically. Exposures were taken at 30 second intervals for 125 minutes.

RESULTS

The break up of a planar interface of different materials is shown in Figures 2(a) and 2(b). Figure 2(a) shows break up in the succinonitrile-acetone binary system. Figure 2(b) shows break up of a planar interface in the pivalic acid-ethanol binary system. The primary difference between succinonitrile and pivalic acid which concerns solidification properties is the interface anisotropy properties. Succinonitrile has been shown [4] to have a surface energy anisotropy an order of magnitude lower than pivalic acid. This difference in anisotropy can be observed in Figure 2(b) where the cells are growing slightly asymmetrically. Whereas both Figures 2(a) and 2(b) have cells which have crystallographic directions nearly identical, only pivalic acid grows with cells which are asymmetric. This is because heat flow controls the cellular growth for succinonitrile, but both heat flow and crystallography are important to cellular growth of pivalic acid.

The development through time of the asymmetry of the cellular growth is shown in Figure 3 and plotted in Figure 4. The angle given was calculated by measuring the motion of the cell tips as a function of time during the break-up process. Studying the angle as a function of time shows that the growth starts out in the direction of heat flow and then, turns toward the [001] growth direction. The anisotropic growth velocity, defined as v_x/V, was between 17% and 25% of the growth velocity V.

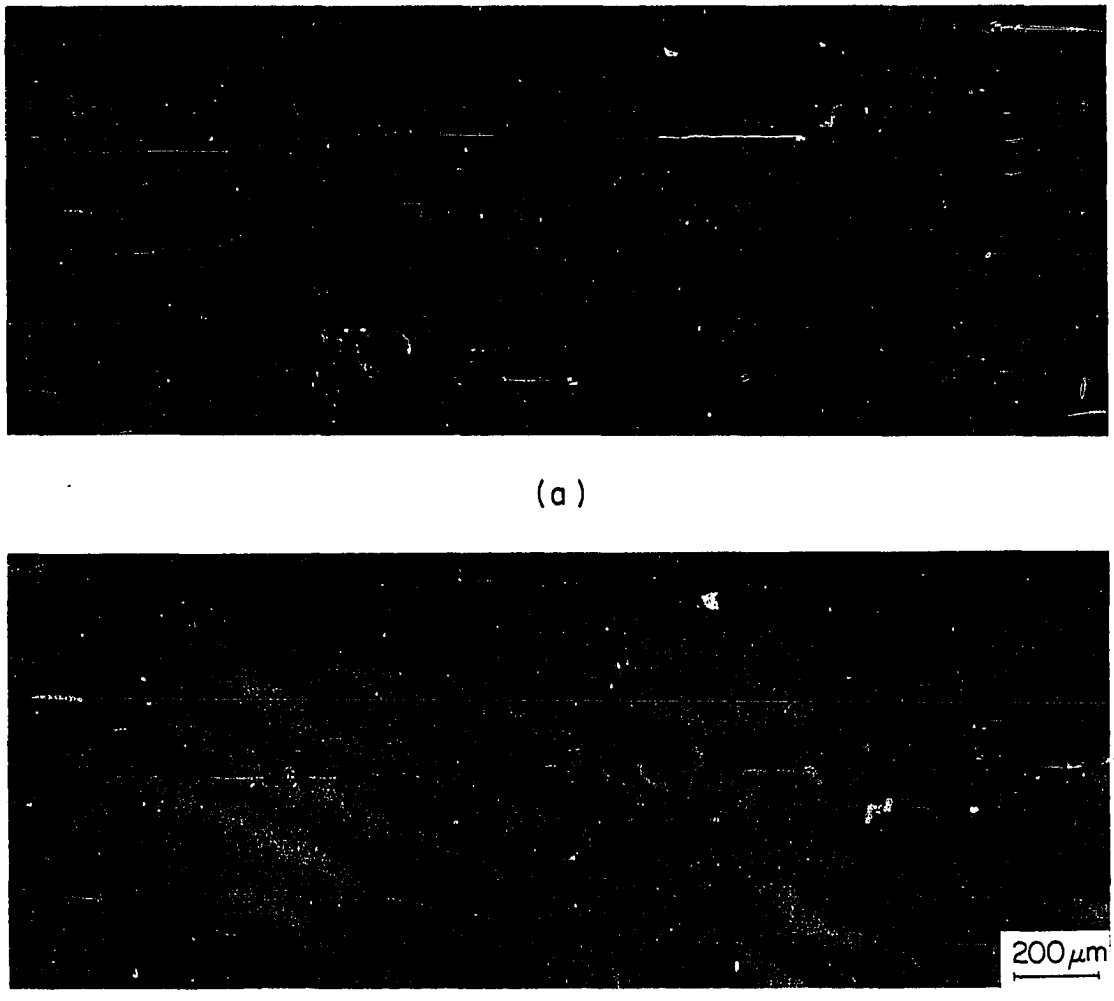

Figure 2. Interface patterns just after planar interface break up in pivalic acid 0.2 w/o ethanol, G = 2.98 K/mm, V = 0.5 μm/s. (a) [001] crystallographic orientation aligned with the heat flow direction; (b) [001] crystallographic orientation is at 25° to the heat flow direction

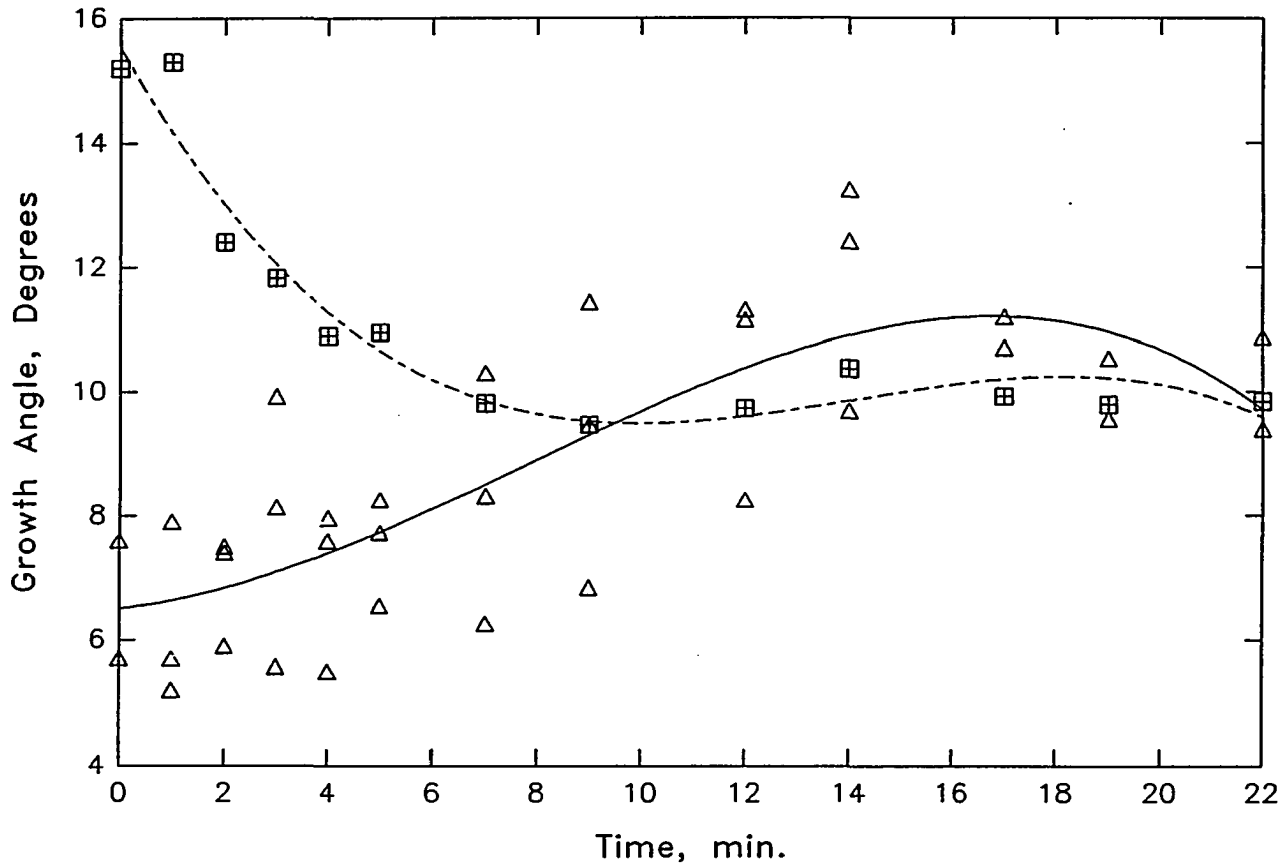

Figure 3. Growth angle $\theta = v_x/V$ as a function of time for growing perturbations in pivalic acid 0.2 w/o ethanol, G = 2.98 K/mm, V = 0.5 μm/s

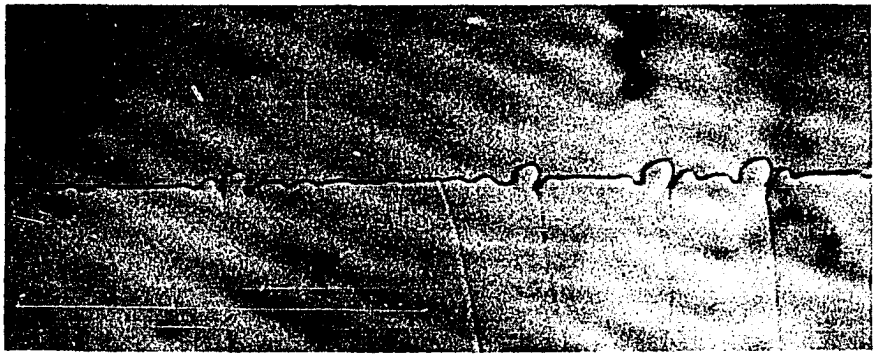

(a)

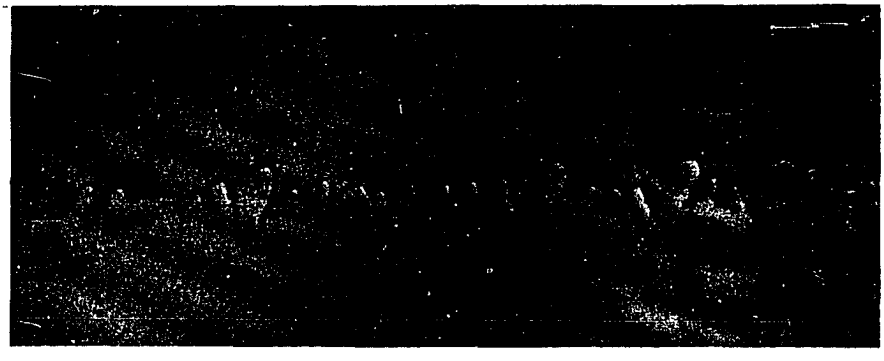

(b)

(c)

Figure 4. Interface pattern formation after planar interface break up. Times are (a) 13 minutes, (b) 16 minutes, and (c) 20 minutes after planar interface break up

In order to determine the [001] growth direction precisely, the velocity was increased at the end of the experimental run to form dendrites as shown in Figure 5. The dendrites form on the leading tip of the cells, and there is a one-to-one correspondence between the cellular and dendritic spacings. Careful inspection of Figure 5 shows that there are several initial perturbations on the opposite side of the cell where the dendrite does not form. These perturbations which did not form dendrites are in the [011] direction. The respective growth angles are given in Figure 5. It is interesting to notice that the [011] perturbations do not form dendrites even though they are more closely aligned to the heat flow direction and therefore, should have more favorable growth conditions than the [001] direction, which actually does form the dendrites. The angle between the heat flow and the [001] direction is 25 degrees. The angle between the heat flow and the [011] direction is 20 degrees.

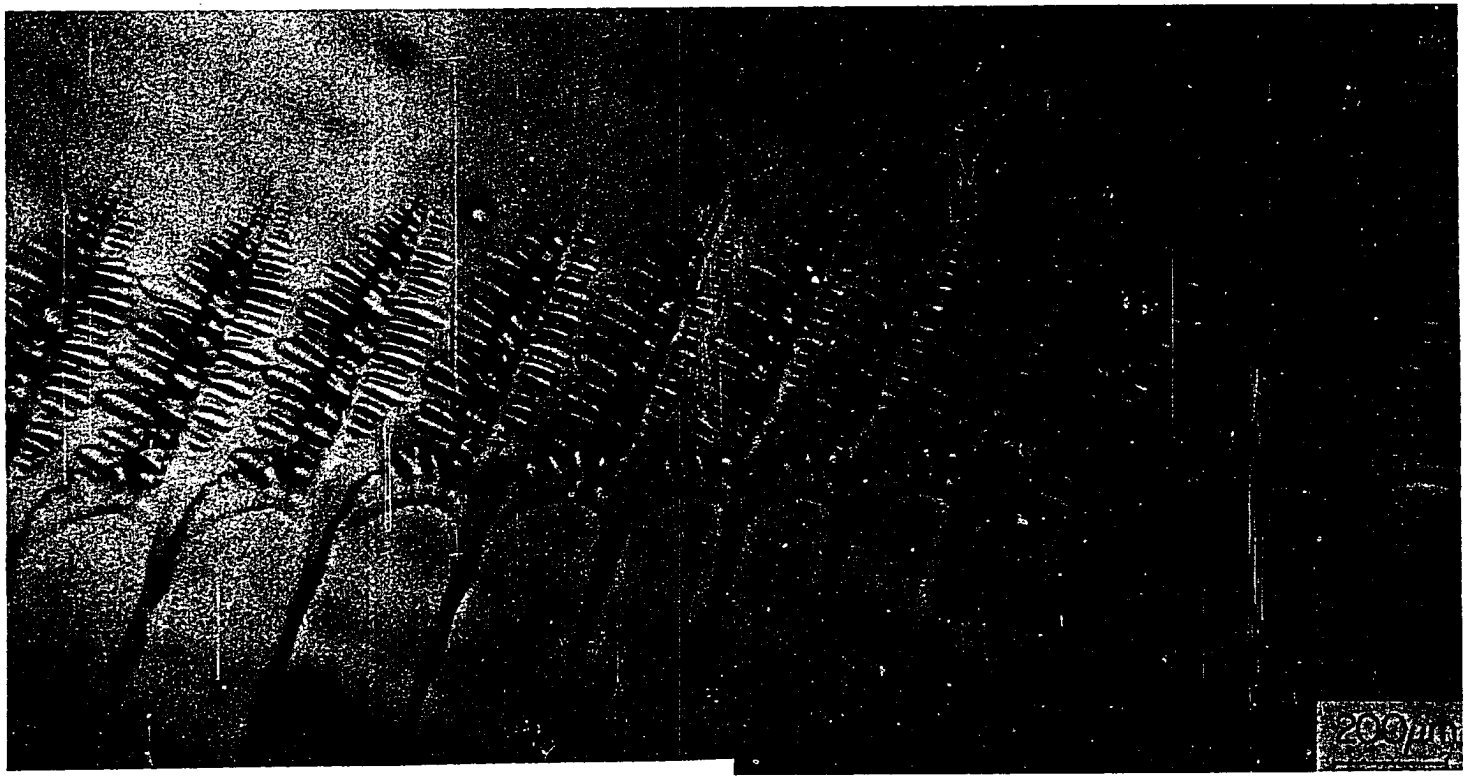

Figure 5. The planar to cellular transition in pivalic acid 0.2 w/o ethanol, G = 2.98 K/mm, V = 0.5 μm/s

DISCUSSION

From Figures 2(a) and 2(b), it is clear that anisotropy is important to the process of interface break up, or pattern formation, from the point of instability onward. Even the very small perturbations can be seen to be misshaped. Since the structures in Figure 2 are dynamic growth structures, the misshapen nature of the structures is due to difference in growth rates for different orientations. This means that the anisotropy responsible for the asymmetry is interface kinetic anisotropy.

The degree to which the kinetic anisotropy is affecting the growth as a function of time following break up can be obtained from Figure 3. This plot shows that the velocity component parallel to the interface ($V_x = -(2j\mu_x/\mu_T)$ increases as a function of time after break up. This was generally the case for the wave growth velocities plotted. In a few cases, particularly for those waves which formed before the bulk of the interface broke up, the parallel velocity component at early times was higher than the final value. In these cases, the parallel velocity component decreases with time to the steady-state value. The reason for this discrepancy is that those cells which form while the bulk of the interface is still stable, grow without being inhibited by other cells. They grow more like isolated cells. The cells which form later as a group are constrained by other cells in the growth array.

From the value of the growth angle, the velocity component parallel to the interface, and the value of μ_x/μ_T could be approximated if j(k)

was first specified. This is not yet possible because j(k) contains several poorly established parameters. The importance of the μ_x/μ_T is that it affects the growth velocities and growth shapes.

The fact that the dendrite growth direction picks a direction not favored by the heat flow, as shown in Figure 5, shows the importance of growth orientation on dendritic growth. It would be valuable to study the cell-dendrite transition as a function of concentration in other transparent metal analog systems to see when, or if, the dendrites change their growth orientation from the [001] growth direction to some other direction. A solution to this problem would be valuable for directionally grown material where orientation is important to some material property.

The shapes of the steady-state cells are shown in Figure 6. Examining the shapes of the cells closely, and knowing the [001] growth direction (from Figure 5), the two facets seen in Figure 6 were determined to be type (111) and type (011) growth planes. The type (111) plane is on the front of the cell, and the type (011) plane is on the side of the cell.

Figure 4(c) is a photomicrograph from the competitive growth region. Examining the figure reveals that facets exist on many of the larger cell structures. Knowing the crystallography from Figure 5, the crystallographic planes on each of the facets can be determined. This has been done in Figure 7. The facets that were observed are of types (111), (112), (011), and (001). These facets are marked where they were observed in Figure 4(c).

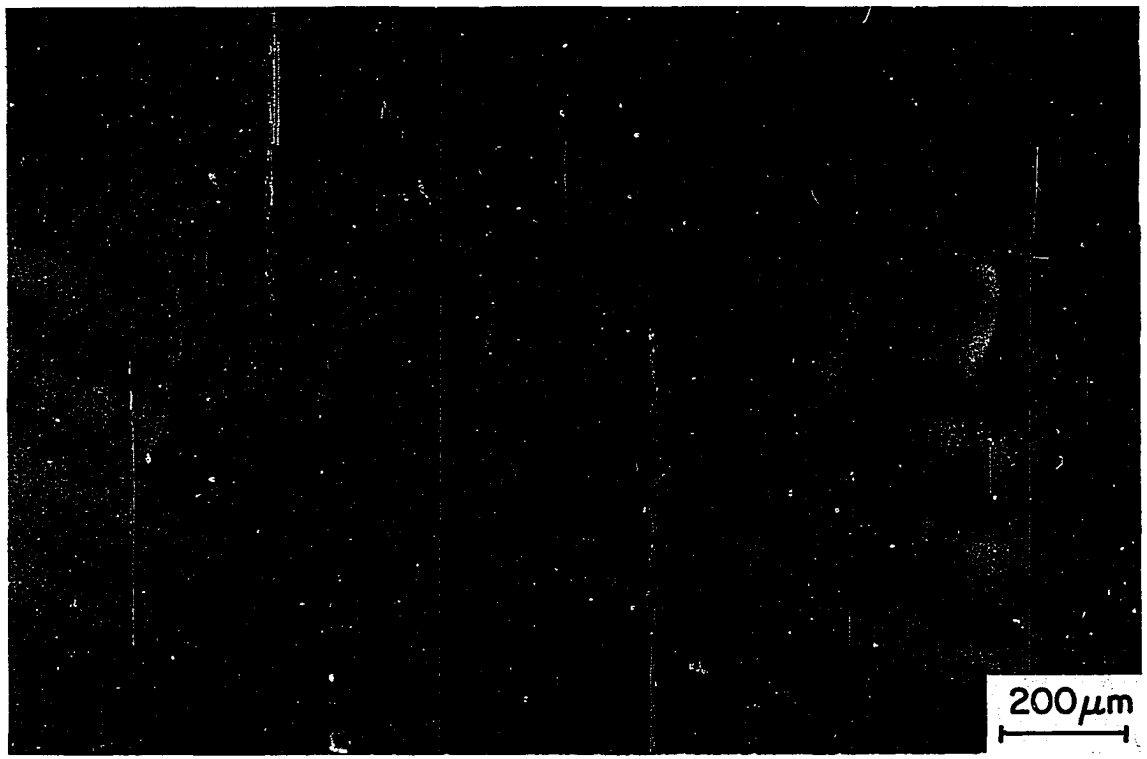

Figure 6. Steady-state cells showing facets in pivalic acid 0.2 w/o ethanol, G = 2.98 K/mm, V = 0.5 μm/s

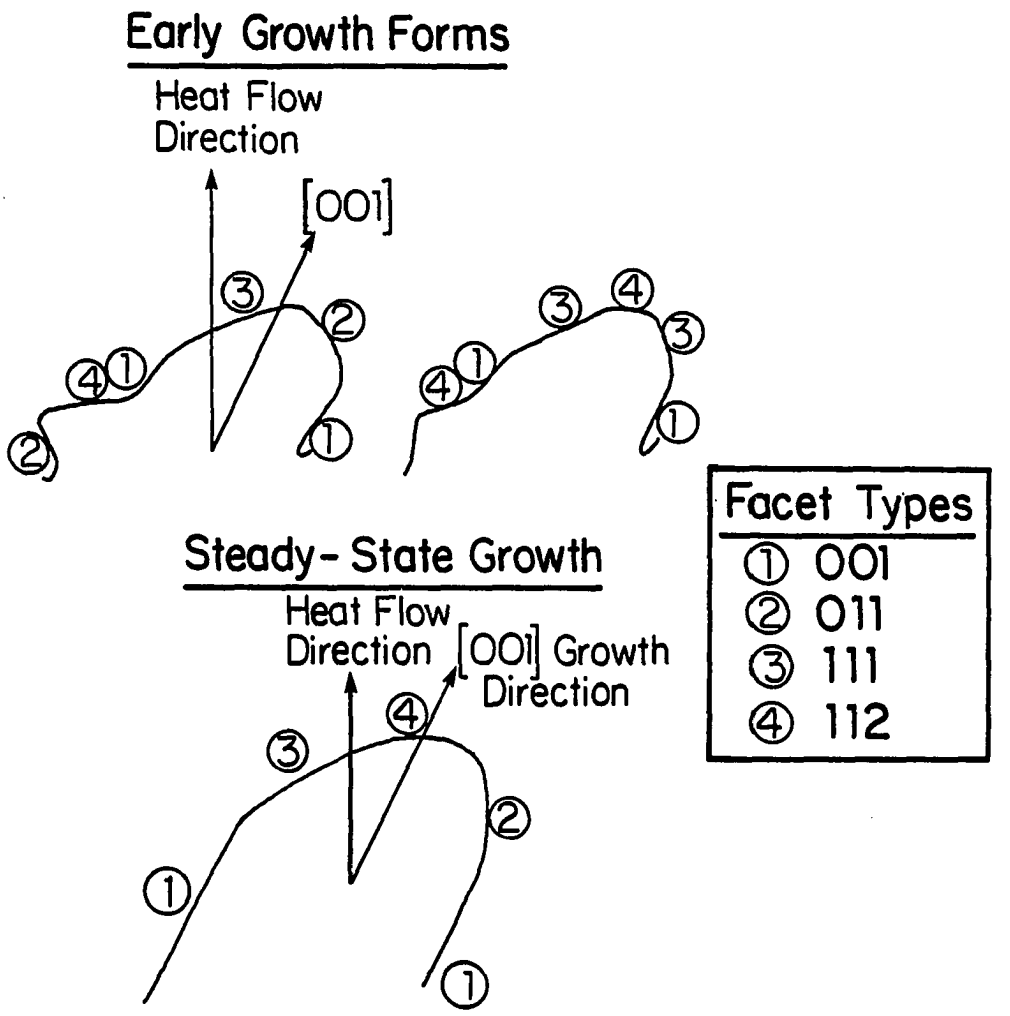

Figure 7. Schematic diagram of faceted cells showing growth planes. The cells here are the prominent cells shown in Figure 4c

The presence of the facets in Figures 6 and 7 and their relative sizes give some approximation of the degree of anisotropy which exists in the kinetic anisotropy parameter at different orientations. This also shows which orientations contain strong anisotropy variations with a variation in crystallography. If a schematic kinetic anisotropy versus orientation plot is constructed from the orientations and relative sizes of the facets seen in Figures 6 and 7, the plot shown in Figure 8 results.

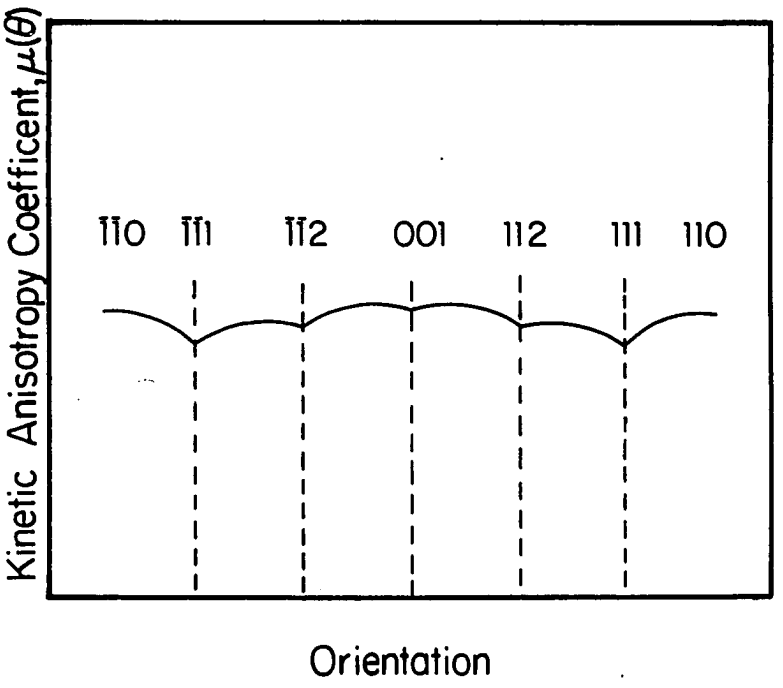

Figure 8. Schematic diagram of the orientation dependence of the kinetic anisotropy coefficient

CONCLUSIONS

Interface anisotropy affects both cell shape and cell growth velocities. Anisotropy introduces a velocity component for growth which is parallel to a perturbed directionally growing interface. This parallel velocity component was measured in the pivalic acid-ethanol alloy system and found to be 21% $\pm$ 4% of the growth velocity at velocities near the critical planar interface velocity. This velocity component is for cells that have a crystallographic orientation 25 degrees off of the heat flow direction.

In addition, cells were seen to facet along (001), (011), (111), and (112) type planes during interface break up. Dendrites were also shown to prefer a nonfavored growth direction due to their crystallography during the cell-dendrite transition.

REFERENCES

1. Gibbs, J. W. In "The Scientific Papers of J. Willard Gibbs"; Dover Publications, Inc.: New York, 1961; Vol. 1.

2. Hoffman, D. W.; Cahn, J. W. Surface Sci. 1972, 31, 368.

3. Cahn, J. W.; Hoffman, D. W. Acta Metall. 1974, 22, 1205.

4. Glicksman, M. E.; Singh, N. B. ASTM Tech. Publ. 1986, 890, 44.

5. Cahn, J. W. J. Phys. Chem. Solids 1967, Supplement, 681.

6. Coriell, S. R.; Sekerka, R. F. J. Crystal Growth 1976, 34, 157.

7. Mullins, W. W.; Sekerka, R. F. J. Appl. Phys. 1964, 35, 444.

8. Mullins, W. W. "Metal Surfaces"; American Society for Metals: Metals Park, Ohio, 1963; p. 17.

GENERAL SUMMARY

In summary, there are a number of important conclusions which can be drawn from the critical experiments done in this work. From the work done on the critical velocity measurements at which planar interface breaks up, it was shown that the velocity predicted by Mullins and Sekerka's linear stability analysis [2] gives a value very close to the value observed experimentally. This is true even in systems where the nonlinear effect of subcritical bifurcation is present. The commercial importance of these findings is that Mullins and Sekerka's estimate of the true critical velocity can be used for single crystal growth. The commercial importance of the existence of subcritical bifurcation, which exists where $K_o < 0.45$, is that a perturbed interface will continue to be perturbed far below V_c. It is, therefore, important to keep the growth velocity substantially below V_c where subcritical bifurcation is present because regaining a planar interface is difficult once it is perturbed.

While the critical velocity for break up of a planar interface is accurately given by Mullins and Sekerka's linear stability analysis [2], the wavenumbers observed at initial break up are three to four times smaller than predicted. The reason for the discrepancy is still unknown.

A second major conclusion that can be drawn from the study of pattern formation. It was observed in the study of pattern formation that the interface breaks up into wavenumbers that are larger than the steady-state values. The interface then goes into a region where a set

of discrete wavenumbers are present. There is, in fact, a dominant transition wavenumber which is present. Following the transition region, a wavenumber corresponding to the steady-state wavenumbers is established. The key points from this analysis are (a) the pattern formation process is not entirely chaotic. There is instead, a transition region which exists which has several wavenumbers present. (b) The interface is stabilized by surface anisotropy properties.

A third major conclusion comes from the study of steady-state cellular spacings. It was found there that none of the existing models of cellular growth accurately predict the decrease, increase, and subsequent decrease with spacing that occurs as the velocity is increased. The cell model of Trivedi [62] does, however, give a good estimate of the maximum spacing observed just prior to the cell-dendrite transition. There is, therefore, a need for a theoretical model to be developed which can describe the entire cell growth region. The study done here clarifies the current confusion in the literature which exists in the area of cell spacing trends as the velocity is increased. This work clarifies the cell growth region which is important commercially in determining material properties.

A fourth conclusion that comes from the dynamic studies of cell spacings is that care must be taken when doing cell spacing measurements because dynamics are important to the observed spacings. This is especially true for systems which contain considerable anisotropy in interface properties.

A fifth conclusion which comes from the work on anisotropy during and following pattern formation is that anisotropy is important to the growth structures observed. Cells will show facets during the pattern formation process and even in the steady state. These cells will also translate down a growing steady-state interface. The translation velocity in the pivalic acid-ethanol system studied was 21% of the growth velocity.

Work is required to establish anisotropy parameters. This work is of interest commercially because one could then calculate the velocity of growing facets along an interface during in situ growth in metals. This could be an important factor in single crystal or slowly grown commercial materials.

This work helped solve some fundamental questions in material science such as modes of bifurcation present, the accuracy of linear stability analysis of planar interface break up, and the general nature of pattern selection. But, work clearly still remains in the areas of pattern formation modeling, cell-dendrite bifurcation modes, and establishing the role of anisotropy in growth structures.

REFERENCES

1a. Spangenberg, K. "Handworterbuch der Naturwissenschaften"; Dittler, R. et al. Eds.; Verlag von Gustav Fischer: Jena, 1935; Vol. 10.

1b. Bentley, W. A.; Humphreys, W. J. "Snow Crystals"; McGraw-Hill: New York, 1931.

2. Mullins, W. W.; Sekerka, R. F. J. Appl. Phys. 1964, 35, 444.

3. Tiller, W. A.; Jackson, K. A.; Rutter, J. W.; Chalmers, B. Acta Metall. 1953, 1, 428.

4. Wollkind, D. J.; Segel, L. A. Phil. Trans. R. Soc. London 1970, 268A, 351.

5. Spittle, J. A.; Hunt, M. D.; Smith, R. W. J. Crystal Growth 1968, 3, 647.

6. Coriell, S. R.; Sekerka, R. F. Physiochem. Hydro. 1981, 2, 281.

7. Hurle, D. T. J.; Jakeman, E.; Wheeler, A. A. J. Crystal Growth 1982, 58, 163.

8. Favier, J. J.; Rouzand, A. J. Crystal Growth 1983, 64, 367.

9. Hurle, D. T. J. J. Crystal Growth 1983, 61, 463.

10. Wollkind, D. J.; Maurer, R. N. J. Crystal Growth 1977, 42, 24.

11. Sriranganathan, R.; Wollkind, D. J.; Oulton, D. B. J. Crystal Growth 1983, 62, 265.

12. Wheeler, A. A. J. Crystal Growth 1984, 64, 8.

13. Huggins, R. A.; Elwell, D. J. Crystal Growth 1977, 37, 159.

14. Shewmon, P. G. Trans. Met. Soc. AIME 1965, 233, 736.

15. Coriell, S. R.; McFadden, C. B.; Sekerka, R. F. Ann. Rev. Mater. Sci. 1985, 15, 119.

16. Morris, L. R.; Winegard, W. L. J. Crystal Growth 1969, 5, 361.

17. Davis, K. G.; Fryzuk, P. J. Crystal Growth 1971, 8, 57.

18. Hecht, M. V.; Kerr, H. W. J. Crystal Growth 1970, 7, 136.

19. Sato, T.; Ohira, G. J. Crystal Growth 1977, 40, 78.

20. Sato, T.; Shibata, K.; Ohira, G. J. Crystal Growth 1977, 40, 69.

21. Shibata, K.; Sato, T.; Ohira, G. J. Crystal Growth 1978, 44, 419.

22. Jamgotchian, H.; Billia; Capella, L. J. Crystal Growth 1983, 62, 539.

23. Kim, K. M. J. Crystal Growth 1978, 44, 403.

24. Reynolds, O. Phil. Trans. Roy. Soc. 1883, 174, 935.

25. Bohr, N. Phil. Trans. Roy. Soc. 1909, 209, 281.

26. Noether, F. Z. Angew. Math. Mech. 1921, 1, 125.

27. Heisenberg, W. Ann. Phys. Lpz. 1924, 74, 577.

28. Landau, L. D. C. R. Acad. Sci. URSS 1944, 44, 311. Also in Landau, L. D.; Lifshitz, E. M. "Fluid Mechanics"; Sykes, J. B. and Reid, W. H., Translation; Pergamon Press: London, 1959; Vol. 6.

29. Caroli, B.; Caroli, L.; Roulet, B. J. Physique 1982, 43, 1767.

30. Wollkind, D. J.; Notestine, R. D. IMPJ Appl. Math. 1981, 22, 85.

31. Kerszberg, M. Phys. Rev. 1983, 27B, 3909.

32. Kerszberg, M. Phys. Rev. 1983, 27B, 6796.

33. Kerszberg, M. Phys. Rev. 1983, 28B, 247.

34. McFadden, G. B.; Coriell, S. R. Physica 1984, 12D, 253.

35. Unger, L. H.; Brown, R. A. Phys. Rev. 1984, 29B, 1367.

36. Unger, L. H.; Brown, R. A. Phys. Rev. 1984, 30B, 3993.

37. Unger, L. H.; Brown, R. A. Phys. Rev. 1985, 31, 5931.

38. Unger, L. H.; Bennett, M. S.; Brown, R. A. Phys. Rev. 1985, 31B, 5923.

39. Karma, A. Department of Physics, California Institute of Technology, Pasadena, CA (unpublished work), September 1986.

40. McCartney, D. G.; Hunt, J. D. Metall. Trans. 1984, 15A, 983.

41. Langer, J. S.; Turski, L. A. Acta Metall. 1977, 25, 1121.

42. Langer, J. S. Acta Metall. 1977, 25, 1121.

43. Dee, G.; Mathur, R. Phys. Rev. 1983, 27B, 7073.

44. Ben-Jacob, E.; Goldenfeld, N.; Langer, J. S.; Schön, G. Physica 1984, 12D, 245.

45. Ben-Jacob, E.; Goldenfeld, N.; Langer, J. S.; Schön, G. Phys. Rev. 1984, 29A, 330.

46. Somboonsuk, K. Ph.D. Dissertation, Iowa State University, Ames, Iowa, 1984.

47. de Cheveigne, S.; Guthmann, L.; Lebrun, M. M. J. Crystal Growth 1985, 73, 242.

48. de Cheveigne, S.; Guthmann, L.; Lebrun, M. M. J. de Physique 1986, 47, 2095.

49. Langer, J. S., Institute for Theoretical Physics, University of California, Santa Barbara, CA (unpublished review), 1986.

50. Esaka, H. Ph.D. Dissertation, Ecole Polytechnique Federale Lausane, Switzerland, 1986.

51. Eckmann, J.-P. Rev. Mod. Phys. 1985, 57, 617.

52. Drazin, P. G.; Reid, W. H. "Hydrodynamic Stability"; Cambridge University Press: Cambridge, MA, 1981; Chapter 7.

53. Trivedi, R.; Somboonsuk, K. Acta Metall. 1985, 33, 1061.

54. Coriell, S. R.; Sekerka, R. F. J. Crystal Growth 1976, 34, 157.

55. Jackson, K. A.; Hunt, J. D. Acta Metall. 1965, 13, 1212.

56. Mason, J. T.; Eshelman, M. A. IS-4906, Ames Laboratory, Iowa State University, Ames, Iowa, 1986.

57. Caroli, B.; Caroli, L.; Roulet, B. (submitted to J. Crystal Growth).

58. Pfann, W. G. "Zone Melting"; John Wiley & Sons: New York, 1958.

59. Chopra, M. A. Ph.D. Dissertation, Rensselaer Polytechnic Institute, Troy, New York, 1983.

60. Mason, J. T.; Noack, M. A. Ames Laboratory, Iowa State University, Ames, IA (unpublished work), 1986.

61. Kaukler, W. F.; Rutter, J. Mat. Sci. Eng. 1984, 65, L1.

62. Trivedi, R. Metall. Trans. 1984, 15A, 977.

ACKNOWLEDGMENTS

The process of learning can go on in most any situation, or under nearly any circumstances, but there are those who have given me specific tools and inspired their use to whom I am grateful and wish to express this acknowledgment. Although on the doctoral level one tries to refine and specialize problems so that solutions can be concretely obtained and discussed, yet there is and should continue to be philosophy, a part of the name of the degree itself, which helps make the problems both interesting to investigate and of value to other areas of life. The principles of working out problems and coming to consistent solutions which have been taught me are, and will continue to be of great benefit, not only as my study of materials science continues, but also in life in general. These principles should and have caused me to search out answers in areas of life I would never previously have ventured into. This is as it should be, since in discovering a part of nature's processes, the whole is more completely understood.

Those at Iowa State University to whom I am grateful are more than the space here justifies, but some of the key people will be mentioned here. I am grateful to Dr. R. Trivedi for his hours of fruitful discussions, for encouraging me to think deeply and concretely, for direction in research, and for including me in some of his cross-cultural experiences. I am grateful to John Mason for showing me research methods, for sharing information and ideas, and for help during many of the experiments conducted. I am grateful to Dr. V. Seetharaman for assisting during a critical time in this research, and also a very

important time in my life. And I am grateful to Dr. K. Somboonsuk for paving the way in this research work by his own study of solidification.

On a very personal level, I am grateful to my parents, Dr. and Mrs. Frank Eshelman, who I believe, had the dream that this was possible long before I did and encouraged me to investigate the dream and to continue on to make it a reality. I am grateful to my wife, Carol, who has come along side to assist, encourage and support me in good and difficult times, and to be my best friend throughout this life. One of her Proverbs aptly speaks in saying, "He who finds a wife finds what is good and receives favor from the Lord" (Prov. 18:22 NIV), and again, "Pleasant words are a honeycomb, sweet to the soul and healing to the bones...." (Prov. 16:24 NIV). Finally, I am grateful to him of whom "The heavens declare glory..." and "... the skies proclaim the work of his hands..." (Psalm 19:1 NIV). He is the only unchanging integration point for all of life.